U.PORTO
FEUP FACULDADE DE ENGENHARIA
UNIVERSIDADE DO PORTO

Study of a hybrid concentrating solar power plant for Portuguese conditions

Bruno André da Costa Coelho

Dissertation presented for the degree of:

Doctor in Mechanical Engineering

by the

University of Porto

Porto 2014

SUPERVISORS:

Armando Carlos Figueiredo Coelho de Oliveira, Associate Professor

Adélio Miguel Magalhães Mendes, Associate Professor

Joaquim Gabriel Magalhães Mendes, Auxiliary Professor

FUNDAÇÃO
CALOUSTE
GULBENKIAN

Acknowledgments

I am grateful to the Portuguese Calouste Gulbenkian Foundation for their belief in my capabilities and financing my PhD grant (Grant Ref.: 104299); to UNET, FEUP and DLR for providing the conditions to develop my work.

I will always be thankful to my supervisors Prof. Armando Oliveira, Prof. Adélio Mendes and Prof. Joaquim Gabriel for their guidance, for always being available (even when there was no time) and for our long discussions and brainstorming, which made possible to build this thesis.

I thank my UNET labmates Szabolcs Varga and João Soares for their friendship; and to Peter Schwarzbözl and Klaus Hennecke for welcoming me in DLR. Also, thanks to all my friends for the coffees, the talks and the laughs that made all the difference.

A special thank you to my father and my mother for always being there for me, for the unconditional help, for all the values and advices you gave me, which made me grow into the person I am today, and still do...

Many thanks to my family for all moments we spent together, to my grandparents, my godmother Gustinha, my godson Alfredo, all my uncles, aunts and cousins.

Last but definitely not least, thank you Eli for the love, patience and support during all these years, especially in the most difficult moments, gmdt.

In memory of my godfather Avelino

Contents

This page was intentionally left blank

Abstract

The world suffers from an increasing dependence on fossil fuels, either for electricity generation, transportation or industrial processes. Central receiver systems (CRS) are one of the most promising concentrating solar power (CSP) technologies. Portugal has a great potential for concentrated solar power and namely for atmospheric air volumetric central receiver systems (CRS). Several CSP projects were selected in a recent Portuguese call, namely a 4 MWe atmospheric air volumetric CRS.

An innovative methodology for performance and cost optimization of CRS plants was developed to solve the power plant optimization complex and iterative process. Several variables affect this process: the power block selection, the selected design direct normal irradiance (DNI), receiver flux limit impact, solar multiple and storage capacity; they all have a significant impact on the power plant levelized electricity cost (LEC), and their optimization and adequate control strategy can save significant costs for the investors. For Faro (Portugal) conditions, the best 4 MWe power plant configuration was obtained for a 1.25 solar multiple and a 2 hour storage, a design DNI of 750 W/m^2 and a power block that generates 80 bar and 480 °C steam at nominal conditions, with a resulting levelized electricity cost (LEC) of 0.234 €/kWh and a capital expenditure (CAPEX) of € 22.3 million (CRS#3). This LEC is significantly lower than the feed-in tariff defined by the national law (0.273 €/kWh), and can be reduced down to 0.232 €/kWh if the receiver flux limit is increased (CRS#11 or CRS#12). The investment has an internal rate of return (IRR) of 9.8 %, with a payback time of 14 years and a net present value (NPV) of € 7.9 million, assuming an average annual inflation of 4 %. In the case of annual average inflation of 2 %, the power plant NPV increases to € 13 million and the payback decreases to 13 years.

The economic turnover of a solar-only CRS is positive (for the Portuguese case), but depends on bonus feed-in tariffs. CSP plants originate moderate electricity costs, in most cases quite low capacity factors and transient problems due to the high inertia. On the other hand, with the existing biomass feed-in tariffs and raising biomass prices, the viability of current biomass power plants is at risk. Hybridization can help solve these problems, and if done with the integration of forest waste biomass, the “renewable goal” can also be maintained. It could also have a positive impact on the reduction of forest fires and expand CSP markets to specific target areas. The local conditions, resources and feed-in tariffs have a great impact on the economic and technic evaluation of the solutions; therefore, the Portuguese Algarve region

was selected to support this study. Due to the innovation associated with the concept, a conservative approach was considered.

In this perspective, the integration of biomass into CSP was studied for the Portuguese SOLMASS project: a hybrid CRS (atmospheric air volumetric receiver)/biomass 4 MWe power plant to be built in Algarve, Portugal. The integration of biomass in the steam cycle is more favourable with the hybrid CRS/biomass power plant with shared power block (FRB4#CRS#12) This hybrid solution reduces the energy dumping, start-up and shut-down periods, and reduces the LEC to 0.146 €/kWh. FRB4#CRS#12 has a 0.086 €/kWh lower LEC than a solar-only CRS#12 and an increase of 0.041 €/kWh when compared to a typical biomass-only power plant (FRB4), with a reduction of 7500 tons/year on biomass consumption. Considering the national feed-in tariffs, the hybrid plant (FRB4#CRS#12) presents an internal rate of return (IRR) of 6.6 % (FRB4#CRS#12), compared to 9.7 % (CRS#12) and 7.4 % (FRB4).

The integration of biomass into the air cycle of a CRS can be done considering a large spectrum of technologies: wood gasification, refuse-derived fuel pellets, biogas from a waste water anaerobic digester, biogas from a landfill and natural gas. The solution with lower LEC was obtained for the hybridization of the 4 MWe CRS with biogas from an anaerobic digester using sludge from a wastewater treatment plant (WWTP) (LEC of 0.15 €/kWh). This power plant returns the investment in 13 years (assuming sludge collection and transport without cost) with the best NPV (15 million euro) and IRR of all the hybrid options. A hybrid CRS/wood residues gasification technology that can be used in a larger number of cases is WG#CRS#3 - LEC of 0.17 €/kWh. This power plant can makes biomass gasification economically viable to operate under the Portuguese conditions (with an IRR of 5.5 % and a NPV of 3.3 million euro), reducing the biomass consumption by 11 000 tons per year when compared to the base case.

Concentrated solar power (CSP) has been proven to be a valid means not only for the electricity generation but for fuels and chemicals generation from renewable sources – water, sun and biomass. A technological revolution in hydrogen and electricity production is important to support the future needs and lead the world towards a better future. For that, several projects in motion are presented and compared, but technic and economic barriers still have to be broken. Although solid steps should be taken to solve the current limitations and increase the viability of these projects, there are conditions to begin this revolution and connect factual bridges from the current fossil fuel technologies to renewable technologies.

Sumário

A nível mundial existe uma crescente dependência de combustíveis fósseis, seja para a produção de eletricidade, combustíveis ou para processos industriais. Para contrariar esta tendência é necessária uma aposta nas tecnologias de conversão de recursos renováveis. Os sistemas de torre solar (CRS) são uma das tecnologias mais promissoras de concentração solar (CSP). Portugal tem um elevado potencial para implementação de torres solares. Vários projetos de CSP foram selecionados numa recente candidatura para pontos de integração de potência na rede elétrica nacional (PIP), entre eles o projeto SOLMASS, um destes resulta de uma parceria FEUP/EFACE para construção de uma torre solar com recetor volumétrico de ar atmosférico de 4 MWe.

Neste âmbito foi desenvolvida uma metodologia inovadora para simular/otimizar o desempenho e custo de uma central CRS. Diversas variáveis afetam este processo: a seleção do bloco de potência, a irradiação direta normal (DNI) nominal da central, os limites de fluxo solar no recetor, a capacidade de armazenamento e o múltiplo solar. Todas estas variáveis têm um impacto significativo sobre o custo da eletricidade (LEC) e a sua otimização pode criar valor para os investidores. Para condições de Faro (Algarve), a central solar seleccionada é uma configuração de 4 MWe com um múltiplo solar de 1,25, um armazenamento de 2 horas, uma DNI de projeto de 750 W/m^2 e um bloco de potência que gera vapor a 80 bar e 480 °C em condições nominais, resultando num LEC de 0,234 €/kWh e um investimento (CAPEX) de 22,3 milhões de euros (CRS#3). Este LEC é significativamente menor do que a tarifa definida pela legislação nacional (0,273 €/kWh) e pode ainda ser reduzido para 0,232 €/kWh, se o limite de fluxo solar de recetor for aumentado (CRS#11 ou CRS#12). O capital investido tem uma taxa interna de retorno (TIR) de 9,8 %, com um período de retorno do investimento de 14 anos, e um valor atual líquido (VAL) de 7,9 milhões de euros (considerando uma inflação média anual de 4 %). No caso da inflação média anual ser inferior (2 %), o investimento na central solar pode ser mais vantajoso, com um VAL próximo dos 13 milhões de euros e um retorno do investimento em 13 anos.

O projeto de construção de uma CRS é viável (para o caso Português), mas depende das tarifas de venda de eletricidade bonificadas. Acresce que as centrais de CSP, na maioria dos casos, apresentam fatores de capacidade bastante baixos e problemas nos transientes solares, devido à alta inércia. Por outro lado, com as tarifas de biomassa existentes, a viabilidade de centrais termoelétricas de biomassa está em risco. A hibridização pode ajudar a resolver esses problemas, e se feito com a integração de resíduos de biomassa florestal, o

"objetivo renovável", pode ser mantido. Se geridas de uma forma sustentável, as centrais híbridas podem também ter um impacto positivo na redução dos incêndios florestais e abrir novos mercados para o CSP.

A integração de biomassa no circuito de vapor e de ar da CRS foi estudada no âmbito do projeto SOLMASS. A integração de biomassa no ciclo de vapor é mais favorável para a central híbrida de biomassa (FRB4#CRS#12). Esta solução híbrida reduz a energia desperdiçada e os períodos de arranque e paragem, reduzindo o LEC para 0,146 €/kWh. O LEC da central híbrida FRB4#CRS#12 é 0,086 €/kWh inferior à central solar CRS#12 e tem um aumento de 0,041 €/kWh quando comparado com uma central de biomassa (FRB4), reduzindo o consumo de biomassa em 7500 toneladas anuais. Considerando as tarifas nacionais atuais, a central híbrida FRB4#CRS#12 apresenta uma TIR de 6,6% em comparação com 9,7% de uma central solar CRS#12 e 7,4% da central de biomassa FRB4.

A integração da biomassa no ciclo de ar de uma CRS pode ser feita considerando-se um amplo espectro de tecnologias: gaseificação de *pellets* ou resíduos de madeira, gaseificação de RDF, biogás gerado a partir de um digestor anaeróbico de águas residuais, biogás de aterro e gás natural. A solução com menor LEC foi obtida para a hibridização da CRS de 4 MWe com biogás de um digestor anaeróbico, utilizando lamas de uma estação de tratamento de águas residuais (LEC de 0,15 €/kWh). Esta central tem retorno do investimento em 13 anos (assumindo coleta e transporte de lamas sem custo) com o melhor VAL (15 milhões de euros) e TIR de todas as opções híbridas. Outra configuração interessante é a central híbrida CRS/gasificação de resíduos de madeira (WG#CRS#3), com um LEC de 0,17 €/kWh, tornando esta tecnologia de gasificação viável para Portugal, o que não acontecia no caso base.

A energia solar concentrada (CSP) tem provado ser válida não só para a geração de eletricidade, mas para gerar combustíveis e produtos químicos a partir de fontes renováveis como a água, biomassa e sol. A revolução tecnológica na produção de hidrogénio e eletricidade é importante para apoiar as necessidades futuras e levar o mundo em direção a um futuro mais sustentável. Para isso, vários projetos em curso são apresentados e comparados. Embora falte ainda tomar medidas para resolver as limitações atuais e aumentar a viabilidade técnica e económica dos projetos, há condições para começar essa revolução e criar pontes das atuais tecnologias fósseis para as tecnologias renováveis.

Figure captions

This page was intentionally left blank

Table captions

Acronyms and abbreviations

BIPV – building integrated PV;

CAPEX – capital expenditure;

CHP – combined heat and power;

CPC – compound parabolic concentrator;

CRS – central receiver system;

CS – control strategy;

CSP – concentrated solar power;

DC – direct costs;

DE – dish/Stirling engine;

DNI – direct normal irradiance;

DLR – Deutsches Zentrum für Luft- und Raumfahrt (German Aerospace Centre)

DP – Design point;

DSC – dye-sensitized solar cells;

EBSILON – Ebsilon Professional software;

ECOSTAR – European concentrated solar thermal road-mapping;

EPC – engineering, procurement and construction;

ES – energy stored;

EU – European Union;

FEUP – University of Porto-Faculty of Engineering;

FICFB – fast internal circulating fluidised bed;

GREENIUS – the green energy system analysis tool;

HFLCAL – Heliostat Field Layout CALculation;

HP – high pressure;

HRSG – heat recovery steam generator;

HVAC – heating, ventilation, and air conditioning;

HTF – heat transfer fluid;

IC – indirect costs;

IRR – internal rate of return;

KAM – Kraftanlagen München GmbH;

LEC – levelized electricity cost;

LF– linear Fresnel;

LP – low pressure;

MENA – Middle East and North Africa;

MSW – Municipal solid waste;

NCV – net calorific value;

NPV – net present value;

NREL – National renewal energies laboratory form U.S. Department of Energy;

ODP – ozone depletion potential;

O&M – operation and maintenance;

ORC – organic Rankine cycle;

PB – power block;

PIP – network integration request call;

PV – photovoltaic systems;

PT – parabolic trough;

REN – Portuguese electricity network, managed by the company REN (Rede Eléctrica Nacional)

RDF – refuse-derived fuel;

RH – re-heater;

SAM – solar advisor model;

SM – solar multiple;

SL – Stoppage loss;

ST – solar thermal;

TES – thermal energy storage;

UPorto – University of Porto;

WWTP – wastewater treatment plant;

Codes

CRS#_SM#_#S_CS# – central receiver power plant (# option) with (# multiple) of solar multiple, (# equivalent hours) of storage capacity and applying control strategy (# CS);

Currency exchange rates and Units

USD/EUR= 0.75;

GBP/EUR=1.15;

SEK/EUR= 0.11;

kWe – kilowatt electrical;

kWth – kilowatt thermal;

MWe – Megawatt electrical;

MWth – Megawatt thermal;

Variables

α – escalation factor;

$C_{E,W}$ – cost of the reference equipment at reference size or capacity;

$C_{E,Y}$ – cost of equipment at the required size or capacity;

C_{rf} – insurance and debt interest coefficient rate;

E_{gross} – gross generated electricity;

E_{net} – net generated electricity;

K_{fuel} – annual fuel costs;

$K_{\text{O\&M}}$– annual operation and maintenance costs;

P_intercept – Receiver intercept power;

P_in_th_Biomass – Biomass thermal energy to power block;

P_in_th_Total – Total thermal energy input to power block;

P_gross – gross generated electricity;

P_net – net generated electricity;

Pth_receiver – Receiver thermal energy to power block;

Pth_storage – Storage thermal energy to power block;

$Q_{intercept}$ – receiver intercept power;

$Q_{dumping}$ – power dumping;

Q_{PB} – power input to power block;

$Q_{receiver}$ – receiver output power;

$Q_{storage}$ – power to/from storage;

Q_{DNI} – power intercepted by the solar field;

Q_{Int} – receiver intercept power;

Q_D – power dumping;

Q_{PB} – power input to power block;

Q_{Rec} – receiver output power;

Q_S – power to/from storage;

S_{max} – storage maximum;

X_W – size or capacity of the reference equipment;

X_Y – size or capacity of the required equipment;

X_W – size or capacity of the reference equipment;

Chapter 1

Introduction

This page was intentionally left blank

1. Introduction

Worldwide concerns about safe energy and energy independence are driving many countries to use renewable energy sources such as solar energy and namely concentrated solar power (CSP) for large scale for electricity generation. Algarve region in Portugal is a premium European location for CSP power plants. In addition to excellent solar resources, Algarve has also significant biomass resources. In this perspective, Portuguese authorities published recently calls for network integration (PIP) of electricity generated by CSP and biomass. These initiatives are part of the 2020 national strategic plan for renewable energies, where Portugal assumed to produce 31 % of the annual energy consumption from renewable sources and to reduce CO_2 emissions to meet the environmental 2020 goals.

SOLMASS project won the CSP-PIP call for a CRS. Based on this project, innovative models were developed and run for central receiver system (CRS) design, simulation and optimization. These models are described in the next chapters, and the main advantages and drawbacks of CSP discussed. To overcome some of the limitations of CSP it was proposed the hybridization of CSP and biomass for electricity and chemicals/fuels generation. Hybrid CRS/ biomass power plants are pioneer options, which minimize both technologies drawbacks and gather the main advantages of CSP and biomass. The following chapters present the results of these hybrid power plants, comparing the performance and economic indicators with the solar-only and biomass-only power plants.

1.1 Concentrated solar power (CSP) and Biomass outlook

Portugal has several important renewable resources: solar, geothermal, hydropower, biomass, wind, wave and tidal. Several studies estimate the renewable electricity generation based on the technical potential (which could be used for power generation in the present technological state of the art) and economic potential , for several countries in the region of southern Europe (including Portugal) and the Middle East / North Africa (MENA region) [1].

In the case of Portugal, the largest economic and technical potential is attributed to concentrated solar power (CSP). The CSP technical potential for Portugal is equal to 436 TWh/year and the economic potential to 142 TWh/year, which is sufficient to support twice the current national electricity consumption [1, 2]. The biomass economic potential is the second largest compared to all other technologies, with about 27 TWh/year.

In terms of project implementation, the scenario changes in the case of Portugal. It is anticipated that the technology with the greatest economic implementation potential in 2050 has the lowest rate of execution, with about 7%, which would give a total electricity generated by CSP of about 10 TWh/year, about the same value that is expected to be produced based on biomass [1].

1.2 Concentrated solar power (CSP)

CSP is already described by the Greeks back to 213-221 BC as a mean for firing enemy wood made ships. However, CSP technologies for commercial deployment began only in the 1980s. Currently, there is a significant investment on CSP in the Mediterranean region, led by countries such as Spain, Algeria, Morocco, Israel and UAE, who are currently building large scale CSP power plants, with different technologies [3]. Also, in the USA, mainly in California and Nevada, several power plants have been recently inaugurated.

There are four main CSP systems for electricity generation: central receiver systems, parabolic trough, dish/Stirling engine, and linear Fresnel. Although with minor expression, other solar concentrating systems can also be found, such as the solar furnace (used for chemical applications). These systems are illustrated in Figure 1.1.

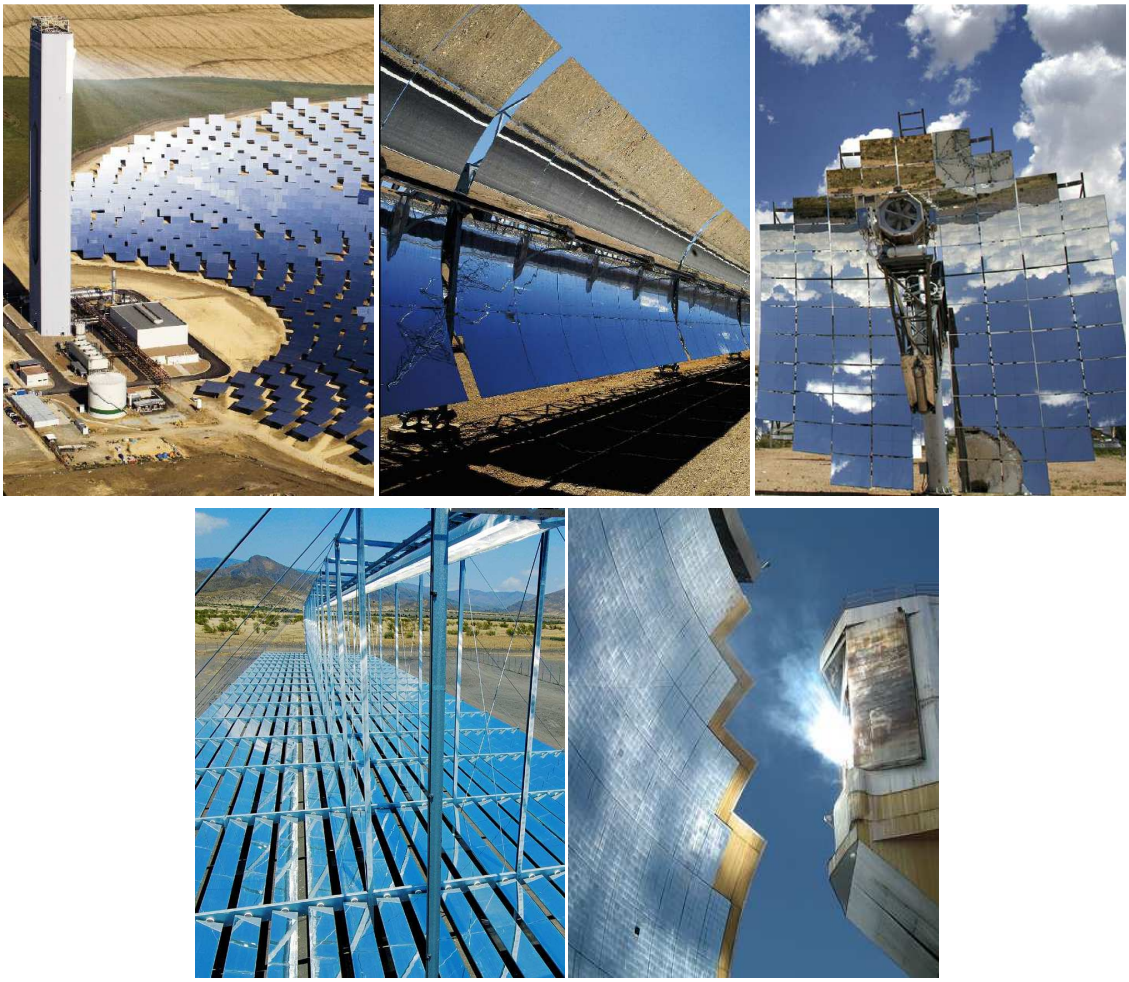

Figure 1.1: Central receiver system (CRS – up left), parabolic trough (PT – up centre), dish/Stirling engine (DE – up right), linear Fresnel (LF – down left), Solar furnace (SF – down right).

The parabolic trough, linear Fresnel and central receiver systems can be coupled to steam cycles up to 200 MW of electrical capacity, with thermal cycle efficiencies around 30-40%. On the other hand, the dish/Stirling engines are typically used for decentralised electricity generation, in the range 10 - 20 kW [1].

1.2.1 Why CRS?

From all the commercial solar concentration technologies the most mature is the parabolic trough. Despite that, in recent years, the technology with more R&D attention has been the central receiver technology, mainly because it can reach very high temperatures (over 1000 °C). New prototypes are capable of producing hot air for the gas turbine operation, which can be used in combined cycles, generating higher conversion efficiency, and approximating these power plants to commercial natural gas power plants, with power efficiencies above 50%, as shown in Table 1.1 [1].

Table 1.1: Performance of several CSP technologies [1].

Technology	Installed Power (MW)	Solar concentration	Max. Sun-electricity efficiency	Annual efficiency	Power block efficiency	Capacity factor	Land Use (m^2MWh^{-1} $year^{-1}$)
CRS	10 - 150	300 - 1000	20 % (d) 35 % (p)	8-10 % (d) 15-25 % (p)	30-40 % (ST) 45-55 % (CC)	25-90 % (p)	8 - 12
PT	10 - 200	70 - 80	21 % (d)	10-15 % (d) 17-18 % (p)	30-40 % (ST)	24 % (d) 25-90 % (p)	6 - 8
DE	0.01 - 0.4	1000 - 3000	29 % (d)	16-18 % (d) 18-23 % (p)	30-40 % (EN) 20-30 % (GT)	25 % (p)	8 - 12
LF	10 - 200	25 - 100	20 % (p)	9-11 % (p)	30-40 % (ST)	25-90 % (p)	4 - 6

(d) = demonstrated, (p) = projected, ST – steam turbine, GT – gas turbine, CC – combined cycle, EN – Stirling engine. Solar efficiency = net electricity generated / solar field incident irradiation. Capacity factor = Solar hours or power plant operating hours / 8 760 hours per year.

The most promising present solution in terms of efficiency is the CRS. Also, the solar energy can be concentrated into a selected focal point, which opens the application of CSP for a great number of applications, e.g. electricity or chemicals generation.

1.2.2 Central receiver system (CRS) technologies

CRS technology began its pioneering solar concentration existence with various projects between 0.5-10 MW in the early 1980s. Among these projects are:

• The Eurelios solar plant (1980-1984) that was built by an Italian/French/German consortium funded by the Commission of the European Communities, in Adrano, Sicily. With an installed power of 750 kWe and molten salts storage, it used a water/steam cycle, reaching peak temperatures of 512 °C. The power plant had an estimated cost of 8.2 million U.S. dollars (Figure 1.2) [4, 5 and 6];

• The IEA-CRS (1981-1985) and CESA-1 (1983-1984) solar power plants were built with the support of the European Community in Almeria, Spain. The IEA-CRS power plant had an installed capacity of 500 kWe and used sodium for storage and operating fluid, reaching temperatures of 560 °C. The power plant had an estimated cost of 18 million U.S. dollars and worked with a peak solar to electricity efficiency of 8.1% (Figure 1.2) [4, 5 and 6];

• The Sunshine solar power plant (1981-1984) was built by the Japanese government, in Nio, Japan. It had an installed capacity of 800 kWe and used steam as working fluid and storage medium, reaching temperatures of 249 °C. The power plant had an estimated cost of 25 million U.S. dollars and worked with a solar to electricity efficiency of 9.2% [4, 5 and 6];

• The Solar One (1981-1986) and Solar Two (1995-1999) solar power plants were built by the North American Department of Energy, in the Mojave Desert, California. Solar One had an installed power of 11.7 MWe and used oil at 302 °C as working fluid and storage, operating the power block with steam and reaching temperatures of 510 °C. The power plant had an estimated cost of 141 million U.S. dollars and worked with annual average solar to electricity efficiency of 5.8% and a peak efficiency of 8.7%. This plant was demolished in 2009 (Figure 1.2) [4, 5 and 6];

• The Themis solar power plant (1983-1986) was built by EDF, in the region of Cerdanya, in the Pyrénées-Orientales, France. It has an installed capacity of 2.3 MWe and uses molten salts as working fluid and storage (in two tanks). The power plant had an estimated cost of 37 million U.S. dollars and worked with annual average solar to electricity efficiency of 17% (Figure 1.2) [4, 5 and 6];

• The C3C-5 solar power plant (1985 -1988) was built by the Soviet Union government, in Crimea, now part of Ukraine. It had an installed power of 5 MWe and used steam as operating fluid and storage, reaching temperatures of 256 °C [4, 5 and 6].

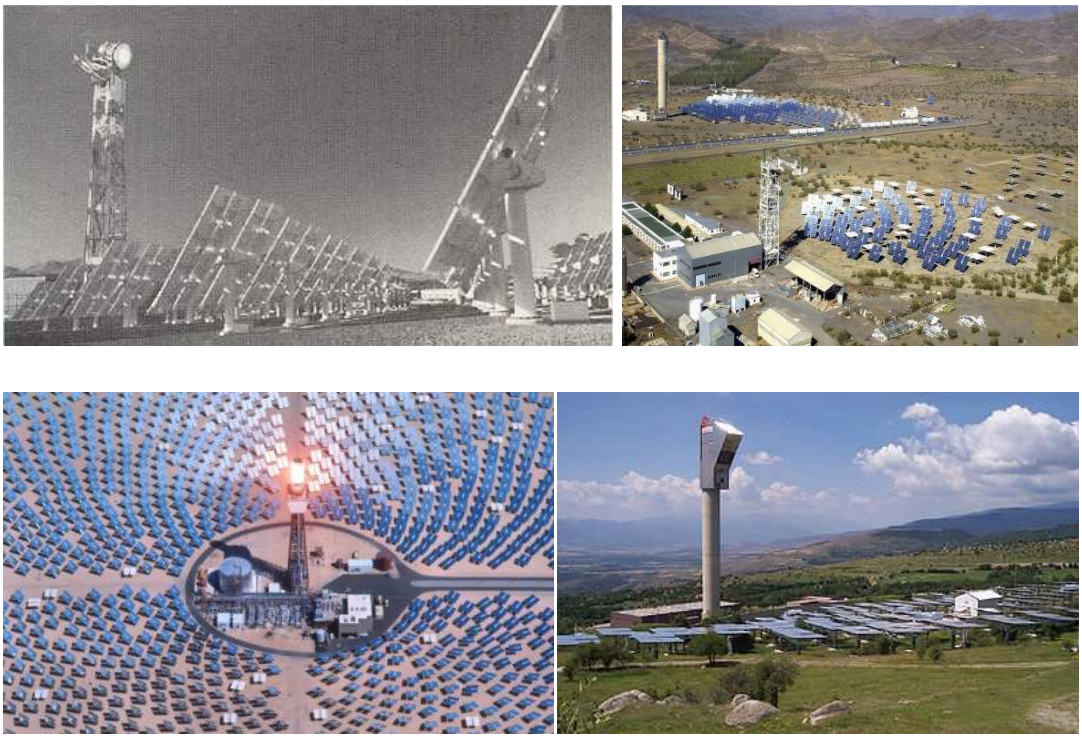

Figure 1.2: CRS pioneer projects: Eurelios (up left), IEA-CRS e CESA-1 (up right); Solar One (up left); Themis (up right) [9, 10 and 11].

All of these different solar towers or central receiver systems may be described in terms of the following components:

• Solar field, consisting of a number of mirrors with two axis solar tracking and optimally distributed through the field - heliostats;

• Solar receiver, where the flow of concentrated solar radiation is absorbed;

• The heat transfer system, where a heat transfer fluid (HTF) is used to carry thermal energy from the receiver to the turbine circuit;

• Thermal energy storage (TES) system, which ensures the dispatchability of the system during periods of low radiation and allows adapting power to the demand curves;

• Backup of fossil fuels/renewable resources for hybrid systems;

• Power block, e.g. steam generator, turbine and electric generator;

Figure 1.3 represents a simplified schematic for a solar tower/CRS solar concentration power plant.

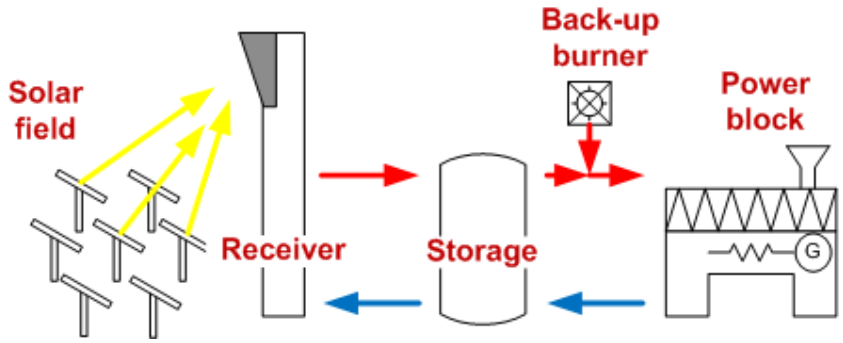

Figure 1.3: CRS power plant scheme.

Many of the pioneering central receiver systems (Figure 1.2) no longer operate, and are now disabled or have been demolished. During their lifecycle many setbacks were registered in key components, such as heliostats and solar receiver. The subsequent improvement of all essential components, in many international projects during the last 30 years, resulted in an significant growth of CRS power plants in recent years and a diversification of the technologies, namely with the use of different heat transfer fluids.

Today, the CRS commercial projects with more success, are the *"Plantas Solares"* PS10 (2007) and PS20 (2009), built by the Abengoa group in Sanlúcar la Mayor, Seville. The PS10 has an installed power of 11 MWe using saturated steam as heat transfer fluid and steam pressure storage (1 hour range), reaching temperatures of 250-300 °C. The estimated construction cost was 45 million U.S. dollars (Figure 1.4) [7, 8];

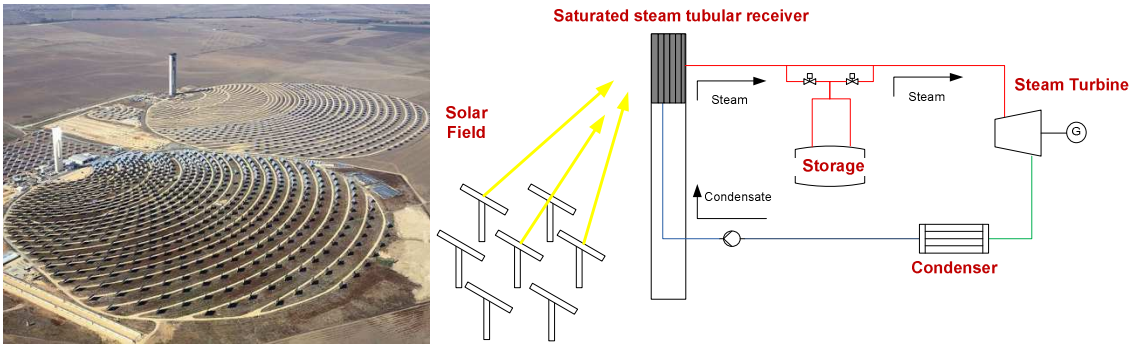

Figure 1.4: PS10 e PS20 (left) [7] and power plant scheme (right).

Following this project, several companies have announced power plants of large dimension and using steam at much higher temperatures, such as Ivanpah Solar Electric Generating Station (2013), built by the company BrightSource Energy, Primm, California. BrightSource planned to build several plants in California, totalling 370 MWe, with superheated steam as heat transfer fluid, reaching temperatures around 565 °C, nearly twice the steam temperature used by Abengoa's PS10 and PS20 (saturated steam). The company recently acquired loan guarantees from the USA Department of Energy estimated in 1375 million U.S. dollars (Figure 1.5) [9];

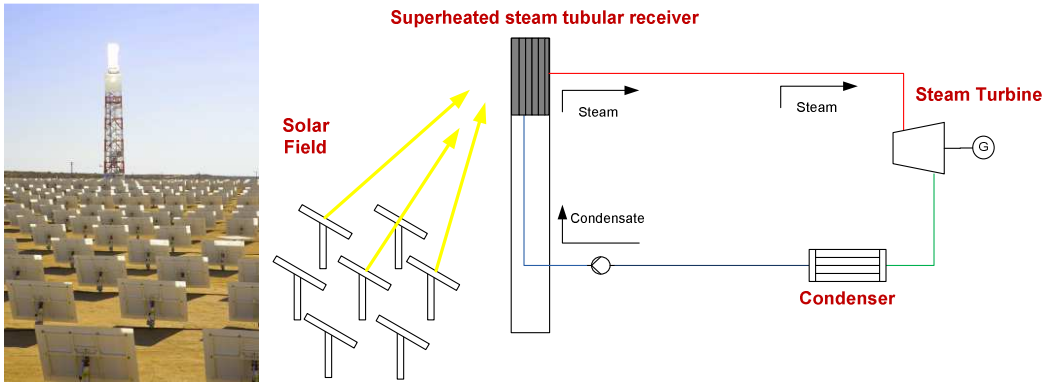

Figure 1.5: BrightSource CRS (left) [9] and power plant scheme (right).

A different approach was used by the company e-solar, also using saturated steam technology, in the Suntower Sierra (2009) project, at Lancaster – California. The 5 MWe power plant reaches temperatures of 440 ° C using a multi-tower/receiver concept with heliostats of small dimensions. The company hails costs competitive with conventional fossil fuel technologies, but did not disclose the final costs associated with this project. The same company has announced two more projects (in progress): Alpine Suntower (2012, 92 MWe) and New Mexico Suntower (to be determined, 92 MWe) (Figure 1.6) [8, 10];

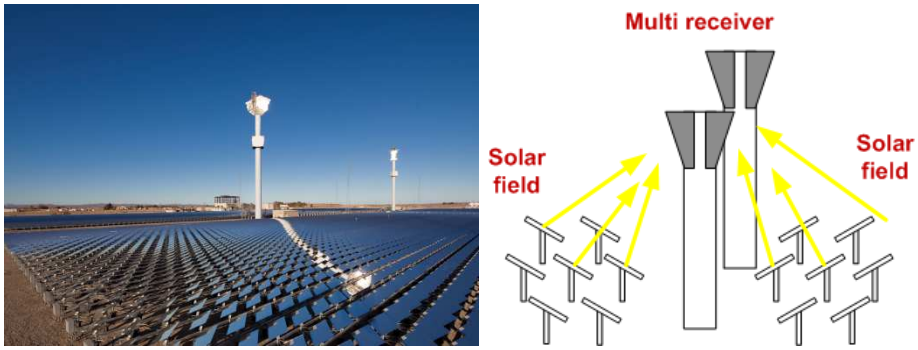

Figure 1.6: Sierra SunTower (left) [8] and power plant scheme (right).

An alternative CRS design is to use a secondary concentrator which concentrates the solar image into a receiver placed at ground level. These systems are called "beam down" and the two reference prototypes are the solar tower at the Weizmann Institute in Israel - 3 MWth and the 100 kW concentrator in the city of Masdar at Abu Dhabi, UAE (Figure 1.7) [11, 12];

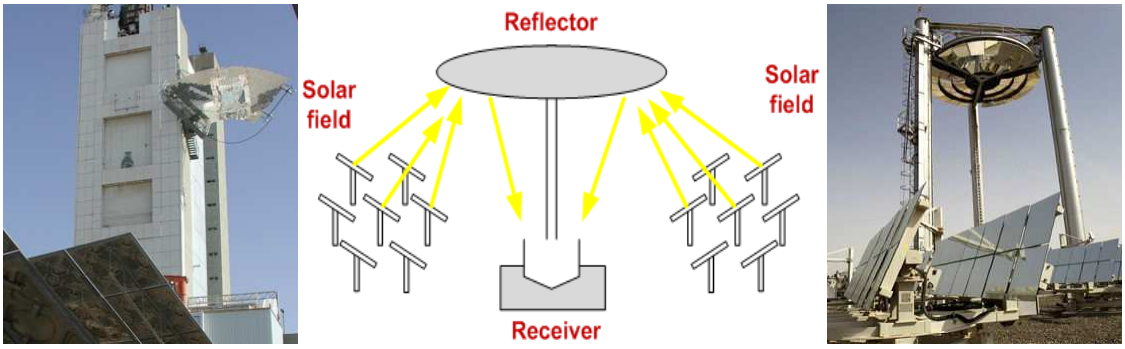

Figure 1.7: Solar tower of the Weizmann Institute (left), power plant scheme (centre) and the Masdar Institute concentrator (right).

A different heat transfer fluid used in power CRS are molten salts. The solar plant Gemasolar or solar three (2011), built by the group Sener in Fuentes de Andalucía (Seville) has an installed power of 17 MWe, two molten salt storage tanks (15 hour equivalent), and the heat transfer fluid reaches temperatures of 565 °C. This plant was built based on the experience gained from the design and operation of solar 1 and solar 2 power plants, in California. The Spanish group Sener announced an estimated funding of 309 million U.S. dollars for the construction and commissioning of the plant (Figure 1.8) [13];

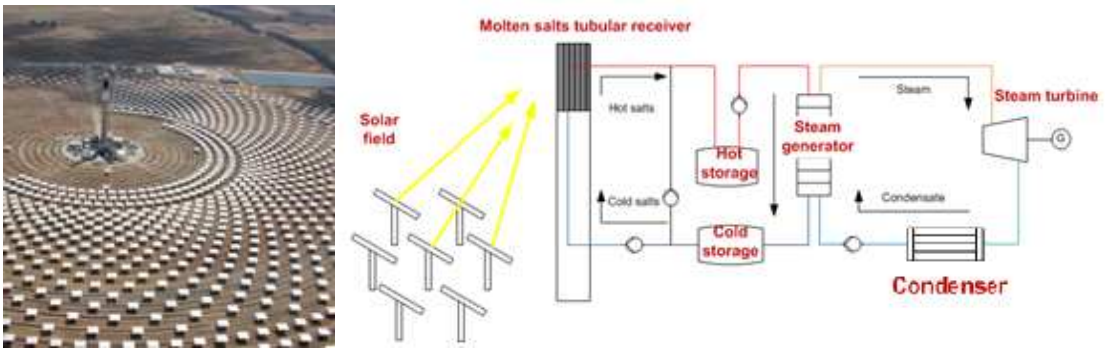

Figure 1.8: Gemasolar power plant (left) [13] and scheme (right).

The company United Technologies Corp. - Pratt Whitney Power Systems, recently inaugurated two large projects using a molten salt as heat transfer fluid: the project Crescent Dunes Solar Energy Project (2013, 100 MWe), built for Tonopah Solar Energy, LLC, in Tonopah,

California; and the Rice Solar Energy Project (2013, 150 MWe), built for the Rice Solar Energy in Rice, California [10, 14].

The current largest commercial power plants use steam or molten salts as heat transfer fluids. A different concept is to use air (atmospheric and pressurized) as heat transfer fluid. Various prototypes and pre-commercial plants were already built. The atmospheric air technology current reference is the Jülich solar tower (2009), designed by DLR and the company KAM in Jülich, Germany. It has an installed capacity of 1.5 MWe, with a ceramic storage and atmospheric air as working fluid, reaching temperatures of 700 °C. The estimated cost of construction was approximately 32 million U.S. dollars (Figure 1.9) [15];

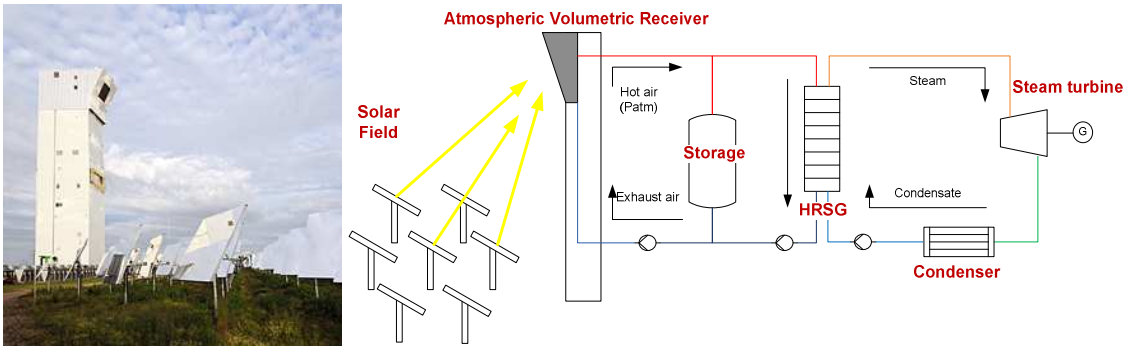

Figure 1.9: Jülich solar tower (left) [15] and power plant scheme (right).

An alternative concept to the use of air as heat transfer fluid, is by "closing" the volumetric receiver, pressurizing the air and reaching higher temperatures, which enable the use of a more efficient combined cycle (Brayton-Rankine). The project with the highest relevance in this technology was the project SOLGATE, held in 2001 at the Plataforma Solar Almeria, which built and tested a full hybrid system with an installed power of about 250 kWe, Figure 1.10 [11].

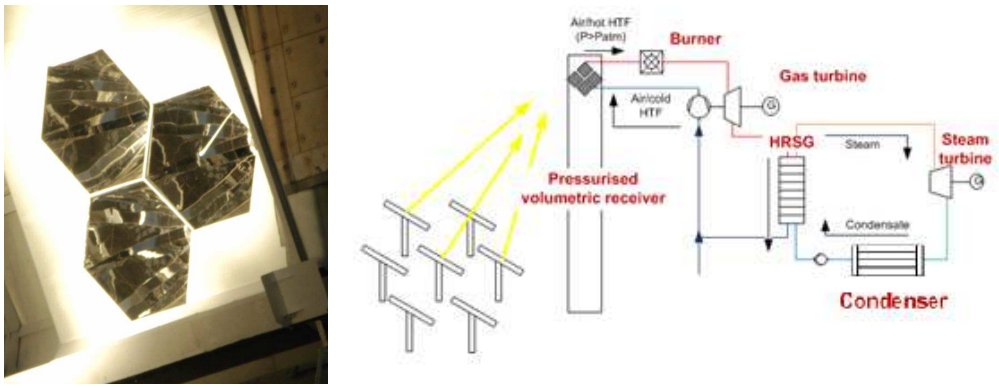

Figure 1.10: SOLGATE project volumetric pressurised air receiver (left) [16] and possible configuration for power plant integration (right).

There are still many other concepts and technologies for a CRS. One of the concepts with high interest for investigation and development is the use of particles (e.g., graphite) to absorb solar radiation and use downstream heat exchangers to feed a thermal cycle (e.g. with air - Brayton cycle). The particles are also used as high temperature heat storage medium. The air under pressure can reach temperatures of about 995 °C [17]. This concept is still in the research stage and there are no commercial or pre-commercial power plants using this technology, Figure 1.11.

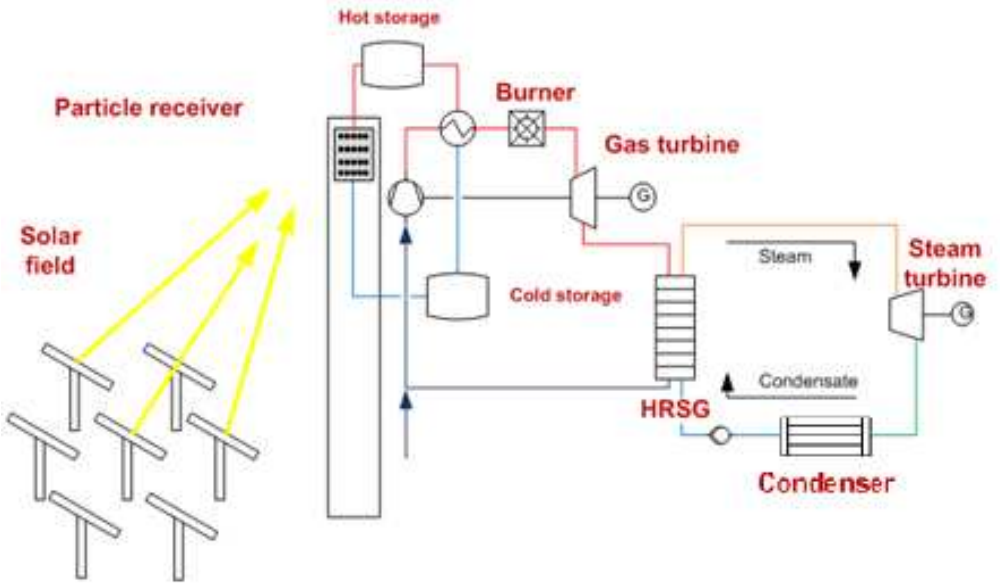

Figure 1.11: Scheme of a particle CRS [17].

1.2.3 CRS components

1.2.3.1 Solar field

The CRS solar field is composed by a set of concave mirrors, which follow the sun trajectory in two axes during the day, focusing and concentrating its direct normal irradiance (DNI) at a position set by the operator. The positioning and distribution of the heliostats in the solar field is dependent on the power plant location and the type of receiver used. There are three types of solar fields: only north of the solar tower (typically in positions in the northern hemisphere); only south of the solar tower (typically in positions in the southern hemisphere); and surrounding solar fields (typically in equatorial positions). The field type also depends on the size of the plant.

The reflective surface of the heliostats is formed, in most commercial heliostats, by facets of thin mirror, with low iron content to improve reflectivity. There are a large number of different heliostat concepts: varying the geometry, dimensions, number of mirrored surfaces and mechanism of action. Figure 1.12 shows two types of different heliostats: large area - Sanlucar 120 heliostat (121 m^2), and small modular area - eSolar heliostat (1.14 m^2) [7, 10].

Figure 1.12: Abengoa PS 10 - Sanlucar 120 heliostat (left) and Esolar heliostat (right) [7, 10].

The heliostat concepts presented in Figure 1.12 are two extreme approaches to the optimization of a solar field. In the 11 MWe PS10 power plant at Sanlucar la Mayor, Spain, there is a north solar field with 624 heliostats of 121 m^2 each - total mirror area of 75 716 m^2 [7]. A different perspective was used by eSolar, with a 100 times lower area but high-precision heliostats. This approach seeks to facilitate the process of heliostat manufacture (is not using an optimized layout for each site but is planning to use the same for all sites) and assembly (do not require deep foundations), but usually requires a multi towers and/or receivers concept to obtain similar power. eSolar prototype power plant has a field with 24 360 heliostats of 1.14 m^2 each - total mirror area of 27 670 m^2, but requires two receivers to achieve 5 MWe nominal power in Lancaster, USA [10].

1.2.3.2 Solar receiver

In a CRS, the solar receiver is mounted on the top of a tower and its surface receives the concentrated solar irradiance from the solar field of heliostats, with solar concentration factors between 200-1000 suns. A CRS operates at high solar flux (between 300 and 1000 kWm^{-2}), which allows operation at very high temperatures (up to 1000 ° C) and the use of more efficient thermal cycles [18]. While in a heliostat, for instance, if there is a fault, the power plant performance just suffers a small drop, if there is any problem in the receiver, the entire power plant is stopped until resolution. The solar receiver is therefore one of the most important parts of a CRS power plant [19].

Nowadays, there are different types of solar receivers, varying the geometry, concept and heat transfer fluid used [19]. They are an essential part for the power plant definition, either influencing the receiver upstream (solar field) and downstream (storage and power block). The following sub-chapters present the different types of the state-of-the-art receivers.

Tubular receiver

The most common receiver concept commercially used is the tubular receiver. In these receivers the irradiance is concentrated on tubes (coated with a selective absorbing material), and transferred into the working fluid through the tube's wall (metal or ceramics). Various working fluids have been used in tubular receivers: water/steam, sodium and molten salts, for temperature ranges up to 500 to 600 °C. There is less information available on the use of tubular receivers with gas, although it is possible to obtain temperatures around 800-900 °C [18]. The tubular receivers were extensively tested mainly in France (Themis) and Spain (IEA - CRS and CESA-1) with multiple heat transfer fluids.

PS10 and PS20 power plants used cavity tubular receivers; in the case of PS10, Figure 1.13, the receiver is mounted on the top of a 115 m tower and is composed by a cavity with four receiver tube panels, 12 meters high and 5.5 m wide [20]. At design conditions, the receiver is capable of delivering 50 MWth of saturated steam at 257 °C and 40 bar pressure, with efficiencies above 92%, Figure 1.13 [20].

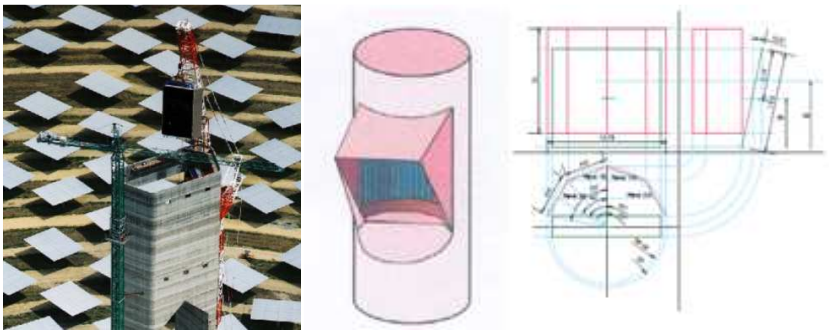

Figure 1.13: PS10 receiver (left) and scheme (right) [20].

Although a cavity can be used to reduce thermal losses, as in the case of PS10, it adds restrictions to the solar field (only north or south fields). The alternative is an external receiver, e.g. a cylindrical tubular receiver that can be used in combination with a surrounding solar field. This concept was used in Solar One and Solar Two power plants, with superheated steam and molten salts, respectively. In Solar One, the 42 MWth receiver generated steam at a 516 °C and 100 bar, with efficiencies of 82%, Figure 1.14 [21].

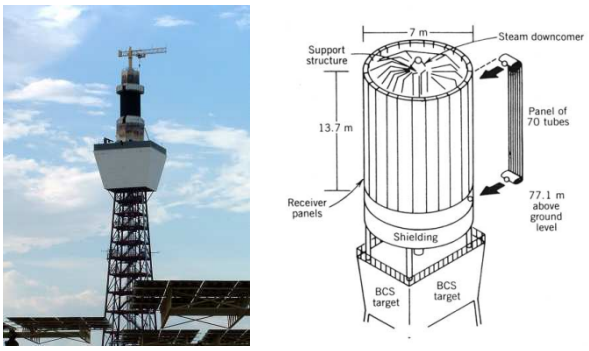

Figure 1.14: Solar One receiver (left) and scheme (right) [21].

However, Solar One had some operational problems; mainly with deformation of the receiver superheating section, [18] due to the transient nature of the DNI and poor heat transfer properties of the tubes. Solar Two used a molten salt as heat transfer fluid; the cold salt (290 °C) was pumped from a reservoir into the solar receiver where it was heated up to 565 °C. The receiver had a power of 42 MWth and was composed by 768 tubes (of 2 cm diameter) in a cylinder of 6.2 m diameter and 5.1 m height. It reached efficiencies of 88 % and peak solar fluxes of 800 kW/m^2, with average solar fluxes of 400kW/m^2. The use of molten salts provides a number of benefits, as the absence of phase change and the ability to heat up to 565 °C. However, the salts have a high solidification point (about 220 °C), which brings complex problems of solidification, especially during solar transients and stop periods, affecting the receiver, storage tanks, piping and valves [20]. Solar two had some problems with the design and application of measurement equipment and heating resistances. Moreover, the parasitic energy costs were significant. However, solutions have been developed to correct the known errors and, in 2011, the Sener group in Spain inaugurated the central Gemasolar or Solar three, which is the first fully commercial power plant of its kind [22].

Volumetric receiver

A different concept of receiver is the volumetric receiver, currently, with two available alternatives: the atmospheric volumetric receiver or the pressurized volumetric receiver. It is also common to use the terms open and closed volumetric receiver, respectively.

In the case of the atmospheric volumetric receiver, the working fluid used is atmospheric air. The selection of air has intrinsic advantages, such as its availability from the environment, being environmentally-friendly, having no phase change, ability to achieve high working temperatures, ease of operation and low maintenance. In the early development of CRS technologies, and after operating problems identified in the production of superheated

steam in tubular receivers for Solar One, CESA-1 or Eurelios power plants, various CRS designs changed to air volumetric receivers, which conferred an impulse to this technology. One of the first proposals for volumetric receiver was presented in the Phoebus project, using a receiver of metal wire mesh to heat atmospheric air to temperatures of 700 °C, used to produce steam at 480-540 °C and 35-140 bar in a heat recovery steam generator (HRSG) with superheater, reheater, evaporator and economizer [18]. The system incorporated a ceramic thermal storage, capable of storing heat for several hours and work under loading and unloading cycles, by reversing the air flow with two axial fans. However, there are some limitations to the storage capacity in this type of power plants (between 3 and 6 h) [20], and if higher annual capacity factors are required hybrid solutions must be considered.

The PS10 power plant initial design used a receiver based on the Phoebus concept, coupled with its 10 MWe commercial power block. The receiver inlet temperature was 110 °C and reached 680 °C at the output. Due to the insulation of the air pipes, air speed could not exceed 33 m/s. The energy storage of hot air was made with alumina pellets and the steam generator produced a steam flow rate of 10.73 kg/s at a temperature of 460 °C and 65 bar. The turbine generated 11 MWe power (gross), with an efficiency of approximately 30% [20]. The projected atmospheric volumetric receiver thermal efficiency was modest when compared with the tubular receivers: 74% rated efficiency and 61.4% efficiency annual average. PS10 design was changed to saturated steam.

Currently, on this technology most of the benefits of using high heat transfer fluid temperatures are sacrificed by the receiver losses; nevertheless, it allows to generate superheated steam without some of the problems still present in tubular receivers [23]. A pre-commercial prototype of this technology is the solar power plant Jülich in Germany, Figure 1.15 [23, 24]. Jülich is an example that can bring important results for the development of efficient volumetric receivers.

Figure 1.15: Volumetric atmospheric receiver (left) and its cups (centre and right) [23, 24].

It is expected that the natural evolution of volumetric receivers will be the pressurization of the heat transfer fluid, leading volumetric receivers to greater efficiency, much higher temperatures and the possibility to use combined cycles. This concept can be applied to a wide range of power ratings (from 1 to 100 MWe); even for low power systems, gas turbines with heat exchangers may be used instead of the combined cycles. However, it is expected that this receiver has better performances in larger systems, coupled to combined cycle systems which can achieve efficiencies up to 70%, while traditional Rankine cycle systems may have peak efficiencies of 30 to 40%. Hybridization of the power plant with other fuels is also possible, because the receiver outlet temperature can be chosen with some ease, Figure 1.16 [16].

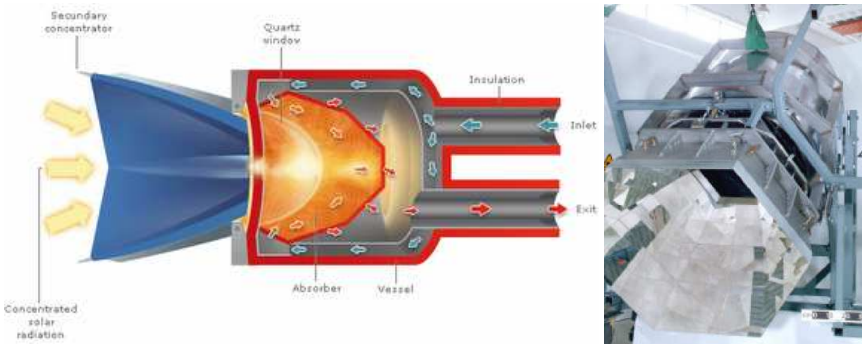

Figure 1.16: SOLGATE receiver (left) and high temperature module (right) [16].

State-of-the-art pressurized volumetric receivers are normally divided in three modules: low temperature, medium temperature and high temperature, to guarantee high thermal efficiency, low pressure drop, low manufacturing cost and high durability. Tubular receivers are used for the low temperature module, e.g. in the case of the SOLGATE design, 16 connected parallel tubes each with a length of 2.3 m and a diameter of 28 mm were used. The nominal temperature increase in this module is around 200 °C, with an associated pressure drop of 100 mbar. The maximum temperature on the tube surface is 950 °C and the exit air temperature is 550 °C [16].

The SOLGATE medium term module was equipped with a metal wire mesh absorber, designed for an air exit temperature of about 800 °C (average temperature module); while the high temperature module, with a quartz window and porous ceramic absorbent, had a air outlet temperature of 1000 °C. In the SOLGATE design all modules had secondary concentrators (aperture area of 1.28 m², hexagonal geometry and an acceptance angle of 21°).

The pressure drop for high and medium temperature volumetric receiver modules is 20 mbar. The overall thermal efficiency of the receiver was 77% at 800 °C and 70% at 950 °C [24].

The SOLGATE project defined an optimized system for three power plant configurations: 1.2 MWe (gas turbine with HRSG), 4 MWe (gas turbines with HRSG) and 16 MWe (Combined Cycle, CC), to be implemented in Seville, Spain, and Daggett, California [16]. The average LEC can be competitive with current fossil fuel power plants (€ 0.06/kWh – 16 MWe combined cycle, outlet receiver air temperature of 800 °C, solar fraction of 16%, operating 24 hours/day). For this case, the solar incremental LEC, which is the cost for the solar contribution, is about € 0.118/kWh [16].

1.2.3.3 Storage

Thermal energy storage (TES) can be divided into two groups: sensible heat storage systems and latent storage systems [24]. In sensible heat storage systems the storage device releases or absorbs energy from a fluid, changing the storage temperature and maintaining its physical state. When there is a phase change, from solid into a liquid, or from liquid into a gas, the heat released or stored is called heat of fusion (solid to liquid) or heat of vaporization (liquid to gas). Both are commonly referred as latent heat, and differ from sensible heat as there is no temperature change associated. Another perspective of heat storage is to use reversible chemical reactions which use heat for progressing in either direction. TES can also be classified considering the type and utilization. TES can be used for short-term operation, providing operational short-term stability, or medium/long term operation, increasing the power plant capacity factor and decoupling the electricity generation period from the solar collection period. TES types can also be divided into active direct storage (the HTF is the same as the TES fluid – does not require additional heat exchangers), active indirect storage (different HTFs using a heat exchanger) and passive storage (e.g. heating a solid material such as concrete or ceramics) [24]. All TES systems operate using three steps: charging, storing and discharging.

The type of thermal energy storage system used for a specific CSP power plant depends on the specifications of the heat transfer fluid, the definition of the required storage capacity (number of hours desired for the storage to support the power block at nominal conditions) and the power plant dispatch strategy. There is a strong ongoing R&D in this topic, since it is considered by many as the greatest advantage of CSP compared to other renewable systems; nowadays, five solutions emerge in terms of TES for CSP [20]:

• Storage using molten salts and ionic liquids;

• Storage using concrete modules;

• Storage using ceramics modules;

• Phase change materials (PCM) storage;

• Steam storage.

In the following sub-chapters these technologies are presented and discussed.

Storage using molten salts and ionic liquids

The state of the art of molten salt storage technology is two-tank storage. This solution was extensively tested in Solar Two power plant, in combination with a molten salt solar tubular receiver. There are different salts under study, but the combination that best fits the temperature range of operation of a Rankine cycle is a mixture of 60% sodium nitrate and 40% nitrate potassium. This was the chosen solution for the Gemasolar (Solar 3) solar plant.

The molten salt two-tank storage [25] was applied in the Gemasolar power plant, Figure 1.17, but was also used in parabolic trough systems as indirect storage. Andasol uses a heat exchanger to transfer heat from the oil to the salts. If molten salt were used as heat transfer medium, it may cause problems in the parabolic trough receiver tubes, because salts solidify at temperatures of 220 °C. Using oil directly as storage material might also be an alternative, however is not normally used because the vapour pressure of 12 bar and the high price.

Figure 1.17: Salts (left) and Andasol two-tank storage solution (right) [25].

The use of ionic liquids can bypass this drawback, since these materials are liquid even at low temperatures. Ionic liquids are organic salts with negligible vapour pressure at the relevant temperature range and melting temperature below 25 °C. The ionic liquids at ambient temperature are still materials with unknown results to CSP, and it is uncertain that they are

stable at the temperature level required for CSP systems, and also if they can be produced at a competitive cost [20].

Storage using concrete modules

The concept of storing sensible heat in concrete has been studied by Wespe and Wanda projects for parabolic trough systems. The projects studied two possible solutions: concrete with inner tubes and tubeless. Since the use of steel pipes within the storage material is very expensive (accounts for 45-55% of total storage cost), storage without tubes may result in reduced costs, however still requires extensive research [20].

Advanced loading/unloading modes can significantly increase storage capacity for a given size and material. The basic idea of modular storage is to increase the storage capacity by changing between the two modes of operation. Extensive simulations have shown that in those designs the ability of a given storage size can be increased by about 200% over the base case operation [26]. Storage in concrete is highly modular and is easy to apply loading and unloading, creating different temperature modules. However, the implementation of a concrete storage system is still risky for both cases (with or without tubing) and require further investigation before commercial application, Figure 1.18.

Figure 1.18: Concrete storage systems.

Storage using ceramics modules

The storage of sensible heat using solid materials (e.g. ceramics) is usually used in combination with atmospheric or pressurized volumetric receiver systems. In these high temperature systems, heat needs to be transferred to another carrier, which may be several types of solids, provided they have high heat capacity and density. The materials size and shape of the solids is also important, as an optimized size and shape would minimize pressure drop and increase heat transfer, thereby reducing energy consumption. Apart from solid storage materials, there are other emerging concepts such as the use of silica sand. The Jülich

power plant has a 10 MWth ceramics storage, which provides storage heat at 700 °C for 1 equivalent hour of the power plant consumption. The layout of these ceramic materials and their integration in the solar plant are shown in Figure 1.19 [33, 34].

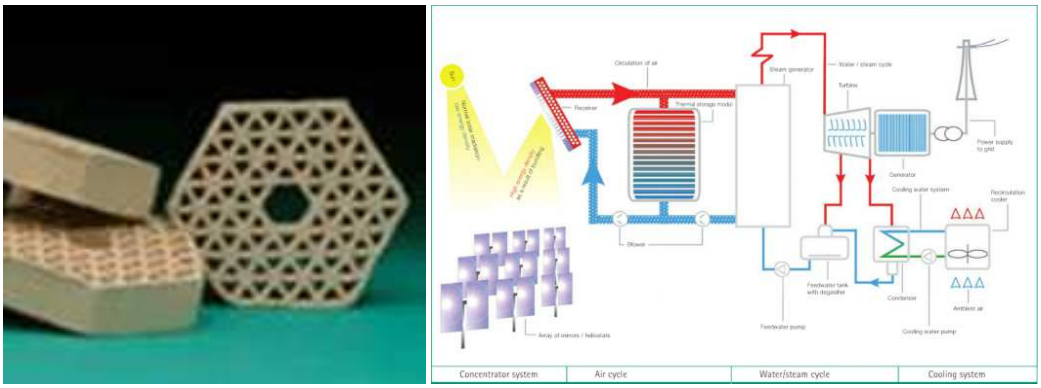

Figure 1.19: Ceramic modules (left) and integration into the Jülich CRS (right) [27, 28].

Another possibility of storage development for pressurized volumetric receivers are insulated storage containers resistant to pressure up to 16-20 bar (depending on the pressure ratio of the gas turbine) [20].

PCM storage

Phase change materials (PCM) can be the future for heat storage, which is particularly important in direct steam generation systems, since the temperature remains constant in the enthalpy range of phase change. PCM storage does not use exclusively solid-liquid transitions, but may also use solid-gas or liquid-gas transitions. However, solid-liquid transition is the most studied and applied. The two main R&D areas of PCM storage are [29]:

• Encapsulation of small amounts of PCM;

• Incorporation of PCM into a matrix made of another solid material with high heat conduction.

The first line of research aims to find a way to reduce the distances within the PCM, while the second line of research aims to increase the PCM heat conduction. The solid PCM is the limiting factor for heat transfer between the fluid and storage, once it agglomerates between the pipe and the PCM liquid phase. Developments in these areas will enable PCMs to overcome the early stages of development and move to the first prototypes in real-scale, after some initial laboratory experiments, Figure 1.20.

Figure 1.20: Interior (left) and exterior of a PCM storage module (right).

Steam storage

The steam drum, which is a common part in many steam generators, is a type of storage as it contains a quantity of boiling water under pressure. Steam could be produced from that component only by reducing the pressure. This type of storage is used many times as heat storage process for several industries. The main problem is scaling to larger capacities and the degradation of steam quality during unloading. This type of storage is ideal for short periods of time, in the range of several minutes, to compensate for the solar area shading in the case of rapid passage of small clouds. Such a system is used in PS10 in Seville, with a thermal capacity of 20 MWh of saturated steam (equivalent to 50 minutes of power block operation at 50 % load). The system is composed by four tanks that are operated in sequence as they are loaded. During operation of the plant at full load, and according to the strategy defined by the operator, the steam at 250 °C and 40 bar pressure, from the receiver, is used to charge the thermal storage system. When energy is needed, it is recovered from the storage tanks (Figure 1.21) to feed the turbine [7].

Figure 1.21: 4 steam tanks storage solution used at PS10 [7].

In the future, the use of encapsulated PCMs within the storage tanks, could improve the storage capacity, because the latent heat content can be used to reduce the falling of temperature and pressure, thus allowing larger heat capacity with the same storage tanks [20].

1.2.3.4 Power block

Thermal cycles

State-of-the-art CSP plant thermal cycles are based on the Rankine cycle, Figure 1.22 [30]; the water is pumped from a low pressure to a high pressure, with external power consumption. The pressurized water then enters a boiler/receiver (heat source) where it is heated at constant pressure until it becomes saturated/superheated steam. The saturated/superheated steam then expands through a turbine to generate work. With this expansion, both pressure and temperature are reduced. Finally, the steam enters a condenser where it is cooled to liquid condition. This water is then pumped and the cycle is repeated [30].

For a CRS, in the case of tubular steam receivers, the operation diagram is similar to Figure 1.22, because the receiver acts as a solar boiler and directly feeds the turbine. In the case of a molten salt tubular receiver, there is an intermediate step, the molten salt/ water-steam heat exchanger. This intermediate step is also applied in the volumetric receiver power plants that use a steam generator to recover heat from the hot atmospheric air and generate superheated steam to be fed to the turbine. Both molten salts and air technology have a decrease in efficiency due to this intermediate step, which is counterbalanced by better control.

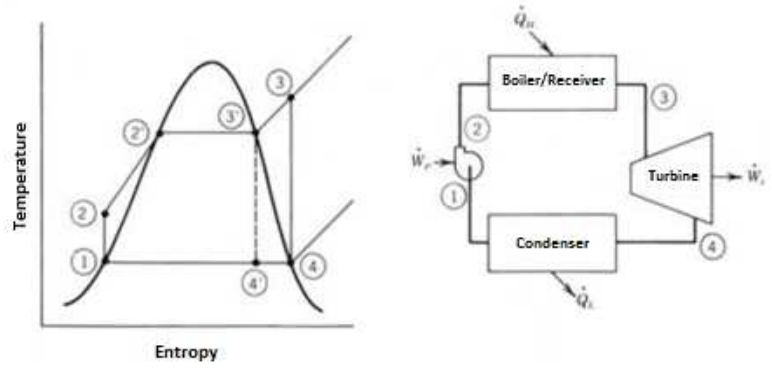

Figure 1.22: Rankine cycle (left) and its application to CRS (right) [30].

Commercially, the main power block companies have been developing series of turbines/generators specifically oriented towards CSP applications. This is the case of Siemens [31], Man Turbo [32] (Project Andasol 3) and General Electric [33] (Project PS10).

In the case of pressurized volumetric receivers it is possible to operate a gas turbine under the Brayton cycle, Figure 1.23 [30], reducing the impact of the very inefficient compression of hot gases. Currently, this solution was only tested in prototype scale, and a

large part of the power was obtained using a backup fossil fuel without recovering the gas turbine exhaust gases. Nevertheless, some pre-commercial power plants for this technology were already announced, as the case of the Themis power plant renovation [34].

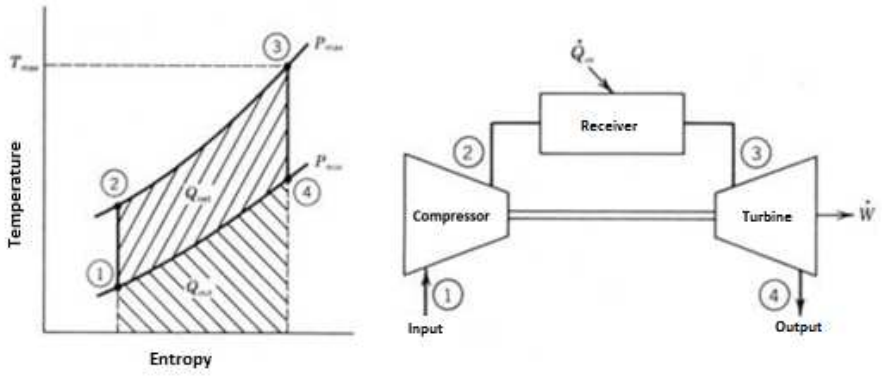

Figure 1.23: Brayton cycle (left) and application into CRS (right) [30].

The main advantage of the Brayton cycle is that the remaining energy is rejected from the combustion in the form of heat in the hot exhaust gases, but can be recovered by a HRSG to run a Rankine cycle in what is called a combined cycle. These combined cycles could be the future of CRS technology, increasing efficiency of the power plant. However, turbine resistance to high temperatures is an extremely critical point for the technology viability, as well as turbine poor adaptability to transient heat flow situations. These issues deserve further R&D towards a full implementation of combined cycles in CRS power generation.

Heat rejection

The CRS technology usually consider two heat rejection systems: water and air cooled condensers. The use of water condensers leads to higher system efficiency, but also large water consumption (a problem in most countries with good CSP resources). The use of air-cooled condensers usually requires an increase in electricity consumption, thus reducing the overall efficiency. It is also possible to use a hybrid scheme, with water and air cooling, but usually with an increase in the project cost, Table 1.22 [35].

Table 1.2: Heat rejection technologies and performance/cost impact [35].

Technology	Cooling	Capacity (dm^3/MWh)	Performance decrease*	Cost increase **
Coal / Nuclear	Once through	87000 to 102000		
	Recirculation	1700 to 2800		
	Air	200 to 250		
Natural gas	Recirculation	750		
CRS	Recirculation	1900 to 2800		
	Hybrid	350 to 950	1 to 3 %	5 %
	Air	350	1.3 %	
PT	Recirculation	3000		
	Hybrid	400 to 1750	1 to 4 %	8 %
	Air	300	4.5 to 5 %	2 to 9 %
DE	Washing	75		
LF	Recirculation	3800		

* Loss in the annual electricity generation in comparison with the most efficiency technology;

** Additional cost to the electricity generation.

Water cooling condensers were extensively used in the SEGS U.S. system, but consumed approximately 800-1000 litres of water per MWh generated; the Rankine cycle heat rejection system represents approximately 90 % of water consumption of the plant; and the other 10% of water consumption includes the water replacement in the steam cycle (8%) and water used for washing the solar field mirrors (2%) [36]. Commercial CRS power plants (Abengoa's PS10 and PS20, Sener's Gemasolar and e-solar's Sierra Suntower) all use water cooling condensers, Figure 1.24. The use of air cooled condensers can only be found on the Jülich Solar power plant and on BrightSource Ivanpah power plant [37]. The Crescent Dunes Solar Energy power plant will be the first CRS commercial project using a hybrid heat rejection mechanism [37].

Figure 1.24: Jülich power plant air cooled condensers (left) and hybrid condenser (right).

1.3 Why CRS hybridization?

Central receiver solar only power plants have some limitations, inherent to the solar irradiance characteristics: transient daily operation; unavailability of energy resource during the night; high capital investment per installed power; and difficulty in market entry. This restrictions lead to low capacity factors or over-dimensioned and expensive storage devices. Overall, and because of these issues, CSP and CRS have quite high levelized electricity costs. Hybridization can be a solution to these concentrating solar power shortcomings, providing energy for night operation or to support transient daily operation, increasing the power plant capacity factors and reducing market entry difficulties.

CRS hybridization can be done with different objectives: for electricity generation, for chemicals or fuels generation or even for fresh water generation. Several resources can be used for this hybridization, e.g. fossil fuels or renewable resources such as: biomass, geothermal, photovoltaic or wind. Each solution has a specific approach and current different R&D status. Hybridization with geothermal energy is possible but more restrict, since good CSP coincident with good geothermal spots around the world are limited, and are usually subjected to frequent earthquakes that are not good to CRS, because it affects the heliostat structure and misaligns the reflected irradiance. Fossil fuels and biomass are very interesting hybridization possibilities, as the electricity conversion cycles are similar to the CRS ones, and they can answer to the major limitations from CSP. Both solutions are studied in this thesis, with the main emphasis in biomass hybridization, so the “renewable goal” is maintained.

The hybridization makes sense also from the biomass perspective. As it will be presented in the following chapters, biomass only power plants shortcomings can be minimized in hybrid CRS/ biomass power plants.

1.3.1 Incentives in Portugal for CSP and biomass

There are no incentives for hybrid CSP biomass power plants in Portugal. The network integration (PIP) calls are specific either for CSP or biomass power plants. Nevertheless, the Portuguese feed-in tariff for renewable energy projects is calculated by a formula which can consider contributions from different resources.

Regarding CSP, a call was opened in Portugal for network integration (PIP) of CSP and concentration photovoltaic (CPV) power plants on September 2009, by the order no. 18838/2009, published on the national republic journal DR n.157, 2nd Series, from the 14th August 2009 [38]. 87 proposals were presented and 65 were accepted, but only 15 were selected. From these projects, 5 CPV projects were selected totalling 5 MW of installed capacity, Table 1. [38].

Table 1.3: PIP results for CPV power plants [38].

Promoter	Location	Power (MWe)	Technology
Reciclamas, SA	Tavira	1	SOLFOCUS
SAPEC – Química, SA	Sapec	1	MAGPOWER
Tecneira – Tecnologias Energéticas, SA	Alqueva	1	OPEL
LUZ.ON – Solar Energy, SA	LUZ.ON	1	CONCENTRIX + AMONIX
Glintt – Global Intelligent Technologies	Évora	1	EMCORE

The intention of national authorities with the PIP was to create a commercial demonstration platform for the main CSP technologies available, approving 4 projects with dish/Stirling engines, 2 projects with the parabolic trough technology, 2 projects with linear Fresnel technology and 2 projects with central receiver technology. The total installed power approved for dish/Stirling engines was 5.5 MWe while the other 6 projects total 24 MWe; divided into 6 power plants of 4 MWe installed power each, Table 1.4 [39].

Table 1.4: PIP results for CSP power plants [38].

Promoter	Location	Power (MWe)	Technology
Ramada Holdings, SGPS	Évora	1.5	DE
Hyperion Energy Portugal	Évora ou Reguengos	1.5	DE
Selfenergy	Silves	1	DE
Bragalux	Évora	1.5	DE
Efacec	**Tavira**	**4**	**CRS**
Abengoa/Fomentinvest	Moura	4	CRS
Energena SLU	Évora	4	PT
Martifer Energia	Évora	4	PT
Dalkia	Faro	4	LF
Tom	Moura	4	LF

The Faculty of Engineering, University of Porto (FEUP) was the national scientific partner for the project led by EFACEC to build a 4 MWe CRS in Tavira. The CRS technology uses an atmospheric air volumetric receiver, and included the participation of the German Aerospace Center (DLR) as international scientific partner and the company Kraftanlagen München (KAM) as engineering, procurement and construction (EPC) contractor. FEUP gathered the consortium that applied to the call and was responsible for the call's technical proposal. The EFACEC-FEUP proposal got the first position in the CRS call, and this thesis work was built to support the construction of a 4 MWe atmospheric air volumetric CRS power plant in Portugal, developing innovative models for the SOLMASS project and proposing innovative options for the hybridization with biomass.

For the location selected, CRS and biomass hybridization can also interesting from the government perspective. It could allow reaching the objectives set for the renewable electricity strategic plan. In 2006, Portuguese authorities launched a PIP call to support biomass power plants grid connection allocating up to 100 MWe (equivalent to the annual consumption of one million tons of biomass), mainly in areas of with large biomass resources and risk of fire [40]. Following the call, connection points were defined and several projects were approved, Figure 1.25 [41].

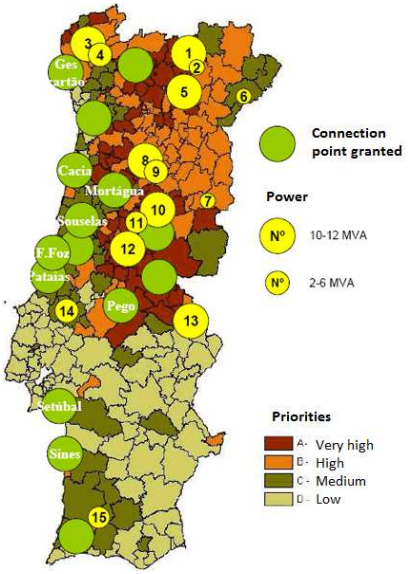

Figure 1.25: Biomass power plants and connection points approved under the 2006 Portuguese strategic programme [41].

However, the objectives of the strategic plan 2006 [42] were unaccomplished, with only a few power plants built. In 2009 a new call was launched for 15 projects, corresponding to a total of 100 MWe [43] adding up to 150 MWe of electricity from forest biomass already allocated. Despite that a low implementation rate remained. The strategic plan was then reworked and in March 2010 a new strategic plan was launched [44]. Portugal, as part of its European commitments, agreed a target of 31% of the average annual electrical consumption from renewable sources by 2020. For biomass, the need for implementation of the 250 MWe capacity already allocated is assumed to be reconciled with the availability of biomass on the forest market.

The feed-in tariff indicated for electricity using biomass as fuel is very low, and this was one of the main reasons for the low implementation of biomass power plant projects approved in 2006. Given the need to create an entire network for the collection and cultivation of biomass, the investments are high and the financial return of these projects is not attractive. This even threatens existing business processes, as in the case of the Mortágua power plant, subjected to biomass price volatility, and operation and maintenance cost increases, while the feed-in tariff remains low, endangering the power plant exploitation. Hybridization of CRS and biomass can be an interesting approach to combine the available permits and resources and build more sustainable power plants to reach the national strategic plan.

If the importance of renewable energy is indisputable, countries debt crisis has to be balanced with policies and measures for the promotion and integration of electricity generated from renewable resources in the national electricity network. This reflection must take into account not only the resources or maturity of technologies available, but above all, the ability to add value to the technology value chain, from design to marketing and industry development, considering job creation and increase of the national gross domestic product (GDP). Interaction with other policies, including: national security, environmental, agricultural, industrial and employment, is essential for development and sustainable growth of Portugal.

To fully apply these policies, the generation of renewable energy should be distributed in the territory and based on the diversity of energy sources: biomass, geothermal, hydro, solar, wave, wind, etc.., both in electricity generation and fuels. Portugal had a large and recent investment in fossil fuel power plants that require amortization, while electricity generation from renewable sources is mainly based on hydro and wind clusters that difficult the penetration of other renewable energies.

1.3.2 SOLMASS Project

The SOLMASS project [50] obtained the best classification in the CSP-PIP call, supported by EFACEC, DLR and KAM consortium, granting a national bonus feed-in tariff to finance the CRS power plant construction, operation and investment amortization. The atmospheric air volumetric CRS is the SOLMASS anchor to future developments. EFACEC also enquired several companies to acquire a biomass PIP call permit to Algarve. The SOLMASS project was divided in three phases:

1. Design and optimization of the CSP and biomass independent power plants:
    - Design and optimization of the CSP-only and biomass-only power plants;
    - Definition of the best technologies for hybridization;
    - Technic and economic analysis CSP-only, biomass-only and hybrid power plants.

2. Construction and operation of the power plants:
    - Build-up of the power plants;
    - Commercial operation of each unit to create market credibility;
    - Definition of the units control strategies and optimal hybridization solutions;
    - Hybridization optimization and testing.

3. Commercialization of the individual and hybrid power plants:
    - Implementation of larger individual and hybrid units;
    - Implementation of a R&D platform at SOLMASS;
    - Solar-chemical research and development.

The SOLMASS vision, approached on this thesis, is the implementation of CSP and biomass power plants for renewable electricity and fuels (chemicals) generation, in an integrated solar-chemical concept, Figure 1.26.

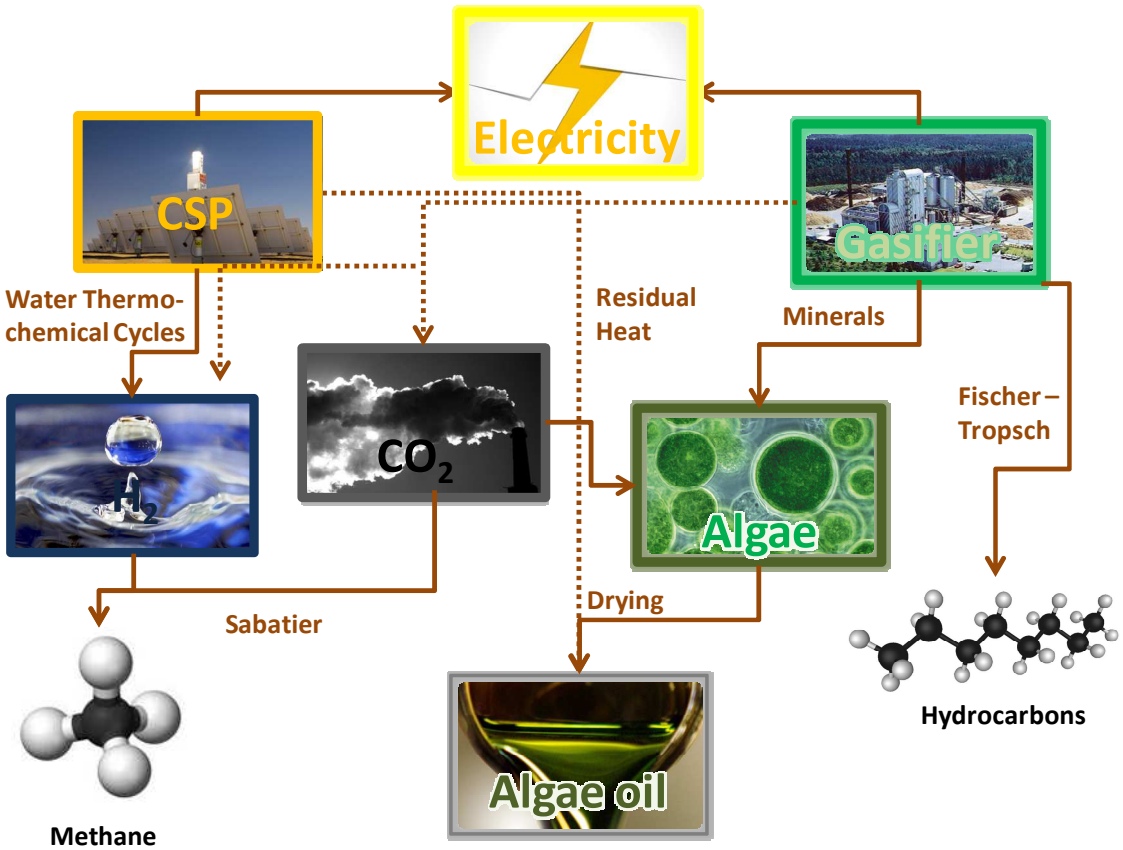

Figure 1.26: SOLMASS solar-chemical concept.

1.4 Biomass integration: resources and conversion technologies

The European directive 2001/77/EC [46] defines biomass as the biodegradable fraction of products and residues: from agriculture (including vegetal and animal); forest and related industries; as well as the biodegradable fraction of industrial and municipal waste. Biomass as a fuel is based on organic materials produced in a renewable way, but presents some difficulties, such as: low energy density (compared to fossil fuels) or its (growing) dispersion, solid physical state and high humidity. In result, the costs for collection and transport of biomass can easily exceed the actual cost of biomass (which often is a residue of low value).

These features constrain biomass as a fuel to be, typically, consumed locally or on short distances (up to 50-80 km) [47].

The safety (availability) and prediction of biomass as a fuel is an important factor. Biomass has a broad spectrum of applications and its use for electricity generation, since large amounts are needed, imposes that biomass availability and its cost must be ensured [46] else wise, the power plant can become unviable. Several sources of biomass as a fuel can be used, which are generally divided as: forest residues, energy crops, waste from agriculture and animals, municipal solid waste, industrial waste and algae, Table 1.5 [47].

Table 1.5: Biomass sources as fuel [47].

Source	Biomass type	Advantages	Disadvantages	Main conversion technologies
Forest	Wood cutting and forest thinning residues	National opportunity for funding biomass power plants, fire reduction, biomass energy value	Deforestation risk, habitat destruction risk, annual variations in the amount of resource, large collection system	Combustion, gasification, pyrolysis
Energy crops	Woody or herbaceous	Uniformity of the resource, supply stability, energy value	Soil erosion, possible conflict with the food industry, cost, pesticides and herbicides	Combustion, gasification, pyrolysis
Agricultural	Non food products (corn stover, etc...)	Uniform Resource	Possible conflict with the food industry, seasonal variations in the amount of resource	Combustion, gasification, pyrolysis
Animal	Animal excrement	Reduced environmental impact	Low energy content, Difficult integration in the livestock industry	Anaerobic digesters
Urban	Biodegradable fraction of municipal solid waste	Reduction of the environmental impact	Combustion complexity, collection structure required	Anaerobic digesters, combustion
Industrial	Furniture and pulp industry	Resource uniformity, supply stability, energy value	Raw material cost	Enzymatic hydrolysis (paper pulp), combustion, gasification
Algae	Micro and macro algae, cyanobacteria	Low environmental impact, no sulphur, no confronts with the food industry	Cost of scale, drying, early development phase	Extraction, fermentation, anaerobic digesters

To each source of biomass are associated one or more technologies for conversion of the biomass into electricity or fuel with higher energy value. All technologies presented in Table 1.5 are commercially available, but have different states of maturity and viability. The main biomass conversion technologies are presented in Figure 1.27 [48].

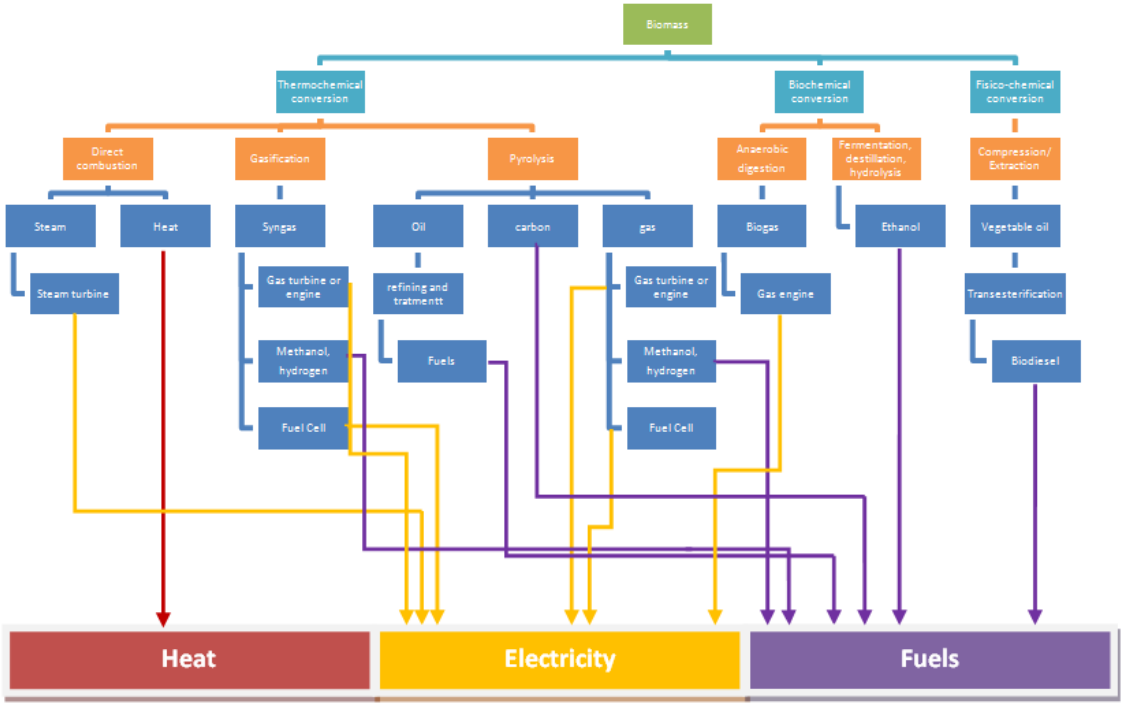

Figure 1.27: Main biomass conversion routes [48].

The main biomass power plant technologies can be divided according to the type of conversion applied: thermochemical, biochemical or physicochemical. The main thermochemical conversion processes are:

• Combustion or direct burning: it is the oldest technology for converting biomass. The combustion process uses the fuel energy, transforming it into heat after ignition, keeping the reaction while oxygen present (or air in stoichiometric excess) and biomass. Ashes are generated as a by-product, which are reapplied in some cases as fertilizers for agriculture or dumped into landfills. The combustion process is applied to most solid biomass power plants, with good performance and relatively low initial investments.

• Gasification: is a thermochemical process for converting biomass in the presence of an oxidizing agent (air or O_2), in lower quantities than the stoichiometric, into a synthetic gas usually known as syngas. This process is done at high temperatures and pressures and the synthesis gas generated is normally composed of carbon monoxide and hydrogen, with small amounts of carbon dioxide and methane. This gas can be burned in a boiler generating steam or be converted into methanol or hydrogen (using catalysts) which can be used in a fuel cell to generate electricity.

• Pyrolysis: In pyrolysis biomass heating is made in the absence of oxidant (usually air or oxygen) and a fuel gas, liquids (tars and pyroligneous acid) and charcoal are obtained. The

pyrolysis of biomass is one of the first processes for woody biomass utilization and had as main objective to obtain charcoal (via slow pyrolysis - a process done at low heating rates and for low temperatures). A fast pyrolysis, flash, or ultrasonic, is also used, applying heating rates between 10 and 1000 (respectively) times higher than the slow pyrolysis (operating with temperatures between 600 and 1000 °C) [48].

The thermochemical conversion processes are mainly applied to woody biomass: from forest, energy crops, agricultural waste or industrial solid, all with reduced humidity. When the biomass has higher moisture content, or comes from animal or urban waste, the most commonly applied conversion technologies are based on biochemical processes such as:

• Anaerobic Digestion: it is the anaerobic conversion of organic biomass by the action of microorganisms to generate biogas (methane and CO_2). The biggest advantage of anaerobic digestion is the valorisation of waste by generation of energy while reducing its environmental impact.

• Fermentation: it is the process of anaerobic conversion of organic compounds by action of microorganisms (in most cases yeast). In the case of alcoholic fermentation the organic substrate is sucrose and the products are essentially carbon dioxide and ethanol [49].

For conversion of biomass resources such as algae into fuels/energy, the conversion processes applied are physicochemical such as:

• Extraction (mechanical and/or solvents): that allows extracting lipids from algae, breaking their cell membranes using solvents or mechanically. The extraction is done with mechanical presses in a similar manner to the oil pressing process, removing up to 75% of the algae oil. This mechanical method can be complemented by using solvents such as hexane removing up to 95% of oils [50].

Alternatively, for conversion of algae fermentation processes can be used to generate methane or ethanol. However, in the case of algae and other biomass resources, there is still a lack in the technological development of extra conversion technologies, such as harvesting and logistics, which are still underdeveloped. It is necessary to create harvesting and distribution networks that provide stable biomass supply to power plants and the constant competitive prices.

In Portugal, the power plants use for biomass conversion the themochemical processes, mostly combustion or direct burning of biomass. The projects presented in Figure 1.28 are the larger biomass power plants in Portugal: the Mortágua power plant, with a capacity of 9 MWe [51] (operating with forest residues); and the Vila Velha de Ródão power

plant, with a capacity of 4 MWe [51] (operating with forest residues, bark residues, pine sawdust and olive bagasse), Figure 1.28.

Figure 1.28: Mortágua biomass power plant (left) and Vila Velha de Ródão power plant (right).

The use of forest biomass for energy production could have negative and positive effects. On one hand, the energy agriculture may be an excellent opportunity to promote sustainable agriculture and low ecological impact, and could be an incentive for the forest products industry to manage their resources more efficiently and thus improve the health of the forest. But it can also provide an excuse under the "green" cover, to explore the forests unsustainably, as unfortunately happened in the past, and many people regard with alarm the prospect of increased wood logging. The solution is to analyse the use of biomass integrated into forestall policies, so that integration in the range of renewable energy is successful. If the source is agricultural, the use of biomass should also be carefully examined to avoid collisions with food industry, especially for surface area required and the selected sources. A massive and inadequate use of biomass for energy purposes can compete with agriculture and possibly increase the basic food prices or influence the quality of soil and agricultural economies. However, if done in a sustainable manner, energy crops can provide a steady income to supplement farmers in periods between stations, stabilize crops susceptible to erosion and flooding, or allow farmers to work without requiring much unproductive additional equipment. Thus, there is also a need for regulation and supervision of the development of energy crops and waste.

With regard to emissions of greenhouse gases, current forest biomass plants generally have similar emissions as coal plants, with the notable difference that biomass emits very little sulphur dioxide and toxic metals (cadmium, mercury and others). The most serious problem is the emission of particulate matter that must be controlled with special equipment. One of the greater environmental benefits of replacing fossil fuels with biomass is that, if done in a sustainable manner, the amount of carbon dioxide emitted when biomass is burned is almost the same as it is absorbed by the biomass growing up, thus forming a sustainable fuel cycle

with virtual none global emissions of carbon dioxide. Some entries of fossil fuel may be needed for growing, harvesting, transportation and processing of biomass. However, the emissions from cultivation should be small, and if the energy to produce and process biomass comes from renewable sources, the net contribution to global warming would be nearly zero.

The most advanced biomass technologies such as gasification should generate very low emissions, comparable to natural gas plants. Biomass gasification processes have a wide range of applications and higher energy conversion efficiency [52, 53] than biomass combustion power plants. Biomass gasification can produce a mixture of methanol, heat, synthesis gas and electricity with efficiencies up to 73% [53]. The wood biomass, although more costly than the forestry residues, has better and more consistent properties which are beneficial to feed a gasifier. Under these conditions most of the problems associated with the fluidized bed gasifier or tars formation are relatively well known, so the biomass gasification industry already has commercial solutions to these issues.

There are however few commercial biomass gasification to electricity generation power plants. Examples of demonstration and pre-commercial projects can be found in the Nordic countries and Central Europe. The 3.5 MW gasification of wood shavings Harboøre power plant is in operation since 1996 and has over 8000 hours of annual operation [54]. In the power plant early days, some problems emerged mainly in the cleaning of the synthesis gas. However, the company that built the process in 2000, Babcock & Wilcox Vølund, solved the problems and at the end of 2003 the general concept of biomass gasification CHP (combined generation of electricity and heat) was considered commercial by this company, Figure 1.29 [54]. One of the most promising biomass gasification power plants network is the Renewable Energy Network Austria, which includes a gasification power plant that is supplying the town of Güssing with 2 MWe power and 4.5 MW of heat, from wood chips, since 2003, Figure 1.29 [55].

Figure 1.29: Harboøre (left) and Güssing power plants (right) [54, 55].

The gasification technologies having been successfully demonstrated, however, they are still relatively expensive, and face economic and non-technical barriers when trying to be introduced into the national electricity generation networks. Most of the new projects address technical aspects of the gasification processes, but also the integration of gasification in existing projects, showing that the overall system offers better economic prospects.

A different possibility is to use refuse-derived fuel (RDF) from municipal solid waste pellets (mainly plastics and biodegradable waste). The gasification of RDF is an interesting solution to solve the environmental impact of municipal solid waste. The Chianti RDF power plant is an example of a power plant using RDF gasification [56, 57]. The Greve plant is equipped with two 15 MWth TPS CFB gasifiers, each with a capacity of 100 t/d of RDF pellets. However, several operational problems occurred at Chianti, namely with gas cleaning and maintaining gas properties. The Chianti operational scheme is presented in Figure 1.30 [58].

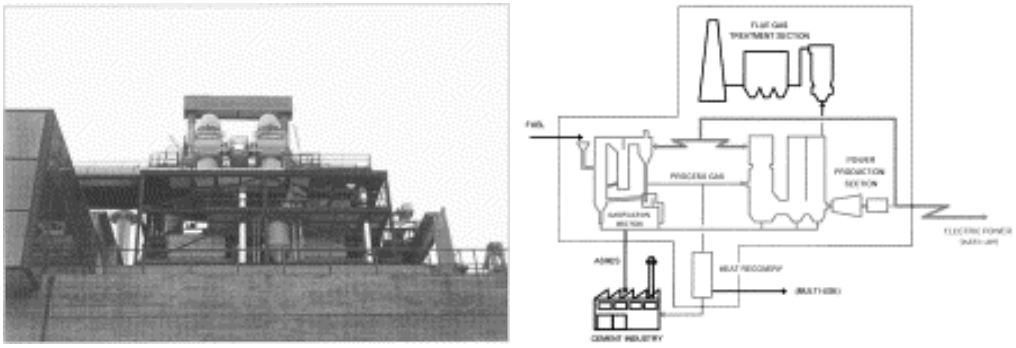

Figure 1.30: Chianti power plant (left) and scheme (right) [58].

Locally there is also an interesting potential of biogas generated from a waste water treatment plant and landfills. The biogas generated from the landfill has different characteristics compared with the biogas generated by a wastewater anaerobic digester [59]. The Barlavento landfill (Algarve) receives 176 thousand tonnes (2011) of waste every year and generates biogas to run the 900 kWe power block (it is in progress the expansion to 1.6 MWe). The Sotavento landfill is the other landfill in Algarve region and started operation in 2011 with a 1.2 MWe power block, Figure 1.31 [60].

Figure 1.31: Barlavento landfill (left) and Sotavento landfill (right) [60].

The biogas can also be generated from a wastewater treatment plant (WWTP). There are five main WWTP in the Algarve region: Vilamoura (140 000 inhabitants), Almargem (50 000 inhabitants), Faro (45 000 inhabitants), Olhão (35 000 inhabitants) and Boavista (25 000 inhabitants). All the Algarve WWTPs have no actual biogas valorisation. The larger national WWTP with biogas valorisation is the Frielas WWTP with a 2 MWe power block, which serves a population of 700 000 inhabitants, Figure 1.32 [61, 62].

Figure 1.32: Vilamoura (left) and Frielas (right) WWTPs [61, 62].

An alternative or supplement to biogas/syngas is the natural gas. Natural gas Rankine and combined cycle power blocks are an established technology, but the “renewable goal” would be lost. Commercial power plants running on natural gas normally use combined cycles up to several hundreds of MWe.

All these base case power plants are analysed through the thesis. The integration of biomass from these sources and using several conversion technologies is also studied for the hybridization of the CRS. The innovative models present interesting results, which is going to be used to analyse the concept of CSP and biomass hybridization.

1.5 Thesis structure, background and outputs

The thesis has 7 chapters. A review of the state-of-the-art on CSP and biomass technologies, and their possible integration, is carried out in Chapter 1. A model for the CRS design was developed by the author, and is presented in Chapter 2. This new model was created in HFLCAL, Ebsilon and Excel, and optimized for the Portuguese conditions and solar only operation in Chapter 3.

The work developed in the thesis started with the participation in a consortium that applied to a PIP call (SOLMASS project), in which FEUP was a scientific partner. Due to the promising local conditions, the SOLMASS project aimed to be the first hybrid Biomass/CRS power plant of its kind in the world. With this perspective, in Chapter 4, several biomass options were analysed for integration into the CRS steam cycle. The integration of biomass into the air cycle is presented in Chapter 5.

Chemical generation, based in renewable resources and CSP, is also analysed, Chapter 6. Chapter 7 presents the main conclusions of the work and perspectives of future work.

References

[1] Schillings, C., Trieb, F., MED-CSP Study, Concentrating Solar Power for the Mediterranean Region, DLR, 2005.

[2] Caracterização da Rede Nacional de Transporte para Efeitos de Acesso à Rede em 31 de Dezembro de 2008, REN, Março 2009.

[3] Richter C., Teske S., Short R., Concentrating Solar Power Global Outlook 09, Greenpeace, Estela and SolarPaces, 2010.

[4] Gordon, J., Solar energy: the state of the art : ISES position papers, International Solar Energy Society, 2001.

[5] Johansson, B., Burnham L., Renewable energy: sources for fuels and electricity, Island Press, 1993.

[6] Lovegrove, K., Luzzi A., Solar Thermal Power Systems, Encyclopedia of Physical Science and Technology, Volume 15, Academic Press, 2002.

[7] PS 10 Final Technical Progress Report, Solúcar, 2006.

[8] www.nrel.gov/csp/solarpaces/power_tower.cfm, accessed on 06-12-2010.

[9] www.brightsourceenergy.com/, accessed on 06-12-2010.

[10] www.esolar.com/, accessed on 06-12-2010.

[11] http://www.weizmann.ac.il/weizsites/solarenergy/, accessed on 16-12-2012.

[12] http://www.masdar.ac.ae, accessed on 16-12-2012.

[13] http://technology4life.wordpress.com/2009/01/25/financing-secured-for-gemasolar-power-tower-from-torresol-energy/, accessed on 06-12-2010.

[14] www.pratt-whitney.com/vgn-ext-templating/v/index.jsp?vgnextoid=f4d1202744f1a210VgnVCM1000004f62529fRCRD, accessed on 06-12-2010.

[15] http://www.ka-muenchen.de/253+M52087573ab0.0.html, accessed on 06-12-2010.

[16] SOLGATE - solar hybrid gas turbine electric power system Final Report, European Commission, 2005.

[17] Giuliano, S., et al., Analysis of solar-thermal power plants with thermal energy storage and solar-hybrid operation strategy, Journal of Solar Energy Engineering, 133 (2011), p. 310071-310077.

[18] Romero, M., Zarza, E., Handbook of Energy Efficiency and Renewal Energy, Chapter 21: Concentrating Solar Thermal Power, CRC Press, 2007.

[19] Romero, M., Buck, R., Pacheco, James., An Update on Solar Central Receiver Systems, Projects, and Technologies, Journal of Solar Energy Engineering 124 (2002), p. 98 – 108.

[20] Pitz-Paal, R., Dersch, J., Milow, B., ECOSTAR roadmap document, DLR, 2005.

[21] Pacheco, J., Overview of recent results of the solar two test and evaluations program, Sandia Report, 1999.

[22] www.torresolenergy.com/TORRESOL/gemasolar-plant/en, accessed on 06-12-2010.

[23] Hoffschmidt, B., Téllez, F., Valverde, A., Fernández, J., Fernández, V., Performance Evaluation of the 200-kWth HiTRec-II Open Volumetric Air Receiver, Journal of Solar Energy Engineering 125 (2003), p. 87 – 94.

[24] http://www.saint-gobain-solar-power.com/heat-receivers-hpr-13, accessed on 06-12-2010.

[25] Kearney, D., Kelly, B., Price, H., Thermal Storage Commercial Plant Design Study for a 2-Tank Indirect Molten Salt System, NREL report, 2006.

[26] Tamme R., Laing D., Steinmann W., Advanced Thermal Energy Storage Technology for Parabolic Trough, Proceedings of the 2003 International Solar Energy Conference, 2003.

[27] KAM technology catalogue.

[28] www.saint-gobain-solar-power.com/solar-thermal-storage-norpro-9, accessed on 06-12-2010.

[29] Luz International, Phase-Change Thermal Energy Storage, NREL report, 1989.

[30] Stine, W., Solar energy fundamentals and design, Wiley, 1985.

[31] Siemens catalogue - www.energy.siemens.com/fi/pool/hq/power-generation/steam-turbines/downloads/E50001-W410-A105-V1-4A00_Solarbroschuere.pdf, accessed on 06-12-2010.

[32] www.mandieselturbo.com/1013241/Press/Press-Releases/Press-Releases/First-steam-turbine-for-solar-power-station.html, accessed on 06-12-2010.

[33] www.gepower.com, accessed on 06-12-2010.

[34] http://www2.cnrs.fr/journal/3160.htm, accessed on 06-12-2013.

[35] U.S. Department of Energy, Concentrating Solar Power Commercial Application Study: Reducing Water Consumption of Concentrating Solar Power Electricity Generation, Report to Congress, 2009.

[36] www.nrel.gov/csp/troughnet/power_plant_systems.html, accessed on 06-12-2010.

[37] www.nrel.gov/csp/solarpaces/, accessed on 06-12-2010.

[38] Despacho n.º 18838/2009, Diário da República n.º 157, 2ª Série de 14 de Agosto de 2009 - http://dre.pt/pdf2sdip/2009/08/157000000/3313233132.pdf, accessed on 06-12-2010.

[39] http://www.dgge.pt/, accessed on 06-12-2010.

[40] CNADS, "Reflexão do CNADS sobre Energia e Sustentabilidade", 2007.

[41] www.renae.com.pt/_fich/22/060630DGGE.pdf, accessed on 06-12-2010.

[42] Estratégia Nacional para a Energia, Resolução do Conselho de Ministros n.º 169/2005.

[43] www.portugal.gov.pt/, accessed on 06-12-2010.

[44] Estratégia Nacional para a Energia 2020, Resolução do Conselho de Ministros n.º 29/2010.

[45] Coelho, B., Domingues, P., Oliveira, A.C., Mendes, A., "SOLMASS project - solar-biomass dual hybrid 4 MW CRS pilot plant", Solarpaces 2010, Perpignan, France, September 2010, paper 295.

[46] http://www.logistica-florestal.pt, accessed on 16-12-2012.

[47] Yakima County Public Works Solid Waste Division, Review of biomass fuels and technologies, R.W.Beck, 2003.

[48] Neto, V., Potencial da Cogeração e Planeamento da Expansão do Sector Eléctrico, 2006.

[49] Queirós, A., Produção de Metanol a partir de Biomassa Vegetal: Um novo processo integrado, Tese de Mestrado, FEUP, 2009.

[50] http://www.oilgae.com/algae/algae/oil/extract/extract.html, accessed on 16-12-2012.

[51] www.energiasrenovaveis.com, accessed on 06-12-2010.

[52] Kayhanian, M., Tchobanoglous, G., Brown, R., Handbook of Energy Efficiency and Renewal Energy, Chapter 25: Biomass Conversion Processes For Energy Recovery, CRC Press, 2007.

[53] Brandberg Å., Hjortsberg H., Sävbark B., Ekbom, T., Hjerpe, C., Landälv I. "BioMeeT, Planning of Biomass based Methanol Energy Combine at Trollhättan region". Final report by Trollhättan Municipality, Ecotraffic R&D AB and Nykomb Synergetics AB, Stockholm, 2000.

[54] www.volund.dk/solutions_references/gasification_solutions, accessed on 06-12-2010.

[55] www.renet.at/english/sites/guessing.php, accessed on 06-12-2010.

[56] Granatstein, D.L., Case study on waste-fuelled gasification project greve in Chianti, Italy, IEA bioenergy agreement—task 36 report, 2003.

[57] G. Barducci, G., Ulivieri, P., Pike, D.C., McDonald, N., Repetto, F., Cristo, F., The Greve in Chianti project, Renewable Energy 16 (1999) p. 1041–1044

[58] Morris, M., Waldheim, L., Energy recovery from solid waste fuels using advanced gasification technology, Waste Management 18 (1998) p. 557–564.

[59] Persson, M., Jönsson, O., Wellinger, A., Biogas Upgrading to Vehicle Fuel Standards and Grid Injection, IEA Bioenergy report, 2006.

[60] http://www.algar.com.pt, accessed on 10-07-2013.

[61] http://www.aguasdoalgarve.pt, accessed on 10-07-2013.

[62] http://www.simtejo.pt/, accessed on 10-07-2013.

Chapter 2

Model of an atmospheric volumetric central receiver system (CRS)

This page was intentionally left blank

2. Model of an atmospheric volumetric central receiver system (CRS)

Presently, only a few simulation tools are available for modelling of atmospheric volumetric CRS power plants. HFLCAL and EBSILON are software packages for the solar field design and for the power block design, respectively. By combining them within Excel and introducing an economic model, CRS modelling was taken a step further, and a complete model was built, with an integrated optimization of the CRS, balancing the performance and economic indicators. Besides, the developed simulator has a powerful and user-friend graphical interface based on EBSILON module. This new model allows sizing the equipment for nominal conditions and to evaluate the operation of the power plant. It is also possible to evaluate the impact of different operational conditions and design variables in the power plant economics and performance. This chapter presents how the model of the 4 MWe power plant was built, the mathematical background and the design strategies and variables.

2.1 CRS solar field model

The solar field of heliostats is responsible for "harvesting" the solar energy, tracking up the sun on two axes and continuously concentrating the sun's rays on the receiver surface or any other point pre-defined by the operator. The distribution of heliostats in the available field is an iterative process with special attention to the geometry and position of the receiver, the nominal power and minimization of the effects of shading, blocking, the cosine factor, atmospheric attenuation and spillage. In addition to the distribution of heliostats in the solar field, other factors affect the performance of the solar field, such as: the reflecting surface, the structure and foundations, the curvature of the mirrors, the drive mechanisms, control instruments and modes of operation, which are detailed in the following subchapters. The heliostat/solar field should address all these factors, optimizing the cost/performance ratio.

Since the distribution and performance analysis of the heliostats field is a complex process and requires a high number of iterations, some simplified models such as SAM-TRNSYS STEC and ECOSTAR/Greenius only consider an array of efficiencies for characterizing the solar field performance using it to calculate the energy sent to the receiver for each pair of solar coordinates. This approach assumes that the performance characteristics of the solar field are identical for all solar fields that use the same matrix (whatever areas, locations, and other specific restrictions). So, the use of a pre-defined matrix (e.g. already known from literature) is limiting and was not the approach used in the models developed for this thesis; instead, individual and optimized solar field configurations were developed for each case studied.

The development of specific tools for the design and optimization of the CRS solar field began in the 1980s, when different codes were written in Fortran for the design and simulation of solar thermal central receiver plants, such as HELIOS, ASPOC, HFLCAL, RCELL, Delsol, Mirval, SOLERGY, etc.. But, in most cases, their interface and structure were not modular, or user-friendly [1]. To address this issue, an IEA/SolarPACES working group was created to develop modular codes and user-friendly interfaces for the layout optimization of the heliostat field. This group developed versions using the Windows interface for HFLCAL (Kiera, 1989) and DELSOL3 (Kistler, 1986), property of DLR and CIEMAT, respectively. Overall, solar field optimization software use one of the two most common approaches: statistical (ray-tracing) or analytical (convolution), Figure 2.1 [1].

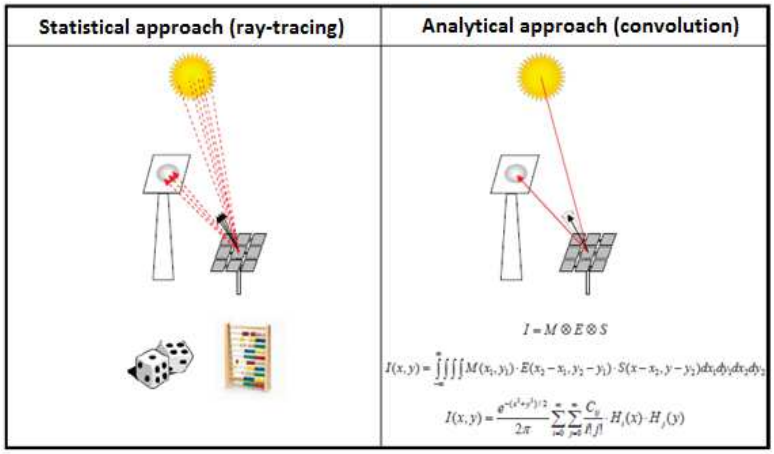

Figure 2.1: Approaches for calculating the solar image incident in the solar receiver [1].

The operation principle of statistical approach or Monte Carlo methods is the random selection of a set of rays emitted from a surface A, determining which arrive to a surface B by reflection. It is then considered that a surface radiance is proportional to the basic number of rays that affect it. The method is applied twice: from the sun (with a distribution that coincides with the sun's shape) and the reflecting surface of the heliostat; and between this surface and the surface of the receiver with a distribution representing the errors from the reflecting surface. The computation time and complexity of this approach increases with the number of rays and the complexity of the surfaces geometry.

In the analytical approach, by convolution methods, the rays reflected by the mirror surface are involved by cones of error usually approximated by normal distribution (Gaussian) for each of the considered errors (sun's shape and errors from the heliostat). These models require less computing time, with relatively low errors - 1 to 2% relative to the peak flux and

mean absolute error - which are in the same range of statistical approach software such as SOLTRACE.

For both approaches the total energy incident on the receiver depends on the sun position and the relative position of the heliostat, the receiver, and the nearby heliostats. As such the layout and optimization of the solar field and receiver is preferably solved by computer simulation, for which different codes are currently used, Table 2.1 [2].

Table 2.1: Software for optimization and distribution of heliostats on the solar field [2].

Name	UHC-RCELL	DELSOL	HFLCAL	MIRVAL	SolTRACE
Institution	SANDIA, Tietronix	CIEMAT, SANDIA	DLR	DLR, SANDIA	NREL, CNRS
Development year	1974	1978	1986	1978	1999
Programming language	FORTRAN/ C^{++}	FORTRAN/ Basic	FORTRAN	FORTRAN	Delphi5
Flux calculation method	Hermite polynomial expansion	Hermite polynomial expansion	Convolution of the flux of each heliostat	Monte Carlo ray tracing	Monte Carlo ray tracing
Receiver type	Plain, cavity, cylindrical, external	Plain, cavity, cylindrical, external	Plain, cylindrical, conical	Plain, cavity, cylindrical, external	Multiples
Secondary concentrators	Beam-down	No	Yes	Yes	Yes
Detailed contribution of each error	Yes	Yes	Yes	Yes	No
Annual performance	Yes	Yes	Yes	Yes	No
Optimized components	Heliostat field, tower height, receiver geometry	Heliostat field [a], tower height, receiver geometry, storage	Heliostat field, tower height, receiver geometry, and orientation	Heliostat field [b]	No
Optimization criteria	Energy or cost with the possibility to define flux and field	Cost with the possibility to define flux and field	Energy or cost with the possibility to define flux and field	Energy [b]	Without optimization

a - Uses RCELL spacing methods;

b - Only with additional module created by DLR.

Most of these software are not commercially available and are property of the institutions that developed it. Due to the developed partnerships, UNET and the author obtained time-limited licenses for the use of windows versions of HFLCAL and DELSOL. Also SOLTRACE is available from NREL website. The software were tested for their functionalities. Statistical approach software such as SOLTRACE was not selected due to the complexity of the simulation and to define the heliostat distribution through the solar field. HFLCAL gained advantage over Delsol due to the software interface, structure of programming and the optimization algorithms and possibilities.

2.1.1 HFLCAL - Heliostat Field Layout Calculation

The HFLCAL code [3] was created during the GAST project (GAS-cooled solar tower, 1981). In 1994 the program was acquired by DLR adding specifications such as: multipoint focusing, radial array of heliostat layouts and optimization of the variables by the Powell method. In 1999 several options were added: a secondary concentrator, measured meteorological data, pressurized air receivers (based on the REFOS design) and CRS optimization to minimize costs. Subsequently the Windows interface of the program was created, including new configurations for the receiver and additional optimization algorithms.

The main objectives of HFLCAL are calculating the performance of a CRS for an initial configuration, optimizing the CRS layout, maximizing the energy generated per heliostat. HFLCAL also allows an annual simulation, based on the energy reflected by individual heliostats and simplified receiver and power block performance interpolation.

2.1.1.1 HFLCAL approach for the analysis of errors

Typically, the size of the sun, irregularities of the mirrors curvature and their imperfections, are responsible for the deviations from the ideal focal point and size of the solar image on the receiver surface. Usually these deviations can be statistically distributed by a cone centred on the vector between the heliostat and the focal point of the receiver. In addition to these deviations, there are also uncertainties related to the solar tracking mechanism and foundations, which contributes to the imprecision of the reflected solar rays.

HFLCAL assumes that the probability of a direction of the reflected rays to occur is well approximated by a normal distribution with a half width - σ:

$$F(r) = \frac{1}{2\pi\sigma^2} e^{\frac{r^2}{2\sigma^2}} \quad (2.1)$$

HFLCAL also considers that all variables influencing the definition of the solar image reflected in the solar receiver can be represented by the sum of normal distributions for each of the errors:

$$\sigma^2 = \sigma^2{}_{sun} + \sigma^2{}_{error\ 1} + \sigma^2{}_{error\ 2} + \ \ldots \tag{2.2}$$

This approach has certain limitations, because the angular distribution of solar rays does not resemble a Gaussian, although it may be statistically approximated by a normal distribution with the same root mean square deviation relative to the central solar beam [3]; this approach produces similar results to ray tracing methods, especially for large mirror errors or smaller incident angles.

2.1.1.2 Heliostat errors

The errors of the mirrors (in the curvature and waviness of the mirrors) are typically referred to as slope errors and are approximated in HFLCAL by normal distributions. They are measured relatively to the surface normal vector and their effects, in combination with the mirror roughness, lead to deviations on the reflected solar image. The heliostats track the sun in two axes and are driven by motors that also have deviations due to the finite motor step sizes and tolerances of the gearbox, which are measured relatively to the mirror normal vector. The sum of all the heliostat errors is normally called beam error:

$$\sigma_{beam\ error}{}^2 = \sigma^2{}_{sun} + \ \sigma_{beam\ quality}{}^2 + (2\sigma)^2{}_{track} \tag{2.3}$$

HFLCAL assumes that all heliostats have well canted facets and statistically distributed errors. The image reflected by the heliostats with the mentioned features is shown in Figure 2.2 (left) [3]; however, the real image reflected by a heliostat (Figure 2.2 - right) is influenced by non-statistical errors e.g. canting errors and deformations in the structure by gravity or wind loads.

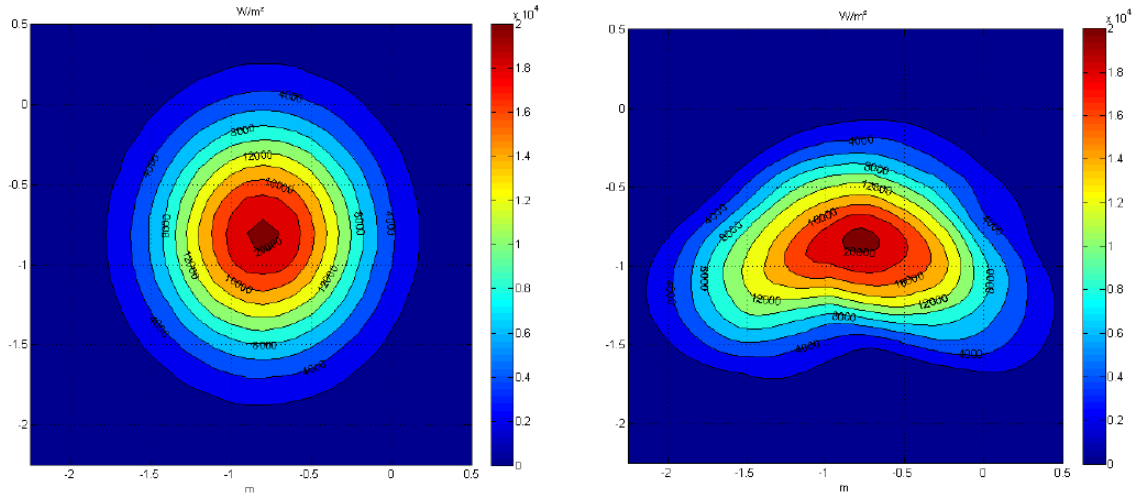

Figure 2.2: Image reflected by a heliostat with normal error distributions (left) and real image reflected by the same heliostat (right) [3].

2.1.1.3 Errors for different incident angles: astigmatism

The solar beam error, defined in equation 2.3, is valid only for design conditions - with incidence angle Ψ = 0 °. For different conditions the astigmatism effect of an image reflected by a concentrating surface has to be considered.

$$\sigma_{total}{}^2 = \sigma_{beam\ error}{}^2 + \sigma_{astigmatism}{}^2 \qquad (2.4)$$

A spherical or paraboloidal solar concentrator concentrates the parallel solar rays in a single focal point only for a specific incidence angle. For other incidence angles the solar radiation is concentrated between two lines (green and red, Figure 2.3). Two planes can be defined: the tangential plane and the sagittal plane. For f/d >> 1, the solar rays in the tangential plan (green) concentrate in the focal point at a f·cos Ψ distance. The rays in the perpendicular sagittal plane (red) are concentrated in a focal length of f/cosΨ, Figure 2.3 [3].

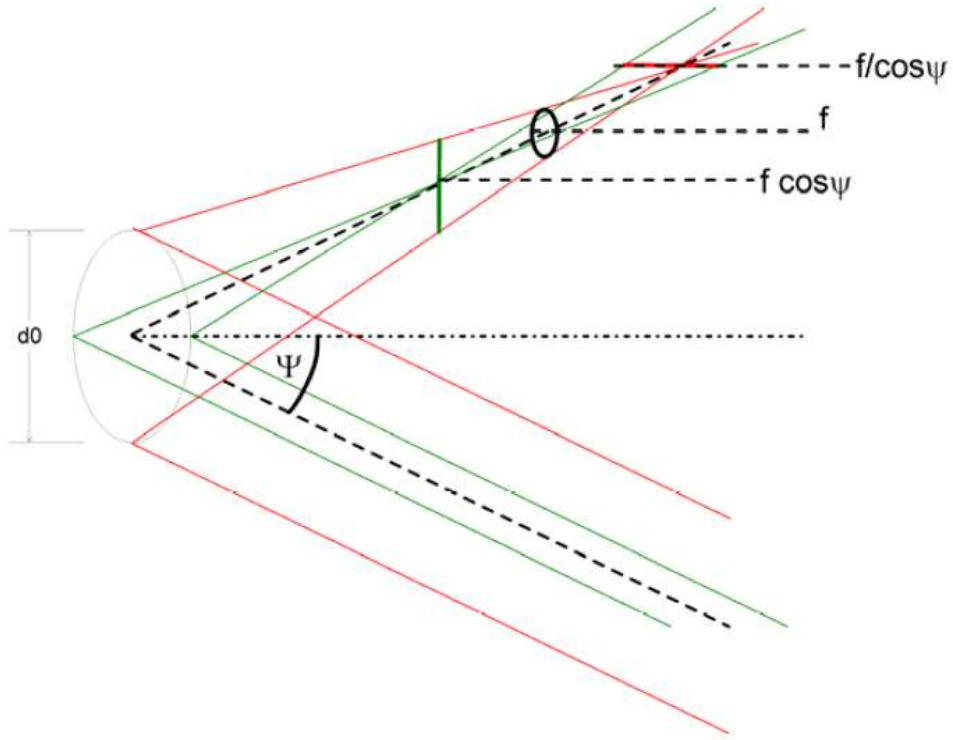

Figure 2.3: Image reflected by a spherical concentrator [3].

For a given slant range - *SLR* distance, from a mirror to the surface - the image reflected has the following dimensions in the tangential and sagittal planes:

$$H_t = d\ \left|\frac{SLR}{f} - cos\ \Psi\right|;\ W_s = d\ \left|\frac{SLR}{f} \cdot cos\ \Psi - 1\right| \tag{2.5}$$

In HFLCAL, the image dimensions due to off-axis reflection can be described as superposition of astigmatism in the heliostat and in the facet:

$$H_t = (d_{\ IH} - d_{\ IM}) \cdot |1 - cos\ \Psi| + d_{\ IM} \cdot \left|cos\ \Psi - \frac{SLR}{f}\right| \tag{2.6}$$

$$W_s = (d_{\ IH} - d_{\ IM}) \cdot |1 - cos\ \Psi| + d_{\ IM} \left|\frac{SLR}{f} \cdot cos\ \Psi - 1\right| \tag{2.7}$$

where $d_{\ IH}$ and $d_{\ IM}$ are the diameters of the heliostat and facets and f is the focal length of the facets.

In HFLCAL, the root-mean-square (RMS) of the reflected solar image (in the tangential and sagittal plane) is treated as uniform distribution and is incorporated as additional error to the reflected solar beam with half width of $\sigma_{astigmatism}$.

$$\sigma_{astigmatism} = \frac{\sqrt{\frac{(H_t^2+W_s^2)}{2}}}{4 \cdot SLR} \quad (2.8)$$

The astigmatism error is mainly associated with the heliostat size (for large incident angles) while for low incident angles the facet size is dominant. For heliostats with astigmatism correction HFLCAL adds the possibility of introducing a correction factor.

2.1.2 Annual simulation

The performance of a heliostat is dependent on several factors, which can be divided into three major groups:

- Regardless of the time and position of the heliostat: reflectivity;
- Dependent only on position: atmospheric attenuation;
- Depending on the time and position: cosine factor, blocking and shading, interception.

Considering these factors, the energy incident into a certain surface (e.g. solar receiver) from a heliostat with an F_{mir} area for a specific instant (t), under a direct normal irradiance $DNI(t)$, is given by the following equation [3]:

$$P(x,y,t) = DNI(t) \cdot F_{mir} \cdot \eta_{ref} \cdot \eta_{atm}(x,y) \cdot \eta_{cos}(x,y,t) \cdot \eta_{b\&s}(x,y,t) \cdot \eta_{Int}(x,y,t) \quad (2.9)$$

From the sum of all heliostats the energy supplied by the field of heliostats to the surface of the solar receiver can obtained for a given time period by:

$$P_{solar\ field}(t) = \sum_i P_i(x,y,t) \quad (2.10)$$

HFLCAL uses about 100 periods of time, typically the daylight hours of the 21st day of each month, to calculate the annual performance, which depends on the location selected for the solar plant (e.g. latitude and height above sea level).

2.1.3 Main factors that influence the solar field layout

The solar field annual efficiency depends on a large number of factors: cosine factor, shading, blocking, atmospheric attenuation and spillage. The solar shape, mirror curvature and defects or imperfections in the mirror surface are also responsible for the final size of the focal point for a given point in time. All these effects overlapped form the solar image incident on the receiver.

2.1.3.1 Reflectivity

The reflective material is an important for the design and efficiency of the solar field. Currently various materials are used and several companies produce specific and optimized reflective materials for application in solar-thermal power plants (cylinder-parabolic, Fresnel, Stirling disks or CRS), e.g. Saint-Gobain, Flabeg and Guardian.

Normally, reflective materials are divided according to the position of the reflective surface: 1st surface, 2nd surface or multi surface. In the case of CRS, the material typically used is a silver film on thick glass support. This is a 2nd surface mirror and has a longer operational experience under real conditions; typically keeps its characteristics for periods of 25 years with only slight breaks in reflectivity. There are also innovative 2nd surface materials such as the silver film on thin glass, which has good features and price, yet still being commercially validated (mainly to maintain the characteristics for periods similar to the silver film in thick glass). 1st surface materials such as the aluminium film polished on a metallic support may enable combining the structure of the heliostat with its reflecting surface, bringing a possible cost reduction; currently these materials have low reflectivity and durability, requiring frequent repositions of the reflecting surface to maintain the overall efficiency of the solar field. An overview of the features and costs of reflective materials is presented in Table 2.2.

Table 2.2: Characteristics of the mirrors available on the market.

Material	Type	Reflectivity	Thickness	Durability	Price
Aluminium film on metallic support	1st surface	0.83 – 0.87	0.3 to 1 mm	5 years	15 €/m^2
Silver film in thick glass	2nd surface	0.935	3.5 to 5 mm	over 20 years	35 - 65 €/ m^2
Silver film in thin glass	2nd surface	0.93	0.4 to 1.2 mm	20 years	15 €/m^2

Prices are dependent on quantities and also vary substantially with the time of acquisition [4].

2.1.3.2 Cosine factor

The cosine factor takes into account the reduction of the surface that effectively reflects the solar radiation at incident angles $\Psi \neq 0$. It is one of the most important factors for an efficient solar field. The cosine factor varies with solar position and the position of each heliostat. It is assumed that the heliostats have a correct tracking, and as such, their cosine factor is defined by the cosine of the angle formed by the incident solar beam and the surface normal vector of the heliostat (Ψ):

$$\eta_{cosine} = \cos(\Psi) \tag{2.11}$$

The heliostat tracking mechanism follows the sun in a way that its normal vector bisects the angle between the solar ray, and a vector pointing to the focal point on the receiver. This can result in a clear decrease in the effective heliostat reflective area, Figure 2.4.

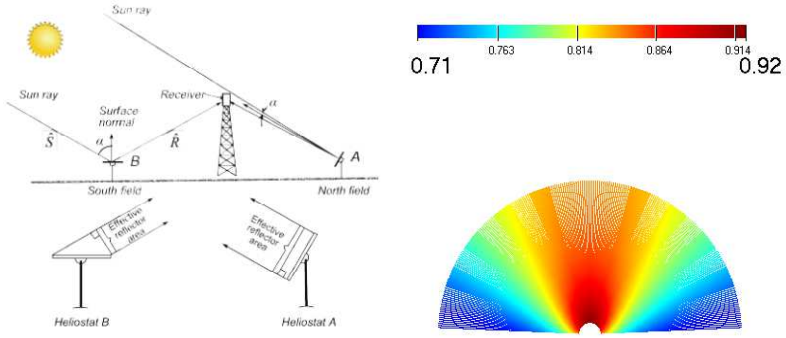

Figure 2.4: Cosine factor (left) [6] and effect on the solar field (right).

For this reason, a heliostat in the northern hemisphere, when placed in the south area (heliostat B – Figure 2.4) has a lower efficiency than the heliostats placed in the north area, which face the sun (heliostat A – Figure 2.4). In a similar analysis, in the morning the heliostats placed west of the tower have higher efficiency than the heliostats placed east, and during the afternoon the opposite occurs.

2.1.3.3 Blocking and shading

For the calculation of heliostat blocking and shading losses, HFLCAL projects the image of the central heliostat in the surrounding group of heliostats. This analysis is carried out in two different directions: between the sun and the heliostat to calculate the shading, and between the heliostat and its focal point (solar receiver) to calculate the blocking. Shadowing occurs when a heliostat, or part of it, is shadowed by one or more neighbours. Blocking occurs when a part of the heliostat sees its solar reflection in the receiver blocked by their neighbours

[5, 6]. Figure 2.5 represents the losses from blocking and shading and the heliostats in the solar field usually most affected by these losses.

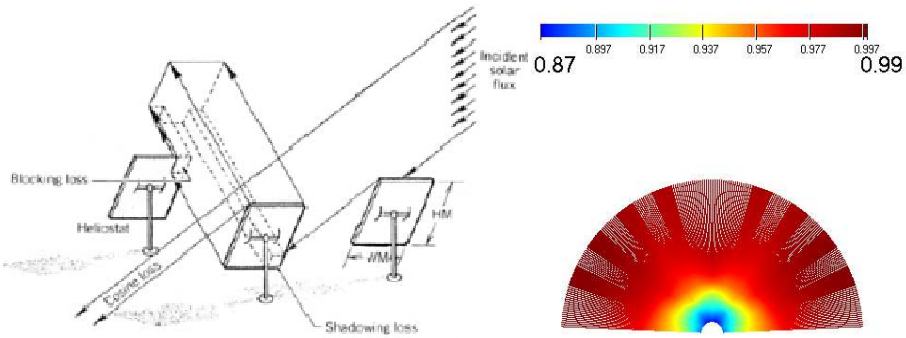

Figure 2.5: Blocking and shading losses (left) [6] and effect on the solar field (right).

The blocking and shading losses are a function of the spacing between heliostats, tower height and solar angles, which are dependent on the respective time of day and position of the heliostats. HFLCAL has different distribution patterns to minimize these losses. The total non-shaded area is calculated and the ratio between this area and the total area is found to obtain the blocking and shading efficiency. Other simulation tools, such as Helios and Delsol2, also use this approach, positioning the heliostats more compactly near the tower and with more spacing far from the tower, so the blocking and shading losses are minimized. An indicator of the solar field layout is its heliostat field density. This is the ratio between the mirror area and the total area of the field or certain zone. It can be calculated by Equation 2.12, where $D_{mirrors}$ is the mirror density (ratio of heliostat mirror area and heliostat total area):

$$\rho_{solar\ field} = \frac{2 \cdot D_{mirrors} \cdot \mathrm{H_{width}} \cdot \mathrm{H_{length}} \cdot \text{number of heliostats in the field}}{field\ area} \quad (2.12)$$

2.1.3.4 Atmospheric attenuation

The atmospheric attenuation of the rays reflected by the heliostats is dependent on the distance between the receiver and the heliostat, the slant range - SLR.

$$\eta_{atmospheric} = 0.99321 - 0.0001176 \cdot SLR + 1.97 \times 10^{-8} \cdot SLR^2 \quad (2.13)$$

For slant ranges of more than 1 km (SLR > 1000 m):

$$\eta_{atmospheric} = e^{-0.0001106 \cdot SLR} \quad (2.14)$$

The models used by HFLCAL are in agreement with experimental data collected by NREL during operation of the solar plant Solar Two in Daggett, California, USA [7] (Figure 2.6), for clear sky models (HFLCAL and Solar Two - 23 km). For the most common slant range of commercial solar fields (up to 1.5 km), HFLCAL variations from measured data are 2 to 3%. Although they are specific to a location in California, the NREL values may be used for other similar locations. However, significant changes are recorded for locations with higher values of aerosols at ground level (commonly referred as visibility) and for locations with different altitudes.

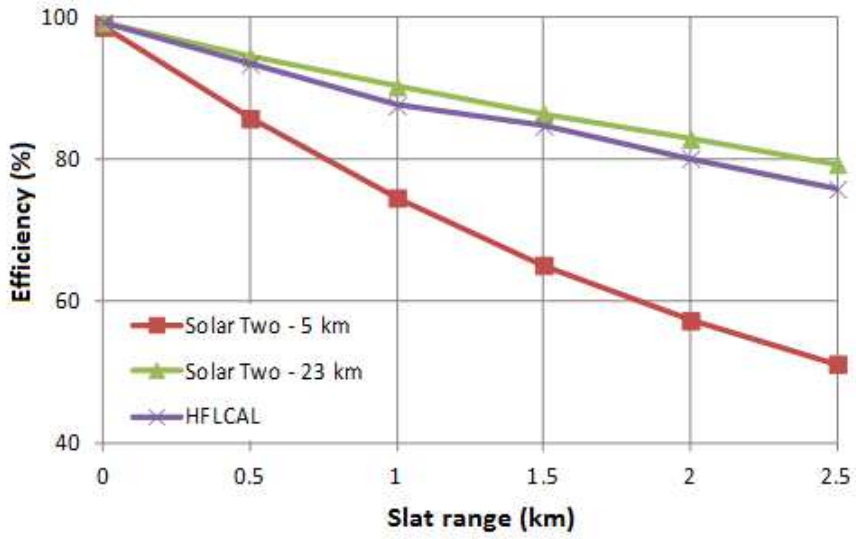

Figure 2.6: Impact of atmospheric attenuation on the efficiency of a solar field for HFLCAL and measured data from Solar Two (lines are for readability).

For hazy days (Solar Two 5 km) the decrease in efficiency (with increasing distance to the solar tower) is more intense - losses closer to 50 % at 2.5 km. Commercial heliostat fields can reach distances of about 1.5 km and atmospheric attenuation losses become significant (≈ 15 %), even considering models of clear sky, Figure 2.7. Atmospheric attenuation losses, associated with interception losses, mean that there is a technical/economic limit for the field area (and ultimately for the CRS installed power).

2.1.3.5 Intercepted radiation

The flow distribution of the solar beams reflected from each heliostat must be integrated over the receiver area to obtain the effective incident energy in the receiver at a certain point in time. In HFLCAL each solar image reflected by a heliostat is described by Equation 2.1 and the reflected image intercepted by the receiver is expressed by the following equation:

$$\eta_{intercept} = \frac{1}{2\pi\sigma_{total}^2} \iint_{receiver} e^{-\frac{x^2+y^2}{2\sigma_{total}^2}} dx\, dy \quad (2.15)$$

The beam dispersion width is calculated according to Equation 2.4. In the case of a circular aperture with the heliostat aiming at the centre this integration is solved analytically. In all other cases numerical integration routines are used. The spillage factor (or the ratio of the reflected image that cannot intercept the receiver surface) is a function of the quality of heliostat solar tracking, uniformity of the reflective surface, the shape of the sun, environmental factors such as wind speed, heliostat foundation, controller and tracking algorithm used, Figure 2.7 [5, 6].

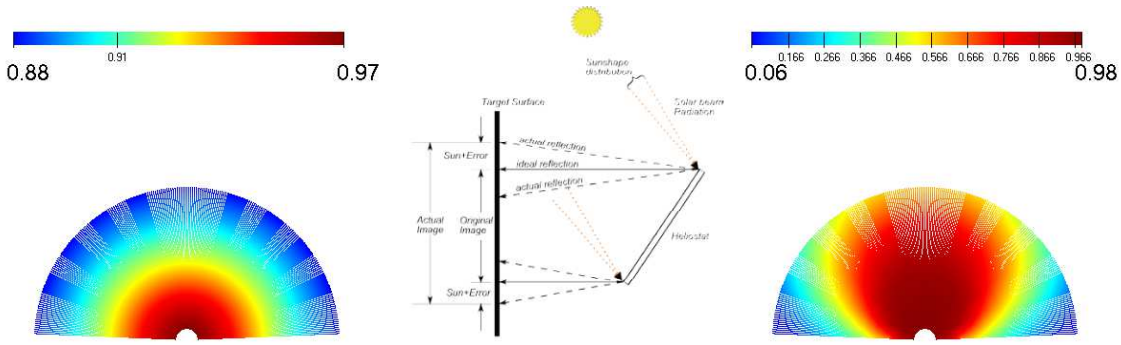

Figure 2.7: Effect of atmospheric attenuation in the solar field (left) spillage (centre) [6] and the respective effect of the solar field (right).

2.1.4 Distribution/optimization of the solar field

2.1.4.1 Heliostats

The starting point for solar field optimization is the definition of the individual heliostat dimensions and the type of heliostat. The most common heliostat configuration is rectangular, with square or rectangular mirrored facets, Figure 2.8. Each facet and heliostat reflects a circular image [3].

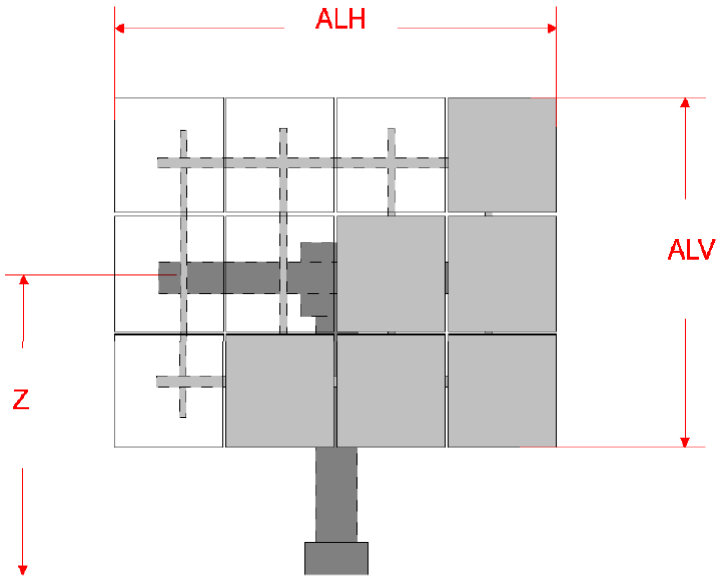

Figure 2.8: Heliostat scheme and dimension [3].

ALV and ALH are, respectively, the vertical and horizontal dimension of the heliostat and Z is the height above the ground up to the centre of the heliostat; HFCAL also requires to define the FMIR and FFAC, respectively the heliostat mirror surface and its facet areas; EFELD and SIG are respectively the annual average reflectivity and total error of the solar beam reflected by the mirror surface. It is also possible to select two options: ideal focus distance - which considers all facets focal points match the slant range; and heliostats with correction of their astigmatism.

The project Helios3S designed a heliostat for application in SOLMASS CRS. The process of optimization of the heliostats size depends on the configuration and characteristics of the receiver and maximizes the energy generated by the plant, but also optimizing the solar field cost. Regarding various commercial approaches to the configuration and dimensions of a heliostat field (Chapter 1), the selected approach was to create a medium-sized heliostat (Helios3S) with the characteristics presented in Table 2.3.

Table 2.3: Characteristics of the Helios3S heliostat.

Characteristic	Value	Characteristic	Value
ALV	7.76 m	FFAC	5.00 m^2
ALH	7.76 m	EFELD	87 %
Z	4.88 m	SIG	3.60 mrad
FMIR	60.32 m^2		

2.1.4.2 Solar field layout

HFLCAL uses an algorithm to distribute the heliostats throughout the solar field, selecting afterwards the most efficient heliostats to generate the thermal energy required by the receiver. The distribution of heliostats can be based on three algorithms: bilinear expanded, bilinear with spacing and slip planes. Each model has different characteristics and may be more advantageous in terms of efficiencies, depending on the type of receiver and the design power, Figure 2.9.

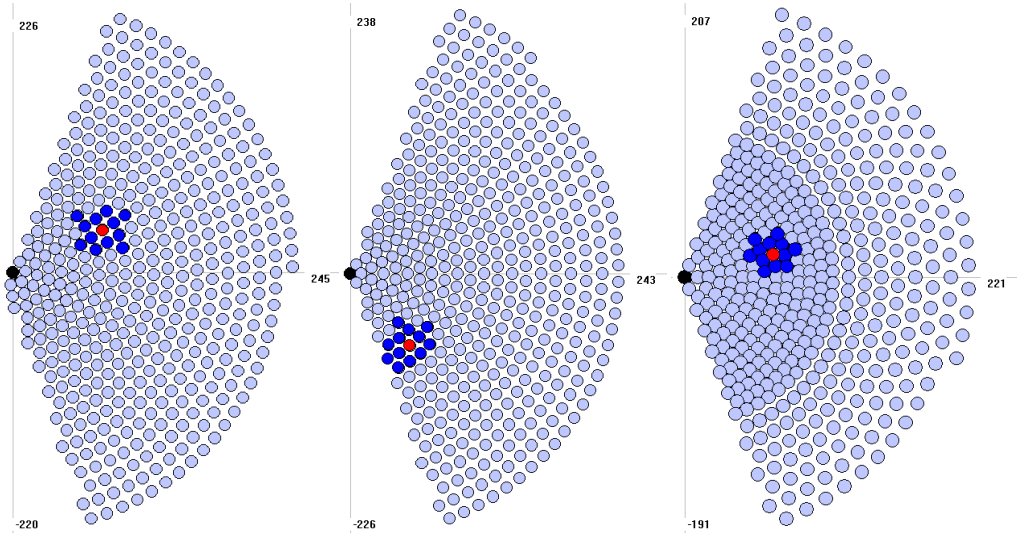

Figure 2.9: Typical heliostat layout for different algorithms: bilinear expanded (left), bilinear with spacing (centre) and slip planes (right).

In the bilinear expanded model the heliostats are considered as concentric spheres arranged in rows; the distance between heliostats in the same line and between lines increases with increasing distance to the tower (r) to minimize blockages and shading, Figure 2.10 [3].

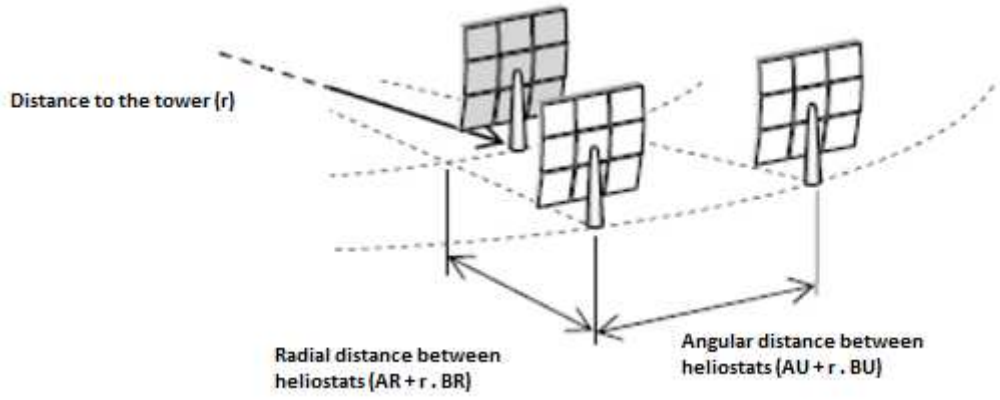

Figure 2.10: Spacing between heliostats in the solar field.

The spacing of the heliostats is defined by two linear functions:

Distance between rows:

$$\Delta r = AR + BR \cdot r \tag{2.16}$$

Distance between heliostats in the same line:

$$\Delta u = AU + BU \cdot r \tag{2.17}$$

AR, BR, AU, BU are variables which are optimized to obtain the best solar field layout. Blockings are proportional to the distance between rows. However it is possible to define optimal spacing to have non-blocking heliostats, Figure 2.11 [3]. For large distances, this spacing is approximated by $br_{block} \approx ALV/ATH$. The counterpart for the position of heliostats at large distances is an increase in atmospheric attenuation losses and spillage losses. Typically the starting values of *br* should be lower than ALV/ATH, e.g. in the range of $0.1\ ou\ 0.5 \cdot ALV/ATH$. Subsequently the values of the coefficients of Equations 2.16 and 2.17 can be optimized to maximize efficiency, by changing the solar field layout.

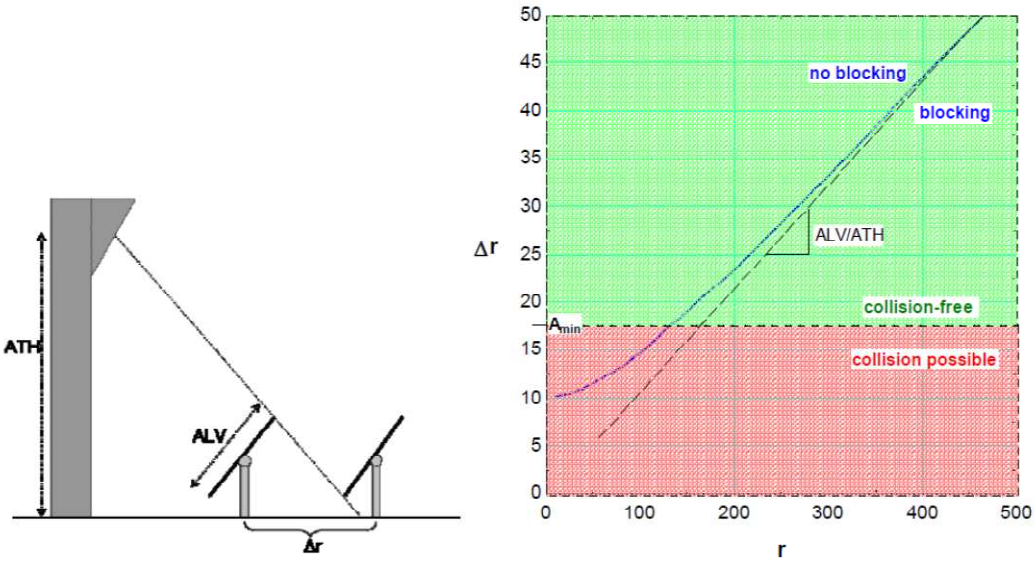

Figure 2.11: Spacing between heliostats to avoid blockings (left) and examples for different distances to the solar tower (right) [3].

To avoid collisions between heliostats, a minimum distance must be kept (A_{min}) that must be at least the heliostat diagonal. A good starting value for *ar* to minimize losses due to blockage can be found in Figure 2.12 [3].

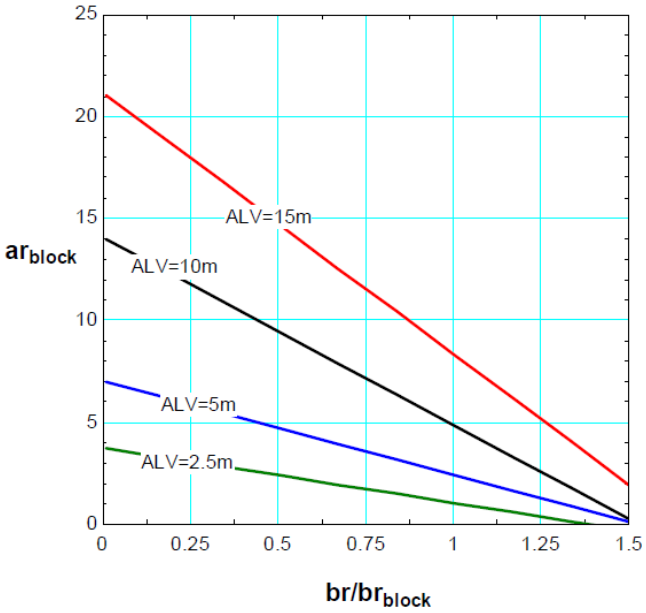

Figure 2.12: Starting values of ar in function of br for different heliostat sizes [3].

A good definition of the starting values facilitates the optimization process and reduces the overall calculation time. Several optimization algorithms are available to obtain a relative or absolute maximum solar field power per heliostat. The starting values for the solar field layout parameters are presented in the Table 2.4.

Table 2.4: Starting values for heliostat distribution in the solar field.

Characteristics	Starting value
AMIN	8.76 m
AR	10
BR	0.02
AU	10
BU	0.02
PHIRAND	1 °
RTURM	10.00 m
Origin height	0 m
Field inclination	0 °

where AMIN is the minimum distance between heliostats (distances Δr and Δu must be higher than this value); AR, BR, AU, BU are the variables of Equations 2.22 and 2.23; PHIRAND is the angle between the field limit and the East-West axis; RTURM is the distance between the tower centre and the first heliostat row. With HFLCAL it is also possible to define the boundaries of a specific solar field and define the best layout for this field geometry and slope.

Alternatively to the standard bilinear expanded model, HFLCAL can use two other distribution models: bilinear with spacing and slip planes. The bilinear model with spacing applies the same distribution pattern as the bilinear expanded model, but distributes alternately heliostats and empty spacing around the tower. This favours more elongated and narrow solar field layouts, as in the case of secondary concentrators and thermochemical applications.

In the case of the slip planes model the heliostats are distributed radially so Δu automatically increases with increasing distance r; when $\Delta u > USTART$, Δu is defined as $USTART$, and the heliostats near the tower are compressed to the maximum (AMIN); this first plane of high compression is limited by FPACK distance (from the tower) and the solar field extension in east-west axis (HFBREITE). The layout of solar fields defined by this method is more adequate for large solar fields.

2.1.4.3 Solar field efficiency

HFLCAL uses the initial heliostat distribution in the solar field to measure the influence of each factor of the solar field, calculating the atmospheric attenuation losses, cosine factor, blocking and shading losses and interception losses, selecting the most efficient heliostats to achieve the design thermal power in the receiver. The example of a typical non optimized solar field is presented in Figure 2.13.

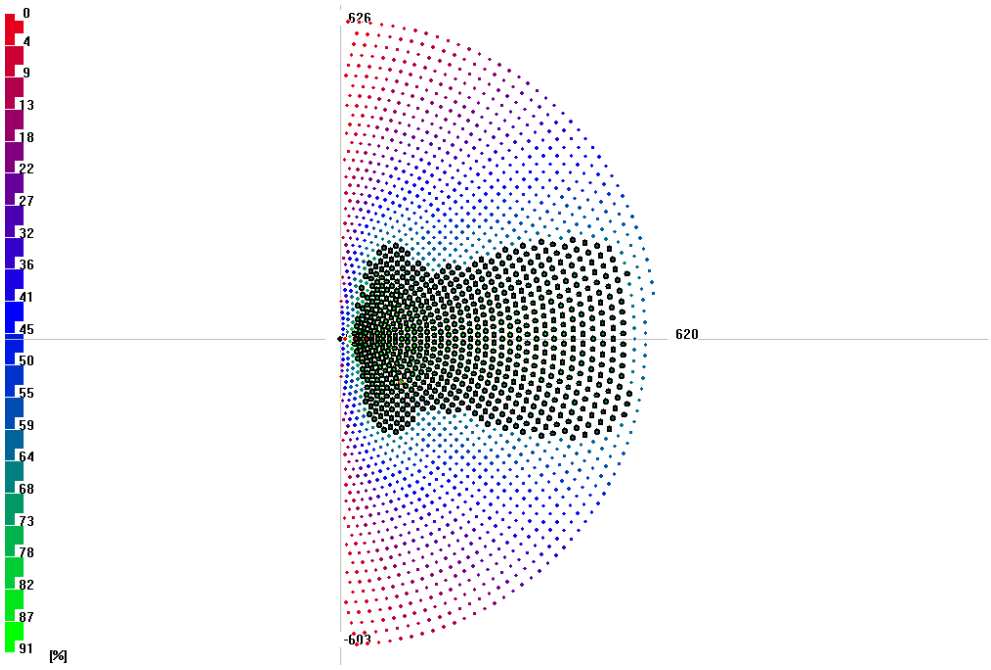

Figure 2.13: Non optimized solar field: highlighted are the best performance heliostats and their efficiency.

The first parameter necessary to calculate the performance/layout of a solar field is the definition of the location and meteorological model used. HFLCAL can use measured local meteorological data. However, to reduce calculation time, decrease complexity and eliminate the influence of stochastic processes some models are usually used, normally for clear sky conditions, such as the Hottel model [8].

$$DNI = I_{extraterrestrial}\left(a_0 \cdot r_0 + a_1 \cdot r_1 e^{-\frac{kr_k}{\cos(zenith)}}\right) \quad (2.18)$$

Either for the calculation (by the Hottel model) of the direct normal irradiance (DNI) or for the definition of solar angles and distribution of heliostats in the field, it is also necessary to define the location of the power plant (latitude and height above sea level). Other key parameters are the height of the tower (ATH) and its orientation angle (PHI). To calculate the

shading caused by the solar tower in the solar field it is also necessary to define the tower diameter. The tower dimensions are one of the optimization parameters, both to maximize the energy reflected by the heliostats and reduce the cost. Higher towers allow packed solar fields and have lower losses by blocking and shading. In contrast, higher towers increase cost, as well as shadow on the solar field. Analyzing the latest commercial designs, typically the CRS tower height can be fixed within a range of ± 30% of a power equation of the receiver power, presented in Figure 2.14 [9].

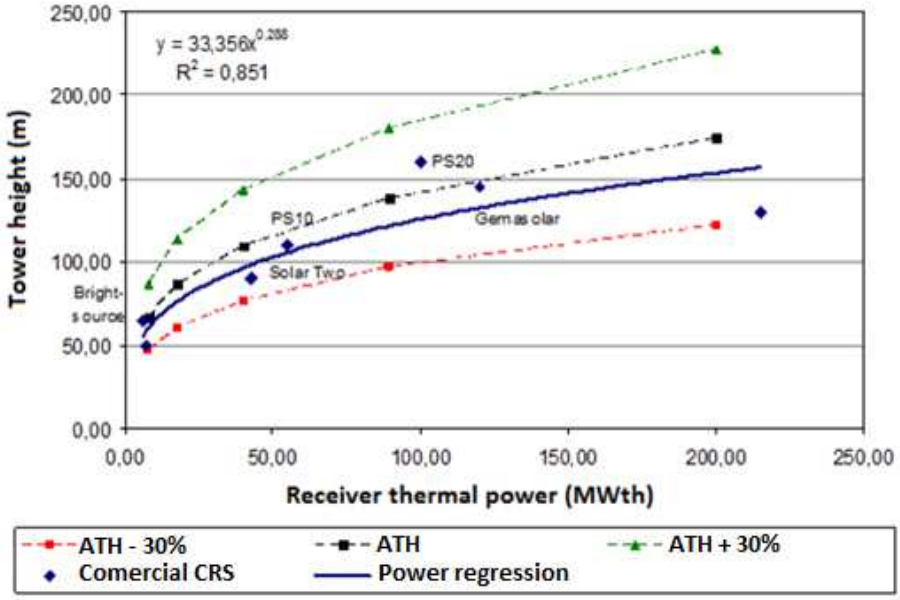

Figure 2.14: Tower height for different commercial CRS [9].

For the specified receiver solar thermal power, the tower height considered was 97 m. The power plant location is in the Tavira/Faro region, Algarve, which has latitude of 37.01 ° and a height above sea level of 8 m.

2.1.4.4 Receiver configuration

The selected CRS power plant technology uses an atmospheric air volumetric receiver pre-commercial solution, with rectangular ceramic composite cups supported by a rectangular metal frame. With HFLCAL, it is possible to simulate rectangular, cylindrical and circular receivers, composed of up to 3 zones, connected in series or in parallel. It is also possible to add a secondary concentrator. The selected solar receiver is a square surface with a width and length of 7.75 m and a total area of 60 m^2. It is an external receiver and has an inclination of 11.2 °, which was optimized to maximize the energy intercepted by the receiver. To optimize the energy generated by the receiver, HFLCAL can use two mathematical models: receiver with

variable temperature model (receiver with constant working fluid mass flow rate and the receiver outlet temperature is lower in part load); and the model with constant thermal losses (constant temperature).

The efficiency of a receiver with constant thermal losses is given by:

$$\eta_{receiver} = \eta_{optical} - \dot{q}_{losses} \frac{A_{receiver}}{P_{receiver}} \tag{2.19}$$

For a receiver with variable temperature model:

$$T_{loss} = T_{receiver\ in} + \frac{T_{receiver\ out} - T_{receiver\ in}}{2} + dT_w \tag{2.20}$$

$$T_{receiver\ out} - T_{receiver\ in} = (T_{receiver\ out} - T_{receiver\ in})_{DP} \cdot \frac{P_{receiver}}{P_{receiver,DP}} \tag{2.21}$$

$$dT_w = dT_{w,DP} \cdot \frac{P_{receiver}}{P_{receiver,DP}} \tag{2.22}$$

$$\eta_{receiver} = \eta_{optical} - A_{receiver} \cdot \frac{\epsilon \cdot \sigma \cdot (T_{loss}^4 - T_{amb}^4) + \alpha \cdot (T_{loss} - T_{amb})}{P_{receiver}} \tag{2.23}$$

However, for the design of the CRS a three dimension interpolation method was used, based on real measured data form DLR at Jülich power plant, Figure 2.15.

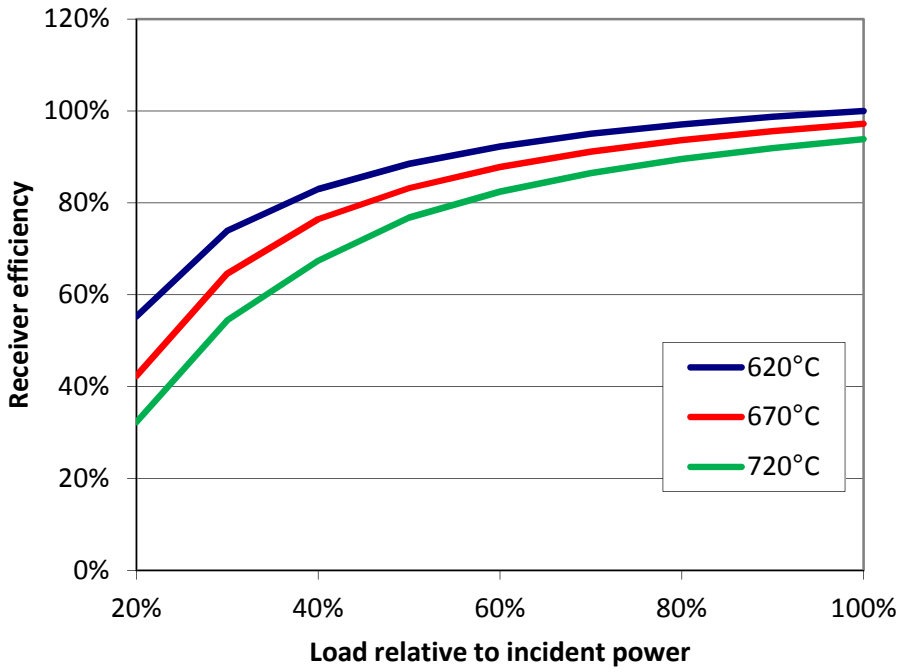

Figure 2.15: Measured operating efficiencies of Jülich atmospheric air volumetric receiver (relative values).

The receiver design conditions and its operating temperatures and efficiencies were set in combination with the power cycle model, which was designed in Ebsilon. The receiver performance was interpolated from Figure 2.15.

2.1.4.5 Receiver solar flux

The mapping of solar fluxes incident on the receiver is essential to analyze the performance of the solar receiver. A correct distribution of the solar flux over the entire area of the receiver allows an increase of the receiver efficiency and longevity. Too high fluxes may cause structural deformations in the receiver cups and structure. Typically, for SiC receivers, currently used in commercial CRS, peak flows should be max. 1100 kW/m^2. For large power this is only possible by defining a strategy with several focal points, each focusing on solar images of a certain group of heliostats, usually using groups of heliostats closer to the solar tower to focus on points nearer to the receiver boundaries and farther heliostats (with larger solar image) to cover the points of focus in the centre of the receiver. HFLCAL allows using different strategies and focal points in the receiver, Figure 2.16.

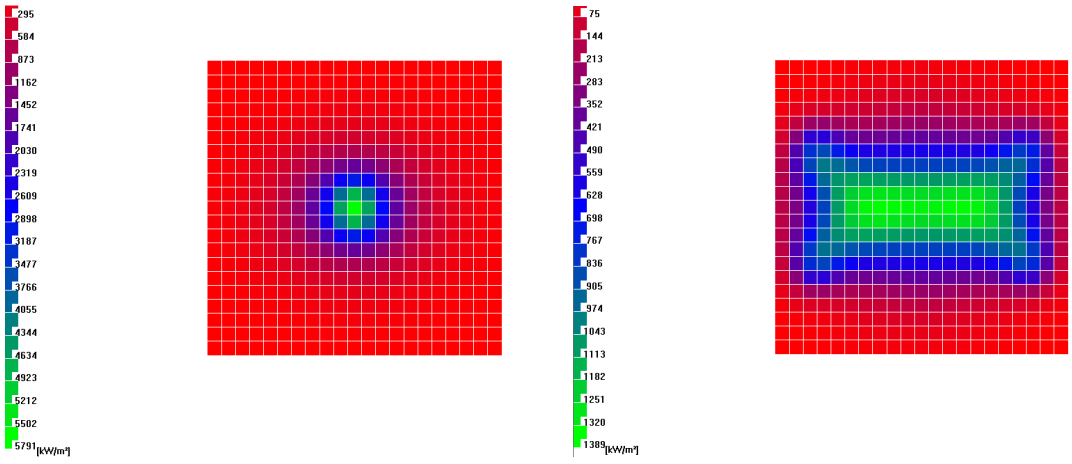

Figure 2.16: Strategies for solar field focusing: central point (left) and several points on a centre line (right).

The central point focussing strategy is used in various micro power plants or for thermochemical solar applications, normally using circular receivers or reactors (e.g. quartz window). For a 4 MWe power plant this strategy would reach very high concentrations in the centre of the receiver (Figure 2.16 - left), and so it is advisable to use more focal points in the receiver. One possible strategy is to use three focal points (similar to what is used in Jülich power plant); however, the level of concentration reaches more than 1300 kW/m^2 (Figure 2.16 - right) and should be avoided. HFLCAL has a distribution algorithm for the heliostat focal

points into receiver, according to their image. It is also possible to optimize the focal point distribution, which is itself an iterative process. The goal is to limit the maximum incident solar peak flux and get a uniform flux profile throughout the area of the receiver. A good solar flux distribution may allow using a smaller receiver and consequently lower heat losses and cost. Nevertheless, a decrease in the solar receiver area, can lead to increased spillage losses and a consequent reduction in receiver efficiency and output power.

2.1.4.6 Solar field optimization

The process of solar field optimization has the utmost importance for the overall life-time performance of the solar power plant. HFLCAL has algorithms for optimization based on two principles: maximizing the performance of the power plant or minimizing the cost associated with it. It is necessary to estimate several initial values and a first performance of the power plant is calculated; subsequently, each iteration step is defined and new variable values (one by one) are defined and the new solar field configuration performance is calculated; the process is repeated, step by step, until a relative or absolute maximum is obtained. HFLCAL contains three optimization algorithms: iso-scan; genetic and Powell method. Each algorithm has specific characteristics and can be used at different stages in the optimization process. The iso-scan algorithm (all possible combinations) permits a scan of all selected parameters, combining them with each other, for a selected range of values (usually wide) in order to obtain an idea of what could be the values of interest to start the detailed optimization process. The computation time of this algorithm increases rapidly with the number of parameters selected and the range of values chosen. The genetic algorithm initiates a random collection of configurations with different values for the selected parameters and in accordance with the algorithm starts an internal convergence process for obtaining the maximum overall optimization function for the parameters selected. The algorithm is efficient in getting the maximum, by phasing elimination of not maximum function values; however, this algorithm needs further optimization processes to obtain the specific values of the parameters that the algorithm estimates. This optimization can be done using the Powell method. This method gives only a good approximation (with reasonable times) when the initial values of the parameters are chosen close to the maximum values. Since this is a directional method, it will progressively increase values of the selected parameters until a maximum is found, and the selected parameters should be reviewed as they may exceed the permissible physical values.

Several optimization algorithms were used to find the best solar field layout. The process is limited by equipment operability and physical barriers (when a minimization of costs is selected) and by the cost of the equipment (when a maximization of the performance is selected). The whole process is repeated in order to maximize the performance and minimize cost of the solar field according to all design parameters. The optimization process is briefly described in the decision tree of Figure 2.17.

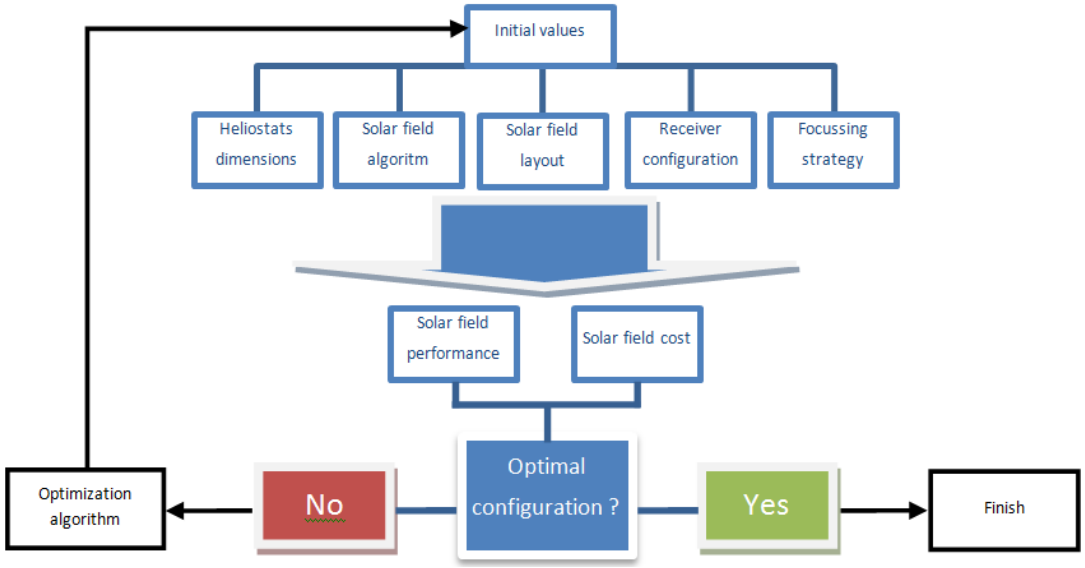

Figure 2.17: Solar field optimization strategy.

2.2 Power circuit model

2.2.1 Ebsilon Professional

Ebsilon Professional software simulates thermodynamic cycle processes and is used for engineering, designing, and optimizing power plants [10]. During the design process, it can be used to identify optimal cycles and evaluate various options and configurations. It can also be used during plant operation to evaluate losses and suggest improvements. Ebsilon uses a graphical interface that allows the models to be built using single components, groups of components, sub systems or complete systems. Ebsilon has an extensive component library (e.g. heat-exchangers, boilers, pumps, steam and gas turbines, fans, etc) and different fluid media property libraries and tables [10]. It has a design mode and an off-design mode; the power plant design mode sizes the equipments for nominal operational conditions. Off design operation, necessary for annual simulation, is usually defined by characteristic lines. Conventional (natural gas or coal) power plants usually operate in close to nominal conditions almost all year round. This is not the case of a CRS, which is more dynamic (because solar irradiance is not constant), and because of that, several operational profiles are necessary, Figure 2.18.

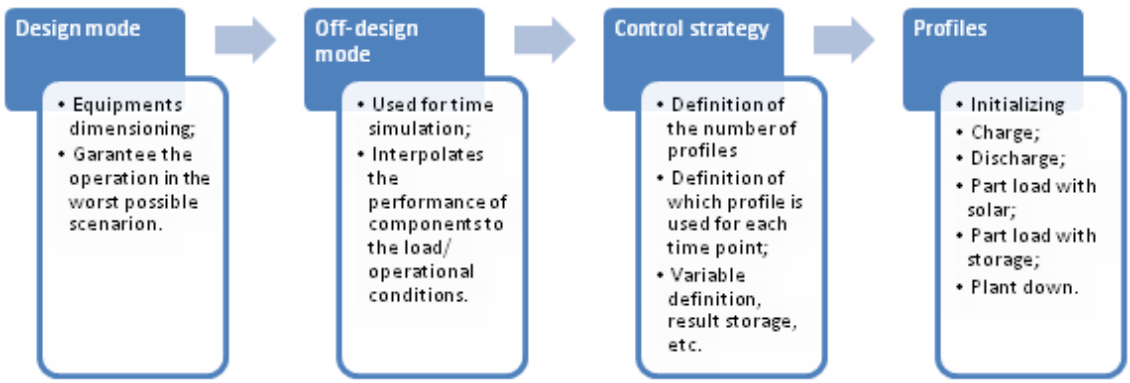

Figure 2.18: Ebsilon structure.

2.2.2 Power circuit optimization approach

Solar power has several peculiarities that influence the power circuit equipment selection and how the power plants are designed to incorporate it. As mentioned in Chapter 1, for commercial systems three types of CSP thermal cycles may be considered: Rankine, Stirling and Brayton cycles. The choice of thermal power cycle depends on the type of technology selected. For CRS (as in the case of LF and PT) a Rankine or Brayton cycle is usually selected, which may unfold in several power circuit configurations and operational conditions.

To determine the best power circuit configuration for the CRS, several variables are of great importance: e.g. the electrical power to inject into the network (4 MWe), the available solar irradiance (Faro, typical meteorological year, DNI of 2183 $kWh \cdot m^{-2} \cdot yr^{-1}$), power block operational conditions, solar multiple, storage capacity and control strategy. The final variable definition is an optimization process including the entire solar plant: solar field layout, solar receiver configuration, thermal cycles used among others. This optimization process should be carried out in accordance with technical and economic criteria so that the CRS has the highest possible performance with the lowest possible costs.

In parallel to this process it is vital to validate the solar power plant components and models with commercial equipment. This is an extremely laborious process since there are often conflicting interests among different equipment manufacturers, as well as difficulty in disseminating performance characteristics for reasons of confidentiality. Moreover, the number of suppliers is reduced and typically composed of an oligopoly of large multinationals (SIEMENS, MAN TURBO; ALSTOM, etc.), who impose signed confidentiality agreements to transfer only partial information. There are components, such as the solar receiver and the heliostat field, that are still in early commercial phase and as such the information on their performance is reduced and extremely confidential. In the following chapter is presented the design process and optimization of the power circuit of a CRS of 4 MWe, to be implemented in the region of Algarve (Faro).

As shown in Figure 2.19, the design of CRS is typically done from downstream to upstream. The first variable to be set is typically the peak power to be injected into the grid. In the case of the considered CRS power plant, the installed power is 4 MWe and a power block for this power should be found. The detailed definition of the power circuit equipments and their operational conditions is not only dependent on the installed power but also the thermal

cycle to be applied, which is influenced by the receiver technology, the solar field, local conditions and control strategy.

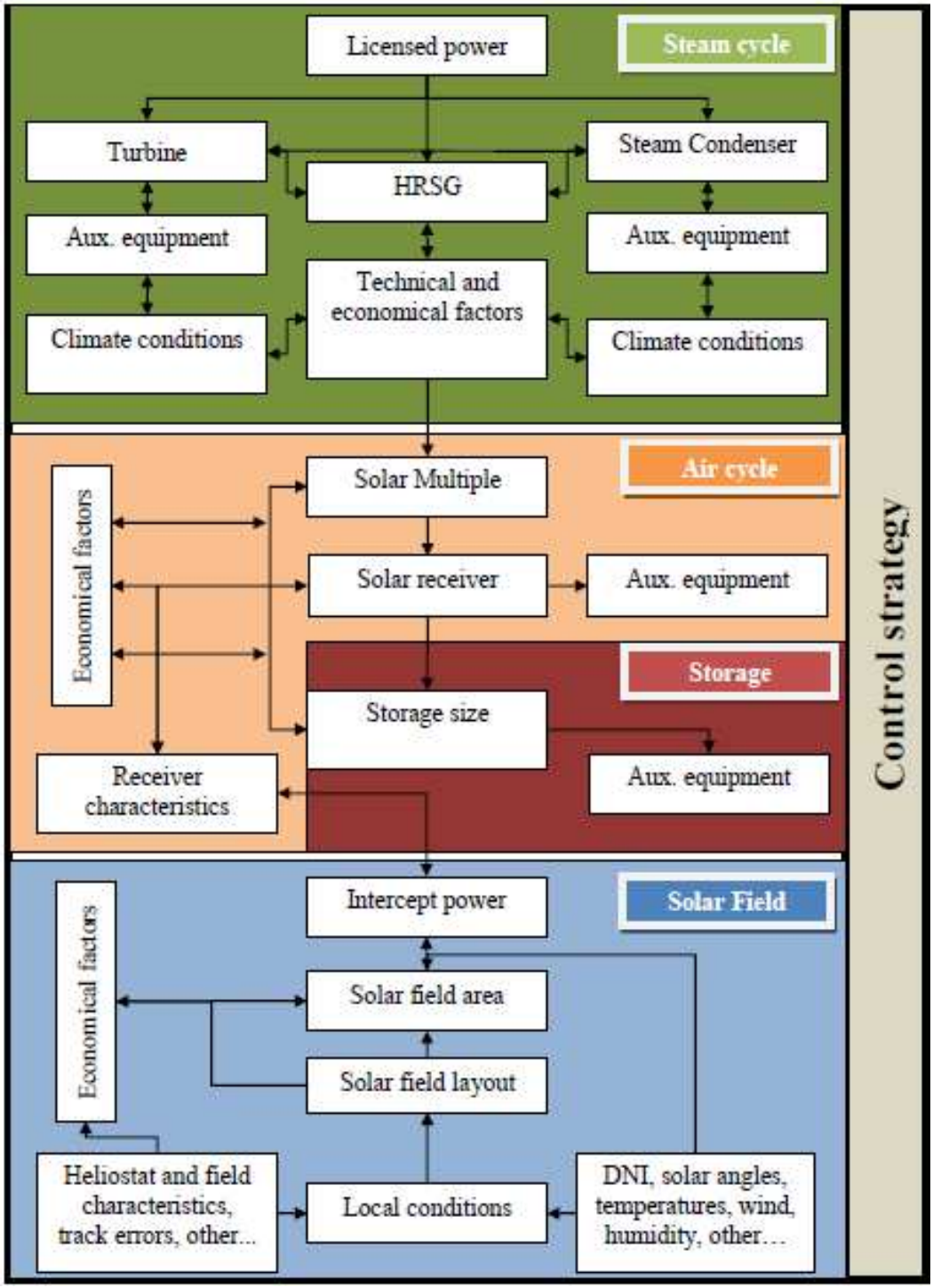

Figure 2.19: Power circuit optimization strategy.

Thermal engines and machines have a theoretical maximum efficiency when converting energy to work: the Carnot efficiency. During this conversion, entropy accumulates in the system, and is removed by dissipating heat. The power cycle receives thermal energy at high temperature, converts some of that energy into mechanical work, and rejects the remaining at a lower temperature. The thermal efficiency of an engine operating under Carnot cycle is defined as:

$$\eta_{Carnot} = \frac{work\ generated}{heat\ input} = 1 - \frac{T_{out}}{T_{in}} \tag{2.24}$$

where T_{out} and T_{in} are the absolute temperatures at which heat is added and rejected by the Carnot heat engine, respectively. The thermal efficiency of an engine is therefore proportional to the ratio between the input temperature of the cycle and the temperature of heat rejection. The wider the difference in temperatures, the more efficient the conversion of heat into work by the Carnot engine is. Because it is a limiting scenario, real engines operate in other cycles than the Carnot cycle. Those cycles operate at lower efficiencies than the Carnot cycle. However, the effect of temperature on the efficiency is still valid for real engines, Equation 2.25. The variation in efficiency of a real engine can then be represented by:

$$\eta_{Real} = K_{Real} \times \eta_{Carnot} \tag{2.25}$$

where K_{Real} represents the fraction of the Carnot efficiency reached by the real engine and η_{Carnot} the equivalent Carnot cycle efficiency.

Equation 2.24 indicates that power circuit efficiency increases with the increase in input temperature T_{in}. The use of very high temperatures is limited by the materials applied and the costs associated to the power block. Contrarily, the solar receiver has higher efficiencies for lower operational temperatures, mainly due to the radiation losses, Equation 2.26 and 2.27 [8].

$$\eta_{Receiver} = \frac{\dot{Q_{out}}}{\mathrm{I}_{b,a}\ A_a} \tag{2.26}$$

$$\eta_{Receiver} = \eta_{Opt} - \frac{U_l(T_r - T_a)}{\mathrm{I}_{b,a}\ CR_g} - \frac{\epsilon\ \sigma_B\left({T_r}^4 - {T_a}^4\right)}{\mathrm{I}_{b,a}\ CR_g} \tag{2.27}$$

where A_a is the receiver area (m^2); CR_g is the geometrical concentration ratio; $I_{b,a}$ is the radiation flux into the receiver ($W \cdot m^{-2}$); $\dot{Q_{out}}$ is the receiver output heat (W); T_a is the atmospheric temperature (K); T_r is the receiver operational temperature (K); U_l is the receiver heat transfer coefficient ($W \cdot m^{-2} \cdot K^{-1}$); ϵ is the receiver emissivity and σ_B is the Stefan-Boltzmann constant (5.6696×10^{-8} $W \cdot m^{-2} \cdot K^{-4}$).

According to Stine et at. [8] the overall efficiency of the system is well approximated by the product of the real machine efficiency and effectiveness of the collector. The analysis of the overall efficiency versus the operating temperature curve allows finding an operating temperature ($T_{rec,max}$) that maximizes system efficiency, Equation 2.28 and 2.29 [8] which, applied to the selected receiver, results in Figure 2.20.

$$4C_3{\theta_{max}}^5 - 3C_3{\theta_{max}}^4 + C_2{\theta_{max}}^2 = C_1 + C_2 + C_3 \quad (2.28)$$

$$\theta_{max} = \frac{T_{rec,max}}{T_a};\ C_1 = \eta_{Opt};\ C_2 = \frac{U_l T_a}{I_{b,a}\ CR_g};\ C_3 = \frac{\epsilon\ \sigma_B {T_a}^4}{I_{b,a}\ CR_g} \quad (2.29)$$

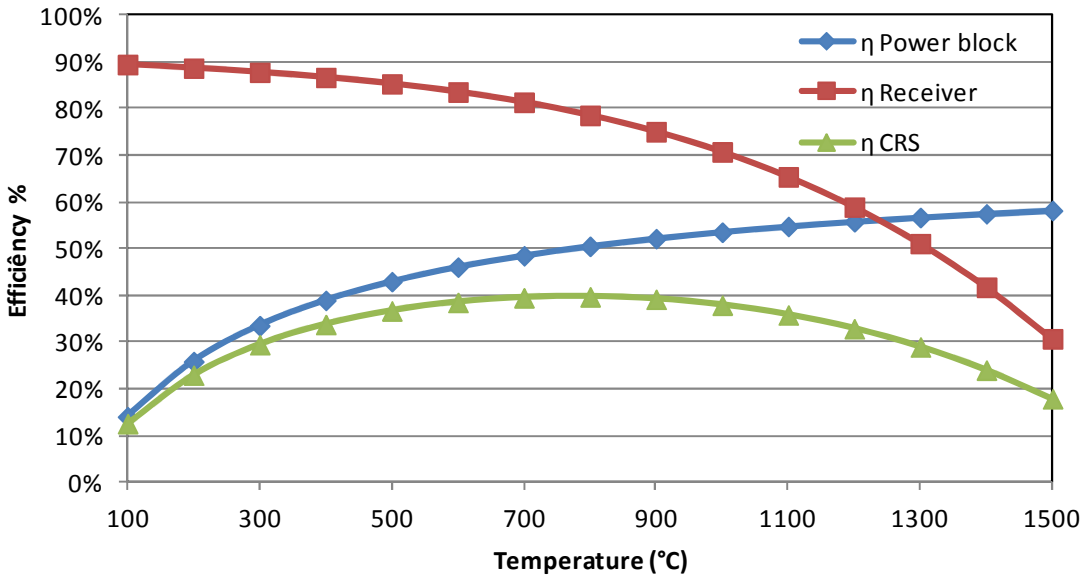

Figure 2.20: Definition of the best power plant operational temperature range.

For CRS the range of ideal operating temperature is between 600 and 900 °C, Figure 2.20. For this temperature range, the CRS efficiency is maximized, although it may be extended from 500 to 1100 °C with only a small drop in efficiency.

2.2.3 Steam cycle

2.2.4.1 Steam turbine

Turbines are the most commonly used equipment for expansion in solar Rankine cycles. Typically, the efficiency of these devices is measured in relation to the ideal adiabatic and reversible expansion. An ideal turbine operates at constant entropy, unlike commercial turbines, which have higher entropy at steam outlet than at inlet. As already mentioned, there are several manufacturers of steam turbines, and each is in the process of developing new equipments to use in CSP plants. The process of modelling a commercial steam turbine in detail can be extremely complex. Ebsilon has a simplified steam turbine model that was used, adding some characteristic lines for off-design operation, Figure 2.21.

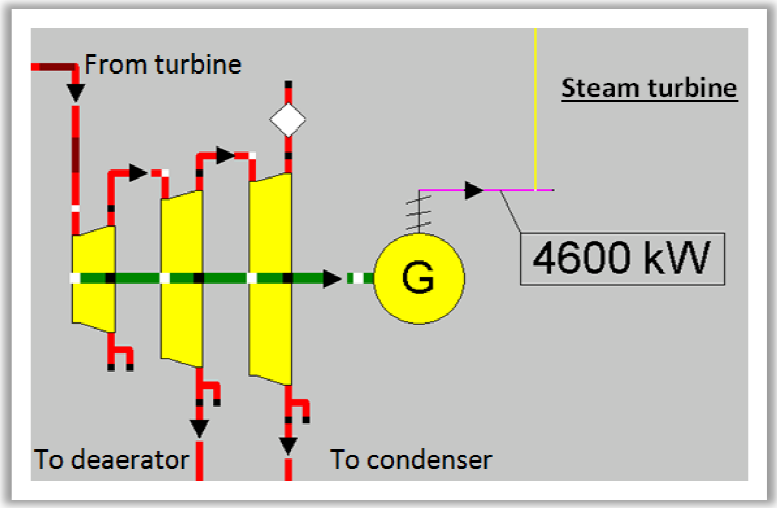

Figure 2.21: Ebsilon steam turbine graphical representation.

In Ebsilon the turbine number of stages and extraction can be defined. In the case of the last stage, the pressure must be set by the user to indicate the existence of back pressure, or not, in the turbine system. Regarding turbine losses (at the entrance and exit), they can be calculated using the parameter QLOSSM - which is a constant parameter of mechanical losses, regardless of the load. Alternatively, two characteristic lines can be defined (CKIN1 and CKIN2), representing losses in the entrance and exit of the turbine stage, respectively, when the operational mode (FSPEC) is set to "Total isentropic efficiency".

A turbine manufacturer (SIEMENS) was contacted to determine which would be the most suitable steam turbine for application in the specific CRS, and that would allow a future adaptation of a biomass module running in parallel/series to obtain the installed power

granted by the PIP (SOLMASS project). The suggested turbine was the SST-110 Model (Figure 2.22), characterized for its quick starts without preheating and by a "twin" structure, which is based on two individual "twins" that allow a great versatility of operation; an advantage in terms of increased hybridization possibilities and part load operation.

Figure 2.22: SIEMENS steam turbine SST-110 Model **[11]**.

Alternatively, a concept of three stages composed of three TSS-060 modules has been proposed [12], which also increases the versatility of integration, but showed a 10% higher cost compared to the SST-110 solution. Both options can be tuned to operate under different conditions: so, a large spectrum of options was requested to the manufacturer. Unfortunately, only a few configurations were given by the manufacturer and theoretical models were developed to study different possibilities/concepts to be applied in the power plant. These models were subsequently adjusted to agree in terms of performance with commercial data from the manufacturer. In the case of power plant construction the models should be readjusted to exactly match the commercial solution. This was also the methodology in the case of the electric generator and the heat recovery steam generator.

2.2.4.2 Heat recovery steam generator (HRSG)

HRSGs are usually classified according to firing, layout and configuration. One of the ways to classify the HRSG is based on the use of auxiliary power: with or without duct burner. Some HRSGs only use exhaust gases (e.g. from a gas turbine or other process as a power source) and have their performance affected by this upstream equipment: e.g. in the case of a gas turbine part load operation, the HRSG steam production can be reduced, affecting its operation. To avoid such situations, a duct burner or supplementary firing equipment can be added. Another way of classifying the HRSG is the gas flow path: vertical or horizontal. In terms of performance and cost, these are equivalent systems and its use is only dependent on the type of manufacturer or customer preference regarding the layout. A different way to classify

HRSGs is their operational configuration, e.g. the pressure levels: single pressure HRSG, or multi-pressure, or if they have re-heater. The smaller HRSGs are typically single pressure, in a manner similar to a combustion boiler. In larger HRSGs, to optimize the performance, steam generation occurs in circuits of different pressure. A more recent concept for larger HRSGs is the once-through HRSG (or Benson type). The Benson HRSG retains all the virtues of the proven natural circulation principle of drum-type steam generators, yet replaces the high-pressure drum with thin-walled components. Figure 2.23 presents the different commercial types of HRSG [13, 14, and 15].

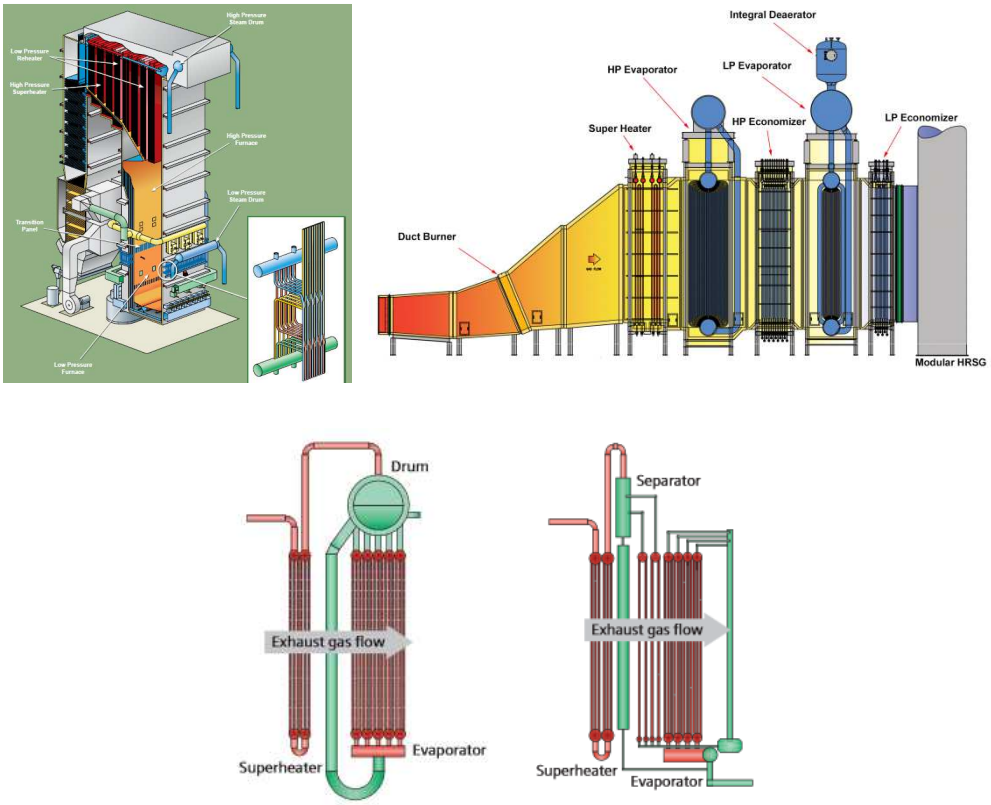

Figure 2.23: Different HRSGs: vertical (up left), horizontal (up right), single pressure with steam drum (down left) and Benson type (down right) **[13, 14, 15]**.

Two of the most important HRSG design variables are the Pinch Point and Approach Temperature. These variables define the equipment characteristics, Figure 2.24.

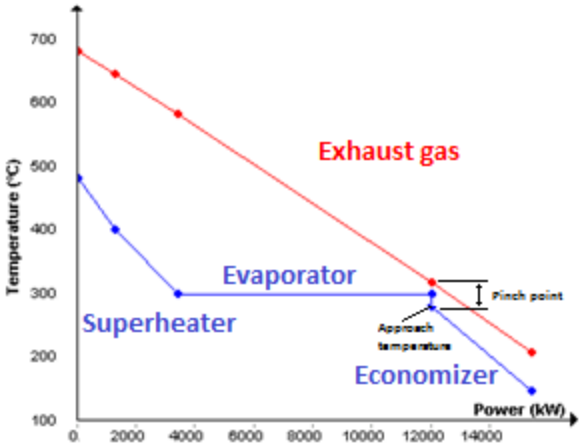

Figure 2.24: **Single pressure HRSG temperature and energy transfer profile.**

Equipments with low pinch point and approach temperature maximize the generated steam, but also increase the heat exchange area leading to an increase in equipment cost. Typically, a HRSG with an 8 °C to 14 °C pinch point will have a 50 % higher heat exchanger area, compared to a HRSG with a 22 °C to 28 °C pinch point [16]. In the case of high pinch point and approach temperatures, the HRSG evaporator performs inefficiently. Also, the incorrect definition of pinch point and approach temperatures could lead to errors on the analysis; e.g. the utilization of low approach temperatures for high saturation point temperature lead the HRSG economizer to heat the fluid up to high temperatures, with the possibility of generating steam in the economizer [17]. Several manufacturer and references for pinch point and approach temperature ranges for the HRSG evaporator are presented in Table 2.5.

Table 2.5: HRSG evaporator pinch point and approach temperature ranges.

Evaporator type	**Bare tubes [17]**		**Finned tubes [17]**		**Garioni Naval [18]**	**Bertsch [19]**
Gas temperature (°C)	350-650	650-1000	350-650	650-1000	< 950	< 1500
Pinch Point (°C)	44-72	72-83	5-17	17-33	3-14	8-33
Approach Temp. (°C)	5-22	22-39	5-22	22-39	8-17	11-27

The selection of the pinch point and approach temperature is done regarding technique and economic factors. Also, it is important to associate the pinch point and approach temperature to the HRSG operational conditions. An increase in pressure from 40 to 80 bar represents an increase of 4 % in the global efficiency of the power circuit, Figure 1.1 [13]. Nevertheless, high pressure HRSGs are only viable for large power blocks, because otherwise the flow rates of the equipment would be low and could cause physical problems.

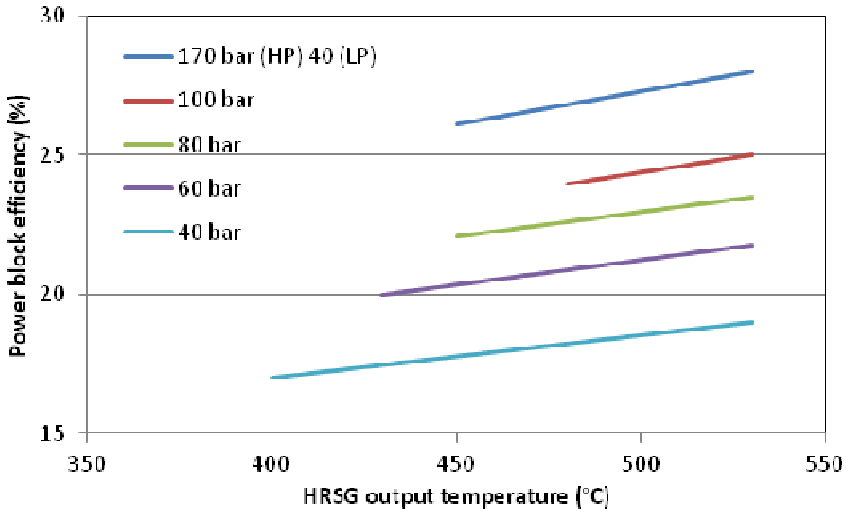

Figure 2.25: Babcock & Wilcox HRSG output steam temperature influence in the power circuit efficiency [13].

2.2.4.3 Air cooled condenser

The turbine exhaust is sent to the condenser with a specific enthalpy and pressure. The condenser selected for the power plant is an air cooled condenser. On one side, atmospheric air is forced by an aero-generator to the condenser to condense the steam in the other side. The air cooled condenser Ebsilon model is composed by the combination of a condenser and an air ventilator that feeds the condenser, Figure 2.26. In design mode, the flow and properties of the exchanger $(k \times A)$ are calculated based on the vapour pressure and the design temperature difference specified by the user. The off-design performance assumes that the component performance is known and is specified by a characteristic line. The exhaust pressure is calculated for complete condensation of the steam. Heat losses to the periphery are represented by a loss factor - DQLR.

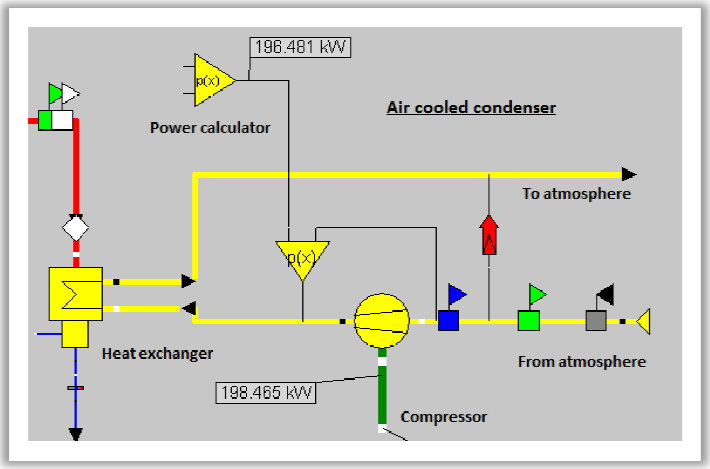

Figure 2.26: Air cooled condenser Ebsilon model.

The heat dissipated by the heat exchanger is fixed by the properties of the steam, and the cooling air flow is calculated. The condenser pressure is, in practice, limited by the properties of the coolant and by the turbine exhaust system conditions, with a minimum pre-defined pressure (FP3MIN) - in this case considered as 1 mbar. The condenser fan electricity consumption is defined by the following equation [20]:

$$N_V[kW] = (140\ to\ 150)\frac{\dot{M_D}\left[\frac{t}{h}\right]}{(T_{condenser} - T_{ventilator})[K]} \quad (2.30)$$

where $\dot{M}_D$ is the mass flow rate of steam that is multiplied by a factor between 140 and 150 (in this case 145 was used) and divided by the temperature difference between the condenser inlet and the ventilator air inlet.

2.2.4.4 Steam cycle configuration

The steam cycle can be designed to have different heat recovery / extraction streams, increasing or decreasing its complexity, efficiency and cost. The steam cycle configuration applied on early atmospheric air volumetric CRS is the Rankine cycle with superheating, Figure 2.27.

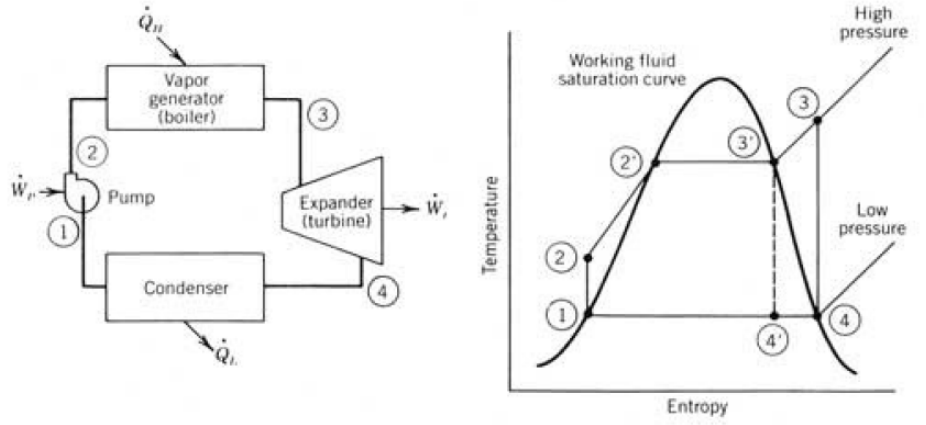

Figure 2.27: Rankine cycle with superheating scheme (left) and respective Temperature-Entropy diagram (right) [8].

The water from the condenser outlet (point 1) is pumped (in the case of Figure 2.27 by an ideal pump in reversible adiabatic operation) and the pressure increases up to the state 2 where it will feed the HRSG. The compressed fluid is heated at constant pressure (pre-heating) to achieve a state of saturated liquid (point 2'); then it is evaporated at constant temperature and pressure until all the liquid has evaporated to saturated steam (evaporator - point 3'). At this point the saturated steam enters the superheater part of the HRSG, where, at constant pressure, the steam increases its temperature to state 3. The superheated steam is then conduced to the expansion device (turbine) and expands (adiabatically) down to the pressure set by the condenser (point 4). The condenser converts exhaust from the turbine into liquid, releasing heat to the environment $(\dot{Q}_L)$.

To reduce the heat load on the boiler (heat necessary to raise the fluid to the superheated state), and to elevate the average temperature of heat addition, a Rankine cycle with reheat is used. This steam cycle configuration allows increasing the temperature at which heat is added to saturated liquid by the boiler, but also assures that the steam leaves the turbine still relatively dry. As illustrated in Figure 2.28 [8], partially expanded steam is removed through a turbine intermediate stage, point 7, which is led back to the steam generator, re-heating the steam to state 8. The reheated steam generally reaches similar (or lower) temperature than the steam at point 6, but is at lower pressure. The steam is then reintroduced in a second turbine stage (operating at low pressure) which generates more work as it expands to the condenser pressure. This process generally results in improved thermal efficiencies.

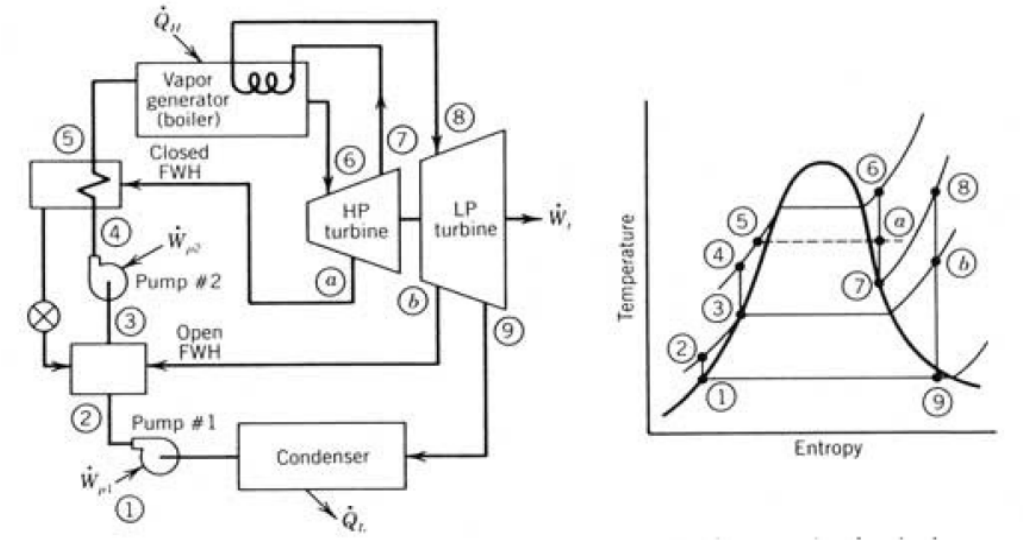

Figure 2.28: Rankine cycle re-heating scheme (left) and respective Temperature-Entropy diagram (right) [8].

The regeneration of a Rankine cycle can be accomplished in two ways: a) and b), Figure 2.28. The first (a) is commonly called feed water preheating; the steam which is partially expanded in the first turbine stage is extracted from point (a) and is used for preheating the liquid before entering the boiler, point 5. In the second option (b), part of the steam from the second turbine stage flows through a heat exchanger heating the compressed fluid before it enters the boiler. Both (open and closed) feed-water heaters are commonly used: the open preheater heats the feedwater from state 2 to state 3 by mixing it with steam extracted from the turbine at point b. The extracted steam pressure must be the same as that defined by pump # 1. Pump # 2 raises the liquid pressure to the pressure of the boiler; the closed preheater is used for higher pressure applications, since it preheats the liquid from state 4 to state 5 using extraction of high pressure steam from the turbine at point (a), which can afterwards be drained, as condensate, to the open preheater. The extracted steam pressure does not need to be the same as the compressed fluid, since they are independent and isolated streams.

Large solar power plants can use two or more stages of reheating to improve their efficiency, as well as several pre-heaters and turbine stages. However, there is a balance between the number of components and the gains in terms of efficiency and cost. For each power plant (and its particularities) several commercial consultations should be done.

2.2.4 Air cycle

2.2.5.1 Receiver and solar multiple

A particularity of solar thermal applications is that usually the energy is given by an external source (solar receiver) that heats a heat transfer fluid (HTF), as opposed to internal combustion engines where the potential energy is already intrinsic to the fluid. Therefore, it is necessary to choose the HTF, which can be pumped directly to the receiver or by incorporating an additional intermediate HTF between the receiver and power circuit. There are advantages and disadvantages to both. The incorporation of an intermediate HTF results in the need for another pump, a heat exchanger and a second HTF (results in increased system complexity, but often will reduce the size of the receiver due and the cost of high pressure piping). Pumping the working fluid directly to the power cycle can make the system difficult to control, especially in transient periods, because for Rankine cycle systems, preheating, evaporation, and overheat would occur in the receiver. Despite that, the concept is quite simple, may work more efficiently and with less initial investment, since less components are necessary.

Receiver flux design is another variable to consider. Tubular receivers are difficult to operate at incident fluxes above 600 kW/m^2 (peak) [21], because the tubes may not resist the continuous thermal and mechanical stresses. In volumetric receivers (applied in atmospheric air technology), highly porous structures operate as convective heat exchangers absorbing the concentrated solar radiation. Air is forced through the porous structure (cooling the structure) and is heated by convective heat transfer, allowing incident fluxes larger than 1000 kW/m^2 (peak) [21]. Table 2.6 presents the operating temperatures and flux ranges of the available CRS solar receiver technologies [21].

Table 2.6: Operating temperatures and flux ranges of CRS solar receivers [21].

Fluid	**Tubular receiver**			**Volumetric Air**
	Water/Steam	**Liquid Sodium**	**Molten Salt (nitrates)**	
Average Flux (kW/m^2)	100-300	400-500	400-500	500-600
Peak Flux (kW/m^2)	400-600	140-2500	700-800	800-1000
Fluid outlet temperature (°C)	490-525	540	540-565	700–800 (>800)

The receiver design is dependent on the thermal power necessary for the power block and the excess of power necessary to fill the storage device. This ratio is defined as the solar multiple: the ratio between the thermal power generated by the collector system (solar field and receiver), at the design point (DP) and the thermal power required by the power block at nominal conditions, Equation 2.31.

$$SM_{DP} = \frac{Q_{Rec,DP}}{Q_{PB,DP}} \tag{2.31}$$

In solar-only power plants the solar multiple is always greater than one, so the full load power block operation is not confined only to clear sky solar conditions. The increase in solar multiple also represents a higher capital investment (CAPEX), larger solar field, land area and receiver costs. Also the increase in solar multiple represents an increase in the solar field intercept power, Figure 2.29.

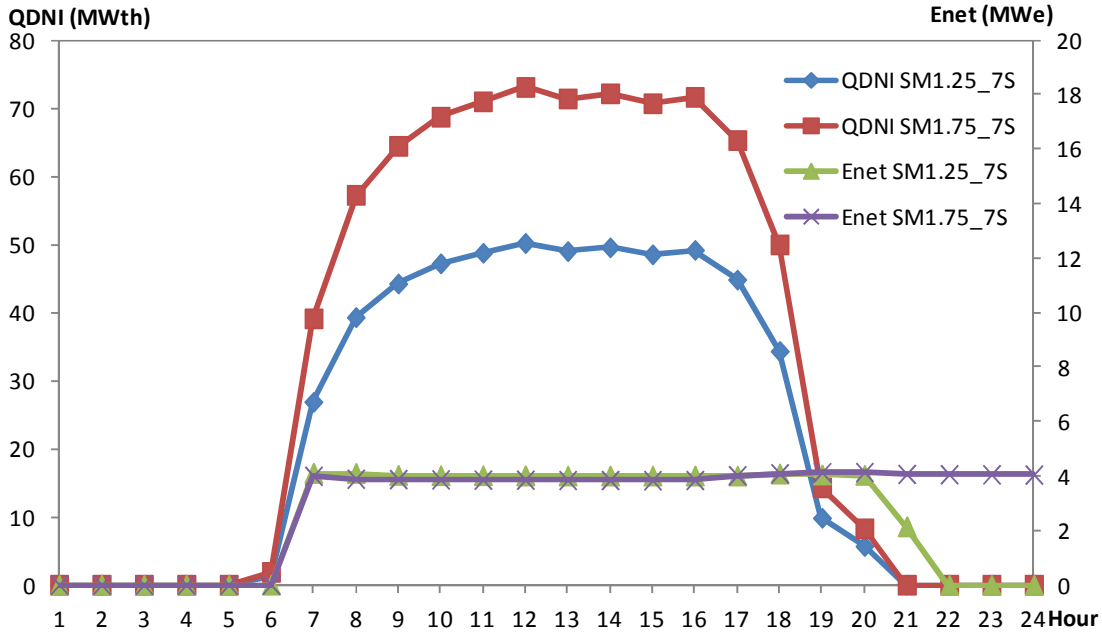

Figure 2.29: Typical summer day history of available power from the solar field and generated electricity as a function of different solar multiples (lines are for readability).

The power plant with 1.75 solar multiple (SM1.75_7S, Figure 2.29) collects more solar energy than the power plant with solar multiple of 1.25 (SM1.25_7S, Figure 2.29) and, as result, the period of power block full load operation is extended. This is only possible using thermal energy storage (TES); otherwise the energy exceeding maximal power block input must be dumped.

2.2.5.2 Thermal energy storage – storage size

With TES it is possible to decouple power generation from the solar resource. Electricity generation can occur without solar resource and/or on demand by the electricity network, Figure 2.29. The TES unit provides an affordable and efficient solution to dispatchable CSP electricity generation. It is thus possible to adapt the electricity generation profile to the national electricity demand, decreasing the need of backup and stand-by power. The Portuguese electricity consumption during a typical summer day is presented on Figure 2.30.

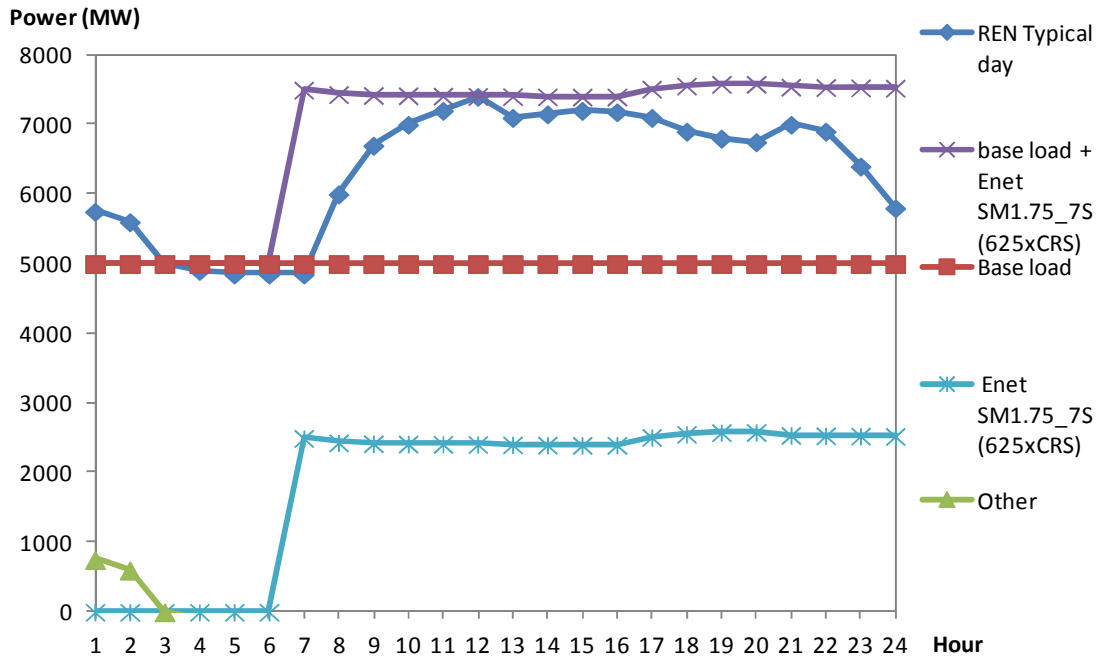

Figure 2.30: Scenario for CSP potential and Portuguese electricity consumption - REN typical day [22] (lines are for readability).

A possible way to supply the electricity demand with CSP is by using large thermal energy storage that allows operating almost on a 24-hour daily base, Figure 2.30. As this is a costly solution, an alternative is to use the CSP hybridization potential. But even using only CSP it is possible to respond to the Portuguese network consumption day peak (7:00 to 24:00) with 625 CRSs (4 MW_e each with SM of 1.75 and 7 hour storage – total 2.5 GW installed power), generating 10.2 TWh of electricity per year. This is far from the 142 TWh economic potential referred by the MED-CSP study [23] for CSP power plants in Portugal. Although this scenario is not probable to occur in the short term, CSP technologies can provide base load power, either in solar only mode or in more cost efficient hybrid solutions. Even in these hybrid solutions the storage unit confers stability and reliability to the electricity generation, preventing component failure and improving power plant performance.

As in the case of atmospheric air volumetric CRS the HTF is atmospheric air, and, because air has very low energy density and conductivity, direct active heat storage is not a good solution. The technology applied in the Jülich solar tower is a regenerator-type storage (passive storage), where a gaseous heat transfer fluid is in direct contact with a solid storage medium and exchanges heat as it flows along a path through the storage medium [24]. The storage device is a rectangular housing of 7 x 7 x 6 m^3 (total volume of 120 m^3), divided into four chambers of identical size, filled with a ceramic storage material, and connected in parallel. The storage system operates between 120 and 680 °C and has a capacity of almost 9 MWh. The total heat loss in a 24 h period is 930 kWh (fully charged storage) with a pressure drop of 15 mbar [24]. There are some limitations on the number of equivalent hours of storage (between 3 and 6 hours), due to technological and economic reasons [25].

The optimal storage capacity depends on the solar multiple and control strategy. The control strategy is the power plant operational strategy and varies during the day, e.g. according to network special needs, contract with the electricity purchase entity, feed-in tariff, technologies used in the power plant and available staff. Several countries have premium feed-in electricity tariffs for producers during the day, while others have fixed feed-in tariffs or forecast obligations [26]. In the Portuguese case, the power plant operator can choose if he wants to receive the same remuneration regardless of the time of day, or a higher tariff for electricity generated during the day than during the night. In the last case, the amount of electricity generated between 8:00 and 22:00 during wintertime and 9:00 and 23:00 during summertime is multiplied by 1.25 and the rest of the electricity is multiplied by 0.6 [26]. As the feed-in tariff calculation formula is complex, the regulators release the value for each project or call; in the case of the latest CSP call, the feed-in tariff is 0.273 €/kWh [26].

2.2.5.3 Ebsilon model for the air cycle

The receiver model was based on the 3D interpolation of measured data from Jülich solar tower, provided by DLR on Figure 2.15. The receiver input is the solar intercept power given by HFLCAL which heats a cold air stream (60 % recycled and 40 % fresh air) up to a temperature of 680 °C (at design conditions) with a flow rate defined by the discharge and charge controllers. Ambient conditions are based on Meteonorm hourly data. The hot air stream is forwarded to the storage device and the HRSG, Figure 2.31.

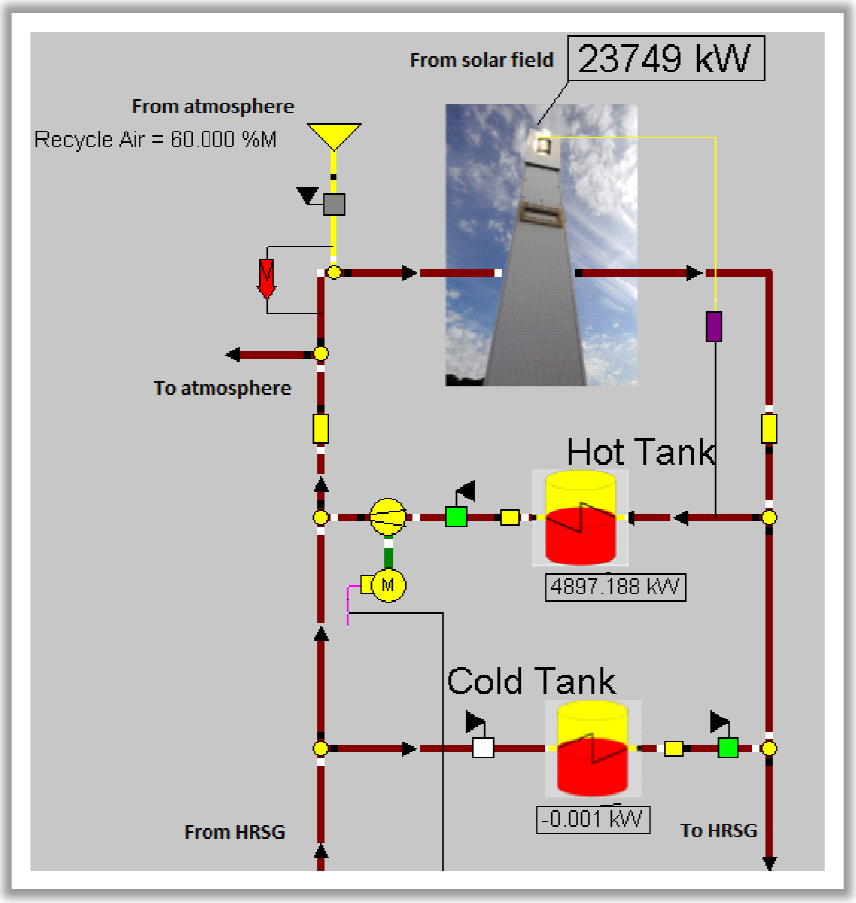

Figure 2.31: Ebsilon model for the receiver and storage.

The quantity of energy that is forwarded to the storage is defined by the solar multiple and the control strategy. At design conditions the HRSG is supplying the power block required energy to generate the 4 MWe net and the excess is stored. The ceramic storage is designed for large contact surfaces so heat transfer is optimized. The air can flow through the storage in both directions (charging and discharging) but the storage temperature varies during charging and discharging. Due to Ebsilon restrictions the storage module was divided into a cold and a hot tank Figure 2.31. However in the power plant there is a single storage device with the temperature profiles presented in Figure 2.31 [27] for charging and discharging.

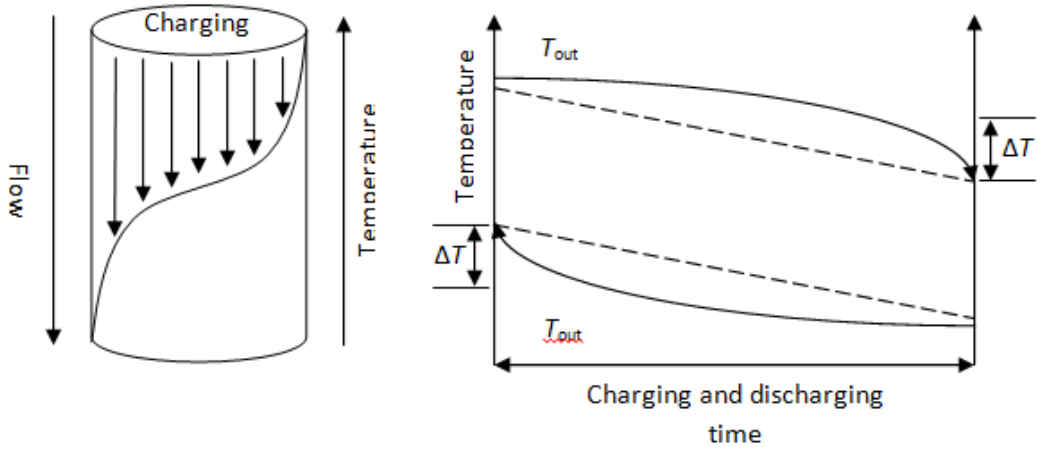

Figure 2.32: Ebsilon storage temperature profile.

The storage output temperature is thus influenced by the HTF properties (temperature, flow rate), the actual available storage capacity and the storage design properties (e.g. materials, layout, etc.). These temperature differences can be estimated by the dashed line in Figure 2.32, which can be defined by the following equations [27]:

$$T_{out\ charge} = T_{min} + 0.1 \times \Delta T_n \times \frac{ES}{SM} \tag{2.32}$$

$$T_{out\ discharge} = T_{max} - 0.1 \times \Delta T_n \times \left(1 - \frac{ES}{SM}\right) \tag{2.33}$$

$$\Delta T_n = T_{hot,nominal} - T_{cold,nominal} \tag{2.34}$$

The hot air then flows from the storage or receiver to the HRSG and its exhaust is sent back to the receiver, closing the power plant air cycle. There are several possible HRSG configurations. The simplest configuration of HRSG is composed by an economizer, evaporator and a superheater, which is illustrated in Figure 2.33. There are several connections to the steam cycle, e.g. a turbine extraction to the deareator or a feedwater extraction to be injected in the superheated steam to prevent sudden temperature increases. Several controllers are considered to maintain stable temperatures.

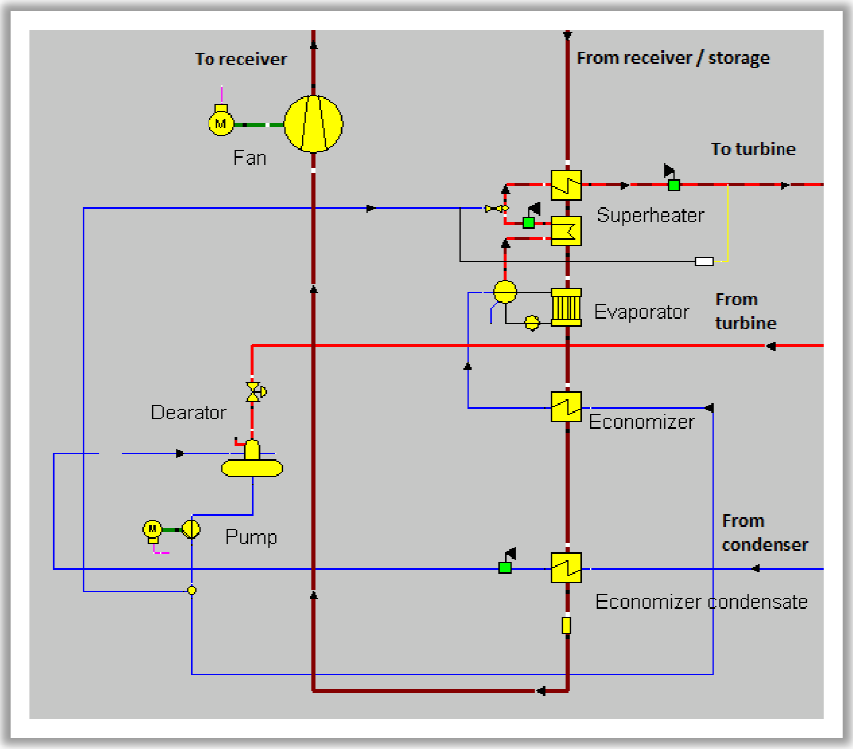

Figure 2.33: Ebsilon model for the receiver and storage.

2.3 Software integration

The design and annual simulation of atmospheric air volumetric central receiver power plants is an iterative process and can be performed with several simulations tools. Some simulation tools such as NREL SAM, DLR GREENIUS or the ECOSTAR methodology use a simplified and intuitive approach, with very low calculation times, that allow studying different power plant configurations for an overall technical and economical perspective. On the other side, there are some complex models and tools that allow studying, with very good precision, individual parts but not the overall plant, e.g. solar radiation, solar field, receiver performance, power block, costs, etc. These models need more calculation time and require detailed estimation of the variables to increase precision.

For the present work, models with good accuracy and reasonable calculation times were created, so that CRS power plants could be optimized up to the detailed engineering and definitive cost evaluation stage. With this purpose, three tools were selected: Heliostat Field Layout Calculation (HFLCAL) for solar field optimization, Ebsilon Professional for power circuit optimization, and Excel for software compilation and economic evaluation.

Microsoft Excel was selected as compilation software because it is highly integrated with Ebsilon. Several models were built and optimized using Ebsilon Professional, while the solar field was designed and optimized using HFLCAL, and power plant economics were defined in Excel. For each time step Excel sends user defined input variables to Ebsilon, runs the Ebsilon model and gathers the results back to Excel. The integration of HFLCAL, Ebsilon and Excel in the model is presented in Figure 2.34.

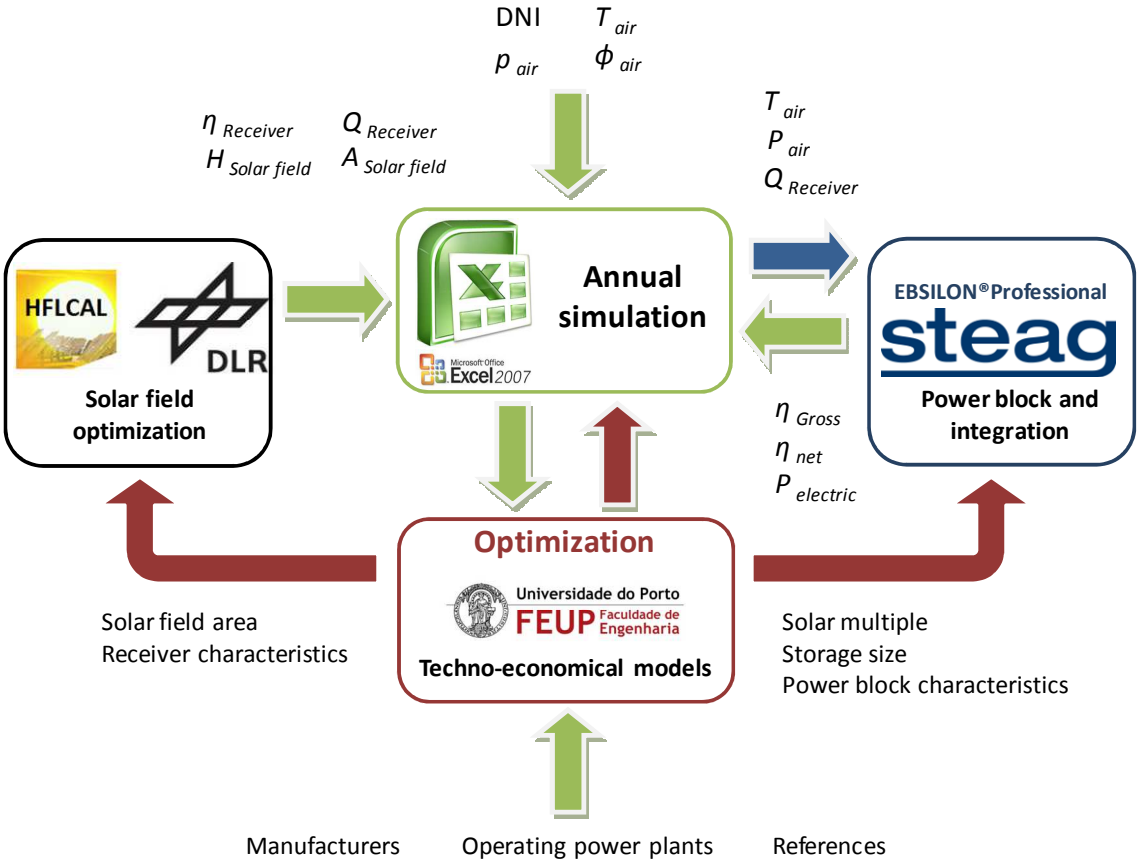

Figure 2.34: Compilation of tools used for the power plant design and annual simulation.

2.4 Economic model

2.4.1 Levelized electricity cost

The power plant LEC was calculated according to the IEA Method [25]. To compare the different approaches, a combination of LEC plus sensitivity analysis was used to choose the best alternative and analyse the impact of different variables on the generated electricity cost. The LEC is dependent on the power plant capital investment (CAPEX), debt interests and insurance rates, annual operation and maintenance costs, annual fuel costs and generated annual net electricity, according to Equation 2.35 [25].

$$LEC = \frac{C_{rf} \times CAPEX + K_{O\&M} + K_{fuel}}{E_{net}} \quad (2.35)$$

where C_{rf} is the insurance and debt interest coefficient rate; CAPEX is the capital expenditure for the power plant; $K_{O\&M}$ is the annual operation and maintenance costs; K_{fuel} is the annual fuel costs and E_{net} is the annual net electricity.

Power plant C_{rf} was considered to be 9.88 %, for a 30 year lifetime expectance. CSP power plants lifetime, for economic calculations, is usually considered between 20 and 40 years. Above this period power plant degradation may require to substitute key components such as the mirrors, receiver, etc., which are unaccounted in the regular maintenance costs. Annual operation and maintenance costs were considered for local conditions, using a percentage of CAPEX for fixed O&M costs, variable O&M costs and water usage costs (mainly heliostat cleaning, etc.) [25, 28].

2.4.2 Cash flow analysis

A more comprehensive economic model was built, calculating the cash flows and finding the investment return rate and period, based on SAM [28]. This project cash flow analysis is dependent on financial factors (fraction of own capital used, amortization structure, debt payment structure and methods used for future cash flow calculation) and power plant technical factors (power degradation, equipment performance and cost). The estimations considered for the cash flow analysis were: a 30 % own capital, a 20-year loan with an interest rate of 8 %, a 1 % annual insurance rate, a linear amortization for 20 years, current national profit taxes and a conservative 1 % of power degradation. The cash flow was done for the 30 years of power plant life time and the cash flow year is indicated by the letter *n* ranging from *n* = 0 (year zero) to *n* = 30 (the last year). The electricity generated for year one is not constant for the remaining years. The power plants suffer degradation of equipments, reducing their performance, usually generating less electricity and therefore lower operational income. The annual generated electricity and the operational income are approximated by the following equation:

$$Energy\ in\ year\ n = Energy\ in\ year\ 1\ \times (1 - Degradation\ rate)^{n-1} \quad (2.36)$$

$$Energy\ value = Electricity\ (kWh) \times feed\ in\ tariff\ (\frac{€}{kWh}) \quad (2.37)$$

The power plant operational expenses are: operation and maintenance (O&M) costs, fuel costs, insurance, financing costs and local taxes. For solar only power plants, the fuel cost

is zero. The O&M costs are divided into the Fixed O&M costs and the variable O&M costs and are defined by:

$$Fixed\ O\&M = Personal\ cost\ \left(\frac{€}{yr}\right) + Fixed\ cost\ per\ capacity\ \left(\frac{€}{kW\ yr}\right) \times System\ capacity\ (kW) \quad (2.38)$$

$$Variable\ O\&M = Variable\ cost\ per\ electricity\ generated\ \left(\frac{€}{MWh}\right) \times Annual\ output\ (MWh) \quad (2.39)$$

$$Annual\ property\ tax = Property\ evaluation\ (€) \times Local\ tax\ (\%) \quad (2.40)$$

The insurance costs were considered constant for the power plant life cycle, as in the case of the LEC analysis with a fixed rate of 1 % of the CAPEX [25]. To define the financing costs several concepts are important: Debt balance, Debt interest, Debt repayment and total payment. The debt balance for the first year is defined by:

$$Debt\ balance = (-CAPEX + Incentives) \times Debt fraction \quad (2.41)$$

If there are no incentives for the subsequent years the debt balance is defined by:

$$Debt\ balance(current\ year) = -Debt\ balance\ (previous\ year) - Debt\ repayment\ (previous\ year) \quad (2.42)$$

The total debt payment per year for the power plant is the amortization to the bank loan (debt repayment) and the debt interest payment to the bank for loaning the money (debt interest payment).

$$Total\ payment = Debt\ interest + Debt\ repayment \quad (2.43)$$

$$Debt\ interest = Debt\ balance + Loan\ interest\ rate \quad (2.44)$$

The last factors to be accounted in the power plant cash flow analysis are the national taxes. In Portugal (in 2012) the following values apply: a 23 % sales taxes (VAT), the local municipally applies a 0.7 % property tax and the corporate profit taxes are 25 % or 12.5 %, depending on the company taxable income being above 12 500 € or not, respectively. The amortization of the equipment was considered with an annual tax of 5 %. This tax model is simplified and a more detailed model should be conducted in the future, as further tax savings can be obtained. Also the Portuguese tax model has been suffering some alterations in recent

years so the moment of application is essential for the correct interpretation of the cash flow analysis.

$$Sales\ tax\ deduction = Sales\ tax\ (\%) \times Percentage\ of\ direct\ costs\ aplicable\ (\%) \times Total\ direct\ costs\ (€) \quad (2.45)$$

$$Profit\ taxes = Taxable\ income\ less\ deductions\ \times Tax\ rate\ (\%) \quad (2.46)$$

The after taxes cash flows are the result of the balance from the operational income and expenses, considering the national taxes. The after tax cash flow is influenced also by the inflation (i) during the project life cycle, and it is usual to obtain project economical indicators such as the net present value (NPV), payback period (period of time required by the project to repay the investment to investors) and the internal rate of return (IRR).

$$NPV = \sum_{n=1}^{n} \left(\frac{C_{after\ tax,n}}{(1+i)^n} \right) + C_{after\ tax,0} \quad (2.47)$$

The net present value is the present value of the after tax cash flow discounted to year one using the nominal discount rate, plus the after-tax cash flow in year zero. The net cash flow for each year is the difference between the revenue and cost in that year. A project's net present value is a measure of a project's economic feasibility that includes both revenue and cost. In general, a positive net present value indicates an economically feasible project, while a negative net present value indicates an economically unfeasible project. The year when the NPV equals zero is the payback period.

The internal rate of return on an investment or project is the rate that makes the net present value of all cash flows equal to zero. It can also be defined as the discount rate at which the present value of all future cash flow is equal to the initial investment. IRR analysis is used to evaluate the attractiveness of investments or projects. For similar CAPEX projects, the project with the highest IRR would be considered the best. The IRR is an indicator of the efficiency, quality, or yield of an investment and is a contrast to NPV, which is an indicator of the value or magnitude of an investment. An investment is considered attractive if the IRR is greater than the cost of capital, or at least higher than the predicted inflation for the project lifetime [28].

2.5 Conclusions

HFLCAL and EBSILON are good software tools for solar field and power block design and simulation, respectively. Their use for CRS simulation allowed developing several power plant design options and new concepts. A complete CRS model was developed by integrating HFLCAL and EBSILON with other software tools (Excel, control algorithms) and an economic model. Integration of different technologies and fuels was also done. Robust models were built with reasonable calculation times for the design and optimization of a CRS and possible hybrid solutions. The calculation time of the models is dependent on the time step considered and on the complexity of the CRS control system. The calculation time of the developed models (6-12 hours) is higher than existing CRS models built in TRNSYS, DELSOL or HFLCAL (usually 1-2 hour max.) however, the detail of simulation is higher. The tools developed for software interconnection and definition of economic models, using the performance simulations, allows obtaining a complete technical and economic analysis of CRSs.

References

[1] Pitz-Paal, R., Heliostat field design for solar thermochemical processes, SFERA Winter School on Solar Fuels & Materials, March 2011, Switzerland.

[2] Garcia, P., Codes for solar flux calculation dedicated to central receiver system applications: A comparative review, Solar Energy 82 (2008) 189–197.

[3] Schwarzbözl, P, The user's guide to HFLCAL: A Software Program for Heliostat Field Layout Calculation, DLR internal manual, 2009.

[4] Curso de Sistemas Solares de Concentração CIEMAT, Volume 1, Madrid, 2009.

[5] Johansson, B., Burnham L., Renewable energy: sources for fuels and electricity, Island Press, 1993.

[6] Wagner, M., Simulation and predictive performance modelling of utility-scale central receiver system power plants, Thesis, University of Visconsin-Madison, 2008.

[7] Winter, C.J., Sizmann, R.L., Vant-Hull, L.L., Solar power plants – fundamentals, technology, systems, economics, Springer-Verlag, 1991.

[8] Stine, W., Harrigan, R., Solar energy fundamentals and design, Wiley, 1985.

[9] Schwarzbözl, P., DLR, personal communication, 22-02-2011.

[10] EBSILON®Professional,www.steag-systemtechnologies.com/, accessed on 23-01-2012.

[11]http://www.energy.siemens.com/hq/en/fossil-power-generation/steam-turbines/sst-110.htm, accessed on 23-01-2012.

[12] Siemens Portugal, personal communication, June 2011.

[13] Babcock & Wilcox, Dual Pressure Reheat Recovery Boiler, brochure 2009.

[14] Cleaver-Brooks, Energy recovery solutions, brochure 2012.

[15] Siemens, Benson® Once-Through Heat Recovery Steam Generator, brochure 2006.

[16] Petchers, N., Combined Heating, Cooling & Power Handbook: Technologies & Applications. An Integrated Approach to Energy Resource Optimization, The Fairmont Press, Inc., 2003.

[17] Ganapathy, V., Optimize energy efficiency of HRSG, Hydrocarbon processing, 2001.

[18] http://www.garioninaval.com, accessed on 23-01-2012.

[19] http://www.bertsch.at, accessed on 23-01-2012.

[20] Bohn. T.; Hrsg. Handbuchreihe Energie; Band 5: Konzeption und Aufbau von Dampfkraftwerken, Technischer Verlag Resch; Köln; Verlag TÜV Rheinland, 1985.

[21] Romero, M., Zarza, E., (2007). Handbook of Energy Efficiency and Renewal Energy, Chapter 21: Concentrating Solar Thermal Power, CRC Press.

[22] REN, Caracterização da rede nacional de transporte para efeitos de acesso à rede em 31 de dezembro de 2011, 2011.

[23] Schillings, C., Trieb, F., MED-CSP Study, Concentrating Solar Power for the Mediterranean Region, DLR, 2005.

[24] Zunft, S., et al, Jülich Solar Power Tower - Experimental Evaluation of the Storage Subsystem and Performance Calculation, Journal of Solar Energy Engineering 133 (2011) 1-5.

[25] Pitz-Paal, R., Dersch, J., Milow, B., (2005). ECOSTAR roadmap document, DLR.

[26] Arne Klein *et al.*, (2010) Evaluation of different feed-in tariff design options, 3rd edition, Fraunhofer ISI and EEG.

[27] Giuliano S., DLR, personal communication, February 2011.

[28] NREL, System Advisor Model (SAM), Version 2010.11.9, 2010

This page was intentionally left blank

Chapter 3

Optimization of a 4 MWe atmospheric volumetric CRS power plant

This page was intentionally left blank

3. Optimization of a 4 MWe atmospheric volumetric CRS power plant

The CRS optimization process involves the power block, design DNI, receiver flux, solar multiple, storage capacity and control strategy. Only a few options are presented in this thesis, as well as the results that allowed the selection of the best configuration decision for SOLMASS project. The start case for this study was the Jülich solar tower design scaled-up to the 4 MWe scale. The work presented in this Chapter (and the previous chapter), resulted into the manuscript [1].

3.1 Options analysed

3.1.1 Optimization of power block, design DNI and receiver flux

For the power block, design DNI and receiver flux optimization, several configurations and operating conditions were simulated. The single pressure HRSG systems analysed were:

#1. a HRSG that generates 27 bar and 415 °C steam to feed a 2 stage turbine;
#2. a HRSG that generates 60 bar and 450 °C steam to feed a 2 stage turbine;
#3. a HRSG that generates 80 bar and 480 °C steam to feed a 3 stage turbine;
#4. a HRSG that generates 130 bar and 530 °C steam to feed a 3 stage turbine;

The multi-pressure HRSG systems analysed were:

#5. a 2-pressure HRSG that generates 27 bar and 485 °C steam – based on the Jülich power plant [2] - to feed a 3 stage turbine;
#6. a system based on the previous designed of PS10 project [3], considering a 2-pressure HRSG that generates 80 bar and 515 °C steam to feed a 4 stage turbine;
#7. based on developments from Brightsource that announced their CRS with direct steam generation operated at 530 °C e 130 bar [4]. A similar steam condition 2-pressure HRSG with reheat was simulated to feed a 4 stage turbine at 530 °C and 130 bar.

Options CRS#1 and CRS#5 were based on Jülich solar tower and were used to analyse the impact of multi-pressure HRSG in the technical and economic performance of CRS power plants. Options CRS#2, CRS#3 and #6 were designed to support new research vectors such as the integration of steam generated from the CRS into biomass power plants with similar conditions [5]. Forest waste biomass power plants with these steam characteristics are operating and projected in Portugal [6]. Options CRS#4 and CRS#7 correspond to high pressure and temperature systems, reaching the borderline established for open volumetric CRS and

commercial power blocks [3]. The objective is to operate with high pressure and temperature steam (to improve efficiency) and fully use all the potential of the high temperature air obtained from the open volumetric receiver. Due to water scarcity, a common scenario in high DNI locations (although not in Portugal), an air-cooled steam condenser was considered for all options. Table 3.1 presents the most important design variables considered, to analyse power block cycle selection impact.

Table 3.1: Design values for the power block cycle selection impact analysis.

Option	**CRS#1**	**CRS#2**	**CRS#3**	**CRS#4**	**CRS#5**	**CRS#6**	**CRS#7**
Receiver							
Flow rate (ton/h)	115	104	108	110	116	97	95
Temperature (°C)	680	680	680	680	680	680	680
HRSG evaporator							
Pinch Point (°C)	17	17	17	17	31 (HP) 3 (LP)	31 (HP) 3 (LP)	31 (HP) 3 (LP))
Approach Temperature (°C)	22	22	22	22	39 (HP) 5 (LP)	39 (HP) 5 (LP)	39 (HP) 5 (LP)
HRSG output							
Temperature (°C)	415	450	480	530	485 (HP) 400 (LP)	515 (HP) 400 (LP)	530 (HP) 400 (LP)
Pressure (bar)	27	60	80	130	27 (HP) 15 (LP)	80 (HP) 40 (RH) 15 (LP)	130 (HP) 40 (RH) 15 (LP)
Flow rate (ton/h)	23	20	20	20	20 (HP) 2 (LP)	15 (HP) 15 (RH) 3 (LP)	13 (HP) 13 (RH) 4 (LP)
Condenser							
Temperature (°C)	49	49	46	46	46	46	46
Pressure (bar)	0.12	0.12	0.1	0.1	0.1	0.1	0.1

The solar field layout is influenced by several variables: equipments and space (e.g. limitations on the field available, heliostat beam quality), environmental conditions (e.g. available DNI, solar angles, temperatures, wind, humidity [7]) and by design definitions (e.g. design point DNI, heliostat distribution algorithm, heliostat/receiver dimensions, tower height and inclination).

One of the variables is the design DNI. If the selected design DNI is high, energy dumping would be lower but the power plant would operate in partial load a larger period of time, with lower efficiencies. If the design DNI is low, dumping would be higher but the number of full power hours would also be larger. This can be confirmed in Figure 3.1.

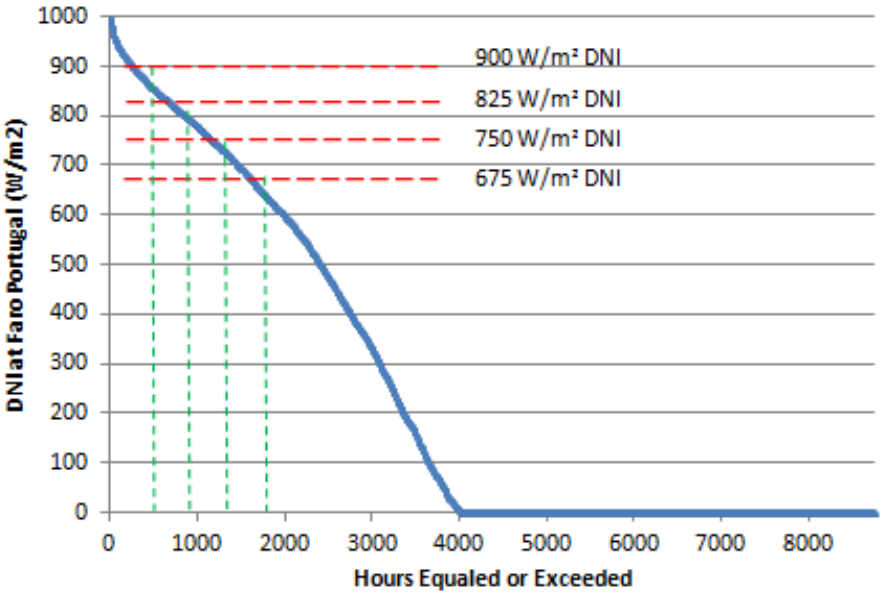

Figure 3.1: Cumulative hours per incident DNI for Faro, Portugal.

With this perspective, and to obtain the optimal design DNI, four different DNI design values were tested for the CRS#3 power plant option:

#8. design DNI 675 W/m^2 and receiver area of 72.6 m^2;
#9. design DNI 825 W/m^2 and receiver area of 55.3 m^2;
#10. design DNI 900 W/m^2 and receiver area of 50.8 m^2.

The heliostat dimensions and tower height were kept unchanged (respectively 60 m^2 and 97 m) and the remaining design definition variables were optimized to maintain similar receiver fluxes, average design fluxes of 550 kW/m^2; the resultant peak solar fluxes for option CRS#8 to CRS#10 were close to 950 kW/m^2. As by experimental testing the receiver solar fluxes

could be higher (≈1000 kW/m^2) [8], to optimize the performance, a design case was considered with a 10 % solar flux tolerance in the receiver before the solar field defocus – option CRS#11:

#11. design DNI 750 W/m^2 and receiver area of 60.0 m^2 with 10 % tolerance in the receiver peak flux.

Option CRS#11 with a larger storage (3 hour at nominal load) was used to study the integration of different biomass based options into open volumetric CRS (option CRS#12), Chapter 4.

3.1.2 Optimization of solar multiple, storage capacity and control strategy

Several options were analysed to find the best solar multiple, storage capacity and control strategy. For each option (set of solar multiple/ storage capacity/ control strategy), different receivers and blowers were simulated. The tested sets of solar multiple/ storage capacities were:

- solar multiples of 1; 1.25; 1.5; 1.75; 2;
- storage capacities of 1; 2; 3; 4; 5; 6 equivalent hours for each solar multiple.

For each solar multiple, a different solar field configuration and layout was optimized using HFLCAL. As for higher solar multiples larger intercept power and solar field aperture are necessary, two alternatives were considered: a different distribution of the heliostats' focal points in the receiver or, if it is insufficient, the receiver area was increased. For the design DNI of 750 W/m^2 the receiver dimensions obtained were:

- solar multiple of 1 – receiver area of 48.6 m^2;
- solar multiple of 1.25 – receiver area of 60.0 m^2;
- solar multiple of 1.5 – receiver area of 72.6 m^2;
- solar multiple of 1.75 – receiver area of 85.0 m^2;
- solar multiple of 2 – receiver area of 96.8 m^2.

Solar multiple and storage capacity are important design variables in the CRS optimization process. Their optimization is also dependent on the operational strategy defined by the power plant responsible. For CRS power plants with large storage devices (or hybrid), a larger staff is necessary for 24 hours daily operation, while power plants with smaller storage devices need a smaller staff team. But it is only possible to find the best control strategy for a specific CRS via an optimization process, involving the thermal storage capacity, solar multiple,

energy dumping, feed-in tariff or the need to generate power on demand. Four different control strategies were considered. The first one is:

- control strategy #1 (CS#1) – it is the most common control strategy in commercial CRS; it uses the solar power to run the power block and the excess heat is stored; this stored energy is used to cover solar transients and extend operation until storage is empty; the staff is scheduled for 2 shifts with extra-hours for extended operation.

In CS#1, during power plant start-up, there is a period of time when solar radiation is not enough to run the power block and begin generating electricity (CS#1, nº1, Figure 3.2). This period is dependent on the inertia of components and on the available solar radiation. To minimize this start-up period, a different control strategy can be used taking advantage of residual energy stored from the previous day. Another alternative to reduce this start-up period and avoid transient problems is the integration of a fuel burner (full or partial hybridization). After start-up, the power block begins generating electricity, and, because the power plant is designed for solar multiples higher than 1, heat from the solar receiver surpasses the needs from the power block. During this period (CS#1, nº 3, Figure 3.2), the excess energy is stored while the power block is generating electricity at nominal power. When the storage device maximum capacity is reached, the excess energy is dumped, normally by defocusing heliostats from the receiver. In the evening (CS#1, nº5, Figure 3.2), the axial blowers reverse the flow and use the energy stored to compensate the solar radiation scarcity, extending power plant operation until the storage is empty.

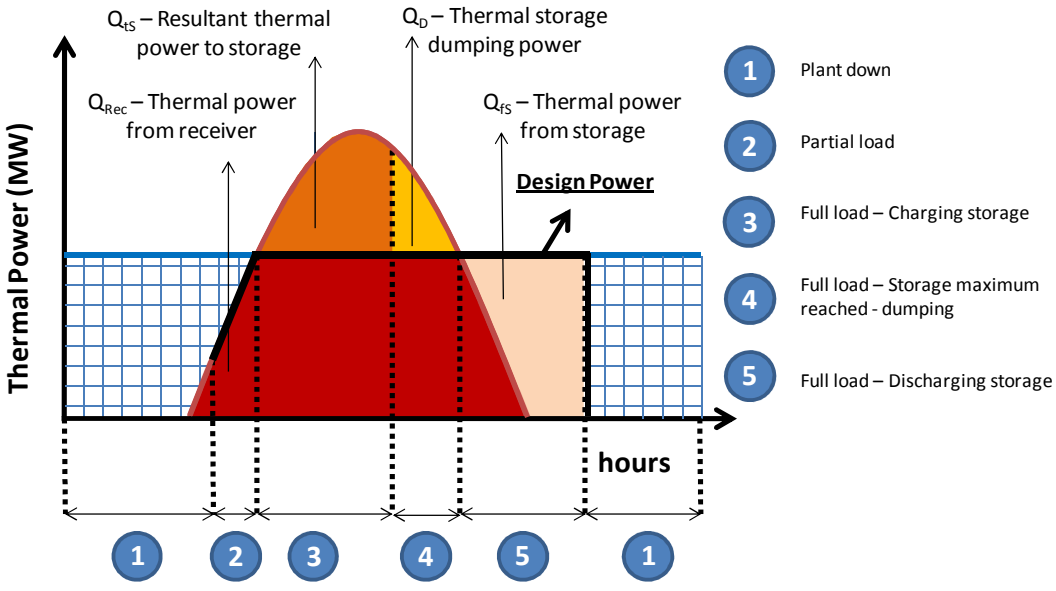

Figure 3.2: Application of control strategy CS#1 to a typical operating day.

The decision diagram for CS#1 is based on C.J. Winter decision diagram [9], Figure 3.3.

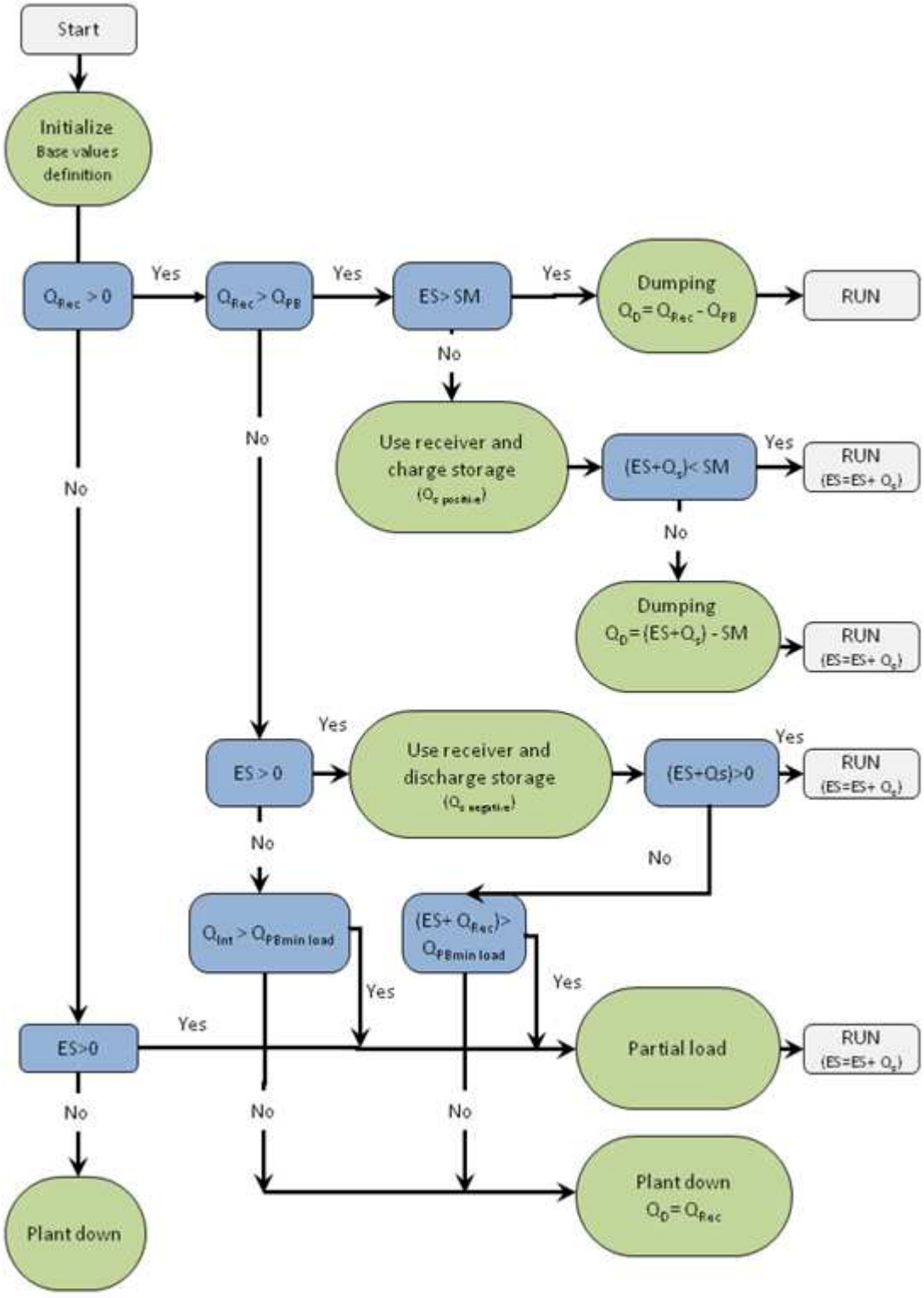

Figure 3.3: Decision diagram for CS#1 control strategy on a CRS.

Other control strategies considered are control strategy #2 (CS#2), with the power plant operating only in two fixed shifts (6:00 to 22:00) and the remaining energy being stored for the next day start-up, and control strategy #3 (CS#3) with the power plant operating only in one shift and reduced personnel costs:

- control strategy #2 (CS#2) – power plant operates during 2 shifts without extra hours (6:00 to 22:00 hours), storing any excess heat for power plant start-up in the next day;
- control strategy #3 (CS#3) – power plant operates during 1 shift (8:00 to 16:00 hours) plus 2 extra hour operation when necessary (16:00 to 18:00), storing any excess heat for power plant start-up in the next day;

The aim of control strategies #1, #2 and #3 is to use the CRS for base load power, with the power plant generating an almost continuous electricity flow to the grid. However, 24-hour operation of an atmospheric air volumetric CRS is not common, due to the thermal storage cost and size. A different perspective for CRS power plants is to generate power on demand, mainly to support the peak electricity consumption periods with bonus feed-in tariffs. Figure 2.30 illustrated the electricity consumption in Portugal for a typical summer day, with consumption peaks from 9:00 to 13:00 and 18:00 to 21:00 (these peaks are even more pronounced during the winter). CSP can also be used to cope with this demand defining a control strategy for these conditions:

- control strategy #4 (CS#4) – the power plant operates at nominal load (4 MW_e) only during hours with high network electricity demand (9:00 to 13:00 and 18:00 to 22:00) and at minimum power block load (2 MW_e) during the remaining period.

3.2 Results and discussion

3.2.1 Optimization of power block, design DNI and receiver flux

There are no commercial open volumetric receiver CRS 4 MW_e power plants in operation worldwide. The most important operating power plant with this technology is the 1.5 MW_e Jülich Solar Tower [10]. In off-design conditions, the solar field performance was obtained by HFLCAL, and the receiver performance was approximated by a model based on experimental data from DLR (Chapter 2.1.4.4); the storage performance was approximated by a constant loss factor (Chapter 2.2.5.3); the HRSG pressure drops were obtained based on data from manufacturers and references; turbine performance was checked with manufacturers for option CRS#2 (2 stage steam turbine) and CRS#4 (3 stages steam turbine) (Chapter 3.4) [11].

Options CRS#1 and CRS#3 were considered to have similar operating nominal isentropic and mechanical efficiencies as options CRS#2 and CRS#4. For options CRS#1 to CRS#7 the receiver design dimensions were considered to be similar to the dimensions of a 60 m^2 heliostat, with design DNI of 750 W/m^2, 1.25 solar multiple and 2 hour storage. Table 3.2 presents the main energy and economic results for CRS#1 to CRS#7 power blocks.

Table 3.2: Power block operating conditions for a 4 MWe atmospheric air volumetric CRS.

Option	**CRS#1**	**CRS#2**	**CRS#3**	**CRS#4**	**CRS#5**	**CRS#6**	**CRS#7**
Performance							
Gross power (MW_e)	4.2	4.2	4.6	4.9	4.5	4.6	4.7
Net power (MW_e)	3.8	3.7	4.0	4.1	4.0	4.0	4.0
Annual net electricity generated (GWh)	10.3	11.1	11.6	12.1	10.8	12.4	12.6
Efficiency							
Power block cycle (gross)	21 %	23 %	24 %	26 %	22 %	26 %	27 %
Power block cycle (net)	19 %	20 %	21 %	22 %	20 %	23 %	24 %
Power block and CRS costs							
CAPEX PB cost (Million €)	2.8	2.9	3.1	3.7	3.7	4.3	4.4
CAPEX CRS cost (Million €)	22.0	22.1	22.3	23.0	23.0	23.8	23.9
Annual O&M cost							
O&M cost (thousands of €)	506	509	517	526	516	526	528

Table 3.2 indicates that, for single pressure HRSG, higher operation temperatures and pressures (options CRS#1 - CRS#4) resulted in improvements of power block cycle efficiency (up to 5 %). The increase in pressure also increases the parasitic losses, so the net efficiency gain is reduced up to 3 % (Table 3.2). However, even in single pressure HRSG, the utilization of higher pressure systems increases the system complexity, the equipments used are more expensive (increase in CAPEX, Table 3.2) and with higher annual maintenance costs (Table 3.2).

The power block (PB) impact in the power plant LEC is significant. Two methodologies were used to analyse the PB cost: a simplified PB cost, obtained by downsize of the ECOSTAR data to 4 MW_e (Table 3.9), while keeping the relative cost constant for all operating pressures; and UPORTO model developed by the author (Table 3.7), Figure 3.4.

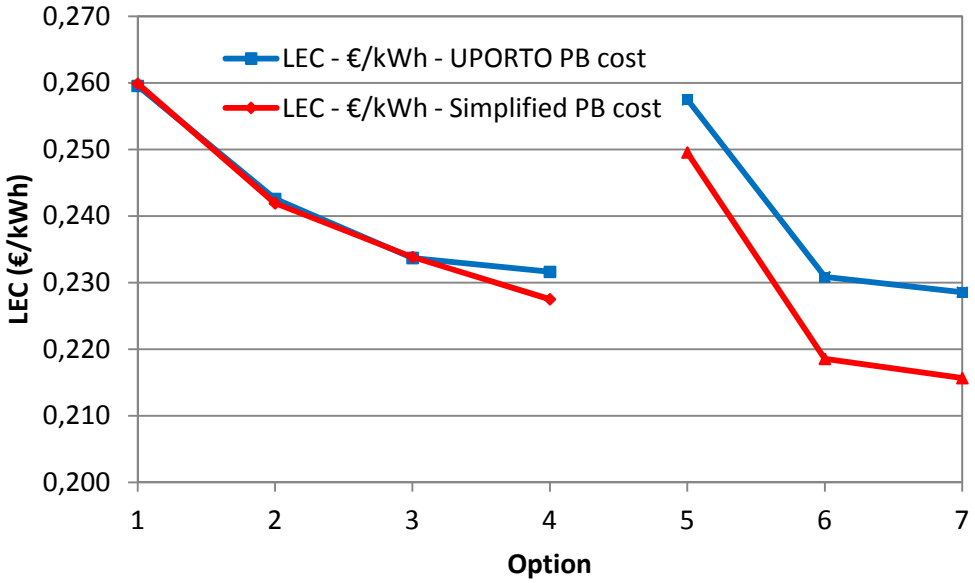

Figure 3.4: LEC variation with power block operating conditions (lines are for readability).

The same reasoning concerning the relation between cost and performance applies to multi-pressure systems, which generally exhibit higher efficiencies for higher pressures. Though, there is a significant overall increase in the cost of multi-pressure systems that justifies the need of a detailed model for the power block cycle cost. The LEC is lower for these multi-pressure systems; however, the LEC analysis does not consider equipments degradation and consequent performance decrease.

The option with the best LEC is CRS#7 (0.229 €/kWh), Figure 3.4. Lower pressure and less complex power blocks, such as options CRS#1 and CRS#2, have a significantly higher LEC, 0.260 €/kWh and 0.243 €/kWh, respectively. Nevertheless, this complexity/cost trade-off should be a factor to analyse in the risk assessment done by the project investor. Between the single-pressure and multi-pressure HRSG there are significant changes in performance and in investment (CAPEX). Multi-pressure HRSG systems have higher costs and O&M than single-pressure HRSGs, but multi-pressure HRSGs are more energy efficient. Despite these differences, their LEC does not vary significantly, e.g. from option CRS#7 to CRS#4 there is a 0.003 €/kWh LEC difference.

Option #3 presents higher efficiency compared to a 4 MW_e CRS with similar operating conditions to Jülich Solar Tower (option CRS#5), without presenting a significant risk increase. If the selected risk management approach is the replication of Jülich Solar Tower operating conditions, there will be a significant increase (of 11 %) in the power plant LEC (0.257 €/kWh), compared to option CRS#3 (0.234 €/kWh).

The author preference was to use single pressure systems, due to lower CAPEX. Comparing option CRS#3 and CRS#4, the LEC differs no more than 0.002 €/kWh. So, option CRS#3 was selected for design DNI analysis. Using the operating conditions similar to CRS#3 power block, several solar field design DNIs were considered, Table 3.3.

Table 3.3: Design DNI and receiver flux impact in a 4 MWe atmospheric air volumetric CRS.

Option	**CRS#8**	**CRS#3**	**CRS#9**	**CRS#10**	**CRS#11**
Performance					
Annual net electricity generated (GWh)	12.0	11.6	11.0	10.3	11.7
Direct costs					
TOTAL DC (Million €)	20.2	18.6	17.5	16.5	18.6
Indirect costs					
TOTAL IC (Million €)	4.0	3.7	3.5	3.3	3.7
CAPEX					
TOTAL CAPEX (Million €)	24.2	22.3	21.0	19.8	22.3

The base case scenario is a 4 MW_e CRS with 2 hour storage and a 1.25 solar multiple, the best design DNI and receiver dimensions are 750 W/m^2 and 60 m^2, respectively (option CRS#3). The main result is that an increase in design DNI results in a decrease of the necessary solar field area and in a lower receiver area (to maintain the average solar flux into the receiver). Therefore, higher DNI results in lower land and receiver costs – overall lower CAPEX (Table 3.3). The impact of receiver design DNI in the power plant LEC can be found on Figure 3.5. Again, two methodologies for cost calculation were compared: a simplified receiver cost, obtained by downsize of the ECOSTAR data to 4 MW_e (Table 3.9), where the cost only varies with the receiver thermal power; and UPORTO model developed by the author (Table 3.7).

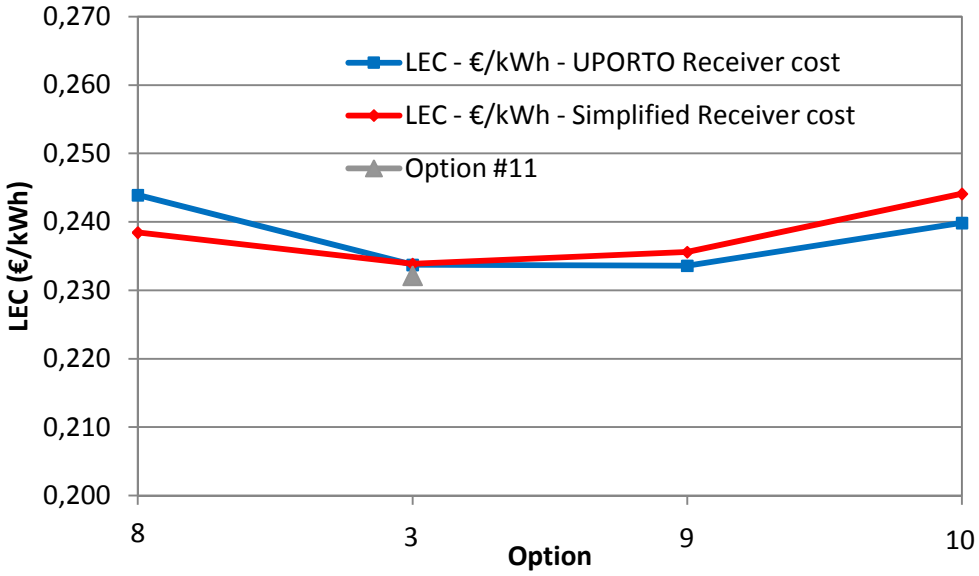

Figure 3.5: LEC variation with receiver design DNI (lines are for readability).

As shown in Table 3.3 and Figure 3.5, the reduction in CAPEX does not correspond to a decrease in LEC, because the power plant does not generate the same annual electricity (lower generation for higher receiver design DNI, Table 3.3). Option CRS#3 still has some margin for LEC improvement if the receiver flux limit is increased by 10 % - option CRS#11. In this case, the power plant LEC decreases by 0.002 €/kWh to 0.232 €/kWh, Figure 3.5. This reduction is limited, because the storage device capacity is low (2 hour) and the receiver output power increase due to higher fluxes (more 3 GWh thermal per year) corresponds only to an increase of 0.1 GWh in the annual generated electricity. A CRS with 3 hour storage generates 11.9 GWh (similar flux limit than option CRS#3 – option CRS#13) or 12.3 GWh (similar flux limit than option CRS#11 – option CRS#12) of electricity, with respective LECs of 0.240 €/kWh (0.060 €/kWh higher than option CRS#3) and 0.232 €/kWh (equal to option #11). As this storage capacity increase does not reduce the LEC, the option selected for the solar-only power plant is option CRS#3.

3.2.2 Optimization of solar multiple, storage capacity and control strategy

In combination with the selected power block operational conditions, receiver flux and design DNI for the SOLMASS local conditions (Option CRS#3 – HRSG which generates 80 bar and 480 °C steam to feed a 3 stage turbine, design DNI of 750 W/m^2, receiver dimensions of 60 m^2 and receiver peak flux of 950 kW/m^2), Table 3.4 presents the main design conditions for the different solar multiple options, operating under Portuguese weather conditions.

Table 3.4: CRS design conditions for the different solar multiples.

	SM 1.25	SM 1.5	SM 1.75	SM 2.0
Solar field				
Heliostat reflective area (m^2)	60	60	60	60
Field density (%)	18	16	15	14
Total mirror area (m^2)	53 580	65 760	78 060	91 020
Land area (hectare)	21	26	31	36
Receiver				
Area (m^2)	60	73	85	97
Design power (MW)	24	29	33	38
Storage				
Capacity nominal hours (hour)	2	2	2	2
Capacity power (MWh)	34	34	34	34
Power block				
Gross electric power (MW)	4.6	4.6	4.6	4.6
Net electric power (MW)	4.0	4.0	4.0	4.0

The solar field mirror area and the receiver design power increases for higher solar multiples. The location of these supplementary heliostats is farer from the receiver and, due to higher blocking and shading losses their distribution is more spaced, resulting in lower field densities, Table 3.4, which affects the solar field efficiency, Figure 3.6.

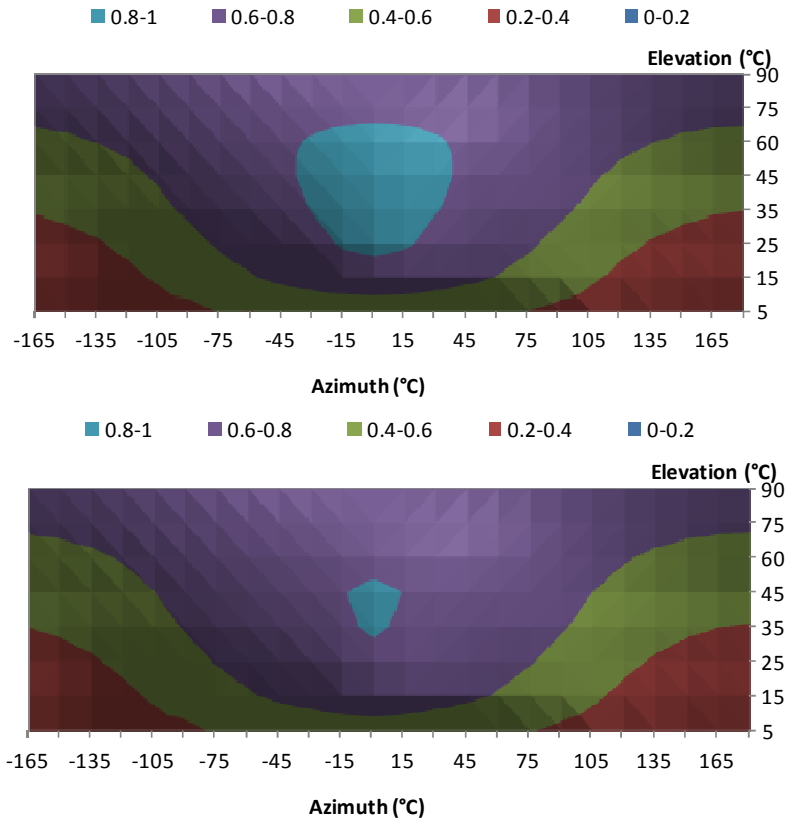

Figure 3.6: Effect of solar multiple in the solar field performance for SM=1.25 (up) and SM=1.75 (down).

As shown in Figure 3.6 (central area), for higher solar multiples the number of solar positions with good solar efficiencies is reduced, and so the annual solar field efficiency is lower. Also, the increase in solar multiple corresponds to a power plant CAPEX increase, due to a significant higher solar field area and receiver power and dimensions, Table 3.5.

Table 3.5: Cost distribution for power plants with different SMs.

Direct costs (million €uro)	**SM 1.25**	**SM 1.5**	**SM 1.75**	**SM 2.0**
Solar field	8.0	9.8	11.5	13.3
Receiver	3.5	4.1	4.7	5.2
Tower	1.0	1.0	1.0	1.0
Storage	2.2	2.2	2.2	2.2
Power block	3.1	3.1	3.1	3.1
Land	0.8	0.9	1.1	1.3
Indirect costs (million €uro)	3.7	4.1	4.7	5.2
CAPEX (million €uro)	22.3	25.2	28.3	31.3

A power plant with a solar multiple of 1 and absence of storage was simulated only for comparison purposes, because its operational viability is reduced. Power plants with solar multiples of 1.25, 1.5, 1.75 and 2.0 were considered, with different storage capacities from 1 to 7 equivalent operating hours, and four different control strategies, Figure 3.7.

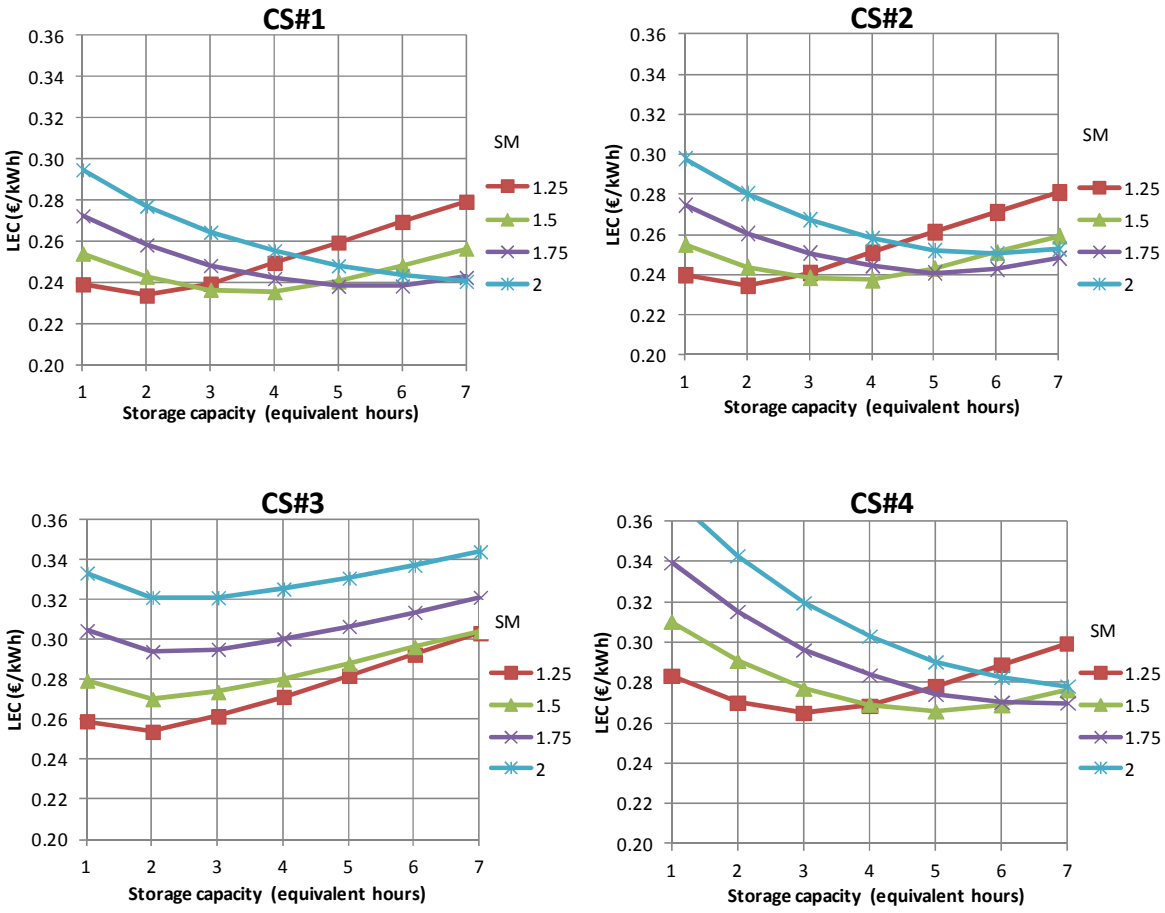

Figure 3.7: Influence of solar multiple, storage capacity and control strategy (CS#1 to CS#4) on CRS LEC (lines are for readability).

The power plant configuration with best LEC (0.234 €/kWh, Figure 3.7) is for 2 hours storage and with a 1.25 solar multiple using CS#1 (CRS#3_SM1.25_2S_CS#1). There are some other power plant configurations using CS#1, such as the CRS with 1.5 solar multiple and 3 or 4 hour storage (CRS#3_SM1.5_3S or 4S), that have a similar LEC (0.001 €/kWh higher) but with higher CAPEX.

For each solar multiple there is an optimal storage size and different configurations result in significant changes in the LEC, e.g. a 1.25 SM power plant with 7 hour storage (CRS#3_SM1.25_7S_CS#1) has a LEC almost 20 % higher than the optimal 1.25 SM power plant (CRS#3_SM1.25_2S_CS#1). Similarly, for each storage capacity there is an optimal solar

multiple, e.g. the 1.25 SM power plant with 7 hour storage (CRS#3_SM1.25_7S_CS#1) has a 16 % higher LEC than the best 7 hour storage power plant configuration (CRS#3_SM2.0_7S_CS#1). These LEC variations are normally due to higher dumping or high periods of partial load operation. For improving the overall efficiency, instead of dumping energy this can be used for e.g. generating chemical products Chapter 6. Figure 3.8 summarizes the LECs of the best power plant configurations for each solar multiple, storage size and control strategies.

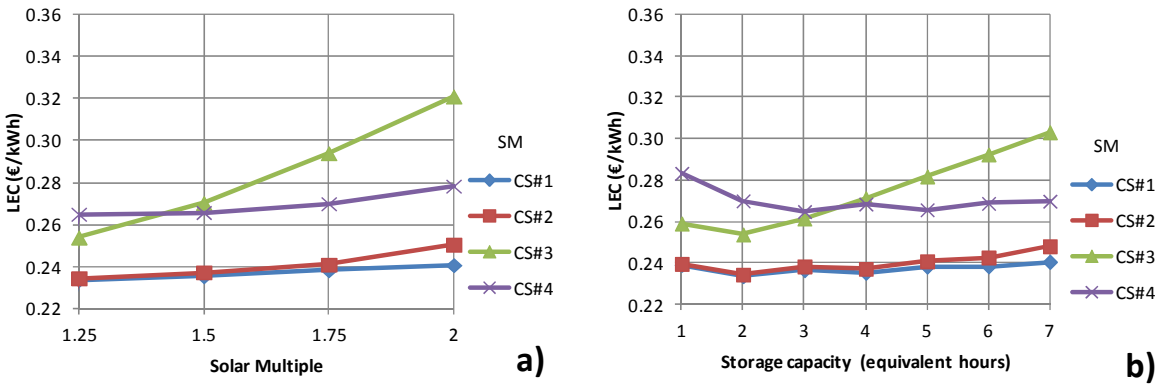

Figure 3.8: Optimal power plant solar multiple (**a**) and optimal storage capacity (**b**) variations with control strategy (lines are for readability).

Figure 3.8 demonstrates that the control strategy has a significant impact on the power plant LEC. If power plant operation is limited to 2 shifts (CS#2), the partial load period and the operation and maintenance (O&M) costs will decrease, but LEC will increase due to higher storage losses. This is clear for configurations with higher storage capacities and solar multiples, e.g. a power plant with 1.75 SM and 3 hour storage using CS#2 (CRS#3_SM1.75_3S_CS#2) has a LEC of 0.241 €/kWh, while for the same power plant, but using CS#1, the LEC is 0.238 €/kWh. If power plant operation is limited to 1 shift (CS#3), the LEC increase is more notorious, especially for higher SM and storage capacities, because the CAPEX increases but the annual generated electricity remains identical (Figure 3.8 – CS#3). Also, since the power plant is located in an abundant solar radiation area, the LEC was further penalised for CS#3 control strategy (this control strategy can be positive for lower DNI locations). For a complete economic analysis, a detailed cash flow model was developed for several power plant configurations, Table 3.6.

Table 3.6: Power plant cash flow analysis and economic indicators.

Plant designation	Feed-in tariff (€/kWh)	IRR (%)	NPV (million €uro) *	Payback period (years) *
CRS#3_SM1.25_2S_CS#1	0.273 (24 hour)	9.8 %	7.9	14
CRS#3_SM1.5_4S_CS#1	0.273 (24 hour)	9.6 %	9.4	15
CRS#3_SM1.75_5S_CS#1	0.273 (24 hour)	9.3 %	10.2	16
CRS#3_SM2.0_7S_CS#1	0.273 (24 hour)	9.0 %	11.4	16
CRS#3_SM1.25_2S_CS#2	0.273 (24 hour)	9.8 %	7.8	15
CRS#3_SM1.25_2S_CS#2	0.341 (from 9 to 22 hours) 0.164 (remaining)	17.0 %	16.9	7
CRS#3_SM1.25_2S_CS#3	0.273 (24 hour)	7.6 %	4.9	20
CRS#3_SM1.25_3S_CS#4	0.273 (24 hour)	6.1 %	3.1	23
CRS#3_SM1.25 _3S_CS#4	0.341 (from 9 to 22 hours) 0.164 (remaining)	11.6 %	10.7	12
CRS#3_SM1.25 _3S_CS#4	0.341 (from 9 to 13 and 18 to 22 hours) 0.164 (remaining)	8.2 %	6.0	18

* - considering average inflation of 4 %.

The investment in CRS power plants is attractive for the selected case (CRS#3_SM1.25_2S_CS#1, Table 3.6), with high IRR (9.8 %) and moderate payback time (14 years), and good NPV for the power plant life cycle (€ 7.9 million) even considering a conservative average inflation of 4 % (well above the December 2012 inflation - 2.2 %, 2.3 % for the Euro Area and European Union, respectively [12]). Power plants with better NPV (up to € 11.4 million) can be considered, but the CAPEX for these power plants is higher and the investment payback time is also higher.

In a different perspective, if the objective is to generate electricity adjusted to the network demand (larger generation during demand peak hours), the power plant would only be viable if a bonus feed-in tariff is obtained (CRS#3_SM1.25_3S_CS#4, Table 3.6). If the bonus tariff is obtained for the period between 9:00 to 13:00 and 18:00 to 22:00 hours, the investment IRR and NPV are below CS#1; however, if the bonus tariff is obtained for the period from 9:00 to 22:00, the investment IRR and NPV are significantly higher than CS#1.

3.3 Optimized 4 MWe CRS power plant

The selected 4 MW_e CRS configuration for Faro conditions is a CRS with design DNI of 750 W/m^2, receiver dimensions of 60 m^2, receiver peak flux of 950 kW/m^2, SM of 1.25, 2 hours storage, a HRSG which generates 80 bar and 480 °C steam to feed a 3 stage turbine and using control strategy CS#1 – option CRS#3 or CRS#3_SM1.25_2S_CS#1. For this power plant a typical operational day is presented in Figure 3.9.

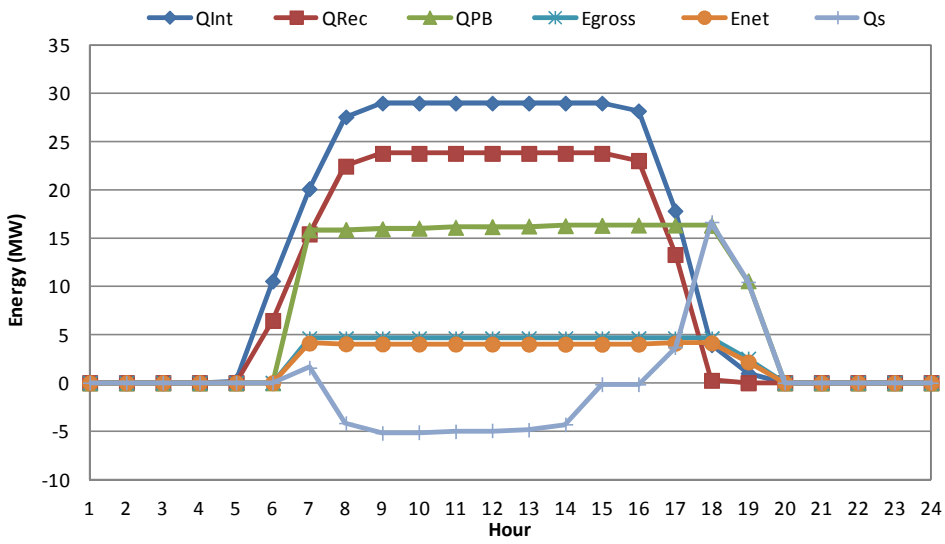

Figure 3.9: Typical operational day for the 4 MWe CRS with 1.25 SM and 2 hours storage for CS#1 (lines are for readability).

The power plant has an initial period when solar energy is available but the power plant is not generating electricity, followed by a period of partial load operation until the power plant begins operating at nominal load (at 7:00 – Figure 3.9). After this period of time, the power plant uses the excess energy to fill the storage (with 5 MWth from 8:00 to 14:00). After this period the storage capacity is full and the excess energy is dumped. At the end of the day, available solar energy is reduced and the storage flow is reversed, extending power plant

operation until 20:00 (Figure 3.9). The 1.25 SM and 2 hours storage 4 MW_e CRS annual performance using CS#1 (CRS#3_SM1.25_2S_CS#1) is presented in Figure 3.10.

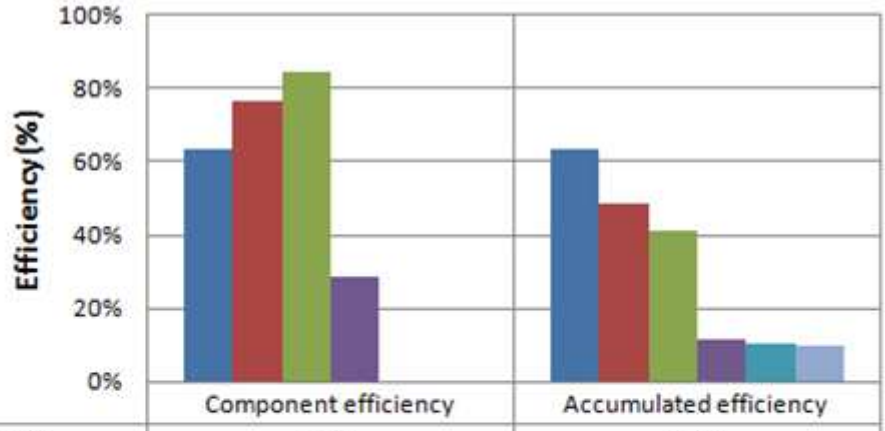

	Component efficiency	Accumulated efficiency
Solar field	63%	63%
Receiver	77%	49%
Storage/Dumping	85%	41%
Power Block gross	29%	12%
Parasitics		10%
Solar-Electricity		10%

Figure 3.10: 4 MWe CRS with 1.25 SM, 2 hours storage and CS#1 annual efficiency.

The solar field annual efficiency (63 % - Figure 3.10) includes the heliostat stow positioning losses (caused e.g. by excessive wind) and the losses due to the solar DNI upper limit. The receiver annual efficiency is 77 % - Figure 3.10 - and the storage unit has an annual efficiency of 85 % - Figure 3.10. The storage unit efficiency includes the dumping losses when excess energy is available but the storage capacity is fulfilled. Up to the power block input the accumulated energy efficiency is 41 % (Figure 3.10). The component with the lowest efficiency is the power block (29 % gross - Figure 3.10); its efficiency could be improved using a combined cycle (gas turbine plus steam turbine) but it would imply changing the receiver technology (e.g. pressurized air receiver) or to consider hybrid solutions. The scale-up of the power plant could also increase power block efficiency, as more efficient turbines can be used. The accumulated efficiency, solar to electricity, is 12 % (Figure 3.10). The parasitic loss, with the consumption of electric equipment, was 1.6 GWh per year, with significant contributions of the air-cooled condenser and blowers. If these parasitic losses are taken into account, the overall solar to electricity efficiency is 10 % (Figure 3.10). Larger power plants can improve the solar to electricity efficiency up to 20 % [13]. The CAPEX for the optimized 4 MWe CRS power plant is expected to be 22.3 M€, with the component costs presented in Table 3.7.

Table 3.7: CRS component costs – option CRS#3_SM1.25_2S_CS#1.

Direct costs (DC)	**UPorto model - 4 MW unit at Faro/Tavira – for best option**
Solar field	150 €/m^2[14]
Storage	64 €/kWh_{th}
Receiver	120 €/kW_{th} - based on receiver power and dimensions) [15]
Tower	1 000 000 € [16]
Power block	671 €/kW_e-based on components design/operating conditions [17,18]
Land	3.6 €/m^2 [16]
Indirect costs (IC)	Local work costs – 20 % of DC

The main components cost share is presented in Figure 3.11.

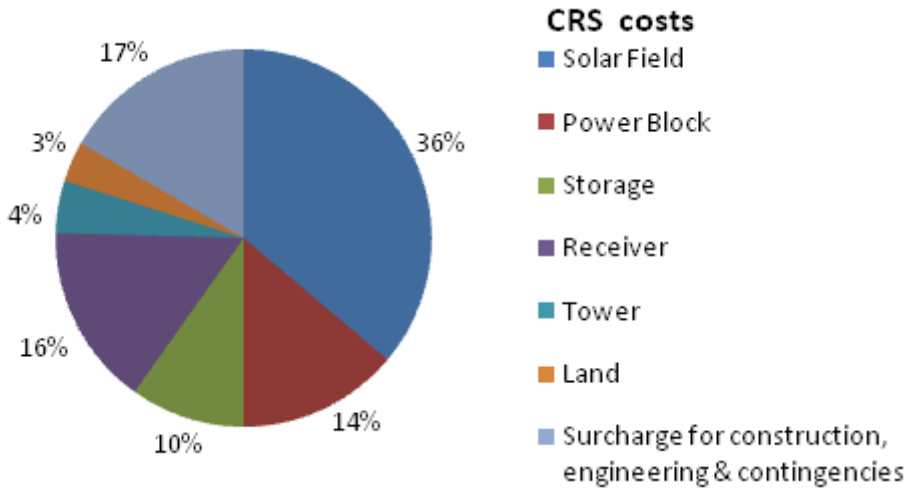

Figure 3.11: Cost structure of a 4 MWe atmospheric air volumetric CRS - option #3.

The main costs associated with the power plant are the solar field (36 %), the solar receiver (16 %), the power block (14 %) and storage (10 %). This indicates the importance of optimizing the power block cycle, receiver design DNI and flux, storage capacity, solar multiple and control strategy.

3.4 Validity

The power plant CAPEX is divided into the direct costs (DC) and indirect costs (IC). Direct costs are the cost attributed to equipment acquisition and their installation. It can be divided into several groups of components: heliostat field, power block, storage, solar receiver, tower and land. Indirect costs are the costs that are not directly attributed to a specific object, as the case of the start-up costs and the surcharge for construction, engineering & contingencies. For the atmospheric volumetric CRS one of the most complete cost reports is the ECOSTAR report [3], Table 3.8.

Table 3.8: ECOSTAR reference costs for an atmospheric volumetric CRS power plant.

	ECOSTAR - 10 MW unit at Seville [3]	**ECOSTAR - 50 MW unit at Seville [3]**
Direct costs (DC)		
Solar field	150 €/m^2	138 €/m^2
Storage	60 €/kWh_{th}	54 €/kWh_{th}
Receiver	115 €/kW_{th}	103 €/kW_{th}
Tower	2 000 000 €	8 934 538 €
Power block	600 €/kW_e	536 €/kW_e
Land	2	2 €/m^2
Indirect costs (IC)		
Flat rate	20 % of DC	20 % of DC
Life cycle	30 years	30 years
Debt interest	8 %	8 %
Insurance	1 %	1 %

The values presented in Table 3.8 are for a power plant located in Seville, Spain with a SM=1.82, and based on PS10 design done by KAM to SOLUCAR, with commercial equipment price consultations. The data presented in Table 3.8 cannot be directly used for the SOLMASS CRS, because the installed power is only 4 MWe. So, the component costs have to be extrapolated from the ECOSTAR data for the 4 MWe case. They can be estimated adjusting a cost curve, with scale factors based on the ECOSTAR report [3] (solar field – 0.95; receiver – 0.87; storage - 0.93).

$$C_{E,Y} = C_{E,W}\left(\frac{X_Y}{X_W}\right)^{\propto} \quad (3.1)$$

where $C_{E,Y}$ is the cost of equipment at the required size or capacity, $C_{E,W}$ is the cost of the reference equipment at reference size or capacity, X_Y is the size or capacity of the required equipment, X_W is the size or capacity of the reference equipment and α is the scale factor. Using the data from Table 3.8, the equipment costs for a 4 MW power plant were calculated and are presented in Table 3.9.

Table 3.9: Economic data for the CRS model.

Direct costs (DC)	**Simplified model - 4 MW unit downsize (using Equation 3.1)**
Solar field	155 €/m^2
Storage	64 €/kWh$_{th}$
Receiver	119 €/kW$_{th}$
Tower	890 572 €
Power block	638 €/kW$_e$
Land	2 €/m^2
Indirect costs (IC)	Flat rate – 20 % of DC

As different configurations were analysed, detailed models were developed to estimate the cost of the equipments. The solar field cost was calculated according to the Helios3s design from UPorto [14], Table 3.7. Heliostat costs are within the range presented at the SolarPaces heliostat catalogue [19] and according to the costs used for a 10 MW$_e$ power plant in ECOSTAR report [3]. A downsize to 4 MW$_e$ based on ECOSTAR report scale factors,

results in a 5 €/m^2 higher cost than Helios3s, but, considering the contacts done with EPC contractors and heliostat developers, the cost of 150 €/m^2 was pointed as realistic for the current commercial heliostat market [20]. Commercial heliostats, e.g. Colon 70 and Sanlucar 90, are operating at Plataforma Solar Almeria (PSA) and had a cost of 130 USD/m^2 (year 2000), for a 1000 heliostat annual production line. Assuming CE index factors of 394 for 2000 and 585.7 for 2011, with an average exchange rate USD/EUR of 0.72, the actual heliostat cost should be near 139 €/m^2, which is 11 % lower than the cost considered. The storage device cost was based on the ECOSTAR report [3]. Novel storage with ceramics can reduce the cost below 20 €/kWh_{th} [21], and so the storage cost used was considered as very conservative.

ECOSTAR receiver cost model is based on the cost per incident power; as different design DNIs and receiver dimensions were selected for the same operating power, a detailed model was created, based on the receiver dimensions and incident power, UPORTO model. The simplified model used cost data from ECOSTAR [3] and a scale factor for the power/cost relation (Equation 3.1). The UPORTO model used data from Solair and Jülich projects [15] to estimate a cost per receiver components (cup, structure, insulation, and tubing) and to find a scale factor for the receiver area and power/cost. Solving Equation 3.1 for each receiver option, led to cost factors (€/m^2 and €/kWth) for the receiver and its respective estimated cost. The land and tower costs were checked by a national company [16].

Because different power block configurations were studied a detailed power block economic model was developed, based on the individual factors from the Guthrie's method [17, 18], using Ebsilon detailed mass and energy balance simulations for equipment sizing, definition of construction materials and labour costs – UPORTO model. This method is referred by Peters et al. [18] as a definitive estimate with a good accuracy (error ± 10 %) to start detailed engineering and definitive cost evaluation. The indirect cost model is based on Guthrie's method [17, 18]. The model used is composed by several components and is influenced by several factors: capacity, material and operational, Table 3.10.

Table 3.10: Power block components cost - for best option.

Equipment	Power factor	Material factor	Operational factor	Cost ($\times 10^3$ USD_{2000})
Condensate economizer	1.2 MW	Steel	1.5 bar (condensate)	20
Economizer (HRSG)	3 MW	Steel	1.5 bar (steam)	91
Evaporator (HRSG)	9 MW	Steel	80 bar (steam)	219
Super-heater (HRSG)	2 MW	Steel	80 bar (steam)	16
Super-heater (HRSG)	1 MW	Steel/ Cr -Mo	80 bar (steam)	21
Condenser	12 MW	Steel	Air cooled condenser	110
Turbine	4.6 MW	-	-	716
Generator	4.6 MW	-	-	9
Deareator	-	-	-	19
Pumps	2 units	-	-	48
Drives for pumps	2 units	-	-	4
Fans	2 units	-	-	33
			TOTAL	1 307

The values are in US Dollar ($) for 2000 with a CE cost index of 394. An actualization of the values to 2011 is necessary, using a cost index of 586 [22]; it is also necessary to convert to EUR using the 2011 average exchange rate of 0.72 EUR for each USD. The component costs in Table 3.10 do not include the costs associated with transport, insurance, assembly, cables, insulation, etc. The method used considers these costs in the bare module factor, which is multiplied by the equipment acquisition costs, Table 3.11 [17, 18].

Table 3.11: Bare module factor for power block equipments.

Equipment		Bare module factor
Fans		2.19
Boilers	Pre-fabricated	2.19
	Locally assembled	1.86
Heat exchangers		3.17
Evaporators		2.45
Air cooled condenser		2.2
Pumps		3.3
Electric generators		2.5
Turbines: steam and gas		3.5
Pressure vessels	Vertical	4.16
	Horizontal	3.05

This method is used to get an estimate of the components costs. The final equipment cost is usually done via a public consultation with manufacturers and suppliers. Because several possibilities were analysed, the reference costs of the main components (HRSG and steam turbine) were requested to some manufacturers for several design cases. The approach used to validate the economic model with real data was to adjust the bare module factor so the equipment cost obtained via model matches the commercial quotation.

The validation of the performance of the different power block options analysed was also done via consultation with manufacturers and reliable references. The power block used on Jülich solar tower uses a HRSG that generates 485 °C and 27 bar steam to feed a steam turbine/generator of 1.5 MWe. As at the time the Jülich solar tower was on early commercial exploration phase, it was not possible to obtain the measured HRSG and turbine characteristic curves. Several contacts were done with the power plant operators (KAM), but it was not possible to obtain this information because of confidentiality issues. HRSG manufacturers were contacted to obtain a solution that would fit the required specifications. The Rentech HRSG pre-assembled commercial series allows obtaining the pressure and temperature used in Jülich but with a steam flow rate of 10 tons/hour. For the 4 MWe power plant (option CRS#1) it would be necessary to have two equipments working in parallel, or a larger HRSG (typically operates at higher pressures and temperatures), or a specially designed HRSG. Option CRS#2 validated steam turbine was used for option CRS#1 (adjusting the operational conditions), and the necessary flow rate to obtain the design power was calculated. Option CRS#2 uses a

commercial SIEMENS SST-110 (2 stages) steam turbine, validated, according to the manufacturer, for the conditions reported on Table 3.12 [11].

Table 3.12: Validation data for the SIEMENS SST-110 turbine.

		Model	Manufacturer data
Input	Temperature	450 °C	450 °C
	Pressure	60 bar	60 bar
	Flow	20.0 t/h	20.0 t/h
Stage 1	Output temperature	196 °C	196 °C
	Output pressure	3.9 bar	3.9 bar
	Output flow	20.0 t/h	20.0 t/h
Stage 2	Output temperature	49.4 °C	49.5 °C
	Output pressure	0.12 bar	0.12 bar
	Output flow	18.5 t/h	18.5 t/h
Generator	Frequency	50 Hz	50 Hz
	Power	4235 kW	4235 kW

The partial load characteristic curves were requested but, as it is confidential information, only several performance values were given at certain loads [11]. These values were used and interpolated by Ebsilon characteristic lines to obtain the turbine performance at partial load, Figure 3.12.

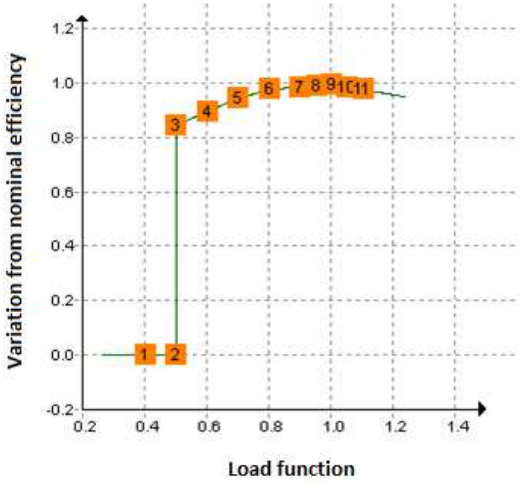

Figure 3.12: Performance characteristics of the steam turbine.

In Figure 3.12, the vertical axis represents the ratio of $\frac{Actual\ efficiency}{Nominal\ efficiency}$ while the horizontal axis represents the turbine load, which is calculated every time step. Afterwards, via characteristic line, the turbine actual efficiency is calculated. Option CRS#2 turbine is coupled with a HRSG based on the operational conditions of a biomass power plant boiler from Babcock & Wilcox Power Generation Group, which generates superheated steam at 450 °C and 60 bar.

Option CRS#3 is based on the original design for PS10 in Seville, now built as a CRS using a saturated steam receiver. This is a configuration that allows the CRS to generate steam, with similar characteristics to a new 10 MWe biomass waste power plant project in Portugal – Chapter 4. The adaptation of a 4 MWe turbine to these operational conditions was done based on a 3 stage concept selected for the biomass plant (10 MWe). The latest equipments allow reaching higher operating temperatures and pressures than the options considered up to this point. The purpose of using higher temperatures and pressures is to increase the power block efficiency, which is the less efficient power plant part. As the pressure in the steam condenser is constant, it is only possible to set the HRSG output pressure; for HRSG systems with superheater and without reheating, to have steam temperatures of 500 °C, the pressure should be between 60-80 bar, while for HRSG with reheat pressures should be above 120 bar. The design of the HRSG to generate steam at these pressures is complex, since the largest portion of the heat transfer is done at temperatures close to the water evaporation, thus dealing with the effects of latent heat (at 100 bar the water evaporation temperature is 311 °C).

The solar receiver exhaust air temperature is typically near 680 °C, and so, the use of a traditional single pressure HRSG that generates high pressure and temperatures steam implies that the temperature of the exhaust air from the HRSG would be about 300 °C, and a large part of the energy contained in the air would be lost to the environment. This problem can be solved by introducing an additional set of economizers, evaporators and superheaters. This system can generate steam at lower pressures (4 to 10 bar) to be integrated in a (low pressure) turbine stage, or at a similar temperature to the first stage of the turbine if there is reheating. As the evaporation temperature of the water at these pressures is much lower, there is a greater recovery of heat from the heat transfer fluid and the temperatures of their HRSG exhaust are reduced to the range of 140-180 °C.

The BrightSource objective is to reach 550 °C and 160 bar in their new Ivanpah solar tower project for direct steam generation. This technological advance was based on the operation of a smaller pilot plant (1.5 MWe) built in the Negev, in Israel. The operating conditions of the pilot BrightSource Negev (530 °C and 130 bar) served as reference for drawing option CRS#7, which is adapted to an atmospheric air volumetric CRS using an HRSG to generate steam, to be used in a turbine set composed by 3 turbines SST-060, validated with operational data provided by SIEMENS Table 3.13 [11].

Table 3.13: Validation data for the three SIEMENS SST-060 turbines.

		Model	**Manufacturer data**
Input	Temperature	530 °C	530 °C
	Pressure	130 bar	130 bar
	Flow	19.3 ton/hour	20.0 ton/hour
Stage 1	Output temperature	361 °C	363 °C
	Output pressure	26 bar	26 bar
	Output flow	19.3 ton/hour	20.0 ton/hour
Stage 2	Output temperature	188 °C	195 °C
	Output pressure	4 bar	4 bar
	Output flow	17.9 ton/hour	20.0 ton/hour
Stage 3	Output temperature	45.8 °C	45.9 °C
	Output pressure	0.1 bar	0.12 bar
	Output flow	17.9 ton/hour	18.5 ton/hour
Generator	Frequency	50 Hz	50 Hz
	Power	4885 kW	4890 kW

The integration of the HRSG and steam turbine is essential for the power plant operation. It is thus crucial to optimize and validate the HRSG to achieve the best performance at the lowest possible cost. With this purpose, some characteristic curves were found in bibliography and/or given by the suppliers, Figure 3.13.

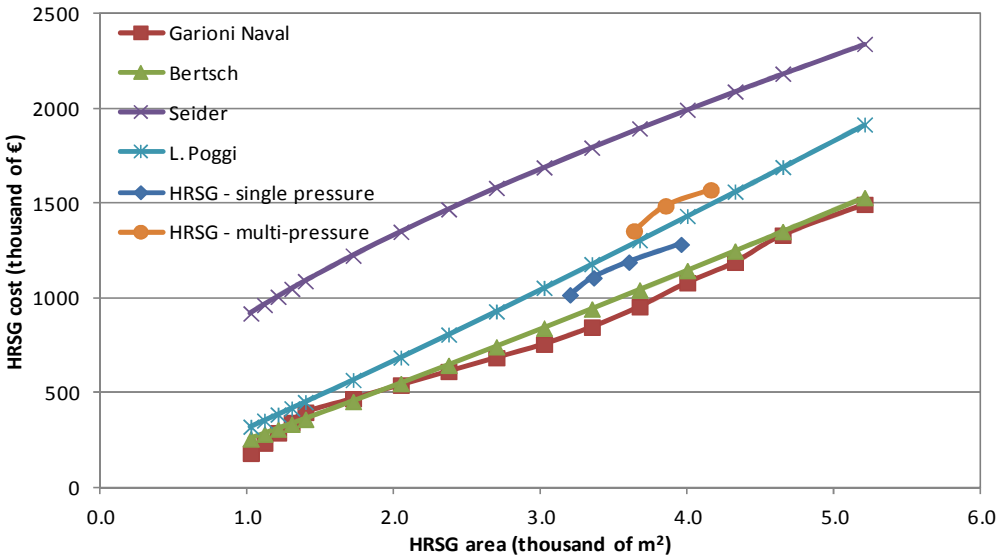

Figure 3.13: HRSG cost/area curves.

The HRSG cost is dependent on the selected pinch point, which defines the respective necessary area. An additional coefficient was added for system complexity (with increased pressure levels and reheat). For the selected conditions, a commercial HRSG should cost between € 0.7 and € 1.2 million, Figure 3.13 (Garioni Naval or Bertsch). The models developed were a little more conservative, resulting in HRSG costs from € 1 to € 1.6 million, Figure 3.13 (HRSG – single pressure and multi-pressure). According to these data, the bare module factors were corrected validating the manufacturers' data, Table 3.14.

Table 3.14: Power block components cost - for best option.

Equipment	Power	Corrected bare module factor	Cost (million USD_{2000})	Cost (million €)
Condensate economizer	1.2 MW	3.2	0.06	0.07
HRSG	16 MW	3.2	1.11	1.19
Turbine + Generator	4.6 MW	1.6	1.16	1.24
Condenser	12 MW	2.2	0.24	0.26
Deareator	-	3.3	0.06	0.06
Pumps + drives	2 units	1.5	0.17	0.18
Fans	2 units	2.5	0.08	0.09
		TOTAL	2.89	3.09

The models developed allow analysing the impact of different receiver and power block configurations in the cost and performance of the power plant. This is essential to optimize the power plant, despite further work still being necessary in terms of detailing the operation viability, maintenance and market availability and equipment costs, which was only briefly approached by this study. Additional validation of indirect costs is also necessary, because only flat rates were considered for the site preparation, contingencies and contractor fees and power plant start-up. This was done according to the methodology of Sieder [17] and totalizes 20 % of the direct costs, which is similar to the flat rate applied in the ECOSTAR report. This additional cost validation is only possible after detailed engineering, e.g. public consultations or a tender to companies.

3.5 Sensitivity analysis

Considering the selected 4 MW_e power plant CRS#3_SM1.25_2S_CS#1 (hereafter mentioned as CRS#3), a LEC sensitivity analysis was performed. Several detailed models were developed to reduce the volatility of LEC and increase the precision of the assumed costs. If some of these estimates are not effectively delivered by the sub-contractors, this could endanger the investment viability. In this perspective, several scenarios were considered: a CAPEX increase (10 % from reference); a power generation reduction (5 % from reference); an O&M cost increase (5 % from reference); power plant longevity reduction (from 30 years to 25); a debt interest rate increase (from 8 to 9 %), Figure 3.14.

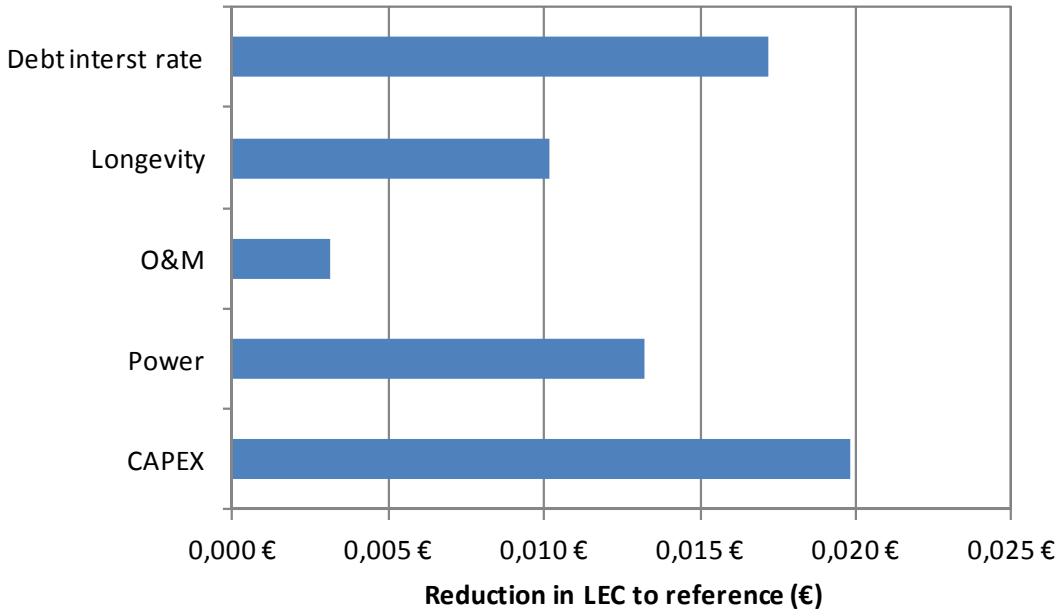

Figure 3.14: Possible impact of several factors in power plant LEC, comparing to reference case - CRS#3.

CAPEX is the variable with greater impact on the power plant LEC, Figure 3.14. The cost estimation method was conservative and several power plant equipments, such as the steam turbine, HRSG, solar field, tower and receiver, were validated with commercial data from the suppliers or references. Power plant performance was based on prestige software: HFCAL and Ebsilon, adjusted with data from the developers. However, some reports have pointed out that solar DNI based on Meteonorm (used for the reference study) could in some cases be overestimated [23]. This factor has great influence in the LEC, and so a local measurement is recommended to improve quality of the simulation results; also, due to actual economic constrains, bank project finance is stricter and the debt interest rate has increased. Debt interest rate has a high impact on LEC (Figure 3.14) and should be further analysed, although alternative finance options could be used for impact reduction.

It is also important to analyse the LEC sensitivity to a possible cost increase of a single component or of several components. With this purpose, an additional 10 % flat rate cost increase in the power plant components was considered: solar field cost increases to 165 €/m^2; receiver cost increases to 131 €/kW_{th}; tower cost increases to 1 100 000 €; the storage cost increases to 71 €/kWh; the power block cost increases to 737 €/kW_e; and the land cost increases to 4.0 €/m^2, considering the reference costs of the main components (Table 3.7). The impact on the final LEC of each of these cost increments is illustrated in Figure 3.15.

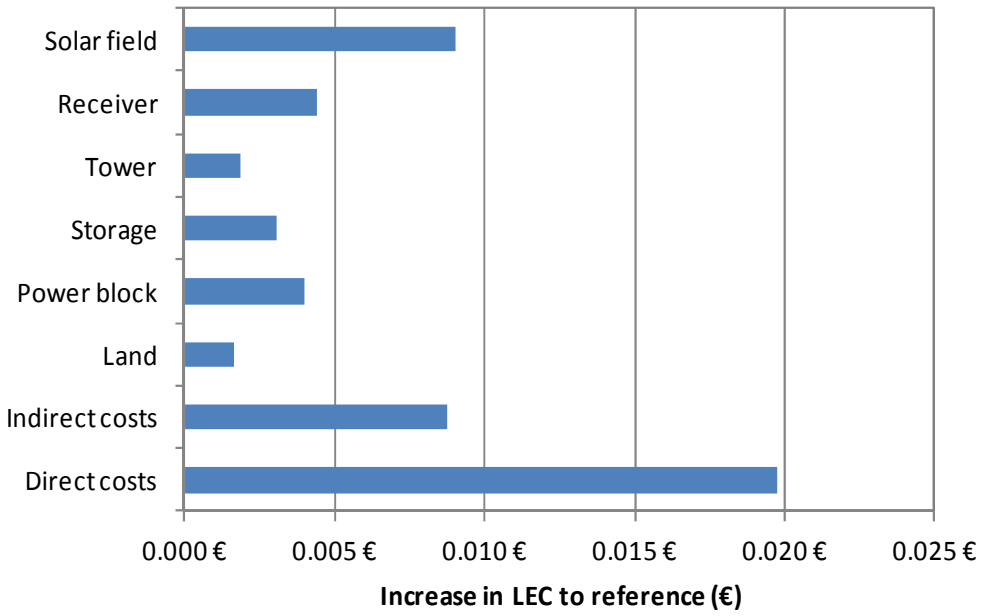

Figure 3.15: Sensitivity impact of several factors in power plant LEC (compared to reference - CRS#3).

The sensitivity analysis can also be used to estimate the impact of several predictable technological and/or production improvements on the final LEC (e.g. component mass production or performance improvements). From this point of view, the impact on LEC of several factors was analysed: a) the application of thin film mirrors (higher reflectivity – 0.955 [24]); b) 20 % reduction in heliostat costs to 120 €/m^2 [3] (dedicated heliostat production line); c) application of new storage materials (phase change materials or solid materials with ceramic saddles - 30 €/kWh_{th} [3]); d) increase in receiver performance by 10 %; and e) higher steam pressure power block. Some of these scenarios are based on products currently in the market (such as thin film mirrors and higher pressure power blocks), which were not considered in the base model due to the conservative approach used. Figure 3.16 presents the impact of these new scenarios in the CRS levelized electricity cost.

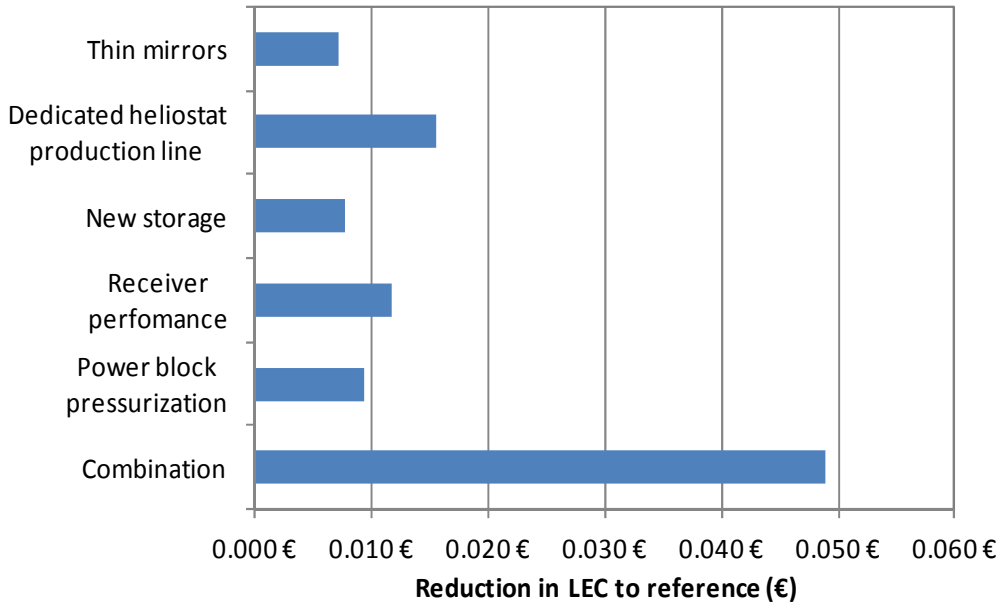

Figure 3.16: Impact of possible mid-term innovations in LEC (compared to reference - CRS#3).

The combination of all these improvements pushes CRS technology towards mid-term grid parity, reducing the LEC to 0.185 €/kWh (reduction of 0.049 €/kWh, Figure 3.16). On the other hand, if a 10 % direct cost overrun is considered, the LEC becomes 0.253 €/kWh (Figure 3.15), which is dangerously close to the feed-in tariff. The LEC methodology does not indicate the most profitable investment, which can be calculated based on the power plant cash flows considering, e.g. technical factors such as the generated electrical energy and power plant degradation; and financial factors such as feed-in tariff, amortization period and local taxes. The cash flow sensitivity analysis to these technical and economic factors is presented in Table 3.15.

Table 3.15: Cash flow sensitivity analysis - CRS#3.

Type	Variation (to reference)	New IRR (%)	New NPV (million €uro) [a]	New Payback period (years) [a]
Technical	Power degradation (+/- 1 % point per year)	7.6 / 11.9	4.2 / 12.2	19 / 12
	CAPEX (+/- 10 %)	7.7 / 12.2	5.6 / 9.9	19 / 11
	Generated electricity (-/+ 10 %)	7.2 / 12.7	4.5 / 11.5	20 / 10
Financial	Depreciation (-/+ 10 years)	10.0 / 8.8	7.6 / 6.9	13 / 18
	Loan time (+/- 10 years)	11.0 / 8.8	7.1 / 8.9	11 / 16
	Insurance rate (+/- 1 % point)	8.7 / 11.1	6.6 / 9.1	17 / 12
	Own capital (All/None)	7.8 / 13.9	10.4 / 6.4	14 / 16
	Debt interest (+/- 1 % point)	8.9 / 10.8	6.9 / 8.8	16 / 13
	Profit taxes (+/- 2.5 % point)	9.7 / 10.0	7.6 / 8.2	15 / 14
	Inflation (+/- 2 % point) [b]	9.8 / 9.8	4.2 / 13.3	17 / 13

a - considering an average 4 % annual inflation, with exception of [b]

The cash flow analysis shown in Table 3.15 is sensitive to several parameters. This reinforces the necessity to perform a complete economic analysis, including a sensitivity analysis. The investment viability is highly influenced by deviations from the reference in the CAPEX, generated electricity and power plant degradation. The financial factors also have considerable impact on the power plant economic viability. Most of the financial factors are defined or influenced by policy makers. One of the major concerns from the power plant operators and investors, is the stability of the national and international financial indicators such as taxes, debt interests, inflation, feed-in tariffs, so that a CRS power plant long-term investment has a positive return. This is reinforced by the results given in Table 3.15. A worse than reference scenario can decrease the NPV by almost € 4 million, or increase the payback period by 2-3 years; however, a more positive scenario, e.g. if the actual annual average inflation is maintained at 2 % (2 % lower than reference), the power plant investment can have

very positive contours, with NPV close to € 13 million and a own capital payback of 13 years. The capital payback can be shortened up to 11 years, with an IRR of 11 %, if the loan is extended to 30 years, but the NPV becomes € 0.8 million smaller (Table 3.15).

3.6 Conclusions

Within the Portuguese reality (Faro conditions) the selected 4 MWe solar only atmospheric volumetric CRS power plant configuration was CRS#3_SM1.25_2S_CS#1 (hereafter mentioned as CRS#3). This power plant has a 1.25 solar multiple, a 2 hour storage, control strategy #1 (CS#1), and a HRSG that generates 80 bar and 480 °C steam to feed a 3 stage turbine. This solution has a good cost/performance/complexity trade-off. It has a higher efficiency than a 4 MWe CRS with operating conditions similar to the Jülich Solar Tower (option #5), and a lower LEC. The optimal design DNI for local conditions is 750 W/m^2 while considering a peak receiver flux of 950 kW/m^2 (power plant LEC is 0.234 €/kWh with a CAPEX of € 22.3 million). If this receiver flux limit is increased by 10 %, the power plant increases the performance by 0.1 GWh per year, reducing its LEC to 0.232 €/kWh, well below the feed-in tariff of 0.273 €/kWh.

Higher pressure and multi-pressure power blocks have higher efficiency, generating more energy. However, the increase in power block operating pressure and pressure levels adds complexity to the system, leads to higher CAPEX and maintenance costs. The solar multiple and storage capacity have a significant impact on power plant LEC and their optimization and control strategy can save significant capital. CS#1 presents better economical results compared to CS#2 and CS#3, due to higher annual electricity generation, despite higher personnel and maintenance costs. This is notorious for larger solar multiple and storage capacity power plants (base load power), with higher investment, but no return on the annual generated electricity. If the objective is to use CSP for power on demand, adjusting the supply to the demand peaks, CS#4 can be an interesting solution, but only if a additional bonus tariff is considered for these periods.

If 30 % own capital, and a 20 year loan with an interest rate of 8 % financing structure is selected, with 1 % of power plant degradation, a 1 % annual insurance rate, a linear amortization for 20 years, feed-in tariff of 0.273 €/kWh and current national profit taxes, the investment IRR is 9.8 %, with a payback time of 14 years and a NPV of € 7.9 million (considering an average annual inflation of 4 %).

The sensitivity analysis indicates that both LEC and power plant cash flow are influenced by variations in CAPEX, generated electricity, financing strategy and economic indicators. Safe margins were considered during the analysis and equipments cost and performance was checked with manufacturers and reliable references. The power plant models are highly sensitive to the debt structure and CAPEX, and so further detailed budgeting and financing options should be considered. In the case of better than reference economic indicators (annual average inflation of 2 % instead of 4 %), the power plant investment has very positive contours, with NPV close to 13 million € and a payback period of 13 years. Also, if some commercial or innovations under development are introduced in the power plant, the LEC can be reduced to a value close to grid parity (0.185 €/kWh).

References

[1] Coelho, B., Varga, S., Oliveira, A.C., Mendes, A., Optimization of an Atmospheric Air Volumetric Central Receiver System: Impact of Solar Multiple, Storage Capacity and Control Strategy, International Journal of Renewable Energy, 2014, Vol.63, pp.392-401.

[2] Project information - solar thermal investigation plant in Jülich brochure (2010), Kraftanlagen München GmbH.

[3] Pitz-Paal, R., Dersch, J., Milow, B., (2005). ECOSTAR roadmap document, DLR.

[4] Silberstein, E., (2009). Brightsource Solar Tower Pilot in Israel‘s NEGEV Operation at 130 bar @ 530°C Superheated Steam, SolarPACES Conference 2009, Berlin, Germany.

[5] Personal communication from EDP and from: http://www.a-nossa-energia.edp.pt/centros_produtores/info_tecnica.php?item_id=72&cp_type=te&section_type=info_tecnica, accessed on 13-07-2011.

[6] Coepro Portugal, personal communication, June 2011.

[7] Meteonorm typical year for Faro 2005, Algarve Portugal.

[8] Romero, M., Zarza, E., (2007). Handbook of Energy Efficiency and Renewal Energy, Chapter 21: Concentrating Solar Thermal Power, CRC Press.

[9] Stine, W., Harriganm, R., Solar Energy Fundamentals and Design”, John Wiley & Sons, Inc., 1985.

[10] http://www.dlr.de/en/desktopdefault.aspx/tabid-5105/8598_read-19289/, accessed on 23-01-2012.

[11] Siemens Portugal, personal communication, June 2011.

[12] http://epp.eurostat.ec.europa.eu/inflation_dashboard, accessed on 03-02-2012.

[13] Sargent and Lundy LLC Consulting Group (2003), Assessment of Parabolic Trough and Power Tower Solar Technology Cost and Performance Forecasts, NREL/SR-550-34440.

[14] Coelho, B., Mendes, J.G, Helios3S: Small Size Solar Precision Tracking Heliostat, UPorto internal report, August 2009.

[15] Fend T., DLR, personal communication, February 2011.

[16] EFACEC Engineering Portugal, personal communication, June 2011.

[17] Seider, W., Seader, J., Lewin, D., Product and process design principles: synthesis, analysis, and evaluation, 2nd edition, Wiley, 2004.

[18] Peters, M., Timmerhaus, K., West, R., Plant design and economics for chemical engineers, 5th edition, McGraw Hill, 2003.

[19] Mancini, T., (2000).Catalog of Solar Heliostats, SolarPaces technical report.

[20] NEM and KAM, personal communication, September 2011.

[21] Tamme, R., Update on the German TES program, presentation from workshop on thermal storage for trough power systems, February 2003, USA.

[22] http://www.che.com

[23] Gueymard, C., (2010).Variability in direct irradiance around the Sahara: are the modelled datasets of bankable quality?, SolarPACES Conference 2010, Perpignan, France.

[24] http://www.flabegsolar.com/index.php?id=144&L=1, accessed on 13-07-2011.

Chapter 4

Hybridization with biomass in the steam cycle

This page was intentionally left blank

4. Hybridization with biomass in the steam cycle

CRS hybridization with biomass is an innovative concept. It was first presented at the SolarPaces 2010 and 2011 conference, under the scope of the SOLMASS project. The models for transient simulation of hybrid CSP/Biomass power plants in EBSILON, HFLCAL and EXCEL generated great interest and the concept received good feedbacks from the CSP community. The work was afterwards detailed and published in an international journal [1]. The approach was to design solar and biomass forest waste only base cases, validated with available data, so that it would be possible to compare the impact of hybridization. Next, several options were considered for the hybrid power plant, either altering the configuration (including storage or not), the design power (4 or 10 MWe) or the control strategy (different solar fractions). All options considered the biomass integration into the steam cycle of the CRS. As done in Chapter 3, the validity of the models and respective assumptions is detailed.

4.1 Options

4.1.1 Base cases

A set of base cases of solar only and biomass power plants were considered, and hybrid systems of these base cases and variants were proposed and assessed. These base cases were also used for validation of models and to build-up hybrid solutions. Two CSP power plants were designed for Algarve's irradiance conditions as base cases: CRS_SM1 - 4 MWe CRS without storage (solar only) – hereafter mentioned as CRS#0; and a 4 MWe CRS with 3 h energy storage (CRS#12_SM1.25_3S_CS#1) – hereafter mentioned as CRS#12. From these base cases it is possible to analyse the effect of a storage device in CRS electricity generation.

For the biomass base cases, two forest waste direct burning plants were considered: FRB4 - 4 MWe biomass forest waste burning plant and FRB10 - 10 MWe biomass forest waste burning plant. The power cycle operational design properties are similar to those chosen for the CRS base cases, so that a comparison would be possible. With this selection, it is possible to analyse a biomass solar-assisted power plant model, or to create a solar-biomass assisted power plant. It is also possible to compare the biomass consumption and electricity generation for two sizes of forest waste biomass power plants.

4.1.2 Hybrid solutions

The hybridization of volumetric open air receivers and forest waste biomass direct burning plants can present several advantages: energy dispatchability, improved power plant capacity factor, adding value to the forest waste biomass through the generation of electricity, a valuable good. The market for hybrid power plants can be the substitution of fossil fuel fired power plants, at end of their life cycle, producing an electricity flow that is proportionally adjusted to the demand by the consumers. Also, it is a sustainable technology, 100 % renewable resource based, which can, in medium-long term, be market competitive.

Integration of biomass in volumetric atmospheric air CRS systems can be done in the steam (power block level) or air cycle (boiler level). The integration should be assessed in terms of reliability and risk. A volumetric CRS power plant can generate a high hot air flow (680 °C) that exchanges its heat on a steam generator, producing a 480 °C and 80 bar steam flow that can be integrated into the biomass boiler power block (FRB10 – Table 4.1) and feed the turbine, with steam on similar conditions, at design point, with 50 % of its steam. At the same time, it is a low risk approach for integration of future concepts of open volumetric CRS on forest waste biomass plants. This concept could easily be tested after the construction of the independent power plants: biomass power plant and CRS power plant – SOLMASS project. The integration should lead to an increase in the solar plant capacity factor and a reduction of biomass consumption. Several cases were analysed:

- FRB4#CRS#0 – hybrid FRB4 biomass boiler steam integration on the CRS#0 power block (independent boilers) – no transients case;
- FRB10#CRS#0 – hybrid FRB10 biomass boiler steam integration on the CRS#0 power block (independent boilers) – no transients case;
- FRB4#CRS#12 – hybrid FRB4 biomass boiler steam integration on the CRS#12 power block (independent boilers);
- FRB10#CRS#12 – hybrid FRB10 biomass boiler steam integration on the CRS#12 power block (independent boilers);

The main operating design values are the electric power output, 4 MW and 10 MW, and two operating scenarios, 24 hour and solar-only operation. Table 4.1 summarises the main routes considered for forest waste biomass burning plant integration on the volumetric air CRS power plant, with and without storage.

Table 4.1: Main routes considered for forest waste biomass burning plant integration on a volumetric open air CRS power plant at design point.

		Plant designation	Plant specification	Operating mode	Receiver/ Boiler	Storage	Power block
Base Cases	**CRS**	**CRS#0**	CRS - 4 MWe	Solar only SM=1	19 MWth (CRS)	No	4 MWe dedicated
		CRS#12	CRS - 4 MWe	Solar only SM=1.25	24 MWth (CRS) + 10 % flux peak allowed	3h full power	4 MWe dedicated
	Biomass	**FRB4**	Forest waste biomass plant – 4 MWe	24 hours	15 MWth (Biomass)	No	4 MWe dedicated
		FRB10	Forest waste biomass plant – 10 MWe	24 hours	34 MWth (Biomass)	No	10 MWe dedicated
Hybrid Solutions	**Without Storage**	**FRB4#CRS#0**	Hybrid steam – Independent boilers	24 hours SM=1	19 MWth (CRS) +15 MWth (Biomass)	No	4 MWe shared
		FRB10#CRS#0	Hybrid steam – Independent boilers	24 hours SM=1	19 MWth (CRS) + 34(17@ DP) MWth (Biomass)	No	10 MWe shared
	With Storage	**FRB4#CRS#12**	Hybrid steam – Independent boilers	24 hours SM=1.25	24 MWth (CRS) +15 MWth (Biomass)	3h full power	4 MWe shared
		FRB10#CRS#12	Hybrid steam – Independent boilers	24 hours SM=1.25	24 MWth (CRS) +34(17@ DP) MWth (Biomass)	3h full power solar part	10 MWe shared

4.2 Results

For the base cases, only state of the art technologies were considered, for a standard design. The meteorological database used was Meteonorm, with the typical year for Faro with a 1 hour semi-steady-state time step (total annual 8760 time steps) [2]. For each time step a position in the control strategy was chosen and the system performance calculated with the use of characteristic lines relative to nominal conditions in Ebsilon.

CRS base cases (Table 4.01) were modelled and validated according to the technology applied on the Jülich Solar Power Plant [3]. CRS#0 did not consider thermal storage, and so the operating strategy is to conduct all thermal energy from the receiver to the power block and operate during daytime, Figure 4.1.

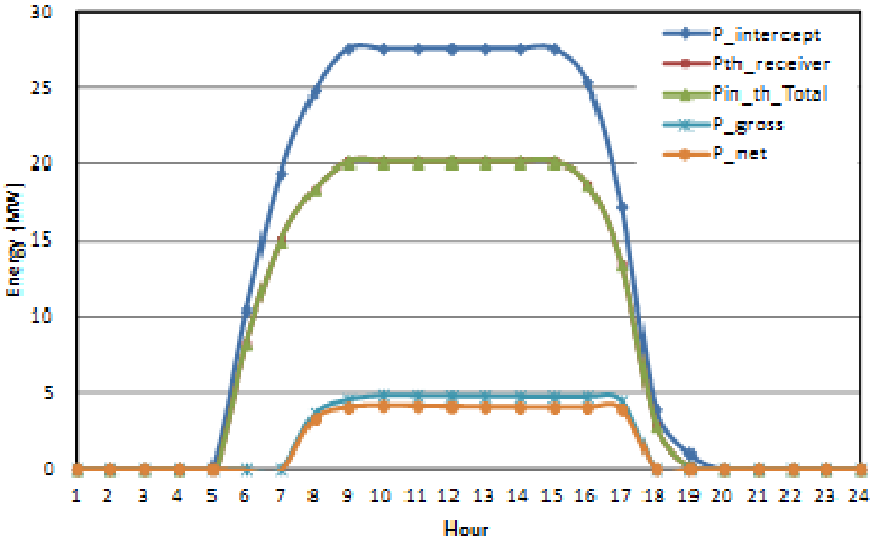

Figure 4.1: Performance on a typical day for CRS#0.

As expected, the solar plant CRS#0, despite having the same nominal power, produces 3.5 times less energy than the biomass plant FRB4, mainly due to the absence of storage. Case CRS#0 is for comparison purposes only, because a power plant without storage should have several operating problems with solar transients. To face these issues the CRS#12 power plant was designed with a SM of 1.25 that fills a thermal storage module of around 50 MWth, which is able to operate the power plant for 3 working hours at full power. The chosen control strategy was to favour the power block operation, and the remaining energy is conducted to storage. During low solar energy transients, the stored energy is used to fill the power block needs. The daily typical CRS#12 performance is presented in Figure 4.2.

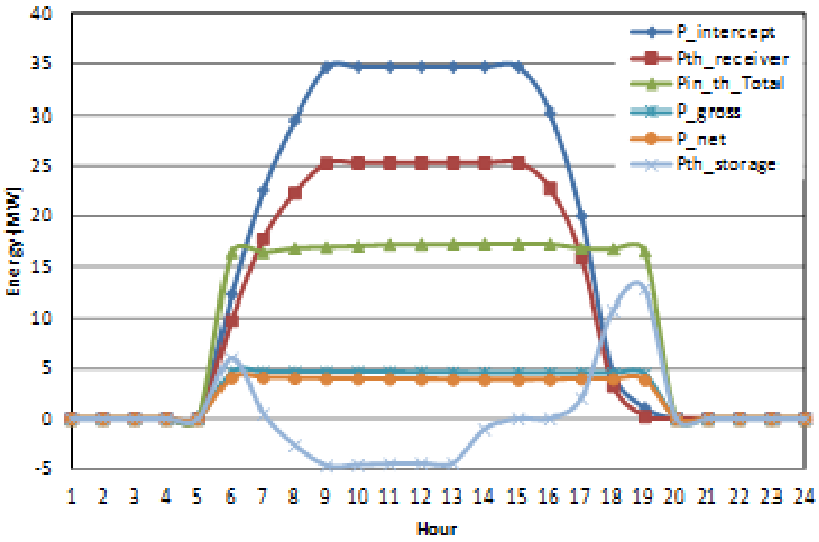

Figure 4.2: Performance on a typical day for CRS#12.

CRS#12 generates about 30 % more energy (12.3 GWh of electricity per year) than CRS#0. However, CRS#12 still generates 2.5 times less electricity than a conventional FRB4 biomass power plant. Also the CRS#12 power plant efficiency from feedstock to electricity is lower. The energy efficiency of the biomass units includes the biomass energy content, neglecting the energy spent for harvesting, storing and feeding. This efficiency from feedstock to electricity of the biomass units is then inflated; on the other hand, the cost balance considers all the previous aspects. CRS#0 LEC is 0.008 €/kWh higher than for CRS#12 and 0.135 €/kWh higher than for FRB4; yet no costs were considered for atmospheric emissions. Moreover, the feed-in tariffs are much lower (0.16 €/kWh) for biomass than for CSP, and so the profit margin of exploiting the CRS#0 is similar to FRB4. The CRS#12 power plant, due to the higher electricity generation, has a higher profit margin compared to CRS#0, and also benefits power plant operation and its feasibility and overall efficiency.

Table 4.2: Main results for biomass and CRS power plant steam integration.

Plant designation	Feedstock (energy content)	Annual gen. electricity*** (GWh/year)	Energy dump. (GWh/year)***	Solar fraction	Efficiency from feedstock to electricity ****	LEC ***** (€/kWh)
CRS#0	Sun (Faro, 2183 $kWh \cdot m^{-2} \cdot year^{-1}$)	8.9 *	7.1	100 %	10 %	0.240
CRS#3	Sun (Faro, 2183 $kWh \cdot m^{-2} \cdot year^{-1}$)	12.1 *	6.9	100 %	10 %	0.234
CRS#12	Sun (Faro, 2183 $kWh \cdot m^{-2} \cdot year^{-1}$)	12.3 *	6.1	100 %	11 %	0.232
FRB4	Forest waste (31.9×10^3 ton/year, NCV – 13806 kJ/kg)	31.6 **	0	0 %	26 %	0.105
FRB10	Forest waste (73.2×10^3 ton/year, NCV – 13806 kJ/kg	78.8 **	0	0 %	28 %	0.093
FRB4#CRS#0	Sun + Forest waste (24.7×10^3 ton/year)	31.7 **	26.6	31 %	18 %	0.120
FRB10#CRS#0	Sun + Forest waste (62.3×10^3 ton/year)	78.8 **	48.5	14 %	24 %	0.100
FRB4#CRS#12_CS#5	Sun + Forest waste (21.2×10^3 ton/year)	31.4 **	37.5	39 %	17 %	0.144
FRB4#CRS#12_CS#6	Sun + Forest waste (27.2×10^3 ton/year)	31.4 **	31.3	24 %	15 %	0.149
FRB4#CRS#12_CS#7	Sun + Forest waste (24.4×10^3 ton/year)	31.7 **	28.0	34 %	16 %	0.146
FRB10#CRS#3	Sun + Forest waste (61.0×10^3 ton/year)	78.9 **	43.6	20 %	23 %	0.108

* Plant availability of 96 %; ** Plant availability of 90 %; *** not considering losses by plant unavailability; **** Annual net values; ***** for a 30 year life time, annual 8 % debt interest rate and 1 % annual insurance costs [4];

For the hybrid solutions, at design point (DP), several points for integrating biomass into the CRS steam cycle were considered. As steam properties were similar for all the base cases, the integration was made into the first stage of the turbine with the assistance of a controller to define the flow required. The biomass boiler is fed by condensate from the economizer, allowing higher system efficiency. All the components from a typical biomass

plant were maintained in the hybrid solutions, with the exclusion of the power block (PB) that is shared with the CRS.

The day operation of the biomass boiler (similar in the case of FRB10#CRS#0) reduces the boiler transients and increases overall efficiency. However, as there is no storage considered in the FRB4#CRS#0 approach, this control strategy would also increase the solar energy dumping, and decrease the solar fraction of total generated energy. So, for comparison purposes, a semi-ideal boiler without inertia was considered, that may start up or shut down to face solar transients and during night operation, Figure 4.3.

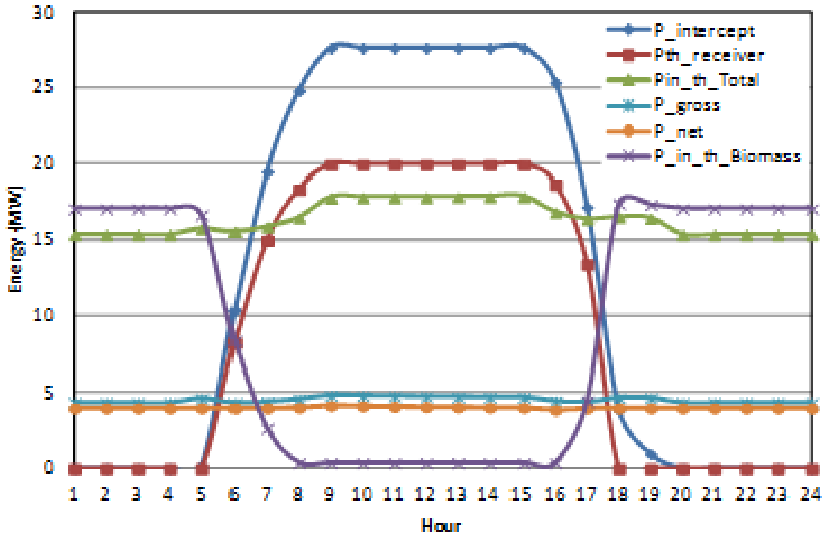

Figure 4.3: Performance on a typical day for FRB4#CRS#0.

The hybrid plant FRB4#CRS#0 was set to operate with solar power and, when absent, biomass is used to achieve the 4 MWe nominal power. The CSP fraction of the total annual energy production is around 31 %, Table 4.2. Again, the integration of a storage device can significantly improve this factor. Furthermore, there is a considerable loss in efficiency of the biomass boiler, due to the daily start-up and shut down. Also, the manufacturer does not recommend frequent start-ups and shut downs of the biomass boiler.

Similarly to the FRB4#CRS#0 power plant, the FRB10#CRS#0 power plant did not contemplate an energy storage system. However, due to the design power of this power plant, a conventional biomass boiler would take at least 2 hours to stabilize during start-up and shut down, mainly due to high inertia [5]. The control strategy of FRB10#CRS#0 should take this factor into account, maintaining the boiler under continuous operation. During the night, the strategy is to operate the plant at 100 % biomass load, while during the day the biomass load is

reduced to around 50 % and the CRS power is used to generate the remaining energy. However, even considering a low inertia boiler, and due to load restrictions of the CRS receiver, the CSP fraction of the total annual energy production is only around 14 % (Table 4.2) - FRB10#CRS#0. A typical operating day for FRB10#CRS#0 is presented in Figure 4.4.

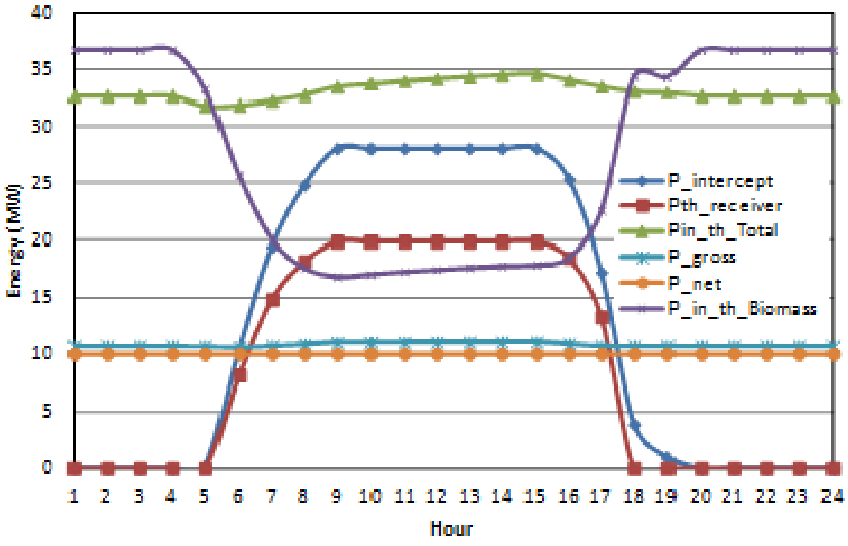

Figure 4.4: Performance on a typical day for FRB10#CRS#0.

Regarding the hybrid solutions, FRB4#CRS#0 presents a LEC of 0.120 €/kWh (Table 4.2), with lower biomass energy contribution due to its 31 % solar share. However, with storage absence, the biomass boiler is highly exposed to solar transients.

The FRB10#CRS#0 biomass boiler operates continuously, and despite the disadvantages of a minimum load operation for long periods, results in a better response to solar transients. Both boilers should be further studied, in agreement with manufacturers, as well as their off-design operating conditions, mainly in the response to solar transients.

In the case of CRS#0, FRB4#CRS#0 and FRB10#CRS#0, a minimum required radiation was set to start operating the CRS. Although it would be difficult to precisely predict the operation of the CRS power plant, a sensibility analysis indicated that a 10 % variation in the annual generated electricity would result in a variation of 0.027 (11.3 %), 0.013 (10.8 %), 0.011 (11.0 %) €/kWh of the CRS#0, FRB4#CRS#0 and FRB10#CRS#0 respective LEC. These variations confirm that a deviation in the generated electricity has a significant impact on the power plant LEC. External factors, such as a correct resource measurement and part load operation, can therefore have a big impact in the power plant LEC. A variation similar to this could easily

occur if the local conditions and the commercial equipment do not respond as predicted by the models used. This would reduce the LEC below the hybrid cases with storage.

The storage device can increase the efficiency of the CRS, since it reduces the solar transients. For the hybrid 4 MWe power plant, several control strategies were analysed: control strategies CS#5, CS#6, CS#7. The control strategy impact in these cases was significant, and its correct incorporation in the project determines the CRS viability. CS#5 control strategy was simulated to minimize the solar energy dumping. It considers operating the power plant with solar energy only during daytime, storing any solar energy excess. The biomass boiler operates during night time and solar transients. In the case of low solar conditions, the preferred source of energy is the storage, and only in the absence of stored energy is the biomass boiler started. However, due to the biomass unit stoppage (SL), the energy not generated by the boiler, because it is operating at partial load, is higher. FRB4#CRS#12_CS#5 design is more viable than the FRB4#CRS#0. Still, the daytime shutdown of the biomass boiler, and frequent start-ups, could be a problem and should be further studied. Performance on a typical day for FRB4#CRS#12_CS#5 is presented in Figure 4.5.

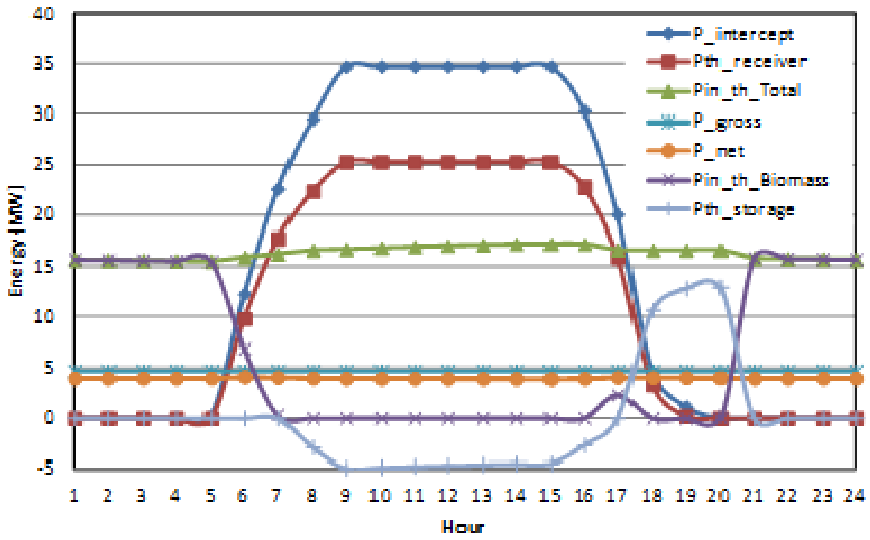

Figure 4.5: Performance on a typical day for FRB4#CRS#12_CS#5.

Control strategies FRB4#CRS#12_CS#6 and FRB4#CRS#12_CS#7 consider the boiler working 24 hours per day, despite efficiency penalties, because of the part-load operation. CS#6 control strategy objective is to never turn down the biomass boiler, using it at full power during night time, and reducing to minimum load during the day. The preferred source of energy is the biomass boiler, reducing its part load operation to a minimum, and the solar

power and storage were only used for transient solar conditions during daytime operation. A typical operating day for CS#6 is presented in Figure 4.6.

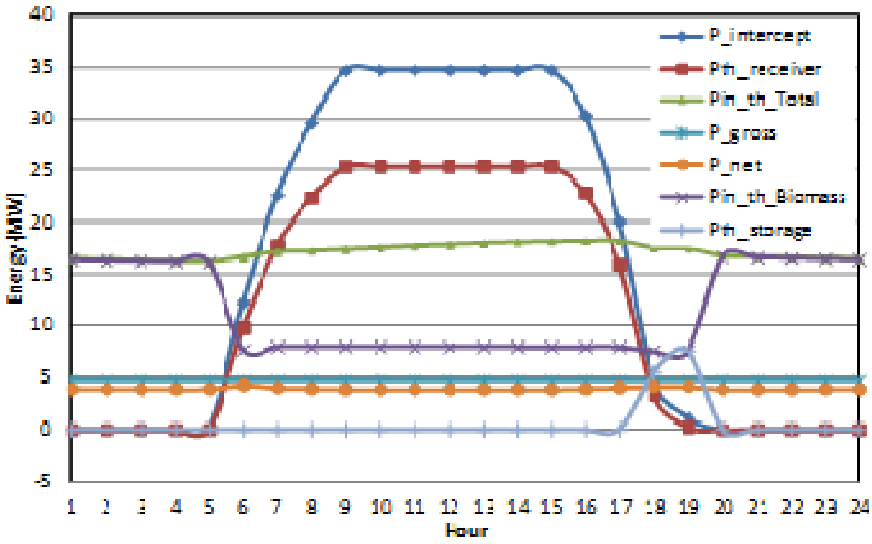

Figure 4.6: Performance on a typical day for FRB4#CRS#12_CS#6.

The CS#7 control strategy is similar to CS#6: it considers that the biomass boiler is never turned down and is run at full power during the night, reducing to a minimum load during daytime. Contrarily to CS#6, CS#7 control strategy sets the preferred sources of energy to be the solar energy and storage. Solar energy storage is used to store the energy excess, support the PB in solar transients and extend operating hours. In these hours the biomass boiler is used at minimum load conditions. A typical operating day for CS#7 is presented in Figure 4.7.

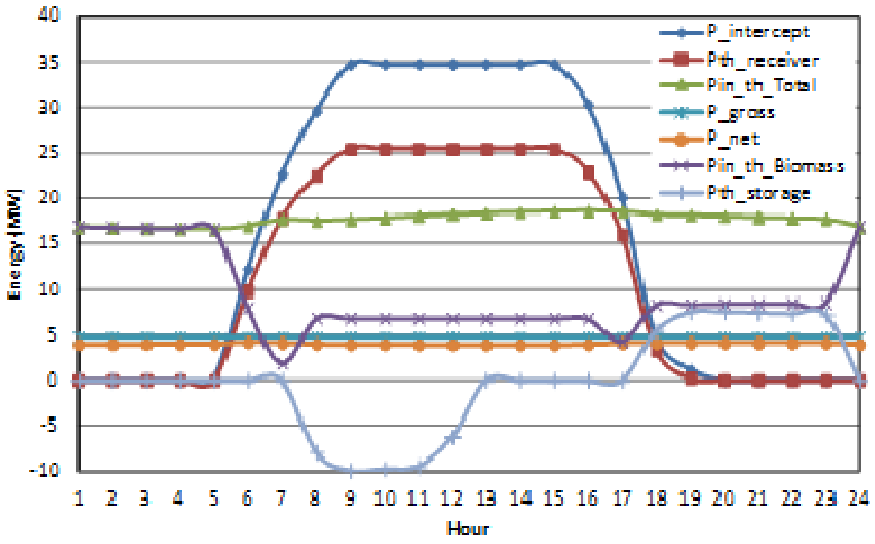

Figure 4.7: Performance on a typical day for FRB4#CRS#12_CS#7.

The main difference between FRB4#CRS#12_CS#6 and FRB4#CRS#12_CS#7 is the solar share: 24 % and 34 %, respectively; this parameter has, however, a small influence on the LEC – 0.003 €/kWh favourable to FRB4#CRS#12_CS#7. Adding to that, FRB4#CRS#12_CS#6 is more biomass dependent and is more exposed to its price volatility; it also presents a large solar and storage dumping. Comparing these three control strategies (Table 4.2), the one that presents lowest energy dumping on the CRS, and stoppage time on the biomass plant, is FRB4#CRS#12_CS#7; still this is a high value, 28 GWh/year, and the actual limitations of state-of-the art technologies should improve to reduce this value and further reduce the LEC.

The last hybrid configuration considered, FRB10#CRS#12, integrates a 4 MWe CRS with 3 hour storage into a 10 MWe biomass power plant. The biomass boiler and the CRS share a common 10 MWe power block, similar to the one used in FRB10#CRS#12. The control strategy applied is similar to CS#7, with the constant operation of the biomass boiler (night at full load; day at minimum load) and the preferential use of storage to sustain the PB during solar transients and to extend daytime operation. A typical operating day for FRB10#CRS#12 is presented in Figure 4.8.

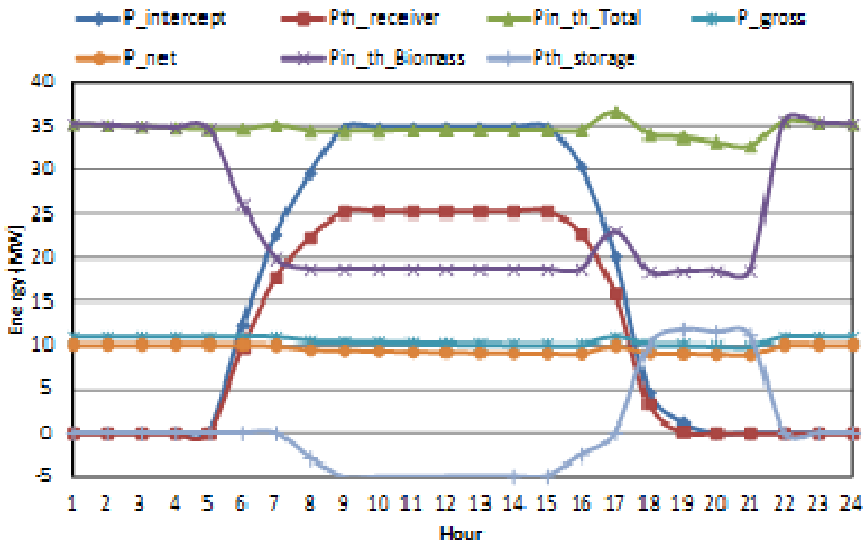

Figure 4.8: Performance on a typical day for FRB10#CRS#12.

Economic indicators are normally the decision factor for the construction of these power plants. As this is still an under-developed technology concept, the technical viability is still unproven, and the technical models have a significant importance.

A cash flow analysis of the project is dependent on several financial factors: fraction of own capital used, amortization structure, debt payment structure and methods used for future cash flow calculation, and production factors such as: power plant degradation, variation on operation and maintenance (O&M) costs, and volatility of biomass costs. Due to the uncertainty of these values, a cautious analysis of the results is recommended. Also, the validation of these values is restricted to the assumptions of the models; a cash flow analysis for each solution was conducted, considering 30 % own capital; a linear amortization structure during the 30 years of the project, and a 20 year loan with an interest rate of 8 %. A 1 % of power plant degradation was used, with fixed biomass (27 €/ton – based on Mortágua power plant [5] actual biomass cost in 2011) and O&M costs; also, a 1 % annual insurance and national profit taxes were considered. Table 4.3 presents the results of the economic analysis for the different power plants.

Table 4.3: Economic analysis for hybrid power plants in the Portuguese Algarve region.

Plant designation	Internal rate of return - IRR (%)	Net present value - NPV (Millions of €uro)*	Payback period (years) *
CRS#0	8.7 %	6.2	16
CRS#12	9.7 %	11.1	14
FRB4	7.4 %	3.3	19
FRB10	14.0 %	22.4	7
FRB4#CRS#0	12.2 %	18.1	9
FRB10#CRS#0	14.6 %	35.9	7
FRB4#CRS#12_CS#5	6.8 %	7.9	21
FRB4#CRS#12_CS#6	5.9 %	5.1	23
FRB4#CRS#12_CS#7	6.6 %	7.1	21
FRB10#CRS#12	11.0 %	27.7	11

* - considering an average 4 % annual inflation.

The cash flow analysis of the hybrid design FRB4#CRS#0 results in an internal rate of return (IRR) of 12.2 %, while for FRB10#CRS#0 the IRR is 14.6 % (Table 4.3). If a 2 % degradation in production per year is considered, the IRR should decrease to 9.8 % (in the case of FRB4#CRS#0) and to 11.7 % (in the case of FRB10#CRS#0). This performance degradation could be expected in the units without storage, due to high equipment fatigue, reducing the IRR of FRB10#CRS#0 to values closer to FRB10#CRS#12 - IRR of 11.0 %.

FRB10#CRS#0 presents a LEC only 0.015 €/kWh higher than the conventional FRB10, and only a 3 % lower IRR, with a predicted NPV of 27.7 M€ and a payback period of 11 years (Table 4.3); this investment has positive contours and a low dependence on biomass (approximately 12 thousand tons less per year than FRB10).

The hybrid solutions with storage present a lower IRR (6.8% - FRB4#CRS#12_CS#5; 5.9% - FRB4#CRS#12_CS#6; 6.6% - FRB4#CRS#12_CS#7) than the hybrid solutions without storage. The most balanced technical control strategy is FRB4#CRS#12_CS#7. Comparing with the other control strategies, the FRB4#CRS#12_CS#7 NPV is 10 % lower than FRB4#CRS#12_CS#5 and 28 % higher than FRB4#CRS#12_CS#6. The FRB4#CRS#12_CS#7 control strategy would reduce energy dumping, reduce the number of plant start-up and shut-down periods, and this can have an influence in long-term operation of the power plant. In the

case of FRB4#CRS#12_CS#5, if 2 % degradation in production per year is considered, the IRR should decrease to 4.2 %, 36 % less than the IRR of FRB4#CRS#12_CS# 7 (6.6 %). This reveals that the IRR is sensitive to the generated electricity and depends on equipment reliability to deliver the design power. It also backs-up the use of conservative control strategies that can deliver the proposed electricity, and preserve equipment.

FRB4#CRS#12_CS#7 IRR was 6.6 % and the LEC (0.146 €/kWh) was 0.086 €/kWh lower than CRS#12 (9.7 %, 0.232 €/kWh) with a 2.9 % lower IRR, and only 0.041 €/kWh higher than FRB4 (7.4 %, 0.105 €/kWh) but with IRR only 0.8 % lower, with a 7500 ton annual reduction on biomass consumption.

As the present Portuguese annual average inflation is around 4 %, this means that the investment is more attractive for larger power plants (10 MWe) than for the smaller power plants. This factor confirms a tendency for smaller projects to have lower profit perspectives, but in return they also have lower capital expenditure - CAPEX (FRB4#CRS#12_CS#7 – 34 M€, FRB10#CRS#12 – 50 M€). National authorities are aware of this reality and are considering allowing a percentage of alternative fuel (e.g. biomass) included in the CSP tariff [6], which would make these small projects more appealing to investors.

The evolution of the concept and application of larger future power plants seems promising. Still, some technical barriers should be overcome and concepts tested before large-scale implementation. However, this is a technology based on renewable resources, capable of supplying power on demand or base load power.

4.3 Validity

The models presented were validated for the base cases with experimental data, published references and suppliers' information. There is no commercial 4 MWe open volumetric receiver CRS plant in operation in the world. For this reason, CRS#0 and CRS#12 design conditions were based on designs presented on chapters 2 and 3. Regarding the biomass power plants, the design conditions of FRB10 were based on a Portuguese biomass power plant design [7], Figure 4.9.

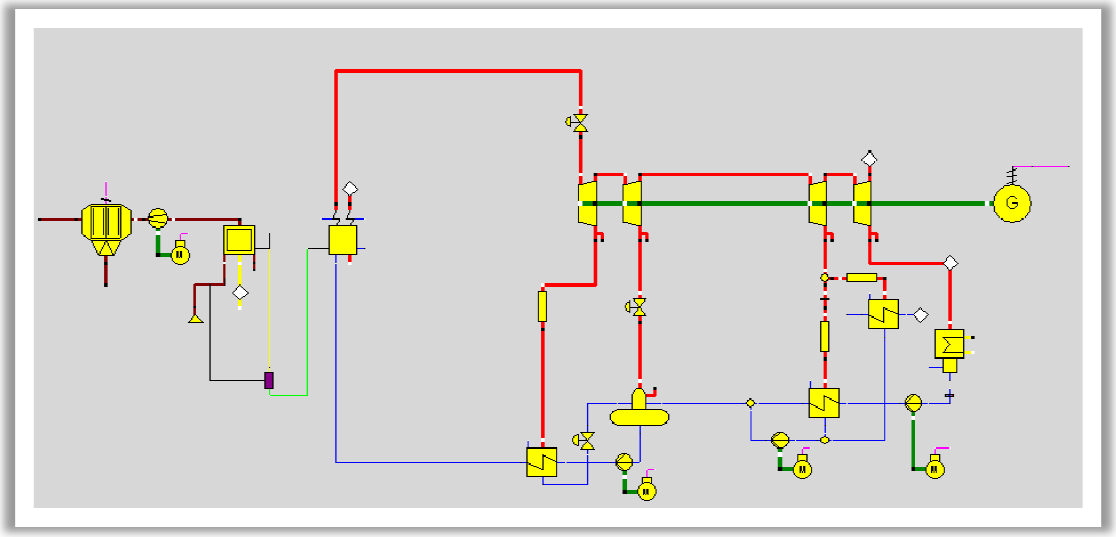

Figure 4.9: FRB10 Power plant configuration.

This power plant was considered to be working at design conditions with an estimated availability of 90 %. Economic models were built with distributed component costs, according to several references [8, 9], adjusting the final costs with consultations with engineering, procurement and construction (EPC) contractors [7, 10 and 11].

FRB4 performance was based on FRB10 components performance (based on commercial equipment). Turbine operating conditions were adjusted to smaller turbine 4 MWe characteristics, according to a personal communication from a turbine manufacturer (chapter 3). The remaining components were optimized with EBSILON Professional software. Component costs were based on the above mentioned references and EPC contractors, developing a detailed model for several installed powers. The model validation results are presented in Table 4.4.

The hybrid cases are a completely innovative concept and there are no commercial power plants in operation to validate this concept. The strategy used was to choose several validated components from the base cases and combine them to obtain the hybrid power plant. Further validation of off-design operation of biomass boilers is needed. The same methodology was used for economic models. The feed-in tariff for the hybrid power plants was calculated based on the national law [6] and considering a weighted contribution of each technology.

Table 4.4: Validation of the biomass boiler model.

	Real – 11 MWe [7]	Model – 11 MWe	Model – 10 MWe	Model – 4 MWe
Boiler input				
Biomass input (kg/s)	2.9	2.8	2.6	1.1
Air input (kg/s)	20.8	20.8	18.9	8.0
Water/ condensate (kg/s)	13.8	13.9	12.8	5.4
Boiler output				
Exhaust gases (kg/s)	24.4	23.1	20.9	10.0
Ashes (kg/s)	0.05	0.09	0.08	0.01
Steam (kg/s)	13.9	14.0	12.8	5.4
Other effluents (kg/s)	0.23	0.61	0.56	0.24
Power block				
PB efficiency	31.5 %	31.2 %	31.0 %	28.8 %

4.4 Conclusions

For biomass integration into the steam cycle of a CRS, the technical/economical balance is favourable to the FRB4#CRS#12 - applying control strategy CS#7 (hereafter mentioned as FRB4#CRS#12). FRB4#CRS#12 would reduce energy dumping; reduce the number of plant start-up and shut-down periods, with a LEC of 0.146. This LEC is 0.086 €/kWh, lower than CRS#12 and only 0.041 €/kWh higher than FRB4, with a 7500 ton annual reduction in biomass consumption. The economic indicators are nevertheless somehow distant from the base cases, with an IRR of 6.6 % (FRB4#CRS#12), compared to 9.7 % (CRS#12) and 7.4 % (FRB4).

For the 10 MWe power scale, the FRB10#CRS#12 power plant could generate electricity with a LEC of 0.108 €/kWh with the double of annual efficiency (feedstock to electricity) of a conventional 4 MWe CRS. Also, it would represent a 17 % reduction in biomass consumption (approximately 12 thousand tons less per year) when compared with a typical 10 MWe biomass power plant – FRB10, only a 3 % lower IRR than FRB10 and with a predicted NPV of 27.7 M€ and a payback period of 11 years - FRB10#CRS#12.

References

[1] Coelho, B., Schwarzbözl, P., Oliveira, A.C., Mendes, A., Biomass and central receiver system (CRS) hybridization: volumetric air CRS and integration of a biomass waste direct burning boiler on steam cycle, Solar Energy, 2012, Volume 86, Issue 10, pp. 2912 – 2922.

[2] Meteonorm typical year for Faro, 2005. Algarve Portugal

[3] www.ka-muenchen.de/253+M52087573ab0.0.html, accessed on 13-07-2011.

[4] Pitz-Paal, R., Dersch, J., Milow, B., (2005). ECOSTAR roadmap document, DLR.

[5] EDP Portugal, 2011. Personal communication, June 2011.

[6] Decreto-Lei n. 225/2007, 2007. Diário da República, no. 105, 1.ª série de 31 de Maio de 2007.

[7] Coepro Portugal, personal communication, June 2011.

[8] McNeil Technologies, Inc. for Oregon Department of Energy, (2003). Biomass Resource Assessment and Utilization Options for Three Counties in Eastern Oregon.

[9] California energy commission, 2007. Comparative costs of California central station electricity generation technologies.

[10] EFACEC Engineering Portugal, personal communication, June 2011.

[11] Siemens Portugal, personal communication, June 2011.

This page was intentionally left blank

Chapter 5

Hybridization with biomass in the air cycle

This page was intentionally left blank

5. Hybridization with biomass in the air cycle

Due to its design, the atmospheric volumetric CRS power plant offers a different possibility for hybridization of CSP with biomass: the air cycle integration. This concept was presented at SolarPaces 2012, building on the CRS model presented in Chapter 3, after developing several new models for biomass power plants. The models were also developed using EBSILON, HFLCAL and EXCEL, with the same approach followed in Chapter 2. All options presented in this chapter consider biomass integration into the air cycle of the CRS. Several biomass resources are analysed (base cases and hybrid options): wood pellets, wood residues, refuse-derived fuel, WWT biogas, landfill biogas and natural gas. The power plant performance and economic indicators are evaluated, detailing the validity of the models, and respective assumptions.

5.1 Options

5.1.1 Base cases

The process to find the optimal configuration for a 4 MWe atmospheric volumetric CRS power plant depends on several interdependent variables and is highly iterative. Several solar-only CRS power plant configurations were optimized [1] and are used as base cases for hybridization:

- CRS#3 - solar only power plant (4 MWe) with a 1.25 solar multiple and 2 hour storage, design DNI 750 W/m^2 and receiver area of 60.0 m^2 with receiver peak flux of 950 kW/m^2;
- CRS#14 - solar only power plant (4 MWe) with a 1.75 solar multiple and 6 hour storage, design DNI 750 W/m^2 and receiver area of 60.0 m^2 with receiver peak flux of 950 kW/m^2;
- CRS#12 - solar only power plant (4 MWe) with a 1.25 solar multiple and 3 hour storage, design DNI 750 W/m^2 and receiver area of 60.0 m^2 with additional 10 % tolerance in the receiver peak flux.

For Faro (Algarve) conditions, the best solar only power plant configuration is a 1.25 solar multiple, 2 hour storage, with a 4 MWe power block operating under Rankine cycle (steam nominal conditions at 480 ºC and 80 bar), working under a control strategy that uses the daytime solar power to run the power block storing the excess heat (CRS#3). This stored energy is used to cover solar transients and extend operation until storage is empty - see chapter 3.

The integration of biomass in the power plant can be done in the air cycle or in the steam cycle. The biomass integration in the steam cycle was analysed in chapter 4, using a biomass steam boiler. The base case for this power plant was a 4 MWe forest waste burning plant:

- Forest waste burning (FRB) – 24 hours/day operation forest waste (NCV = 13.8 MJ/kg) direct burning power plant with a 4 MWe power block operating under Rankine cycle [2].

The forest waste boiler technology is mature and has good fuel flexibility, but is usually associated with moderate efficiencies and large start-up and response times, to compensate typical solar transients (increased dumping in hybrid solutions). A fast response biomass based technology is biomass gasification with gas storage. Several early commercial prototypes had problems with gas cleaning (tar and ash removal), but latter biomass gasification power plants have been operating without major outages [3]. Despite this, fuel flexibility is still an issue, and a constant properties fuel should be selected for viable long term operation. Biomass forest wastes are not a resource with constant proprieties and usually have a high moisture content, sands and other contaminants. Due to this, alternative biomass resources were considered: wood residues or biomass pellets. The pellets have lower moisture content and are more uniform in terms of properties, but present a significant extra cost for the power plant. Wood residues have a lower cost than pellets but also have lower net calorific value (NCV).

The Güssing power plant is a successful case of biomass gasification. It is designed to supply with electricity and heat the Güssing district in Austria. The Güssing fluidised bed gasifier consists of two zones: a gasification zone and a combustion zone. The gasification zone is fluidised with steam which is generated by waste heat of the process, to produce a nitrogen free syngas. The combustion zone is fluidised with air and delivers the heat for the gasification process. The produced gas is cooled, cleaned and used in a gas engine. The heat produced in the process is partly used inside, e.g. for air preheating, steam production, etc., and the rest is delivered to the district heating system. Based on the reported performance [4, 5], the Güssing FICFB (fast internal circulating fluidised bed) gasifier concept was modelled and validated. Because the power block of commercial available atmospheric volumetric central receiver systems is composed by a HRSG and a steam turbine, and the objective of this study is the integration of biomass in CRS, the base case considers that the produced syngas is integrated in a HRSG (duct burner) and coupled with a steam turbine:

- Pellets gasification (PG) - gasifier operating with air/steam, a 4 MWe Rankine cycle power block operating 24 hours/day using biomass pellets (NCV = 18.6 MJ/kg);
- Wood residues gasification (WG) - gasifier operating with air/steam, a 4 MWe Rankine cycle power block operating 24 hours/day using wood residues (NCV = 16.2 MJ/kg).

A different possibility is to use refuse-derived fuel (RDF) from municipal solid waste pellets (mainly plastics and biodegradable waste). The gasification of RDF pellets is an interesting solution to solve the environmental impact of municipal solid waste. One reference in this technology is the 20 MWe Fukuyama RDF gasification power plant [6]. Another reference is the 6.7 MWe Greve in Chianti RDF pellets gasification power plant. However, several operational problems occurred in this power plant, namely with gas cleaning and maintaining gas properties. Based on the Chianti RDF and gasifier properties, a 4 MWe power plant was considered:

- Refuse-derived fuel gasification (RDF) – RDF pellets gasifier (NCV = 17.2 MJ/kg) coupled to a 4 MWe power block operating under Rankine cycle operating 24 hours/day.

Locally, there is also an interesting potential of biogas generated from a waste water treatment plant (WWT) and landfills. The biogas generated from the landfill has different characteristics compared with the biogas generated by a wastewater anaerobic digester [7]. For both cases the local plants are insufficient to sustain the 24 hours/day annual operation at nominal power (4MWe). For comparison purposes, a biogas waste-water anaerobic digester was considered:

- WWT biogas digester (BD) – biogas WWT digester (NCV = 20 MJ/kg) coupled to a 4 MWe power block operating under Rankine cycle operating 24 hours/day;
- Landfill biogas (BL) – landfill biogas (NCV = 12 MJ/kg) coupled to a 4 MWe power block operating under Rankine cycle operating 24 hours/day.

An alternative or supplement to syngas is natural gas. Natural gas Rankine and combined cycle power blocks are an established technology, but the “renewable goal” would be lost. A Rankine cycle power plant, using similar power block configurations was considered, replacing the feed from syngas and biogas by natural gas from local low pressure pipelines:

- Natural gas burner (NG) – natural gas burner boiler power plant with a 4 MWe power block operating under Rankine cycle operating 24 hours/day using natural gas (NCV = 38 MJ/kg).

The commercial power plants running on natural gas usually use combined cycles, scaling from 50 MWe up to several hundreds of MWe. The use of combined cycles in a the 4 MWe scale is not usual, as the HRSG and steam turbine would be quite small, resulting in higher capital investment (CAPEX), without a significant increase in power block efficiencies. Thus, a steam boiler and turbine operating on Rankine Cycle were used, which is a solution with lower efficiency but also a lower CAPEX.

5.1.2 Hybrid solutions

Using the components from the base case power plants described before, several hybrid solutions were developed. The objective for biomass integration in a CRS is to support the solar transients and increase the power plant capacity, the generated electricity and reduce the power plant LEC. The integration of the biomass/biogas/syngas in the air cycle of a CRS can be done, e.g. via a duct burner in the HRSG, via a combustion chamber of a gas turbine or gas engine. Fuel contaminants are a problem for all types of power systems. Gas turbines are especially sensitive to particulate matter, water and metallic contaminants [8]. Although fuel conditioning and handling systems should be considered for all combustion systems (to minimize fuel quality variations), in general gas turbines operate at higher average pressures and temperatures and are more prone to erosion and corrosion. The integration of a gas turbine would also imply a significant investment (despite the expected efficiency increase) and would imply a significant increase of hybrid fuel consumption (lower solar fraction). Also, the CRS design power (4 MWe) is low for most of the commercial combined cycle power blocks, and the cost/efficiency gain with the implementation of a micro gas turbine or small gas engine combined with a small steam turbine should be further studied. Comparing the integration options, the integration via a HRSG duct burner is a robust solution and with reduced investment. These reasons support the study of syngas/biogas integration via a duct burner in the HRSG, Figure 5.1.

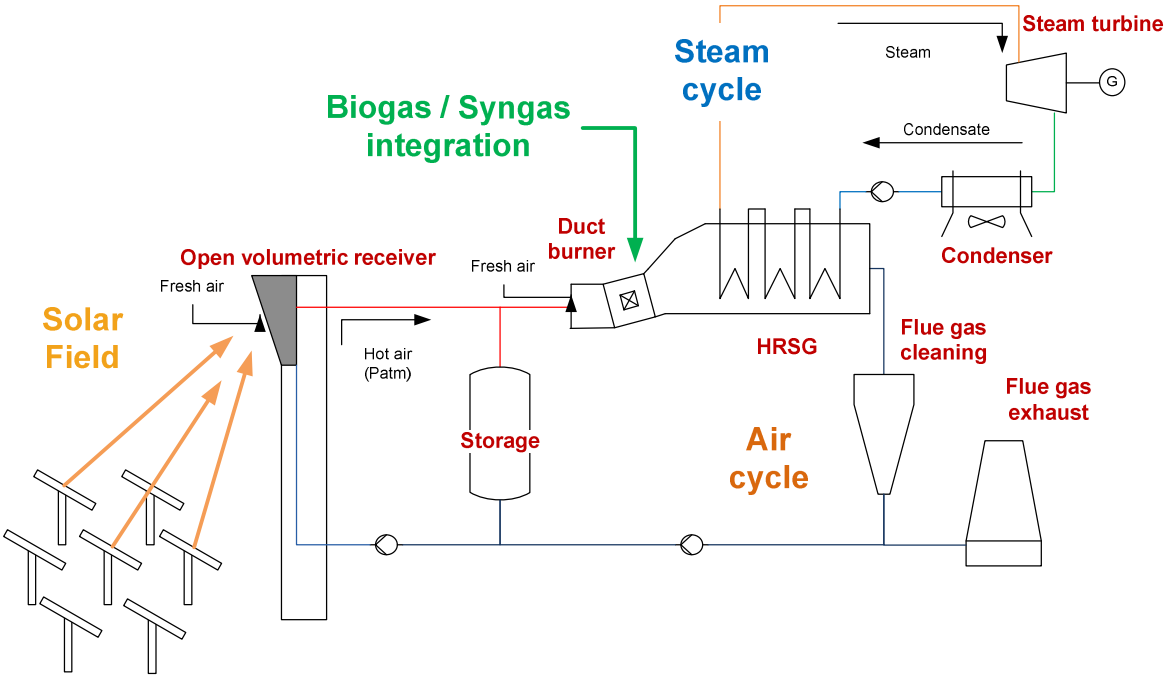

Figure 5.1: Integration of biomass on CRS power plant air cycle, on a duct burner in the HRSG.

Nevertheless, different options can be considered in future studies, e.g. finding the optimal control strategy for the hybrid power plant, utilization of combined cycles, utilization of organic Rankine cycles or power plant optimization for smart power generation - adjusted network demand/supply electricity generation, or utilization of CSP and biomass to generate chemical products such as hydrogen [9].

The comparison with the integration on the steam cycle – Chapter 4, is also positive to define the advantages/ disadvantages of both solutions. Also, other CSP technologies such as parabolic trough can have interesting results, e.g. the largest commercial CSP-biomass power plant worldwide - Termosolar Borges, Spain [10], uses a parabolic trough solar field and biomass boilers to generate 22.5 MWe. This is a hybrid solution that uses mature technologies for biomass integration on the steam cycle. However, the solar field output temperatures are lower, the biomass boilers start-up and transient response is slower when compared to the CRS hybrid biogas/syngas and is less efficient than biomass gasification. For the integration via duct burner in the HRSG (Rankine cycle), different fuels and CRS combinations can be considered for the hybridization, Figure 5.2.

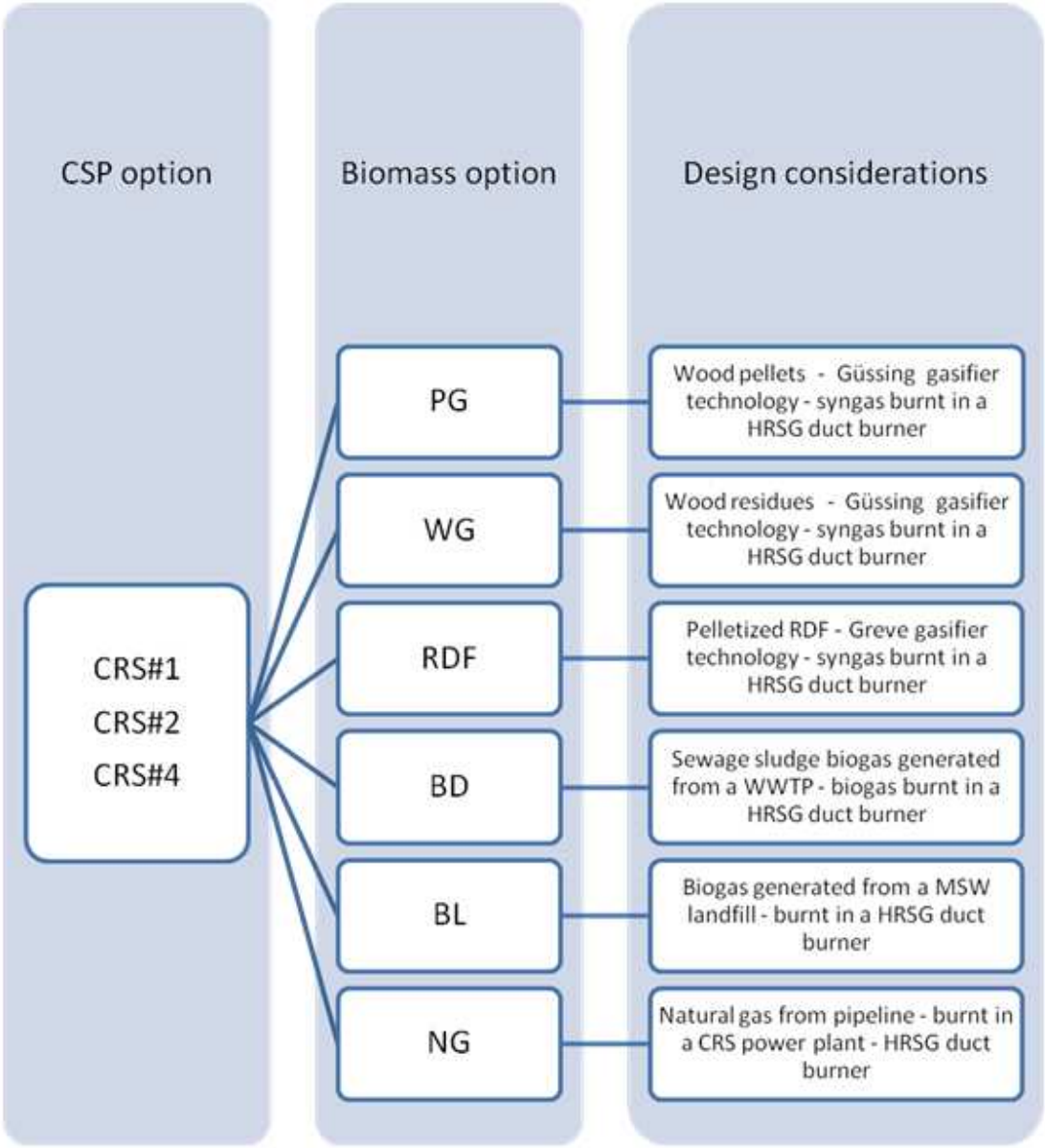

Figure 5.2: Hybridization options for the considered CRSs.

Wood pellets and residues gasification options:

The first two design options in Figure 5.2 consider a Fast Internally Circulating Fluidized Bed (FICFB) gasifier integrating the syngas generated in a duct burner of the CRS HRSG. The CAPEX for the Güssing power plant was 10 million euro and uses a combined heat (4.5 MW) and power (2 MW) gas engine [5] - CAPEX per installed electric power of 5 000 €/kWe. Different references indicate equipment costs for a CFB gasifier and internal combustion engine ranging from 1 850 to 3 460 €/kWe [11]. A pressurized fluidized bed gasifier with gas clean up and steam injected gas turbine engine can have a gross conversion efficiency up to 43 % [12] and a CAPEX per installed electric power cost of 5 325 €/kWe [12].

However, to compare all the gasification options, a model, based on Caputo et al. [13] was developed. For the Güssing power plant (2 MWe) this model resulted in a CAPEX of 5 328 €/kWe (+ 6.6% than the Güssing 2 MWe power plant cost) while for a 4 MWe it results in a power plant equipment cost of 3 175 €/kWe and CAPEX of 4 216 €/kWe, Table 5.1. The model used to estimate the ash disposal cost was based on Caputo et al. [13] and defines a cost of 62 €/ton for ash transport and of 24 €/ton cost for ash disposal [13].

The operation and maintenance (O&M) costs for the Güssing power plant are 1.3 million € per year [5] (including the biomass cost and ash disposal, 66 €/ton [14]). A different model for ash recycling or disposal costs in Sweden estimates: for ash recycle 55-66 €/ton; and for landfill deposit 11-44 €/ton + taxes [15]. As for Portugal the landfill taxes vary between 1 and 6 €/ton [16] the model used was conservative.

One of the major issues in biomass power plants is to have access to a competitive and stable biomass cost. To address this challenge, the power plant is usually located close to the biomass source and the biomass price is set for a long-term contract with different suppliers. There are several indices, e.g. for the pellets price, depending on the origin and destination of the biomass [17, 18, 19], but all recording high volatility in recent years. Also biomass market is demand oriented and there is a significant increase in domestic use of biomass (mainly pellets), which influences the price for the industrial applications. The biomass price for industrial applications in recent years in Germany is 210 – 250 €/ton [18], while in Austria it is 185 – 220 €/ton [17] and the PIX Pellet Nordic Index varied from 120 – 150 €/ton [19]. Based on national quotations, the best biomass pellets spot price for May 2013, including delivery, was 200 €/ton [20]. A different approach is to use wood, locally collected from forest, and industry residues, as in the case of the Güssing power plant, with a lower cost, 24 - 55 €/ton (0.007 - 0.016 €/kWh [5]), but also with lower calorific value. This biomass cost is in line with national forest wastes cost - 27 €/ton.

RDF gasification option:

Municipal solid waste (MSW) is collected from the municipalities and is, in most cases, disposed in a landfill. The use of this waste means a significant positive wealth and logistic solution. The capital investment of Chianti RDF power plant (6.7 MWe) was 3 500 €/kWe [21]. Using the above mentioned economic model (based on Caputo et al. [13]), the CAPEX for the Chianti RDF power plant is 3 235 €/kWe (7.6% less than the Chianti RDF 6.7 MWe power plant cost); for a 4 MWe net power plant the equipment cost is 3 204 €/kWe and the CAPEX is 4 260

€/kWe, Table 5.1. This is a similar CAPEX to the 4 MWe turnkey RDF solution from Chamco [22], which presents a cost of 3 977 €/kWe (6.6% less than the 4 MWe cost model used). In addition, the RDF selection and treatment (eventual pelletizing) represents a cost for the power plant (10 – 21 €/ton of RDF [23]), depending on the process configuration and MSW composition.

Annual O&M costs differ significantly between references: for a Termiska Processer power plant (similar technology applied to the Chianti power plant but with 75 MWe) O&M costs are 21 % of the CAPEX, with waste disposal cost included in the O&M cost [21]; for the Chamco solution the O&M costs are estimated slightly above 13 % of CAPEX per year [22]; a different study from Klein [24] presents an annual O&M cost for RDF gasification power plants from 9 to 20 % of CAPEX, including a 38 €/ton ash disposal cost. The O&M costs used in the model are 12 % of the CAPEX (including a 5% of CAPEX fixed O&M cost, a variable O&M cost of 21 €/MWh, a 62 €/ton ash transport and 6 €/ton disposal costs).

Wastewater treatment plant (WWTP) and landfill biogas options:

In a different perspective, biogas can be recovered from MSW deposited in landfills. The biogas composition and rates are dependent on the composition of the MSW. The Landgem model [25] was used to describe the emissions of biogas from MSW landfills and is based on a first-order decomposition rate equation of the waste mass accepted by the landfill, the methane generation rate (*k*) and the potential methane generation capacity (Lo). For 30 year operation and using average recovery estimates (k=0.04 year^{-1}; Lo= 100 m^3/ton) the consumption of MSW to generate the sufficient biogas to run the 4 MWe power plant is 200×10^3 ton per year (total landfill capacity of 6 000 ×10^3 ton).

The average CAPEX for a landfill biogas power plant is 1 575 – 2 025 €/kWe [11], with equipment cost ranging from 1 010 to 1 125 €/kWe [11] and a biogas extraction cost of 0.02 €/ton [11]. The region has two landfills with 1 900×10^3 ton and 1 800×10^3 ton capacities, which are still insufficient to feed the 4 MWe hybrid power plant. However, the recovery of biogas from landfill and the hybridization with a CRS can be interesting for countries with good solar resources and large landfills.

The same perspective was applied to the biogas from a WWTP digester. About 18.3 L of biogas (on average) can be generated per inhabitant daily [26]. To supply the hybrid 4 MWe power plant, the WWTP should serve a population of about 3 million inhabitants, although the two largest WWTP in the area serve only 140 000 and 50 000 inhabitants. As the digester

retention time should be above 15 days [26] this also implies large digesters and quantities of sludge that are very difficult to collect locally, and so additional sludge from a nearby WWTP should be transported to the local with supplementary costs.

The CAPEX is dependent on the selected digester/power block technologies but, due to the dimension, it is significantly high (2 100 – 4 725 €/kWe [11]), with equipment costs of 1 240 – 1 725 €/kWe [11]. Two possible scenarios were analysed: starting the process with sewage sludge or directly using available biogas with no additional cost. The WWTP biogas generation O&M costs are similar to a conventional biomass power plant (2.1 to 7% of CAPEX-Fixed; 3.2 €/MWh-Variable [11]) but lower than for a landfill power plant (11-20% of CAPEX [11]). The digestate disposal cost can represent a profit for the plant (if sold as fertilizer - commercial value of 14 €/ton), or an expense for the plant (if supplied for free to the farmers covering the spreading costs of 10 €/ton, or if disposed of the power plant with an estimated cost of 55 €/ton) [27].

Natural gas option:

Commercial power plants in Portugal using natural gas have higher design power (centralized solutions using combined cycles) or use co-generation [28]. Despite that, a 4 MWe power plant operating with a steam turbine and a steam generator fed by natural gas was considered. It is possible to connect the power plant to a natural gas local network. The natural gas tariff for large consumers in Portugal is composed by a fixed daily and a monthly cost, plus the natural gas consumption (with different prices for the peak and empty hours) [29]. The annual average natural gas price for the 4 MWe power plant base cases is presented in Table 5.1, as well as all the costs for the base case options.

Table 5.1: Cost considerations for the base cases.

Plant designation	CAPEX reference					
	Biomass cost (€/ton)	Equipment Cost (€/kW)	Power plant CAPEX (€/kW)	O&M costs		Waste disposal cost (€/ton)
				Fixed (% of CAPEX)	Variable (€/MWh) [c]	
CRS#3	n/a	3800	4800	3 %	3	n/a
FRB	26	2800	3400	5 %	3	86
PG	200	3175	4216	5 %	3	86
WG	40	3175	4216	5 %	3	86
RDF	15	3204	4260	5 %	21	68
BD	n/a	1240 – 1725	3790 [a] sludge 2685 [a] biogas	5%	3.2	10
BL	0.03*	1010	1845 [b]	15 %	n.a.	n/a
NG	248	780	920	10 %	3	n/a

a- average equipment cost and CAPEX based on a case study for a 1 MWe internal combustion engine, using biogas from anaerobic digester using sludge provided to the power plant without collection and transport cost; sludge disposal cost not included.

b- average equipment cost and CAPEX based on a case study for a 5 MWe internal combustion engine, using biogas from landfill; biogas collection equipment not included (cost of collection considered under biomass cost);

c- not including waste disposal.

n/a – not applicable; n.a. – not available; * – €/m^3.

5.2 Results

A CRS operating in solar-only mode has several advantages comparing to other renewable energy technologies, but also some limitations. A CRS using efficient thermal energy storage (TES) can decouple the power generation from the solar power. Nevertheless, a 24 hour/day operation requires an over-sized solar field and receiver, as well as large TES devices (in the case of atmospheric air technology this has a high cost and size), which reflects in higher CAPEX and LEC.

Biomass-only power plants have a base load electricity generation characteristic and usually operate in 24 hour/day mode. The major issues with biomass-only power plants is the biomass collection and transport (limited to the power plant surroundings, otherwise the cost is unsustainable). The biomass plant is in most cases limited by this factor, making impossible to use larger and more efficient power blocks. Biomass price stability and availability is also an issue, as they affect the power plant operational profit mainly because the feed-in tariffs are quite low.

Several solar-only and biomass-only power plant configurations were considered. The biomass and CRS base cases performance and cost are presented in Table 5.2. To make the results directly comparable, all the power plants use similar nominal steam conditions and power blocks. These power block conditions were optimized, analysing their impact on a CRS power plant performance and cost. Power plant configurations CRS#3 and CRS#14 are two optimized configurations for different strategies (respectively, small and large storage capacities), while CRS#12 has the same configuration of CRS#3 but an increased peak receiver flux and a slightly larger storage, Table 5.2.

Table 5.2: Biomass and CRS base cases performance and cost.

Plant designation	Solar multiple	Storage	Feedstock	Biomass consumption (Ton/year)	Generated electricity (GWh/year)	Solar fraction	Feedstock to electricity efficiency (net)	LEC [e] (€/kWh)
CRS#3	1.25	2 hour	CSP only	0	11.6 [a]	100 %	10 %	0.23
CRS#14	1.75	6 hour	CSP only	0	16.1 [a]	100 %	9.5 %	0.24
CRS#12	1.25	3 hour	CSP only	0	12.3 [a]	100 %	11 %	0.23
FRB [2]	-	-	Forest residues	32×10^3	31.6 [b]	0 %	26 %	0.11
PG	-	-	Biomass pellets	29×10^3	32.0 [b]	0 %	23 % [c]	0.26
WG	-	-	Wood residues	32×10^3	32.0 [b]	0 %	23 %	0.12
RDF	-	-	RDF	35×10^3	31.9 [b]	0 %	19 % [c]	0.14
BD	-	-	Biogas WWTP	22×10^3	32.4 [b]	0 %	26 % [d]	0.08
BL	-	-	Biogas landfill	37×10^3	32.4 [b]	0 %	26 % [d]	0.10
NG	-	-	Natural gas	12×10^3	32.4 [b]	0 %	26 % [d]	0.13

a - 96 % plant availability; b - 90 % plant availability; c – pelletizing process efficiency not considered; d – biogas/natural gas generation and/or transport process not considered; e - for a 30 year life time, annual 8 % debt interest rate and 1 % annual insurance costs [30].

The steam turbine nominal operating conditions are similar for all options as well as the power plant availability: 90 % for a 24 hour/day operation [31] and 96% for solar-only operation. Different biomass sources were considered for the base cases power plants: forest wastes, biomass pellets, wood residues, refuse derivate fuel pellets (RDF), biogas from a waste water treatment plant (WWTP) and biogas from a landfill. Forest waste biomass was used to feed a combustion boiler; biomass pellets, wood residues and RDF were used to feed a gasifier and generate syngas; it was also considered the generation of biogas from landfill and WWTP

and the use of natural gas form the network, with the compositions presented in Table 5.3.

Table 5.3: Biogas and Syngas calculated compositions.

Technology / Syngas composition	Steam/Air Gasifier		Air Gasifier	Digester [7]		Network [7]
	Biomass pellets	Wood residues	RDF pellets	Landfill	WWTP	Natural gas
H_2 (% volume)	44	39	8.6	0	0	-
CO (% volume)	25	25	8.9	0	0	-
CO_2 (% volume)	18	20	16	40	37	1
H_2O (% volume)	residual	residual	10	residual	residual	-
CH_4 (% volume)	10	12	11.4	45	63	81
C_{2+} (% volume)	Included in CH_4	Included in CH_4	Included in CH_4	0	0	4
H_2S (ppm)	22	25	48	< 100	< 1000	-
O_2 (% volume)	-	-	-	1	0	-
NH_3 (ppm)	128	324	-	5	< 100	-
N_2 (% volume)	3	4	46	15	0.2	14
H_2/CO Ratio	1.8	1.7	0.98	-	-	-
Tars, ash (g/Nm^3)	3	36	130	residual	residual	-
NCV (MJ/Nm^3)	13	12	7.4	16	23	31.6
NCV (MJ/kg)	16	14	5.5	12	20	38

As expected, natural gas has the highest NCV, while the WWTP biogas has a composition closer to natural gas but with higher CO_2 concentration and lower NCV. The syngas composition from gasification depends on the biomass source and technology used; steam gasification can originate streams with high concentrations of H_2 and low concentrations of N_2, whereas atmospheric air gasification originate streams with lower concentrations of H_2 and more N_2, which lowers the calorific value of this syngas.

Hybrid CSP biomass power plants can be an interesting solution for centralized electricity generation and for off-grid locations. The social impact of a power plant with these hybrid characteristics is also interesting. The resources can be collected and transformed locally, contributing to the local economy, with creation and fixation of jobs. The hybrid solar/biomass power plant capacity factor is larger than a solar-only power plant. The advantages of a hybrid power plant are the possibility of 24 hour/day operation with 100 % renewable resources and a reduction in biomass consumption. Furthermore, the hybrid power plant can have a higher feed-in tariff than the biomass-only power plant.

The hybrid power plant burns the biogas or syngas in a duct burner updraft of the HRSG. Duct burners are quite efficient and can be designed for a large range of fuels, satisfying emission limits. However, the reliability of these components can be an issue, in particular for high temperature of the burner body, which may cause significant thermal stresses and even cracks or permanent deformations. Moreover, the syngas metal contaminants (e.g. Co and Ni) should be controlled, because they can endanger the duct burner system (including all piping) operation, e.g. by decomposition in the supply manifold, as well as in the injection nozzles, causing a long-term destruction of the pipe due to the local concentration of thermal stresses; or causing the injection nozzles occlusion, which may require frequent stops for power plant maintenance [32]. The fuel quality control is therefore a vital aspect for the power plant viable operation.

For all hybrid power plants, a gasometer was considered to store the generated syngas or biogas, so that it is available to provide energy to cover solar transients and extend operation. The gasometer also allows the digester/gasifier to be operated without significant transients. Although gas storage is not mandatory, the circulating fluidized-bed gasifier has a high thermal inertia, and intermittent operation of the gasifier is not recommended [33]. The same principles apply to the anaerobic digester system and the landfill. In commercial solutions, also a natural gas backup is recommended to support eventual maintenance or lacks of biogas/syngas.

The complementarity of both technologies improves operational performance, as the duct burner has quick response times, and maintains the HRSG temperature controlled so steam is consistently fed to the turbine. Performance and cost analysis data for the hybrid CRS/ biomass integration via a duct burner in the HRSG (Rankine cycle) are shown in Table 5.4.

Table 5.4: CRS and biomass hybrid power plants performance and cost.

Plant designation	CAPEX (millions of euro)	Hybrid fuel consumption (ton/year)	Generated electricity (GWh/year) [a]	Solar fraction	Feedstock to electricity efficiency (net)	LEC [b] (€/kWh)
FRB#CRS#12	34	24×10^3	31.7	34 %	16 %	0.15
PG#CRS#3	36	18×10^3	32.6	37 %	17 %	0.25
PG#CRS#14	46	14×10^3	32.2	50 %	14 %	0.27
PG#CRS#12	37	18×10^3	32.4	39 %	17 %	0.26
WG#CRS#3	36	20×10^3	32.6	37 %	17 %	0.17
WG#CRS#14	46	16×10^3	32.2	50 %	14 %	0.20
WG#CRS#12	37	19×10^3	32.4	39 %	17 %	0.17
RDF#CRS#3	36	23×10^3	32.4	35 %	15 %	0.18
RDF#CRS#14	46	19×10^3	32.2	48 %	13 %	0.22
RDF#CRS#12	37	23×10^3	32.2	37 %	15 %	0.19
BD#CRS#3	37	14×10^3	32.5	37 %	18 %	0.15
BD#CRS#14	47	11×10^3	32.2	50 %	15 %	0.19
BD#CRS#12	38	14×10^3	32.4	39 %	18 %	0.15
BL#CRS#3	28	23×10^3	32.6	37 %	18 %	0.16
BL#CRS#14	38	18×10^3	32.2	50 %	15 %	0.19
BL#CRS#12	29	23×10^3	32.4	39 %	18 %	0.16
NG#CRS#3	24	7.4×10^3	32.6	37 %	18 %	0.15
NG#CRS#14	35	5.9×10^3	32.3	50 %	15 %	0.18
NG#CRS#12	26	7.2×10^3	32.4	39 %	18 %	0.16

a - 90% plant availability; b - for a 30 year life time, annual 8% debt interest rate and 1% annual insurance costs [30].

The hybrid solutions using wood pellets (PG#CRS) have the highest LEC, mainly due to the pellets high cost, despite lower consumption. The producer gas generated from wood pellets has higher NCV, when compared with the same gasifier technology using wood residues (WG#CRS), but the overall feedstock to electricity efficiency is not significantly increased. WG#CRS#3 and WG#CRS#12 option has an interesting LEC of 0.17 €/kWh, which is 0.06 €/kWh lower than the solar-only optimized power plant (CRS#3) but, for this scale, the LEC is slightly higher than the forest residues biomass boiler integration in the steam cycle of the CRS. The gasification conversion efficiency is higher but, due to the higher wood residues cost (compared to forest waste biomass) and the higher CAPEX, the LEC for WG#CRS#12 is higher than for FRB#CRS#12.

The pelletized RDF air gasifier power plant has similar CAPEX comparing to the wood residues steam/air gasifier power plant. The RDF syngas has lower NCV and implies larger maintenance and so, the power plant LEC is higher. If we analyse the first year cash flow for RDF#CRS#3 operation, the power plant expense is over 2.7 million euro and generates a profit of 2.1 million euro (if the generated electricity is sold at 0.148 €/kWh), resulting in the operational loss of 0.6 million euro. These results can have a positive perspective; if the waste used to feed the power plant was transported and dumped into a landfill without reuse, this would imply an annual cost of over 2 million of euro (33×10^3 ton). This means that the municipality got an investment reduction for MSW disposal of almost 1.4 million of euro (the difference from operating the power plant plus the expense cut with garbage dumping), which is the biggest advantage of using RDF for gasification.

The WWTP anaerobic digester base case option was designed for large cities with centralized sewage collection systems. The WWTP base case supplies the power block with 22×10^3 ton per year of biogas; if these quantities can in fact be delivered, the LEC would be very interesting (0.08 €/kWh). If it is necessary to collect sewage sludge from several smaller WWTP into a centralised digester, additional costs will apply. For example, to transport 30 % from a nearby WWTP (within 30 km distance), an additional CAPEX of 3.2 million euro is estimated. This investment is related to the acquisition of transportation trucks and build a loading/discharging area; additional annual O&M costs of 1.1 euro per m^3 of sludge are also applied (based on US EPA) [34]; this would increase the LEC of the BD base case power plant from 0.08 €/kWh to 0.11 €/kWh. In a different scenario, if the biogas is already available at no cost (e.g. biogas from large livestock with already implemented manure collection systems, like dairy or pig farms) the CAPEX would be lower and the LEC would be even more interesting (0.06 €/kWh for the base case). However, for dairy/pig farms or WWTPs, this is a very large

plant and for this scale (in most cases) it is necessary to transport sludge from other plants, with additional cost. The hybridization with CSP can reduce the biogas consumption, but with significant increases in the LEC. However, as for each technology a specific feed-in tariff is obtained, to fully analyse the impact of the hybridization into the economical balance of the power plant, a detailed cash flow analysis was done for the base cases (Table 5.5) and hybrid options (Table 5.6).

Table 5.5: Economic analysis for base cases.

Plant designation	Majority resource	Feed-in tariff (€/kWh)	IRR (%) [b]	NPV (million euro)		Payback period (years)	
				With taxes and inflation [c]	Without taxes or inflation	With taxes and inflation [c]	Without taxes or inflation
CRS#3	CSP	0.273	9.9	7.9	30	14	10
CRS#14	CSP	0.273	9.2	11	42	16	11
CRS#12	CSP	0.273	10	8.6	32	14	10
FRB	Forest biomass	0.109	4.5	0.5	9.4	27	20
PG	Wood Pellets	0.109	N/A	- 84	N/A	N/A	N/A
WG	Wood residues	0.109	N/A	- 7.2	N/A	N/A	N/A
RDF	MSW RDF	0.074	N/A	- 31	N/A	N/A	N/A
BD	Wastewater sludge	0.117	18	14	41	6	4
BL	MSW	0.104	N/A	- 2.1	N/A	N/A	N/A
NG	Natural gas	0.05 [a]	N/A	- 43	N/A	N/A	N/A

a - MIBEL market price, average estimation; b - considering national taxes from 2012 but without inflation; c - considering an average 4 % annual inflation and national taxes from 2012.

Table 5.6: Economic analysis for hybrid options.

Plant designation	Majority resource	Feed-in tariff (€/kWh)	IRR (%) [c]	NPV (million euro)		Payback period (years)	
				With taxes and inflation [d]	Without taxes or inflation	With taxes and inflation [d]	Without taxes or inflation
FRB#CRS#12	Forest biomass	0.152 [a]	4.4	0.8	21	28	20
WG#CRS#3	Wood residues	0.170 [b]	5.5	3.3	27	24	18
WG#CRS#14	CSP	0.191 [b]	3.4	-1.8	23	N/A	21
WG#CRS#12	Wood residues	0.173 [b]	5.2	2.8	27	25	18
BD#CRS#3	Wastewater sludge	0.175 [b]	11	15	53	13	9
BD#CRS#14	CSP	0.195 [b]	6.4	6.9	42	22	16
BD#CRS#12	Wastewater sludge	0.178 [b]	10	14	51	14	10
BL#CRS#3	MSW	0.167 [b]	7.4	5.3	25	20	14
BL#CRS#14	CSP	0.189 [b]	3.9	0	21	30	20
BL#CRS#12	MSW	0.170 [b]	6.9	4.7	25	21	15

a – calculated by national renewable electricity generation tariff formula, considering the solar and biomass boilers power; b – calculated from base cases tariff using an weighted average from the energy generated from CSP and biomass; c - considering national taxes from 2012 but without inflation; d - considering an average 4 % annual inflation and national taxes from 2012.

The economic analysis is highly sensitive to several variables and should only be used as an indicative of the different technologies impact in CRS hybridization. The Portuguese feed-in tariff is set for each project by the national authorities, using a calculation formula [35] for renewable electricity generation. Its use for hybrid power plants is yet not defined; so, a weighted average from the energy generated from CSP and biomass was used. The impact of national taxes and inflation during the power plant life cycle is significant and can also reduce the investment interest.

The base cases for gasification (wood pellets, wood residues and RDF) do not originate positive investments, due to the low feed-in tariff and high CAPEX. CRS hybridization with biomass wood residues gasification makes the technology viable, reducing biomass consumption by over 11 thousand tons per year compared to the base case. The hybrid power plant is economically viable to operate under the Portuguese scenario, despite having a low attractiveness, with an IRR of 5.5% and a NPV of 3.3 million euro (WG#CRS#3). A hybrid power plant (WG#CRS#14) with higher solar share decreases the biomass consumption by 16 thousand tons per year, but the investment is less attractive, the payback period is higher and the IRR is reduced below the inflation considered.

In previous studies – Chapter 4, a forest waste biomass boiler integrated in the steam cycle of a CRS was studied with a LEC of 0.144 €/kWh, IRR of 6.8 %, NPV of 7.9 with a payback period of 21 years [2]. However, waste disposal was considered without cost. If waste transport and disposal is necessary, the LEC of this power plant would increase to 0.16 €/kWh, the IRR and NPV reduce to 4.4 % and 0.8, respectively, and the investment will have a payback period of 28 years. The forest waste steam boiler integration in a CRS would then be less profitable than the gasification of biomass and syngas integration in a duct burner of a CRS HRSG. In a different perspective, biomass gasification technology is more complex and still less mature than a biomass boiler. In the case of biomass gasification, lower quality/homogeneity biomass can lead to instabilities in the process and higher maintenance costs (that do not occur with the same frequency in biomass combustion boilers), thus the reason of studying biomass pellet gasification. However biomass pellets are not viable considering the Portuguese feed-in tariff.

MSW is a problem in many countries, due to a lack of structures for collection and disposal/reuse. The economical valorisation of MSW, by generating electricity, can provide funds to help the amortization of MSW collection and storage costs. A structural effort to reuse and recycle the MSW is essential in these countries (with priority over energy from waste) to reduce the total waste disposed in landfills. The LEC for RDF gasification is higher than to generate biogas from a landfill; the main reason for this is that, for the deposit in the landfill case, the main equipment costs are the gas extraction, processing and power block (landfill construction and maintenance were not considered); while for the RDF gasification it is necessary to acquire more expensive equipment for triage and pelletizing of the MSW, gasification, gas processing and power block. The Portuguese landfills have a special tariff for the biogas, which makes the investment more attractive than RDF gasification. The investment in a base case or hybrid with CRS RDF gasification, with the actual feed-in tariffs, is not viable

and is only possible from the perspective of reducing the waste disposal costs and the dimension of otherwise necessary landfills. The biogas recovered from landfills has high costs and maintenances and, for the present base case feed-in tariff, the power plant operation generates losses, despite being a very large landfill (only possible in a few locations worldwide); from this perspective, the hybridization with a CRS can reduce the biogas consumption by 14 thousand tons per year from the base case (BL#CRS#3), and as the feed-in tariff would increase, the investment would be more interesting with an IRR of 7.4 % and a payback period of 20 years.

The use of sludge to feed an anaerobic digester generates a high NCV biogas from sludge (without transport cost) and beneficiates from the highest (biomass based) feed-in tariff. However, as in the case of the landfill biogas, the WWTP necessary to generate enough biogas to feed the 4 MWe power plant (base case) implies a large WWTP, only possible in a few locations worldwide; alternatively, it would be necessary to collect sludge from different WWTP into a centralized anaerobic digester, with additional costs. Hybridization with CSP allows the WWTP downsizing, keeping the LEC at interesting values of 0.15 €/kWh and the IRR at 11 %, with a NPV of 15 million euro and a payback period of 13 years.

Natural gas could also be used to fire the duct burner and it is the solution with lower CAPEX. Nevertheless, due to the cost of the fuel, lower conversion efficiency (than a standard combined cycle plant), and national taxes (it would represent almost 70 % of the operational expenses – ND#CRS#3) and the low market electricity feed-in tariff, it is unviable to fully hybridize the CRS with natural gas. However, in several countries (and only in a small percentage) it is possible to use natural gas to start up and support small solar transients without reducing the bonus electricity tariff. This could be an interesting solution (if it was allowed by national authorities) because natural gas can be used to co-fire all the hybrid options and be a safeguard in the case of lack of biogas/syngas supply.

5.3 Validity

The above described models were validated for the base cases with experimental data, published references and information from manufacturers. There is no commercial 4 MWe open volumetric receiver CRS plant in operation worldwide. For this reason, the CRS design conditions were based on designs presented in chapters 2 and 3. Regarding the biomass wood residues and pellets gasification power plants, the design conditions were based on the Güssing power plant, Figure 5.3.

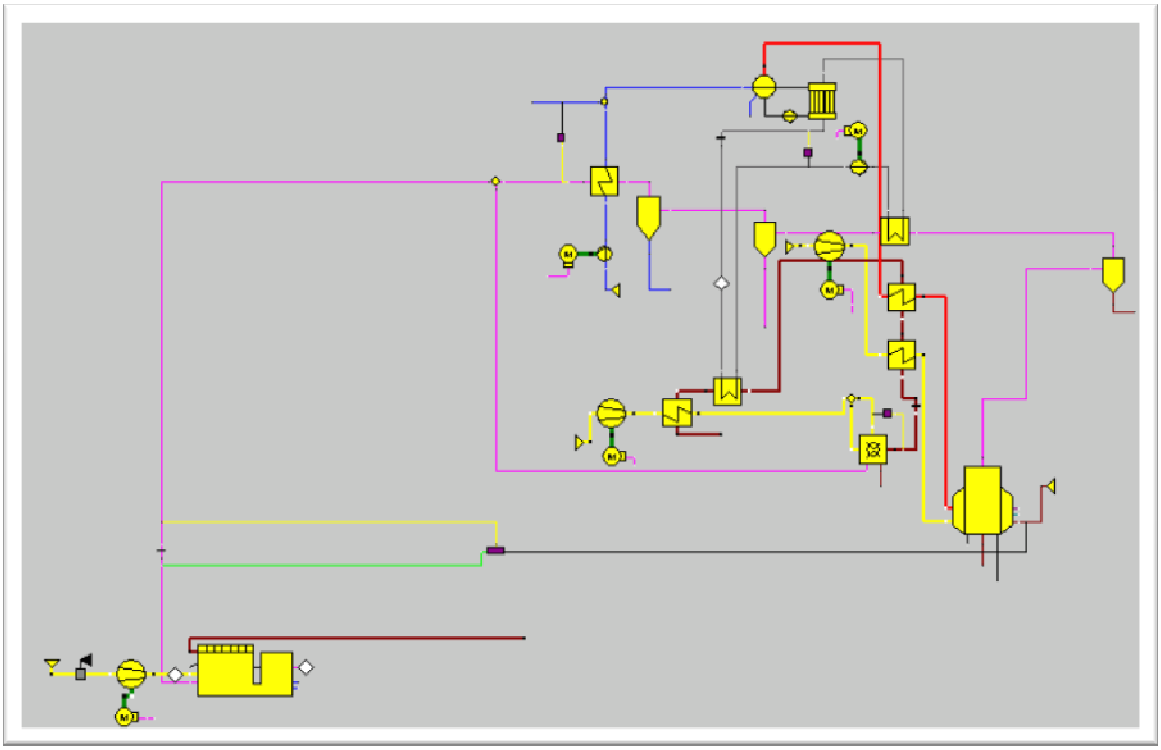

Figure 5.3: WG power plant configuration – model for reference.

The base cases performance was validated with the performance references from the Güssing power plant. Within this model, a simplified model for the gasifier was developed. As the Güssing power plant generates a mixture of electricity and heat, using a CHP engine instead of a turbine, the power block was replaced by a boiler and a 4 MWe turbine, developed in Ebsilon. The model validation results are presented in Table 5.7.

Table 5.7: Wood pellets and residues base case power plant and gasifier validation results.

CHP-plant Güssing	**Reference [36]**	**Model for Reference**	**Model designed for 4 MWe**
Fuel Power (MW)	8.0	7.9	20
Electrical output (MW)	2.0	2.0	4.6
Thermal output (MW)	4.5	4.4	-
Electrical efficiency (%)	25	25 (gross) 23 (net)	22 (gross) 20 (net)
Thermal efficiency (%)	56	55	-
Electrical/thermal output	0.44	0.45	1.0
Total efficiency	81	80 (gross) 78 (net)	22 (gross) 20 (net)
Gasifier	**Reference [36]**	**Calculated**	**Calculated**
Gasifier exhaust temperature combustion zone (°C)	1000 – 1100	1100	1100
Gasifier exhaust temperature gasification zone (°C)	850 – 900	850	850
Scrubber input temperature (°C)	160 – 180	180	180
Scrubber exhaust temperature (°C)	40	40	40
Steam to biomass ratio	0.5	0.5	0.5
Air temperature	500	500	500

The gasifier model was validated for different biomass types, while generating syngas with different compositions, Table 5.8 and Table 5.9.

Table 5.8: Wood pellets and syngas generated - validation results.

Fuel	**Wood Pellets (7% water content) [37]**	**Syngas**	**Reference [37]**	**Calculated**
C (% mass)	49	H_2 (% volume)	41 - 44	44
H (% mass)	6.52	CO (% volume)	25 - 29	25
N (% mass)	0.12	CO_2 (% volume)	18 - 21	18
S (% mass)	< 0.05	$CH_4 + C_{2+}$ (% volume)	8 - 9	10
O (% mass)	44.31	H_2S (ppm)	-	22 ppm
Ash + lime	0.26	NH_3 (ppm)	-	93 ppm
NCV (MJ/kg)	17.1	N_2 (% volume)	residual	2
		H_2/CO Ratio	-	1.8
		Tars, ash (mg/Nm^3)	-	3
		NCV (MJ/Nm^3)	-	13.1

Table 5.9: Wood residues and syngas generated - validation results.

Fuel	**Wood residues (40% water content) [38]**	**Wood residues (40% water content-calculated)**
C (% mass)	47.6	47.6
H (% mass)	6.2	6.2
N (% mass)	0.3	0.3
S (% mass)	0.03	0.03
O (% mass)	42.9	42.9
Cl (% mass)	0.01	0.01
Ash + lime	2.96	2.96
NCV (MJ/kg)	10 – 17.8	16.2
Fuel	**Wood residues (25 % water content) [7]**	**Wood residues (25 % water) NCV calculated**
C (% mass)	48.26	48.26
H (% mass)	5.82	5.82
N (% mass)	0.22	0.22
S (% mass)	0.03	0.03
O (% mass)	45.67	45.67
Ash + lime	0.61	0.61
Volatiles	80 %	80 %
NCV (MJ/kg)	12.4	15.7
Syngas	**Reference [36]**	**Calculated**
H_2 (% volume)	35 – 40 %	39
CO (% volume)	20 – 30 %	25
CO_2 (% volume)	15 – 25 %	20
H_2O (% volume)	-	-
CH_4 (% volume)	8 – 12 %	12
C_{2+} (% volume)	Included in CH_4	Included in CH_4
H_2S (ppm)	20 - 40 ppm	25 ppm
O_2 (% volume)	-	-
NH_3 (ppm)	<400 ppm	324 ppm
N_2 (% volume)	3 – 5 %	4
H_2/CO Ratio	1.6 – 1.8	1.7
Tars, ash (mg/Nm^3)	Tars = 10 – 40; Ash < 5	36
NCV (MJ/Nm^3)	12	12

The RDF gasification power plant model was based on the Chianti power plant, Figure 5.4.

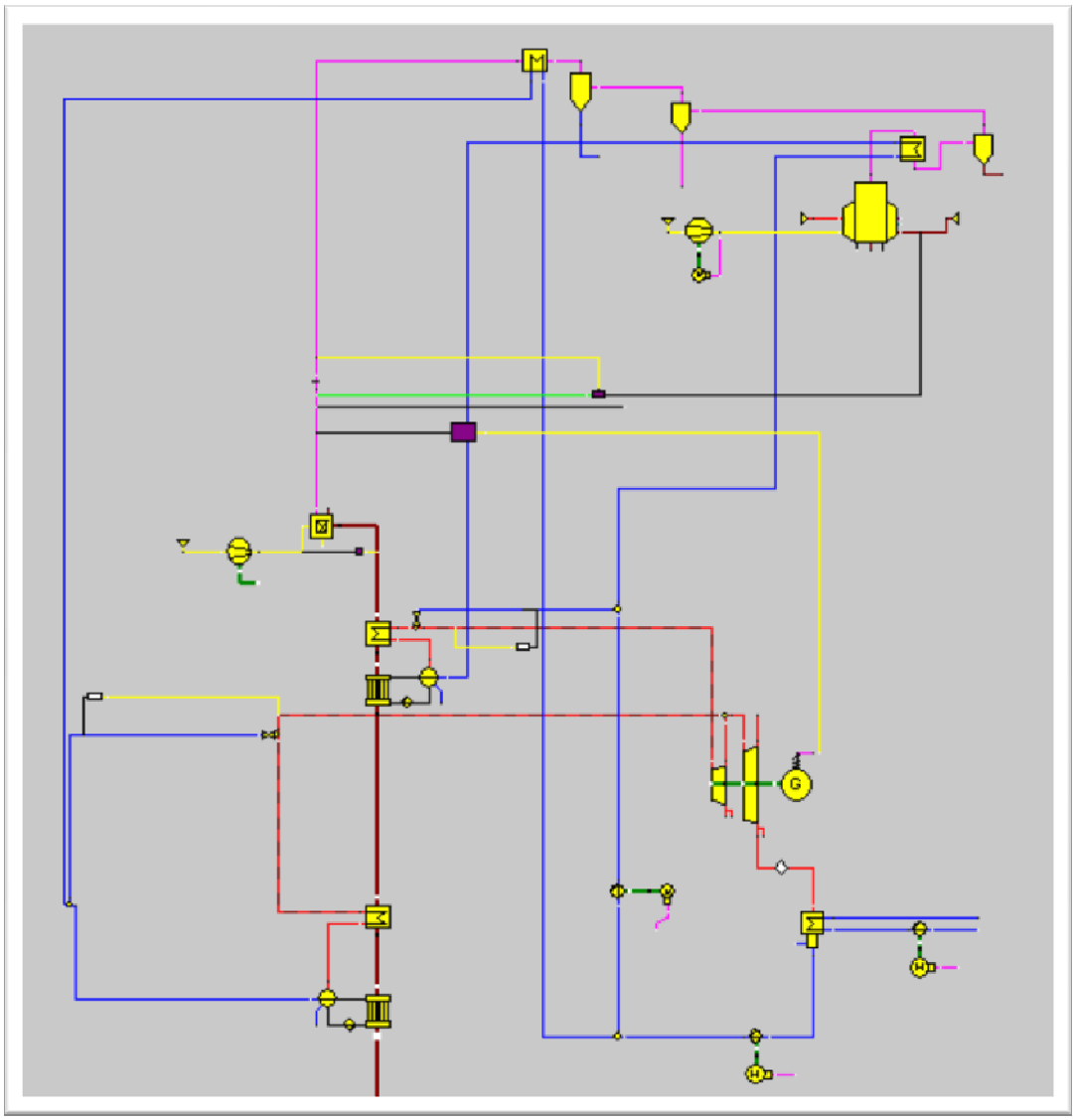

Figure 5.4: RDF power plant configuration – model for reference.

The RDF base case performance was validated with the performance from the Chianti power plant references. Based on the original Chianti power plant, a 4 MWe power plant model was developed to be used as base case for the hybrid solution. The model validation results are presented in Table 5.10.

Table 5.10: RDF base case power plant and gasifier validation results.

Chianti Rankine	**Reference [14]**	**Model for Reference**	**Model designed for 4 MWe**
Fresh air temperature (°C)	15	15	15
Boiler exhaust flow (ton/h)	-	139	140
Boiler temperature (°C)	650	650	650
Boiler exhaust temperature (°C)	200	199	199
Boiler steam temperature (°C)	380	380	380
Boiler steam pressure (bar)	42	42	42
Boiler steam flow (ton/h)	18	18.4	12.4
Electrical efficiency	18 - 20 %	18 % (net) 20 % (gross)	18 % (net) 20 % (gross)
Electrical capacity (gross)	6.7	6.7	4.5
Electrical capacity (net)	-	6.0	4.0
Chianti Gasifier	**Reference**	**Calculated**	**Calculated**
Primary Feedstock	RDF 17 MJ/kg	RDF 17 MJ/kg	RDF 17 MJ/kg
RDF feed (ton/h)	4 - 9	7.0	4.6
Pressure (bar)	1.2	1.2	1.2
Temperature (°C)	700 – 800	749	749
Reactant	Air	Air	Air
Input (kg/kg feed)	-	1.36	1.36
Chianti syngas	**Reference**	**Calculated**	**Calculated**
H_2	8.6	8.6	8.6
CO	8.8	8.8	8.8
CO_2	16	18	18
H_2O	9	8	8
CH_4	6	10	10
C_{2+}	5	(included in CH_4)	(included in CH_4)
H_2S	49 ppm	50 ppm	50 ppm
N_2	46	45.6	45.6
H_2/CO Ratio	0.98	0.98	0.98
Solid waste flow rate, ash (kg/kg feedstock):	0.14	0.11	0.11
Heating Value (MJ/Nm^3)	7.5	7.7	7.7
NCV (MJ/kg)	-	6.5	6.5

As in the case of steam cycle integration, the integration of biomass in the air cycle is a completely innovative concept and there are no commercial power plants in operation to validate this concept. The strategy used was to choose several validated components from the base cases and combine them to obtain the hybrid power plant. In the gasification power plants, for the calculation of the 4 MWe hybrid solutions, the gasifier and syngas treatment equipment were adapted to the CRS power block with the addition of a duct burner into the HRSG. Further validation of off-design operation of each biomass gasifier is needed. The same methodology was used for economic models.

5.4 Conclusions

For biomass integration into the air cycle of a CRS, the lower LEC options are the hybridization of 4 MWe CRS with biogas from a WWTP, with natural gas (LEC of 0.15 €/kWh), with landfill gas (LEC of 0.16 €/kWh) or with syngas from wood residues gasification (LEC of 0.17 €/kWh). Because the Portuguese bonus feed-in tariff is calculated for each renewable energy technology, some of these power plant configurations have negative economic turnovers, and the hybrid power plant investment with best payback period is the hybridization with an anaerobic digester, using sludge from a waste-water treatment plant, which returns the investment in 13 years (sludge collection and transport assumed without cost), presenting also the best net present value (15 million euro). However, for the 4 MWe scale, WWTP biogas would only be possible close to large cities (few limit cases), with centralized plants capable of generating sufficient quantities of sludge or MSW. A different biomass CRS hybridization technology (which can be applied in a larger number of cases) and also presents an interesting LEC is the gasifier of wood residues (WG#CRS#3 - LEC of 0.17 €/kWh), which can reduce biomass consumption by 11 000 tons per year compared to the base case, making biomass gasification economically viable to operate under the Portuguese scenario, despite having a low attractiveness, with an IRR of 5.5 % and a NPV of 3.3 million euro.

References

[1] Coelho, B., Varga, S., Oliveira, A., Mendes, A., Optimization of an atmospheric air volumetric central receiver system: Impact of solar multiple, storage capacity and control strategy, Renewable Energy 63 (2014) 392-401.

[2] Coelho, B., Schwarzbözl, P., Oliveira, A., Mendes, A., Biomass and Central Receiver System (CRS) Hybridization: Volumetric Air CRS and Integration of a Biomass Waste Direct Burning Boiler on Steam Cycle, Solar Energy, Volume 86, Issue 10, October 2012, Pages 2912–2922.

[3] http://www.ieatask33.org/content/thermal_gasification_facilities, accessed on 06-11-2013.

[4] Bődi, K., WP 2.1-2.2 Case Report: Biomass CHP Plant in Güssing, Austria, Biomob FP7-REGIONS-2009-1, Project Report, 2009.

[5] Bolhàr-Nordenkampf, M., et al, Biomass CHP Plant Güssing – Using Gasification for Power Generation, Int. Conference on Biomass Utilisation, Thailand, 2002.

[6] http://www.iswa.org/uploads/tx_iswaknowledgebase/Nagayama.pdf, accessed on 06-11-2013.

[7] Persson, M., Jönsson, O., Wellinger, A., Biogas Upgrading to Vehicle Fuel Standards and Grid Injection, IEA Bioenergy report, 2006.

[8] American Society for Testing and Materials, Manual on Requirements, Handling, and Quality Control of Gas Turbine Fuel: A Symposium Presented at the Seventy-fifth Annual Meeting, Edition 531, 1973.

[9] Coelho, B., Oliveira, A.C., Mendes, A., Concentrated solar power for renewable electricity and hydrogen production - A review, Energy and Environmental Science, 3 (2010) 1398-1405.

[10] http://www.csp-world.com/news/20121213/00652/worlds-first-hybrid-csp-biomass-plant-comes-line, accessed on 06-11-2013.

[11] Gielen, D., Biomass for power generation, renewable energy technologies: cost analysis series, IRENA, 2012.

[12] Sims, R., The Brilliance of Bioenergy: In Business and in Practice, Earthscan, 2002.

[13] Caputo, A., Palumbo, M., Pelagagge, P., Scacchia F., Economics of biomass energy utilization in combustion and gasification plants: effects of logistic variables, Biomass and Bioenergy 28 (2005) 35–51.

[14] Specht, M., Biomass Fluidised Bed Gasification with in-situ Hot Gas Cleaning, AER-Gas II project final report, 2009.

[15] Tollin, J., Reburning biomass fly ash, CADDET Renewable Energy Newsletter: December 2000.

[16] Fischer, C., Overview of the use of landfill taxes in Europe, ETC/SCP working paper, 2012.

[17] www.propellets.at, accessed on 13-05-2013.

[18] DEPV Index, Deutscher Energieholz- und Pellet-Verband e.V., www.depv.de , accessed on 13-05-2013.

[19] PIX Pellet Nordic Index, FOEX Finland, www.foex.fi , accessed on 13-05-2013.

[20] Personal communication from Enerpellets Portugal, May 2013.

[21] Granatstein, D.L., Case study on waste-fuelled gasification project Greve in Chianti, Italy, 2003.

[22] http://www.chamco.net , accessed on 13-05-2013.

[23] Caputo, A., Pelagagge, P., RDF production plants: I Design and costs, Applied Thermal Engineering 22 (2002) 423–437.

[24] Klein, A., Gasification: An Alternative Process for Energy Recovery and Disposal of Municipal Solid Wastes, M.S. thesis in Earth Resources Engineering, Columbia University, 2002.

[25] Alexander, A., Burklin, C., Singleton, A., Landfill Gas Emissions Model (LandGEM) Version 3.02 User's Guide, U.S. Environmental Protection Agency, EPA-600/R-05/047, 2005.

[26] Deublein, D., Steinhauser, A., Biogas from Waste and Renewable Resources, Wiley-VCH Verlag GmbH & Co. KGaA, Weinheim, 2008.

[27] Dolan. T., Cook, M.B., Angus, A.J., Financial appraisal of wet mesophilic AD technology as a renewable energy and waste management technology, Science of the Total Environment 409 (2011) 2460–2466.

[28] http://www.a-nossa-energia.edp.pt/centros_produtores/, accessed on 13-05-2013.

[29] ERSE, Tarifas e preços de gás natural para o ano gás 2011-2012, report, 2011.

[30] Pitz-Paal, R., Dersch, J., Milow, B., (2005). ECOSTAR roadmap document, DLR.

[31] http://www.ficfb.at/renet_d.htm , accessed on 06-11-2013.

[32] Catalano, L.A., Ansaldo Post-Firing System for Combined-Cycle Plants, 31st Meeting on Combustion of the Italian Section of the Combustion Institute, Torino, June 2008.

[33] Personal communication from EDP, on 13-07-2011.

[34] U.S. Environmental Protection Agency, Land Application of Sewage Sludge and Domestic Septage, EPA report EPA/625/R-95/001, 1995.

[35] Klein A., et al., (2010) Evaluation of different feed-in tariff design options, 3rd edition, Fraunhofer ISI and EEG.

[36] Rauch, R., et al, Steam gasification of biomass at chp plant guessing – status of the demonstration plant, 2nd World Conference and Technology Exhibition on Biomass for Energy, Idustry and Climate Protection, 10-14th May 2004, Rome, Italy.

[37] Pfeifer, C., Rauch, R., Hofbauer. H., Hydrogen-rich Gas Production with a Catalytic Dual Fluidised Bed Biomass Gasifier, 2nd World Conference and Technology Exhibition on Biomass for Energy, Industry and Climate Protection, 10-14th May 2004, Rome, Italy.

[38] Bolhàr-Nordenkampf, M., Hofbauer, H., Biomass gasification combined cycle thermodynamic optimisation using integrated drying, Proceedings of ASME Turbo Expo 2004: Power for Land, Sea, and Air, 14-17 June, Vienna, Austria.

This page was intentionally left blank

Chapter 6

Solar-Chemical: Hydrogen production from Water and CSP

This page was intentionally left blank

6. Solar-Chemical: Hydrogen production from Water and CSP

Part of the SOLMASS vision is the implementation of CSP and biomass power plants for renewable electricity and fuels (chemicals) generation, in an integrated solar chemical concept, as mentioned in Chapter 1. Although this is a long-term vision, CSP application for chemicals generation is an interesting topic and with great scope of application. This integrated view was first presented at the HYCELTECH conference in 2009. The work resulted in a publication [1]. The work presented in this chapter is based on this publication. In this chapter, several technologies and cycles for hydrogen generation using CSP are presented, based on electricity, water, biomass or fossil fuels. Hydrogen production cost, efficiencies per cycle and respective operating temperatures are assessed.

6.1 Hydrogen as an energy carrier

Hydrogen has been indicated as the fuel of the future. In addition, the so-called "hydrogen economy" has been receiving great governmental support, public and media attention. However, as there are no abundant natural supplies of hydrogen on the surface of earth, hydrogen has to be obtained from another primary source and should be referred to as an "energy carrier". A foreseen increase in global energy demand, especially due to the progressive industrialization of developing countries in Asia and South America, will culminate in a World net electricity generation increase of 77 per cent, from 18.0 trillion kilowatt-hours in 2006 to 23.2 trillion kilowatt-hours in 2015 and 31.8 trillion kilowatt-hours in 2030 [2] – the economic and geopolitical implications of future limitations in oil supply, and consequently concerns about energy supply security, put the discussion about renewable electricity production and the use of hydrogen as an energy carrier on the agenda.

The transport sector is particularly vulnerable to oil supply scarcity, since it is still 95 % dependent on oil worldwide [3]. It represents 18 % of the primary energy use and about 17 % of global CO_2 emissions, with the vast majority of emissions coming from road transport [3]. Transport is also responsible for 20 % of the projected increase in both global energy demand and greenhouse gas emissions (GHG) until 2030 [4]. For example, using solar hydrogen in Fuel Cell (FC) cars can reduce life cycle GHG emissions by 70 %, compared to advanced fossil fuels [5]. Solar hydrogen production allows the reduction of fossil energy requirements by a factor of 10 compared to conventional technologies [5]. The only environmental impacts are associated with the construction of infrastructures for collecting solar energy, as well as with the hydrogen transport and storage. The major impacts are due to large steel needs for

building a CSP plant, since today's steel production technology is responsible for fossil and mineral resource consumption as well as particulate, GHG, and other harmful emissions [5].

Regarding these scenarios, hydrogen appears attractive as a fuel, because it can solve the major fossil fuel environmental, political and economic down points. Hydrogen takes advantage because it can be produced from water and renewable energy, and can be used in highly efficient fuel cells producing only water as a by-product. This may represent a technological step forward to provide a sustainable energy source that can reduce negative environmental effects on the climate and satisfy the world future fuel demand.

6.2 CSP complimentary characteristics for thermochemical applications

CSP systems have an advantage for thermochemical applications, because they can provide electricity and high temperature process heat to drive endothermic chemical reactions. Within different CSP technologies, each has specific and different operating conditions. PTC and LF are 2D concentrating systems, on the other hand, CRS and DSE are 3D concentrating systems that can achieve higher concentration ratios, between 200 and 1000 for CRS and 1000 to 4000 for DSE, with working temperatures above 1000 °C [6].

Due to a lower concentration capacity of PTC and LF and the size limitations of DSE, the technology with higher potential for hydrogen production is CRS. With a secondary concentration, CRS systems can achieve concentrations over 1500 suns and temperatures above 1500 °C. The collected thermal energy can be used to provide heat, so that hydrogen is produced by chemical reactions that split the water molecule. Many such reaction sets have theoretical efficiencies around 40%. Combined with annual efficiencies for solar thermal systems of about 45 %, the solar-to-hydrogen efficiency of this method could go above 20 % [7].

Solar thermochemical applications are not as developed as solar thermal electricity generation, but they employ the same solar concentrating technologies. In order to scale-up solar reactors, parameters such as the reactor volume and the loading with the required redox/catalyst coating have to be optimized, taking into account the solar flux and the resulting temperature distribution, the heat transfer characteristics, the reaction rates and transient phenomena due to reactor operation at alternating solar flux conditions [8]. The combination of these systems presents interesting synergies that can be explored.

6.3 Renewable hydrogen generation from CSP

6.3.1 Primary resource overview

The different primary energy resources could play important roles in connecting bridges from the current technologies to future hydrogen economy technologies. As presented in Figure 6.1, there are several routes based on CSP technology to produce hydrogen, which can work considering different configurations of the CRS receptor: external, indirect or direct.

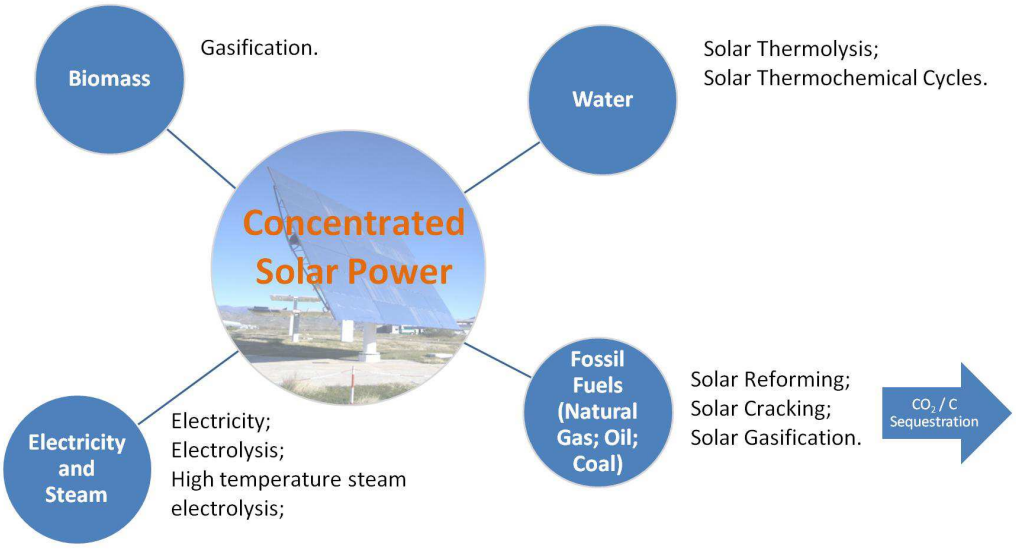

Figure 6.1: CSP routes for renewable hydrogen production.

6.3.2 Hydrogen: supply overview

The "hydrogen economy", even if based in hydrogen production from renewable sources, faces difficulties to its implementation. Hydrogen production, delivery and safety are major problems to a full dissemination of hydrogen as a fuel.

Hydrogen transportation is a major logistics problem. Hydrogen storage in compressed gaseous hydrogen, in lightweight compound bottles or tanks has an energy density of 4.4 MJ/l and represents a cost increase of 0.2-1.0 €/kg [4] in hydrogen production price. These tanks currently have operating pressures up to 700 bar. As tank pressure increases, the energy needed for hydrogen compression also increases. To compress hydrogen to 200 bar, 18 % of the total energy storage in the tank is spent [9].

Depending on the delivery distance, hydrogen liquefaction could also be considered, as the total capital costs could be reduced, despite the decrease of overall energy efficiency and an increase in CO_2 emissions. Hydrogen at atmospheric temperature will become liquid at -253 °C, which is below the critical point (-240 °C, 13 bar). Operating pressures for liquid storage of hydrogen range from 1 to 3.5 bar and can provide energy densities up to 8.4 MJ/l [9]. A typical 40 ton trailer for compressed hydrogen bottles can transport 530 kg of hydrogen, while a cryogenic 40 ton tank trailer would transport 3370 kg of hydrogen. [10] The main problems for liquid hydrogen are the liquefaction required energy, insulation and boil-off losses. About 30 % of the total energy can be consumed in the liquefaction process. Besides, the current pressure vessels, for passenger cars, could boil-off the hydrogen in a 2-3 % volume per day rate [9]. In novel double-walled vacuum insulated tanks, these losses could be reduced to 0.2-0.4 % volume per day [9].

Alternatively, hydrogen may be stored in compounds to make a hydride. Hydrides provide solid state storage compounding hydrogen with solid metals or metallic alloys. Metal hydrides could have very good hydrogen densities, up to 151 kg/m^3 (Aluminium - AlH_3). Even though the storage density of hydrogen in a metal hydride is high, the total mass of the system is large and the gravimetric densities do not exceed 2 % by weight. With auxiliary heating, the gravimetric densities can be increased to 7 % by weight [11]. Higher densities can be reached with the use of chemical hydrides. Such hydrides are usually formed with elements such as B, Al, Mg, and Li. Compounds as $LiBH_4$ can reach gravimetric densities of 18 wt % and Al(BH4)3 can carry 17 wt % hydrogen. But compounds that achieve these high efficiencies tend to have slow hydrogen releasing mechanisms; and the performances are reduced. Also, boron hydrides, which provide the highest storage capacities, produce volatile borates, which have high hysteresis and can potentially damage fuel cell systems [9].

The vehicle autonomy is another problem of using hydrogen as a fuel. Hydrogen storage solutions aren't yet able to provide a range greater than 500 km [4], while meeting all the performance parameters, regardless of the costs. Also, it is necessary to build a new distribution infrastructure. The costs of transportation and building a distribution infrastructure account for 20-40 % of the total hydrogen costs; the remaining 60-80 % share is attributed to hydrogen production [4].

In spite of the presented difficulties for hydrogen use as a fuel, the hydrogen market for other applications is still a growing market. The hydrogen production techniques could be switched towards sustainability, basing hydrogen production in renewable resources.

6.3.3 Electricity and steam: electrolysis

CRS power plants for electricity generation are currently in commercialization phase. These plants are considered one of the most promising CSP technologies for electricity generation, as well as having the potential to support future production of chemicals such as hydrogen [12].

One of the most common hydrogen production technologies is electrolysis. Electrolysis uses electricity, usually from fossil fuels or nuclear power plants, to generate hydrogen from water. These electricity needs could therefore also be supported by a CRS plant, without major changes in current commercial electrolysis equipments. Electrolysis could be performed in an acid or alkaline medium. Despite the discovery of electrolytic water decomposing, first observed in acidic water, in industrial plants the alkaline medium is preferred, because corrosion is more easily controlled and cheaper construction materials can be used. Considering an alkaline electrolyte, hydrogen is generated at the cathode while oxygen is produced at the anode of the electrolyser, as shown in equations 6.1 and 6.2.

$$2\ H_2O + 2\ e^- \rightarrow H_2 + 2\ OH^- \text{ (cathode)} \quad (6.1)$$

$$4\ OH^- \rightarrow 2\ H_2O + O_2 + 4\ e^- \text{ (anode)} \quad (6.2)$$

The charge equalization proceeds by ionic conduction. A porous membrane is located between the two electrodes to prevent the mixture of the product gases.

The major problem of conventional electrolysis is high electricity consumption. It reduces the overall solar to H_2 efficiency (14 % [13]) and increases the cost of hydrogen (2.1 – 6.8 €/kg [14]) when compared with other methods. Other methods of hydrogen production, such as proton exchange membrane electrolysis and steam electrolysis, have been developing in recent years and could lead to good results, especially with the use of CSP. Steam electrolysis is a technology that can reach higher energy efficiency when compared to alkaline and proton exchange membrane electrolysis. That is due to a substantial part of the energy needed for the electrolysis process being added as heat, which is much cheaper and efficient than electric energy. In this system, hydrogen is produced with a solar to H_2 efficiency of 20 % [13] with a cost of 5.5 – 6.7 €/kg [15]. A mixture of steam and hydrogen at 750 to 950 °C is introduced in the high temperature cathode. It goes through the porous cathode and arrives at the interface between the cathode and the solid oxide electrolyte, where a water molecule is electrically dissociated into hydrogen and an oxygen anion by two electrons transported from the anode through externally provided electricity. The hydrogen produced is then back-

diffused to the cathode. Simultaneously, oxygen ions are drawn through the electrolyte by the electrochemical potential, liberating their electrons and recombining to form oxygen molecules on the surface of the anode side [16].

6.3.4 Fossil fuels and biomass

Fossil fuels and biomass already contain a great deal of chemical energy, contrarily to water, and therefore the required solar plant for the same hydrogen production is significantly smaller, leading to lower overall costs and a significantly lower selling price. The costs of biomass and fossil fuels can be, in the near term, more competitive for hydrogen production than for water technologies, and provide a good bridge for the future technologies. However, the evolution of prices and availability of biomass and fossil fuels should be regarded in case of market-wide implementation. Basic research was done since 1975, with several earlier projects [17] and in later years with more effusive projects. Distributed in different branches of fossil plus CSP technologies, some of these assignments are:

- solar steam gasification of petroleum coke [18, 19, 20];
- solar steam reforming of methane, based on the thermal decomposition of methane and steam at about 900 °C [21] (project SOLASYS [22] and SOLREF [23]);
- high temperature solar chemical natural gas cracking for co-production of Hydrogen and Carbon Black (project SOLHYCARB [23]), based on the thermal decomposition of CH_4 into C and H_2 at temperatures in a range of 1225 °C to 2025 °C [24], in various designs of solar reactors [25], with a solar-to-chemical experimental efficiency of 16 % and a predicted efficiency of 31 % to be achieved [26].

Besides current research, there is still a need for new developments, to achieve better performances, overtake the current technological barriers and be competitive. The mid-term strategy should be the upgrading of fossil fuels and biomass, using CSP as a renewable heat source. After establishment of fossil fuels and biomass plus CSP technologies, and development of water plus CSP based technologies, the long-term strategy should naturally tend to the substitution of fossil fuels and biomass by the use of water as primary energy carrier and raw material for hydrogen production.

6.3.5 Water: solar thermolysis

Thermolysis is known as the most direct method to obtain hydrogen, where high temperature heat, provided for example by CSP, induces a one-step direct thermal water molecule decomposition into H_2 and ½ O_2. The technically tolerable reaction temperature limit is around 2225 °C, which theoretically allows dissociation levels around 4 % at atmospheric pressure [27]. Generally the thermolysis reactor is constructed in special refractory materials, capable of enduring chemically active environments and very high temperatures, usually around 1225 °C [27]. The reactor has to tolerate significant temperature gradients and temperature swings during its operation and lifetime, without degradation, so that it is possible to use concentrated solar power to provide heat for its operation. To achieve the requested temperatures with CSP systems, high concentration ratios are required. The solar field should have a secondary concentrator or be over-designed to support several working hours per day at the required temperature, and that, with addition of the special materials required, leads to unsupportable expenses and reduced near-term feasibility and competitiveness. Additionally, direct thermolysis produces a mixture of H_2 and O_2 that requires high-temperature separation. If allowed to cool, the gases would form an explosive mixture that would be hazardous to personnel and plant [6]. Several solutions are proposed for this separation, such as a first very rapid cooling (quenching) of the mixture, with a reduction of more than 1225 °C within milliseconds, followed by traditional hydrogen separation methods, such as diffusion membranes or new hydrogen separation techniques at reaction temperature [27]. At near 2225 °C experiments proved that even at such high temperatures only 25 % of water dissociation was observed [28]. Nevertheless, thermolysis is still a major area for research, but still needs a breakthrough in material, product separation techniques and process design to potentiate its commercial implementation.

6.3.6 Water: solar thermochemical cycles

The search for water thermochemical cycles started worldwide in the late 1960s. During the first 10 years, about 20 publications dealing with thermochemical cycles appeared [29]. After this, activity rapidly increased, especially between 1974 and 1986, indicating a very strong increase in interest [30]. After that period, interest dropped until current days, when the need of investigation for new fuels has increased, as well as the need for new innovations to solve hydrogen production problems from water thermochemical cycles.

The water-splitting thermochemical cycles solve the H_2/O_2 separation problem and allow operation at relatively moderate upper temperatures when compared to thermolysis. Previous studies performed on H_2O-splitting thermochemical cycles were mostly characterized by the use of process heat at temperatures below 925 °C [31]. These cycles required multiple steps (one endothermic high temperature step supported by the CSP heat and then followed by exothermic reaction steps) and suffer from inherent inefficiencies associated with heat transfer and product separation at each step. Currently, the CSP technology has improved, and solar concentrating ratios have improved, and new, more efficient cycles, have been tested at higher temperatures.

There are however, as in the direct water thermolysis process, solar peculiarities in comparison to conventional thermochemical processes: high thermal flux density and frequent thermal transitions, because of the fluctuating solar radiation and weather conditions, e.g. there are reports of a variation of the regeneration temperature of the cycles of about ± 50 °C on the receiver [32]. The two most prominent receiver concepts are the volumetric-air receiver and the solid particle receiver [33].

Therefore, CRS and thermochemical commercial processes need to be adapted and, to reduce the solar transients, it is ideal to store solar high-temperature heat in a thermal storage system, and use the stored thermal energy continuously. However, thermal storage at temperatures above 450 °C is very difficult to achieve in an economically competitive way [14].

From all possibilities, several authors [34] compiled a database of 280 thermochemical water cycles. These cycles can be divided into ‘‘high-temperature’’ (Table 6.1) and ‘‘low-temperature’’ categories (Table 6.2), based on their number of reaction steps and also on the operating temperature, above and below 1400 °C, respectively.

All cycles, including the ‘‘high temperature’’, could use CSP for thermal reduction of the metal oxide. In the simplest version of the cycle, the oxide is completely reduced to a lower valence state. On the following exothermic reaction, the reduced oxide is put in contact with steam to produce hydrogen and regenerate the original oxide. This is the model for the cycles most closely examined in the literature, Zn/ZnO and FeO/Fe_3O_4 [7]. These cycles have only two steps, leading to simple process separations and a low potential for energy losses between cycle steps and during separations. Of all the oxides capable of performing the subsequent hydrolysis, ZnO has the lowest decomposition temperature, and would be predicted to have the highest theoretical efficiency: 29 % in the case of a 5000x solar concentration and 36 % in the case of a 10000x concentration in a plant of 90 MWth [35].

The cycle based on the FeO/Fe_3O_4 pair has also received large amounts of attention in the literature, but its operating temperatures are much higher than in the Zn/ZnO cycle, losing efficiency and having material problems. To avoid these problems, some moderate temperature oxide cycles have been proposed: the case of cadmium carbonate (CdO) and sodium manganese (Mn_2O_3). These oxides, when reduced, do not directly split water, so the process must be achieved through more than one additional step, as shown in Table 6.1. These steps introduce the possibility of unnecessary side reactions and complicated separations steps, and increase the possibility of material and energy losses. Sodium manganese has shown thermal reduction at lower temperatures than ZnO and FeO, without recombination problems. However, the subsequent steps of the cycle form a sodium-manganese compound that requires immense amounts of water from which it is difficult to recover all the sodium [7].

Table 6.1: Thermochemical "high temperature" water splitting cycles [7].

Cycle	Reaction Steps	Temperature (°C)
FeO/ Fe_3O_4	*Fe_3O_4 →3 FeO +* ½ O_2	2000 – 2300
	3 FeO + H_2O →Fe_3O_4 + H_2	400
Zn/ ZnO	*ZnO →Zn +* ½ *O_2*	1600 – 1800
	Zn + H_2O →ZnO + H_2	400
Sodium Manganese	*Mn_2O_3 →2 MnO +* ½ O_2	1400 – 1600
	2 MnO + 2 NaOH → 2 $NaMnO_2$ + H_2	627
	2 $NaMnO_2$ + H_2O → Mn_2O_3 + 2 NaOH	25
Cadmium carbonate	*CdO →Cd +* ½ *O_2*	1450 – 1500
	Cd + H_2O + CO_2 → $CdCO_3$ + H_2	350
	$CdCO_3$ → CdO + H_2O	500
Hybrid Cadmium	*CdO →Cd +* ½ *O_2*	1450 – 1500
	Cd + 2 *H_2O + CO_2 → $Cd(OH)_2$ + H_2* (electrochemical)	25 (ambient)
	$Cd(OH)_2$ → CdO + CO_2	375

Those difficulties are reduced when using a water-splitting cycle, presented on Table 6.2, which is capable of working at lower temperature. However, the difficulties with the use of corrosive reactants in separation are still present, and the cycles with more than three reaction steps suffer from a significant reduction in efficiency, with the use of high temperature solar heat [27]. From this perspective, the Westinghouse cycle: with two reaction steps (Table 6.2); and the General Atomics process: with three reaction steps (Table 6.2), are good solutions. The UT-3 cycle is a clear example of this assessment; when powered by nuclear energy the cycle has an estimated 15 % final efficiency and when operated in solar mode the efficiency is reduced to 8 % [36]. For the hybrid cycles, an important aspect to determine is the equilibrium of the acid concentration and the cell voltage, in order to find the minimum voltage for the best electrochemical efficiency. The hybrid low temperature cycles, which is the case of hybrid copper chloride cycle, use an electrochemical step to reduce cycle operating temperatures, and can lead to more efficient solar operation, eliminating some of the complex steps of similar cycles. However, they will require the use of electricity and could drive up the final hydrogen price [37]. Some of the presented water-splitting thermochemical cycles were and are still being tested in several projects such as SOLZINC [22], HYDROSOL and HYDROSOL II [23], HYTHEC [38], and STCH [39]. The CRS technological experience and knowledge is used to integrate new components and produce a new, high value and potential product such as hydrogen. All of these and other projects explore the synergies of CSP for renewable hydrogen production, experiencing different thermochemical cycles and receiver configurations, to

achieve better efficiencies and competitive prices. The up scaling of the concept reactors to the multi-megawatt scale can also face difficulties, as the reactors are windowed and the aperture designed needs to support a cluster of the several reactors.

Table 6.2: Thermochemical "low-temperature" water splitting cycles [36].

Cycle	Reaction Steps	Temperature (°C)
Westinghouse cycle	$H_2SO_4 \rightarrow H_2SO_4 + H_2O$	875
(or Hybrid Sulphur Cycle)	$H_2SO_4 \rightarrow H_2O + SO_2 + ½\ O_2$	875 – 1275
	$2\ H_2O + SO_2 \rightarrow H_2SO_4 + H_2$ *(Electrolysis)*	80
General Atomics process	$H_2SO_4 \rightarrow H_2SO_4 + H_2O$	875
(or Sulphur-Iodine process)	$H_2SO_4 \rightarrow H_2O + SO_2 + ½\ O_2$	875 – 1275
	$2\ H_2O + I_2 + SO_2 \rightarrow H_2SO_4 + 2$ *HI (Bunsen reaction)*	100
	2 *HI* $\rightarrow I_2 + H_2$	300 – 500
UT -3 cycle	$CaBr_2 + H_2O \rightarrow CaO + 2$ *HBr*	700 – 760
	$CaO + Br_2 \rightarrow CaBr_2 + ½\ O_2$	500 – 600
	$Fe_3O_4 + 8$ *HBr* $\rightarrow 3\ FeBr_2 + Br_2 + 4\ H_2O$	200 – 300
	$3\ FeBr_2 + 4\ H_2O \rightarrow Fe_3O_4 + 6\ HBr_2 + H_2$	550 – 650
Hybrid copper chloride cycle	$2\ Cu_2 + 2$ *HCl* $\rightarrow 2$ *CuCl* $+ H_2$	425
	4 *CuCl* $\rightarrow 2$ *Cu* $+ 2CuCl_2$ *(Electrochemical)*	25 (ambient)
	$2CuCl_2 + H_2O \rightarrow Cu_2OCl_2 + 2$ *HCl*	325
	$Cu_2OCl_2 \rightarrow 2$ *CuCl* $+ ½\ O_2$	550

6.3.7 CSP thermal applications and other solar technologies to produce hydrogen

There are other technologies that allow the production of hydrogen by a combined solution with solar energy. That is the case of water electrolysis using electricity from PV systems [14, 40]. Another technology used is the photo-electrochemical system for hydrogen production [41, 42]. However, the photo-electrode used in the method of photo-electrochemical decomposition, is not yet at the level required for commercialization, and should therefore be further studied and developed to be commercialized [43].

CSP heat can also be used in a great number of different applications other than hydrogen production, such as process heat, handling of hazardous wastes and testing and synthesis of different materials, e.g. carbon nanotubes and refractory oxides [29]. In low temperature applications, CSP can be used for seawater desalinization, supplying heat for Multi-Stage Flash evaporation (MSF), Multi-Effect Distillation (MED), Thermal Vapour Compression (TVC) or supplying clean electricity for Mechanical Vapour Compression (MVC) or Reverse Osmosis (RO) processes [44]. CSP can therefore be a mean to start solving the

alarming water crisis in developing countries with water scarcity, and contribute to the delay of a catastrophic depletion of groundwater resources that would have major effects on economic development and social peace [45]. CSP solar heat can also be used to provide solar cooling in separated [46] or integrated solutions, with production of power, cooling and water support [47].

6.4 Economic perspective

Table 6.3 presents a perspective of the expected hydrogen producing prices for the different techniques. The majority of the technologies are still in project/prototype scale and is still complex to have results in comparable conditions.

However, hydrogen produced by the General Atomics process could have lower production costs than hydrogen produced via the Westinghouse cycle, UT-3 cycle and hybrid Copper chloride. The hydrogen produced from the metal oxide based cycle has the greatest variation in production costs, and is well above all low temperature cycles in the worst price scenario (Table 6.3). This increase in price is mainly due to the high consumption of metal oxide that is not currently produced in large scale. The production cost differences between all the water thermochemical cycles are not very expressive, and due to the early stage of market implementation it is still undefined what cycle could present the cheapest thermochemical method for hydrogen production.

In terms of thermochemical cycle efficiency the metal oxide cycles could achieve the highest efficiencies. Depending on the metal selected, the cycle efficiencies vary from 45 to 60%. Afterwards, depending on the receiver particular configuration, the optical and receiver efficiencies vary from 50 to 55 % and 67 to 78 %, respectively, and determine the solar to hydrogen efficiency, 17 to 22 %.

Comparing renewable technologies with the current methods, there are significant differences in hydrogen production costs. Today's hydrogen is mainly produced from steam reforming of natural gas without carbon sequestration, which has significantly lower costs than hydrogen generated from water. However, the current produced hydrogen from natural gas, releases 7.3 kg of carbon dioxide per kilogram of hydrogen. If the hydrogen production process is from coal gasification, the emissions would increase to 29 kg CO_2/kg H_2 [48]. Even if carbon sequestration is considered, the prices of hydrogen production would still be unmatched to the remaining technologies. But if a natural gas or coal price escalate occurs, the price of

hydrogen produced from fossil fuels would follow that boom. The economy, even if hydrogen based, could still suffer a fuel shortage.

This reinforces the importance of using CSP for fuel and electricity security, especially for small and non-oil producing countries, and encourages the start of solar upgrading of fossil fuels, and in the long-term start the production of hydrogen from biomass and water. Solar steam reforming of methane could be the first step of the integration of CSP in hydrogen production. It presents lower hydrogen cost than methane solar cracking, and is the method with lower hydrogen equivalent cost after current hydrogen production technologies. This method could be the earlier described technological bridge form current technologies to completely renewable hydrogen production from water. The early stage petroleum coke gasification method, based in CSP, could be another interesting method. It uses an unexplored and rich fraction of the refineries products to produce a valued product such as hydrogen, with interesting efficiencies.

Another technology that should be considered is biomass gasification. Although there are still some major difficulties to clean the syngas, the hydrogen best case scenario price could be competitive, as presented in Table 6.3. Photocatalytic water splitting is another technology to consider and that could be quite promising with the use of nanostructured materials [49].

Electricity generated from CSP could also be used to perform water electrolysis. This system could function as a module of the CSP power plant, conferring flexibility and a mean to easily convert electricity excesses into a market added-value product such as hydrogen. Electrolysis nevertheless presents, when compared to water thermochemical cycles, lower overall efficiencies. This is due to significant larger losses in the electricity generation power block. Thermochemical cycles also have better water dissociation efficiencies than electrolysis. The solar to hydrogen efficiency of electrolysis is therefore lower than with thermochemical cycles. However, high temperature solar steam electrolysis is expected to achieve solar to hydrogen efficiencies of about 20 %, and could therefore still be considered a competitive solution.

The solar thermochemical cycles still have a long path to improve in terms of efficiencies, cost reduction and durability of materials. After the current technological and economic barriers are crossed, and with the predicted increase in fossil fuels cost, the water splitting thermochemical cycles have conditions to replace fossil fuels for hydrogen production.

Table 6.3: Hydrogen production cost and efficiencies per cycle.

Cycle	Production costs (€/kg)	Operating temperature of cycle (ºC)	Cycle efficiencies (%)	Efficiencies solar to hydrogen (%)
Metal oxide cycles	3.5 – 13 [a]	1400 - 2300	45-60 [b]	17-22 [b]
Westinghouse cycle	3.9 - 5.6 [a]	875 – 1275	51 [c]	22 [c]
General Atomics process	2.4 - 7.9 [d]	875 – 1275	45 [c]	19 [c]
UT -3 cycle	3.9 – 4.2 [e]	700 – 760	47 [e]	8 [e]
Hybrid Copper chloride	4.0 - 5.5 [f]	550	49 [g]	23 [g]
Water electrolysis with CSP electricity	2.1 - 6.8 [a]	-	30 [g]	14 [g]
High temperature solar steam electrolysis [a]	5.5 – 6.7 [d]	750 – 950	45 [g]	20 [g]
Solar methane cracking	3.0 - 3.9 [h]	1600 – 1900	70 [h]	9.1-31 [i]
Solar steam reforming of methane	1.8 - 1.9 [j]	900	86 [j]	63 [j]
Solar petroleum coke gasification	-	1600 - 2100	48 - 87 [k]	9-20 [k]
Commercial coal gasification (with / without carbon sequestration)	0.8 / 0.64 [l]	600 – 1000	63 [m]	-
Commercial natural gas steam reforming (with / without carbon sequestration)	0.66 / 0.53 [l]	900	83 [m]	-
Biomass gasification	0.85 - 1.7 [l]	1100	40 – 50 [m]	-
Photo-catalytic water splitting	3.5 [l]	-	10 -14 [m]	-

[a] adjusted prices based on a 50 MWth CSP plant [14].

[b] based on a 46 MWth CPC Si-G reactor receiver on a CRS [13].

[c] based on a solid particle 700 MWth receiver [13].

[d] adjusted prices based on current process designs and small scale pilot plants [15].

[e] based on a CRS-CSP with day and night operation for a projected output of 20000 Nm^3/h [36].

[f] hybrid copper chloride cycle coppled with a desalinization plant using nuclear adjusting the capital costs to solar energy [37].

[g] based on a molten salt 700 MWth receiver on a CRS-CSP plant configuration [13].

[h] CRS-CSP with a heliostat field from 2188-8750 m^2 with elemental carbon production based on [50].

[i] based on a 5 kW particle flow reactor in a solar furnace [26].

[j] based on the SOLASYS reformer with 50 MWth [21].

[k] based on based on a 5 kW reactor in a solar furnace [19, 20].

[l] based on [51] and considering a cost increase of 25% for the provision and implementation of the carbon capture costs [14].

[m] process energy efficiency - energy value of produced hydrogen divided by the energy input - based on [51].

6.5 Conclusions

Concentrating solar power for hydrogen production from water could be a long-term solution after the possible implantation of hydrogen as a fuel. Water direct thermolysis and thermochemical cycles have been strongly studied and tested, and could be future processes for renewable hydrogen production. Nevertheless, there is still a need of some breakthroughs that can solve the current technological problems. However, the cost and efficiency estimates are promising for water thermochemical cycles such as metal oxide, sulphur iodine and hybrid sulphur. Hydrogen produced from electrolysis could also be a viable renewable solution for hydrogen production, if the expected electricity generation costs from CSP are accomplished, but with lower efficiencies than water thermochemical cycles. To boost the efficiencies, high temperature steam electrolysis could be used, but the current associated costs are above the best cost scenario for other technologies. Biomass gasification and fossil fuel concentrated solar power cracking/reforming/gasification with carbon sequestration, particularly methane solar steam reforming, can meanwhile act as a bridge to assure the current hydrogen demand in the world and encourage the usage of hydrogen as a fuel, shifting the economy from fossil fuel based to renewable energy based.

References

[1] Coelho, B., Oliveira, A.C., Mendes, A., Concentrated solar power for renewable electricity and hydrogen production - A review, Energy Environ. Sci., 2010, Issue 10, Number 3, pp. 1398 - 1405.

[2] Energy Information Administration (EIA), 2009. International Energy Outlook 2009 (IEO2009)

[3] Ball M, Wietschel M, Rentz O., 2006, Integration of a hydrogen economy into the German energy system: an optimizing modelling approach. International Journal of Hydrogen Energy 32, 1355–68.

[4] Ball M, Wietschel M., 2009. The future of hydrogen – opportunities and challenges. International Journal of Hydrogen Energy 34, 615–627.

[5] Felder, R., Meier, A., 2008. Well-to-wheel analysis of solar hydrogen production and utilization for passenger car transportation. Journal of Solar Engineering 130.

[6] Romero, M., Zarza, E., 2007. Concentrating Solar Thermal Power, in: Kreith, F. Goswami, D. Yogi. Handbook of energy efficiency and renewal energy, CRC Press, Chapter 21.

[7] Perkins, C., Weimer, A.W., 2009. Solar - thermal production of renewal hydrogen, AIChE Journal 55.

[8] C.C. Agrafiotis et al., 2007. Hydrogen production in solar reactors, Catalysis Today 127, 265-277.

[9] Cumalioglu, I., Ertas, A., Ma, Y., Maxwell, T., 2008. State of the Art: Hydrogen storage, J. Fuel Cell Sci. Technol. 5, 034001-1-10.

[10] Linde A.G. communication. www.linde.com

[11] Colozza, A. J., 2002, “Hydrogen Storage for Aircraft Applications Overview,” Report No. NASA/CR-211867.

[12] Pitz-Paal, R., Dersch, J., Milow, B., 2005. ECOSTAR roadmap document, DLR.

[13] Kolb, G. J, Diver, R. B., 2008. Screening analysis of solar thermochemical hydrogen concepts Sandia National Laboratories. Albuquerque: New Mexico; Sandia Report SAND2008-1900.

[14] Graf, D. Monnerie, N. Roeb, M. Schmitz, M. Sattler, C., 2008. Economic comparison of solar hydrogen generation by means of thermochemical cycles and electrolysis, International journal of hydrogen energy 33, 4511-4519.

[15] Pregger T., Graf D., Krewitt W., Sattler C., Roeb M., Moller S., 2009. Prospects of solar ther-mal hydrogen production processes. International Journal of Hydrogen Energy 34, 4256-4267.

[16] Yu, B. Zhang, W., Chen, J., Xu, J., Wang, S., 2008. Advance in highly efficient hydrogen production by high temperature steam electrolysis, Science in China Series B: Chemistry 4, 289-304.

[17] Tamme, R., Buck, R., Epstein, M., Fisher, U., Sugarmen, C., 2001. Solar upgrading of fuels for generation of electricity, J. Sol. Energy Eng. 123, 160.

[18] Trommer D, Noembrini F, Fasciana M, Rodriguez D, Morales A, Romero M, Steinfeld A., 2005. Hydrogen production by steam-gasification of petroleum coke using concentrated solar power — I. Thermodynamic and kinetic analyses. Int J Hydrogen Energy; 30, 605–18.

[19] Z'Graggen A, Haueter P, Trommer D, Romero M, de Jesus JC, Steinfeld A., 2006. Hydrogen production by steam-gasification of petroleum coke using concentrated solar power — II. Reactor design, testing, and modelling Int J Hydrogen Energy; 31, 797–811.

[20] Z'Graggen A, Haueter P, Trommer D, Romero M, de Jesus JC, Steinfeld A., 2007. Hydrogen production by steam-gasification of petroleum coke using concentrated solar power — III. Reactor experimentation with slurry feeding.Int J Hydrogen Energy 32, 992–996.

[21] Moller S, Kaucic D, Sattler C., 2006. Hydrogen production by solar reforming of natural gas: a comparison study of two possible process configurations. Journal of Solar Energy Engineering; 128, 16–23.

[22] European Commission, 2004. European research on concentrated solar thermal energy.

[23] European Commission, 2007. Concentrating solar power, from research to implementation.

[24] Rodat S, Abanades S, Coulie´ J, Flamant G., 2009. Kinetic modeling of methane decomposition in a tubular solar reactor. Chem Eng.J146, 120–7.

[25] Ozalp, N. Kogan, A. Epstein, M., 2009. Solar decomposition of fossil fuels as an option for sustainability, International Journal of Hydrogen Energy 34, 710-720.

[26] Maag, G. Zanganeh, G. Steinfeld, A., 2009. Solar thermal cracking of methane in a particle-flow reactor for the co-production of hydrogen and carbon, International Journal of Hydrogen Energy 34, 7676-7685.

[27] S.Z. Baykara, Experimental solar water thermolysis, International Journal of Hydrogen Energy 29 (2004), 1459 – 1469.

[28] Perkins, C. Weimer, A.W., 2004. Likely near-term solar-thermal water splitting technologies, International Journal of Hydrogen Energy 29, 1587-1599.

[29] Edward A. Fletcher, 2001. Solarthermal processing: a review. J. Sol. Energy Eng 123, 63.

[30] Funk, J., 2001. Thermochemical hydrogen production: past and present, International Journal of Hydrogen Energy 26,185-190.

[31] A. Steinfeld, 2005. Solar thermochemical production of hydrogen – a review, Solar Energy 78, 603–615.

[32] Roeb, M. Neises, M. Sack, P., Rietbrock, P., Monnerie, N. Dersch, J., Schmitz, M., Sattler, C., 2009. Operational strategy of a two-step thermochemical process for solar hydrogen production, International Journal of Hydrogen Energy 34, 4537-4545.

[33] Kolb GJ, Diver RB, Siegel N., 2007. Central -station solar hydrogen power plant. Journal of Solar Energy Engineering 129, 179–83.

[34] Abanades, S., Charvin, P., Flamant, G., Neveu, P., 2006. Screening of water-splitting thermo-chemical cycles potentially attractive for hydrogen production by concentrated solar energy, Energy 31, 2805-2822.

[35] A. Steinfeld, 2002. Solar hydrogen production via a two-step water-splitting thermochemical cycle based on Zn/ZnO redox reactions, International Journal of Hydrogen Energy 27, 611-619.

[36] Kodama, T., Gokon, N., 2007. Thermochemical cycles for high-temperature solar hydrogen production, Chemical Reviews 107.

[37] Orhan, M., Dincer, I., Naterer, G., Rosen, M., 2010. Coupling of copper-chloride hybrid thermochemical water splitting cycle with a desalination plant for hydrogen production from nuclear energy, International Journal of Hydrogen Energy 35, 1560-1574.

[38] Duigou, A., Borgard, J., Larousse, B., et al, 2007. HYTHEC: An EC funded search for a long term massive hydrogen production route using solar and nuclear technologies, International Journal of Hydrogen Energy 32 1516-1529.

[39] Garland, R., Gupta, N., 2009. Hydrogen production roadmap technology pathways to the future, FreedomCAR & Fuel Partnership Hydrogen Production Technical Team.

[40] Gibson, T.A., Kelly, N.A., 2008. Optimization of solar powered hydrogen production using photovoltaic electrolysis device, International journal of hydrogen energy 33, 5931-5940.

[41] Nowotny, J. et al, 2005. Solar-hydrogen: environmentally safe fuel for the future, International journal of hydrogen energy 30, 521-544.

[42] Varner, K., Warren, S., Turner, J.A., 2002. Photoelectrochemical systems for hydrogen production, Proceedings of the 2002 U.S. DOE Hydrogen program review, NREL.

[43] J. Nowotny, C.C. Sorrell, T. Bak, L.R., 2005. Sheppard, Solar-hydrogen: Unresolved problems in solid-state science, Solar Energy 78, 593-602.

[44] Concentrating Solar Power for Seawater Desalination, 2007. German Aerospace Center (DLR), Institute of Technical Thermodynamics, Section Systems Analysis and Technology Assessment, Stuttgart.

[45] Gastli, A., Charabi, Y., Zekri, S., 2009. GIS-based assessment of combined CSP electric power and seawater desalination plant for Duqum - Oman, Renewable and Sustainable Energy Reviews.

[46] Kim, D.S., Infante Ferreira, C.A., 2008. Solar refrigeration options - a state-of-the-art review, International Journal of Refrigeration 31, 3-15.

[47] Trieb, F., Muller-Steinhagen, H., Kern, J., Scharfe, J., Kabariti, M., Taher, A., 2009. Technologies for large scale seawater desalination using concentrated solar radiation, Desalination 235, 33-43.

[48] Kothari, R., Buddhi, D., Sawhney, R.L., 2008. Comparison of environmental and economic aspects of various hydrogen production methods, Renewable and Sustainable Energy Reviews 12, 553-563.

[49] Zhu, J., Zach, M., 2009. Nanostructured materials for photocatalytic hydrogen production, Current Opinion in Colloid & Interface Science 14, 260-269.

[50] Spath, P., Amos, W. A., 2003. Using a concentrating solar reactor to produce hydrogen and carbon black via thermal decomposition of natural gas: feasibility and economics. J. Sol. Energy Eng. 125, 159.

[51] Abbas, H., Wan Daud, W., 2010. Hydrogen production by methane decomposition: A review, International Journal of Hydrogen Energy 35, 1160-1190.

Chapter 7

Conclusions and future work

This page was intentionally left blank

7. Conclusions and Future work

7.1 Conclusions

CSP can generate a dispatchable electricity flow, capable of supplying small or large populations without requiring fossil fuels. The main objective of this thesis work was the development of tools and models to design, simulate and optimize the performance of hybrid CRSs for Portugal, under transient conditions. However, detailed design and simulation of a CRS is complex, due to the interconnections among the various components and the transient behaviour of solar radiation. As CRS hybridization is an unexplored matter, modelling of these systems increases complexity, reducing the software available to perform these simulations. After the analysis of the CRS and biomass state-of-the-art, completely new models were developed in HFLCAL and EBSILON for CRS and biomass base cases design and simulation, demonstrating that these software are suitable for solar field and power block design/simulation, respectively. A 4 MWe solar-only atmospheric air volumetric CRS was design and optimized based on SOLMASS for Portuguese conditions. Afterwards, several biomass power plants (base cases) were designed and simulated for comparison with new and innovative hybrid CRS/ biomass options. This work was very well accepted by the CSP community, with several communications and manuscripts published, and lead to the formation of an international group that will build a prototype and experimentally test the CSP hybridization concept, in the framework of a recently approved FP7-Energy project (REELCOOP).

Solar-only CRS:

Within the Portuguese reality (Faro conditions), the best 4 MWe solar-only atmospheric volumetric CRS power plant configuration uses a 1.25 solar multiple, a 2 hour storage and a heat recovery steam generator that generates 80 bar and 480 °C steam to feed a 3 stage turbine (CRS#3). This solution has a good cost/performance trade-off. It has a higher efficiency than a 4 MWe CRS with similar operating conditions to the Jülich Solar Tower (CRS#5) and a lower levelized electricity cost (LEC). The optimal design DNI for local conditions is 750 W/m^2 while considering a peak receiver flux of 950 kW/m^2. For this configuration, the power plant LEC is 0.234 €/kWh with a CAPEX of € 22.3 million. If this receiver flux limit is increased by 10 % (CRS#11), the power plant increases the performance by 0.1 GWh per year, reducing its LEC to 0.232 €/kWh, well below the feed-in tariff of 0.273 €/kWh. The CRS internal rate of return is 9.8 %, with a payback time of 14 years and a net present value of € 7.9 million

(considering an average annual inflation of 4 %). In the case of an annual average inflation of 2 % instead of 4 %, the power plant investment has very positive contours, with NPV close to 13 million € and a payback period of 13 years. Also, if some commercial or under-development innovations are introduced in the power plant, LEC can be reduced to close to grid parity (0.185 €/kWh).

Hybrid power plants:

Hybrid biomass and CSP power plants are an interesting option for future dispatchable renewable electricity generation. The major drawbacks of solar-only CRS is the moderate capacity factors or high thermal energy storage costs; while the biomass major problems are the necessity to build a large biomass collection structure, the volatility of the biomass price and the low feed-in tariffs. The hybridization of these technologies increases the power plant capacity factors and efficiency (when compared to a solar only CRS) and reduces the biomass consumption (when compared to a biomass only power plant). The results for the hybrid solutions, either in the steam or air cycle, seem quite promising, generating a dispatchable electricity flow with interesting economic indicators. However, due to prototype characteristics of this concept, the margins are low and the relation risk/profit is fairly high, so incentives should be considered to fuel this concept (e.g.: small percentage of alternative fuels allowed in CSP plants with CSP nominal tariff, or financial incentives).

Biomass integration in the steam cycle:

For biomass integration into the steam cycle of a CRS, the technical/economical balance of a hybrid biomass boiler steam integration on the CRS power block (FRB4#CRS#12) presents interesting results, with a LEC of 0.146 €/kWh. This LEC is 0.086 €/kWh lower than for the 4 MWe CRS with 3 h energy storage, SM1.25, design DNI of 750 W/m^2 and receiver area of 60.0 m^2 with 10 % tolerance in the receiver peak flux base case (CRS#12); and only 0.041 €/kWh higher than the 4 MWe forest waste biomass boiler power plant (FRB4), with a 7500 ton annual reduction in biomass consumption. The economic indicators are nevertheless somehow distant from the base cases, with an IRR of 6.6 % (FRB4#CRS#12), compared to 9.7 % (CRS#12) and 7.4 % (FRB4).

Biomass integration in the air cycle:

For biomass integration into the air cycle of a CRS, the lower LEC options are the hybridization of 4 MWe CRS with biogas from a waste-water treatment plant (LEC of 0.15 €/kWh), with landfill gas (LEC of 0.16 €/kWh) or with syngas from wood residues gasification (LEC of 0.17 €/kWh). Because the Portuguese bonus feed-in tariff is calculated for each renewable energy technology, some of these power plant configurations have negative economic turnovers. The hybrid power plant investment with best payback period is the hybridization with an anaerobic digester, using sludge from a waste-water treatment plant, which returns the investment in 13 years (sludge collection and transport assumed without cost), presenting also the best net present value (15 million euro). However, for the 4 MWe scale, waste-water treatment plant biogas would only be possible close to large cities (few limit cases), with centralized plants capable of generating sufficient quantities of sludge or MSW. A hybridization technology that can be used in a larger number of cases is the gasification of wood residues (WG#CRS#3 - LEC of 0.17 €/kWh). This power plant can make biomass gasification economically viable to operate under the Portuguese conditions (with an IRR of 5.5 % and a NPV of 3.3 million euro), reducing the biomass consumption by 11 000 tons per year when compared to the base case.

Fuels generation:

A large piece of the energy market is the fuels. Fuels are high value and highly exchangeable goods that origin mainly from oil. The usage of concentrating solar power for hydrogen production from water could be a long-term solution after a possible implantation of hydrogen as a fuel. Water direct thermolysis and thermochemical cycles have been strongly studied, tested and could be the future processes of renewable hydrogen production. Nevertheless, there is still a need of some breakthroughs that can solve current technological problems. However, the cost and efficiency estimates are promising for water thermochemical cycles such as metal oxide, sulphur iodine and hybrid sulphur. Hydrogen produced from electrolysis could also be a viable renewable solution for hydrogen production, if the expected electricity generation costs from CSP are accomplished, but with lower efficiencies than water thermochemical cycles. To boost the efficiencies, high temperature steam electrolysis could be used, but the current associated costs are above the other technologies. Biomass gasification and fossil fuel concentrated solar power cracking/reforming/gasification with carbon sequestration, particularly methane solar steam reforming, can meanwhile act as a bridge to

assure the current hydrogen demand in the world, and encourage the usage of hydrogen as a fuel, shifting the economy from fossil fuel based to renewable energy based.

Markets and impact:

CSP, and particularly CRS, can be a pioneer technology to develop sustainable centralised electricity generation technologies. However, to achieve full market penetration, CRS needs to reduce the CAPEX and increase the performance of materials and equipment, so the technology would be competitive, in mid-term, with escalating fossil fuel prices. In this perspective, the international incentives were beneficial to mature the technology. However, the present intercontinental debt crisis imposed cuts in the incentives and threatens CSP companies to regression and to abandon investments. The proposed hybridization possibilities open new perspectives to reduce the LEC, maintaining the sustainability and renewable goals. From a national perspective, it also assures local involvement, job creation and strategic national safety issues, assuring electricity and fuel independence, without relying on a single energy resource.

7.2 Future work

In the sequence of the work developed during this thesis, links with international research groups working in the CSP field were established. Discussions with these groups led to the preparation of a proposal submitted to the European Commission FP7-Energy programme, integrated in the REELCOOP project, which was subsequently approved and started in September 2013. REELCOOP stands for REnewable ELectricity COOPeration and addresses different renewable electricity generation technologies, including CSP. Under this project, led by FEUP and where DLR and CIEMAT are some of the partners, a prototype of a hybrid concentrating solar/biomass power plant will be built and tested in Tunisia.

This prototype system, shown in Figure 7.1, is a 60 kWe power plant using a parabolic trough field with direct steam generation. For smaller prototypes, the higher maturity and low complexity/maintenance of parabolic trough solar collectors are an advantage. Energy backup will be provided by a biogas boiler and a storage device. A biomass digester will be fed by locally available organic waste, contributing to the improvement of environmental and living conditions for the population. Energy storage is essential for CSP power plant operation and has higher efficiency and lower costs than conventional electricity storage solutions. Hybridization with bioenergy will eliminate the need for large storage devices to extend power plant operation during the night. There is however the need for storage to compensate the

biomass boiler start-up and short transients from solar power. A novel PCM-storage will also be tested. Simulations will also be carried out for larger output powers.

The consortium objective is to build a fully hybrid prototype, with high solar share, high conversion efficiencies for both solar and biomass parts, and a large capacity factor, up to 24 hours/day of operation. The environmental sustainability and economics of the prototype system will be assessed by means of Life Cycle Assessment studies, and the results obtained will be disseminated to industry and research, as proof-of-concept for this solution. The combination of solar and biomass resources in CSP plants allows maximisation of capacity factors, contributing to lower electricity production costs. This has been demonstrated by the simulation work carried out in this thesis, and will be experimentally demonstrated during REELCOOP.

In the future, the concepts developed in this thesis could be applied/tested in larger scale power plants. When the present economic and financial framework improves, the SOLMASS project might finally take-off, and Portugal could have a hybrid CSP and biomass power plant and possibly explore the solar-chemical concept.

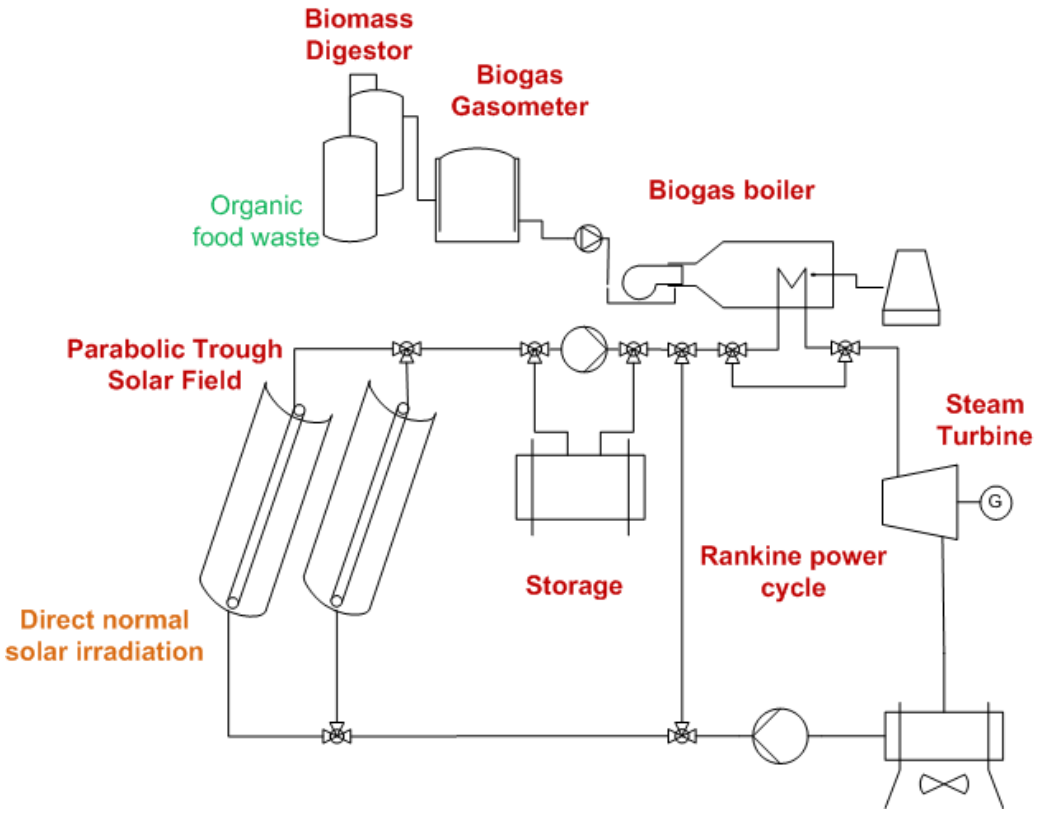

Figure 7.1: Schematic representation of REELCOOP prototype system 3 (hybrid CSP/biomass power plant).

This page was intentionally left blank